NASA-CR 65167

JIS
DIVISION

8100 florissant avenue, st. louis 36, mo, colfax 1-1800

N66-10214
(ACCESSION NUMBER) (THRU)
188 1
(PAGES) (CODE)
33
(NASA CR OR TMX OR AD NUMBER) (CATEGORY)
FACILITY FORM 602

Report Number 1533

Performance Evaluation of "THERMO-LAG" Material for Entry Heat Protection of Advanced Manned Spacecraft

Quarterly Progress Report
1 January 1963 to 1 April 1963

LIBRARY COPY
JUL 1 1963
MANNED SPACECRAFT CENTER
HOUSTON, TEXAS

Prepared for

National Aeronautics and
Space Administration
Manned Spacecraft Center
Houston 1, Texas

NAS 9-877

GPO PRICE $ _____

CFSTI PRICE(S) $ _____

Hard copy (HC) 5.00

Microfiche (MF) 1.25

ff 653 July 65

EMERSON ELECTRIC OF ST. LOUIS
ELECTRONICS AND SPACE DIVISION

8100 florissant avenue, st. louis 36, mo., colfax 1-1800

Report Number 1533

Performance Evaluation of "THERMO-LAG" Material for Entry Heat Protection of Advanced Manned Spacecraft

Quarterly Progress Report
1 January 1963 to 1 April 1963

Prepared for

National Aeronautics and
Space Administration
Manned Spacecraft Center
Houston 1, Texas

(NASA Contract NAS 9-877)

BLANK PAGE

TABLE OF CONTENTS

Section		Page
	SUMMARY	1
	Phase I	1
	Phase II	1
	Phase III	1
	Phase IV	2
	Phase V	2
I	INTRODUCTION	1-1
II	PROPERTY AND PARAMETER EVALUATION	2-1
	Thermal Properties (Virgin and Charred Material)	2-1
	Thermal - Chemical Characteristics	2-9
	Mechanical Properties (Precast and Sprayed Materials)	2-13
III	SPACE PERFORMANCE EVALUATION	3-1
	Reentry Simulation (Convection and Radiation)	3-1
	Modification of Certain Reentry Simulation Tests and Parameter Analyses	3-3
IV	PERFORMANCE ANALYSIS AND PREDICTION	4-1
	Debris Layer Recession	4-1
	Oxidation and Diffusion Model and Analysis	4-3
	Mass Injection	4-6
	Stagnation Effect	4-7
	Downstream Effect	4-12
V	STRUCTURAL CONSIDERATIONS AND APPLICATIONS	5-1
	Structural Applications	5-1
	Analysis of the Structural Model	5-14
VI	BIBLIOGRAPHY	6-1
APPENDIX A	TEST RESULTS	A-1
APPENDIX B	SYMBOLS	B-1
	General	B-1
	Special Symbols for Stress Analysis	B-4

LIST OF ILLUSTRATIONS

Figure		Page
2-1	Thermal Conductivity Test Specimen	2-1
2-2	Thermal Conductivity of Virgin "THERMO-LAG" T-500	2-2
2-3	Thermal Conductivity of Charred "THERMO-LAG" T-500	2-3
2-4	Mean Specific Heat of Virgin "THERMO-LAG" T-500 Versus Temperature	2-5
2-5	Mean Specific Heat of Charred "THERMO-LAG" T-500 Versus Temperature	2-6
2-6	Density of "THERMO-LAG" T-500-4 and T-500-6	2-7
2-7	Coefficient of Linear Thermal Expansion for Virgin "THERMO-LAG" T-500 Materials	2-8
2-8	Coefficient of Linear Thermal Expansion for Charred "THERMO-LAG" T-500 Materials	2-9
2-9	Effect of Temperature at Low Pressure on Weight Loss of "THERMO-LAG" T-500	2-10
2-10	Differential Thermal Analysis of "THERMO-LAG" T-500-4 at 2°C/Minute Heating Rate (T_s = 563°F)	2-11
2-11	Differential Thermal Analysis of "THERMO-LAG" T-500-4 at 5°C/Minute Heating Rate (T_s = 536°F)	2-12
2-12	Differential Thermal Analysis of "THERMO-LAG" T-500-6 at 2°C/Minute Heating Rate (T_s = 545°F)	2-13
2-13	Differential Thermal Analysis of "THERMO-LAG" T-500-6 at 5°C/Minute Heating Rate (T_s = 545°F)	2-14
2-14	Deltatherm Thermogravimetric Analyzer	2-15
2-15	Thermogravimetric Analysis of "THERMO-LAG" T-500-4 at 2°C/Minute Heating Rate (3.78 MG Sample Weight)	2-16
2-16	Thermogravimetric Analysis of "THERMO-LAG" T-500-4 at 5°C/Minute Heating Rate (2.62 MG Sample Weight)	2-17
2-17	Thermogravimetric Analysis of "THERMO-LAG" T-500-4 at 10°C/Minute Heating Rate (4.73 MG Sample Weight)	2-19
2-18	Thermogravimetric Analysis of "THERMO-LAG" T-500-6 at 2°C/Minute Heating Rate (3.3 MG Sample Weight)	2-20
2-19	Thermogravimetric Analysis of "THERMO-LAG" T-500-6 at 5°C/Minute Heating Rate (3.9 MG Sample Weight)	2-21
2-20	Thermogravimetric Analysis of "THERMO-LAG" T-500-6 at 10°C/Minute Heating Rate (4.3 MG Sample Weight)	2-22
2-21	Tensile Strength and Elongation Models for "THERMO-LAG" T-500-4 and T-500-6	2-24
2-22	Research Inc. Material Testing Equipment	2-25
2-23	Specimen Held in Position for Tensile Test in the Cryogenic Chamber	2-26
2-24	Tensile Strength of "THERMO-LAG" T-500-4 and T-500-6	2-27
2-25	Initial Models of "THERMO-LAG" T-500-4 and T-500-6	2-28
2-26	Tensile Elongation of "THERMO-LAG" T-500-4 and T-500-6	2-29
2-27	Specimen Held in Position for Shear Test in the Cryogenic Chamber	2-30

LIST OF ILLUSTRATIONS (Cont'd.)

Figure		Page
2-28	Shear Strength Results of "THERMO-LAG" T-500-4 and T-500-6	2-31
2-29	Specimen Held in Position for Flexural Strength Test in the Cryogenic Chamber	2-32
2-30	Flexural Strength Results of "THERMO-LAG" T-500-4 and T-500-6	2-33
3-1	Percentage of Oxygen Versus Surface Recession for "THERMO-LAG" T-500	3-4
3-2	Heat Blockage Versus Total Enthalpy for "THERMO-LAG" T-500	3-5
3-3	Transient Histories for Stagnation Heat Flux of 35 BTU/FT^2-SEC	3-10
3-4	Transient Histories for Stagnation Heat Flux of 48 BTU/FT^2-SEC	3-11
3-5	Transient Histories for Stagnation Heat Flux of 110 BTU/FT^2-SEC	3-12
3-6	Transient Histories for Stagnation Heat Flux of 170 BTU/FT^2-SEC	3-13
3-7	Transient Histories for Stagnation Heat Flux of 300 BTU/FT^2-SEC	3-14
3-8	Transient Histories for Stagnation Heat Flux of 456 BTU/FT^2-SEC	3-15
3-9	Composition - Radiation Ablation for Radiation Heat Flux of 7.4 BTU/FT^2-SEC	3-16
3-10	Composition - Radiation Ablation for Radiation Heat Flux of 9 BTU/FT^2-SEC	3-17
3-11	Test Gap Model	3-18
4-1	A Physicochemical Model of Partially Dissociated Air Flow Over a Carbon Surface	4-4
4-2	The Variation of h/h_o With m/h_o for Boundary Layer Flow Conditions	4-9
4-3	Effect of Molecular Weight of Gas Injected on Heat Transfer Coefficient	4-10
4-4	Effect of Weight of Gas Injected on Heat Transfer Coefficient	4-11
4-5	Effect of Transpiration of Air on Heat Transfer	4-12
5-1	Effect of Surface Treatment on Bond Shear Strength	5-6
5-2	Bond Shear Test for Mineral Acid CrO_3 Surface Treatment	5-7
5-3	Bond Shear Test for Mineral Acid H_2SO_4 Surface Treatment	5-8
5-4	Bond Shear Test for Mineral Acid H_3PO_4. H_2SO_4 Surface Treatment	5-9
5-5	Bond Shear Test for Sandblasted Surface Treatment	5-10
5-6	Bond Shear Test for Chemically Cleaned Surface Treatment	5-11
5-7	Tensile Test for Mineral Acid CrO_3 Surface Treatment	5-12
5-8	Tensile Test for Mineral Acid H_2SO_4 Surface Treatment	5-13
5-9	Tensile Test for Mineral Acid H_3PO_4. H_2SO_4 Surface Treatment	5-14
5-10	Tensile Test for Sandblasted Surface Treatment	5-15
5-11	Tensile Test for Chemically Cleaned Surface Treatment	5-16
5-12	Comparison of Stresses	5-17
5-13	Comparison of Stresses	5-19
5-14	Comparison of Displacements	5-21
5-15	Comparison of Displacements	5-21
5-16	Potential Energy Curve	5-36
5-17	Shear Stress Versus X	5-47

LIST OF ILLUSTRATIONS (Cont'd)

Figure		Page
5-18	Peeling Stresses Along X Axis	5-47
A-1	Sectioned Model N-2 - After Test	A-2
A-2	Sectioned Model N-6 - After Test	A-3
A-3	Sectioned Model N-9 - After Test	A-4
A-4	Sectioned Model N-11 - After Test	A-5
A-5	Sectioned Model N-15 - After Test	A-6
A-6	Sectioned Model N-21 - After Test	A-7
A-7	Sectioned Model N-22 - After Test	A-8
A-8	Sectioned Model N-26 - After Test	A-9
A-9	Sectioned Model N-29 - After Test	A-10
A-10	Sectioned Model N-30 - After Test	A-11
A-11	Sectioned Model N-35 - After Test	A-12
A-12	Sectioned Model N-36 - After Test	A-13
A-13	Sectioned Model N-46 - After Test	A-14
A-14	Sectioned Model N-48 - After Test	A-15
A-15	Sectioned Model N-53 - After Test	A-16
A-16	Sectioned Model N-54 - After Test	A-17
A-17	Sectioned Model N-64 - After Test	A-18
A-18	Sectioned Model N-65 - After Test	A-19
A-19	Sectioned Model N-71 - After Test	A-20
A-20	Sectioned Model N-73 - After Test	A-21
A-21	Sectioned Model N-75 - After Test	A-22
A-22	Sectioned Model N-82 - After Test	A-23
A-23	Sectioned Model N-92 - After Test	A-24
A-24	Sectioned Model N-94 - After Test	A-25
A-25	Sectioned Model N-105 - After Test	A-26
A-26	Sectioned Model N-106 - After Test	A-27
A-27	Sectioned Model N-110 - After Test	A-28
A-28	Sectioned Model N-112 - After Test	A-29
A-29	Temperature - Time History of Model N-2	A-30
A-30	Temperature - Time History of Model N-6	A-31
A-31	Temperature - Time History of Model N-9	A-32
A-32	Temperature - Time History of Model N-11	A-33
A-33	Temperature - Time History of Model N-15	A-34
A-34	Temperature - Time History of Model N-21	A-35
A-35	Temperature - Time History of Model N-22	A-36
A-36	Temperature - Time History of Model N-26	A-37
A-37	Temperature - Time History of Model N-29	A-38
A-38	Temperature - Time History of Model N-30	A-39
A-39	Temperature - Time History of Model N-35	A-40
A-40	Temperature - Time History of Model N-36	A-41

LIST OF ILLUSTRATIONS (Cont'd)

Figure		Page
A-41	Temperature - Time History of Model N-46	A-42
A-42	Temperature - Time History of Model N-48	A-43
A-43	Temperature - Time History of Model N-53	A-44
A-44	Temperature - Time History of Model N-54	A-45
A-45	Temperature - Time History of Model N-64	A-46
A-46	Temperature - Time History of Model N-65	A-47
A-47	Temperature - Time History of Model N-71	A-48
A-48	Temperature - Time History of Model N-73	A-49
A-49	Temperature - Time History of Model N-75	A-50
A-50	Temperature - Time History of Model N-82	A-51
A-51	Temperature - Time History of Model N-92	A-52
A-52	Temperature - Time History of Model N-94	A-53
A-53	Temperature - Time History of Model N-105	A-54
A-54	Temperature - Time History of Model N-106	A-55
A-55	Temperature - Time History of Model N-110	A-56
A-56	Temperature - Time History of Model N-112	A-57

LIST OF TABLES

Table		Page
3-1	Variation of Oxygen Concentration Tests	3-2
3-2	Stagnation Point Oxidation Results	3-3
3-3	Preliminary Stagnation Point Results	3-7
3-4	Revised Test Matrix - Air-Arc Gap Tests	3-19
4-1	Equilibrium Constants for CO and CO_2 at Elevated Temperature	4-1
4-2	Experimental Data and Results of Oxidation Tests	4-2
5-1	Degress of Artifically Induced Cure by Infrared Source	5-2
5-2	Degree of Electrical Heat Induced Cure (Single Graphite String)	5-3
5-3	Degree of Electrical Heat Induced Cure (Double Graphite Strings)	5-4
5-4	Degree of Chemically Accelerated Cure	5-5

BLANK PAGE

SUMMARY

Primary effort during the second quarter was directed toward specific task accomplishments in all phases of the program. Emphasis was made on obtaining test data for environmental, solid-state thermal, and mechanical properties of "THERMO-LAG" T-500 materials. This was for the purpose of characterizing the materials for the space environment modes of heat transfer and structural loading of a thermal protective coating for a manned spacecraft.

PHASE I.

Solid-state thermal properties that would characterize "THERMO-LAG" T-500 materials for low-vacuum space environment and the modes of heat transfer were conducted. Total normal emittance measurements and gas chromotograph analysis to be reported in the next quarter will complete the thermal property tests of the Phase I task.

An analysis of the design of the model for the gap tests was conducted. These tests which will indicate the effect of gap dimensions on substrate material temperature will be conducted during the next reporting period.

Modifications to the in-house radiation facilities were instituted during this reporting period. The modifications will allow incident heat phases to about 25 BTU/FT^2-SEC to complete the radiation ablation test matrix for 25 to 50 BTU/FT^2-SEC incident heat flux. The facilities and equipment capabilities of appropriate research companies have been investigated. It is anticipated that these high incident heat flux tests will be conducted in the next reporting period. Other thermal performance tests to be conducted within the next reporting period will be for the simulated trajectories of the Apollo spacecraft.

PHASE II.

Tests for tensile strength and elongation, shear strength, flexural strength and ultraviolet exposure mechanical properties were completed during this period. Arrangements have been made to conduct the flexural stiffness and acoustical environment tests during the next quarter.

PHASE III.

Research studies regarding debris layer oxidation were conducted. To accommodate a more rigorous analysis higher shear tests in the plasma-jet tunnel will be required. Program checkouts were conducted on the IBM numerical ablation programs. Air-arc flight simulation tests conducted for transient heating studies were analyzed for parameter evaluation of the ablation model.

PHASE IV.

Surface treatment techniques and secondary bonding materials were investigated. Bond shear and tensile tests were conducted in the selection study of an appropriate bonding material.

PHASE V.

Investigations were performed to determine an artificial technique to cure "THERMO-LAG" T-500 putty for application as joint, gap, and edge filler. Concurrent studies were in progress on field maintenance procedures and methods for the putty application.

Development was completed on techniques to calculate slab stresses in an infinite flat heat shield on a honeycomb structure subjected to a one-dimensional heat flow, and to simulate a material continuum by a truss network. To corroborate the truss analogy a potential energy analysis was performed.

SECTION I

INTRODUCTION

This report is intended to convey, clearly and concisely, all work that has been accomplished during the second quarterly period of the contract. The format designed for the initial quarterly report (Emerson Report 1468) has been followed in this report. The contractural requirements under Schedule, Part V, B, Quarterly Reports have been met.

Sections II through V analyze the tests and accomplishments of the tasks performed during the reporting period.

BLANK PAGE

SECTION II

PROPERTY AND PARAMETER EVALUATION

THERMAL PROPERTIES (VIRGIN AND CHARRED MATERIALS.)

THERMAL CONDUCTIVITY. Thermal conductivity tests were performed on both virgin and charred "THERMO-LAG" by a guarded hot plate method as described in ASTM C177-45. This method of testing is designed to determine the thermal conductivity of the material at various temperatures above, at, and below a standard laboratory atmosphere.

The material test specimens in the virgin state were circular disks 2.5 inches in diameter and 0.125 inch thick. (See Figure 2-1.)

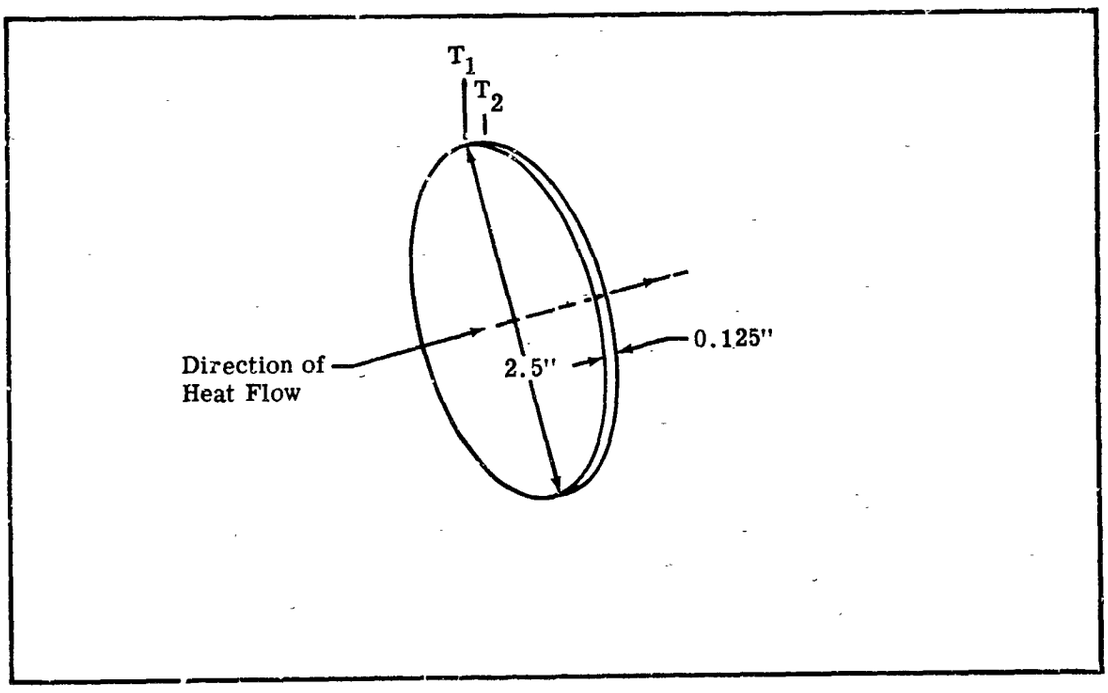

Figure 2-1. Thermal Conductivity Test Specimen

A series of approximately thirteen successive observations were made during each test. The observations were made at intervals not exceeding one hour.

The recorded test results were calculated in the manner described in Quarterly Progress Report No. 1468. Seven tests were conducted on each of the virgin "THERMO-LAG" materials, T-500-4 and T-500-6. The results of the tests are illustrated in Figure 2-2. The data indicates that the thermal conductivity of "THERMO-LAG" T-500-4 is approximately linear over the temperature range of -150°F to the sublimation temperature, and can be reasonably fitted to the empirical expression

$$k = k_o\left(\frac{T}{T_o}\right)^{0.147}$$

where the subscript *(o)* denotes known values.

The plotted data for the T-500-6 material at the temperature range below 0°F indicates the increasing influence the glass mesh material has upon the over-all thermal conductivity of "THERMO-LAG" T-500-6. The thermal conductivity of the glass mesh material increases with decreasing temperatures below 0°F.

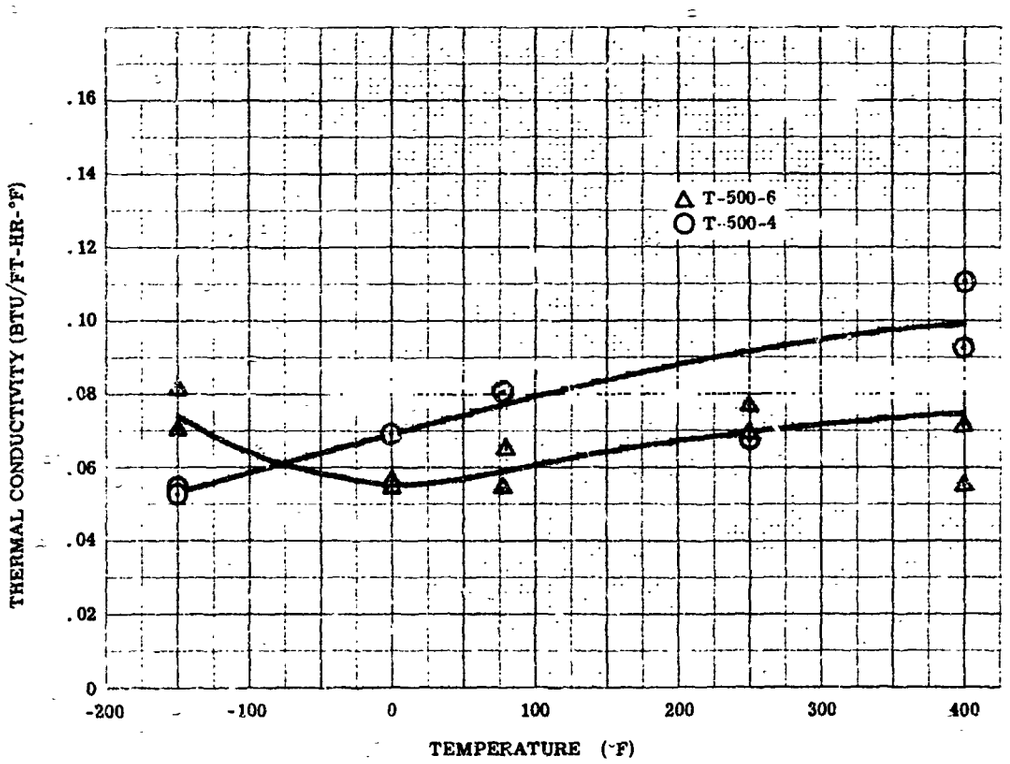

Figure 2-2. Thermal Conductivity of Virgin "THERMO-LAG" T-500

Nine tests were conducted on each of the charred "THERMO-LAG" materials, T-500-4 and T-500-6. The results of the tests are illustrated in Figure 2-3, which indicates that over the test temperature range, the thermal conductivity is essentially constant, being for

"THERMO-LAG" T-500-4	0.036 BTU/HR FT °F
"THERMO-LAG" T-500-6	0.0379 BTU/HR FT °F

SPECIFIC HEAT. Specific heat tests were conducted on both virgin and charred "THERMO-LAG" materials, T-500-4 and T-500-6. The tests were conducted using a method of mixtures with a Parr calorimeter. Mean specific heats were calculated from the tests

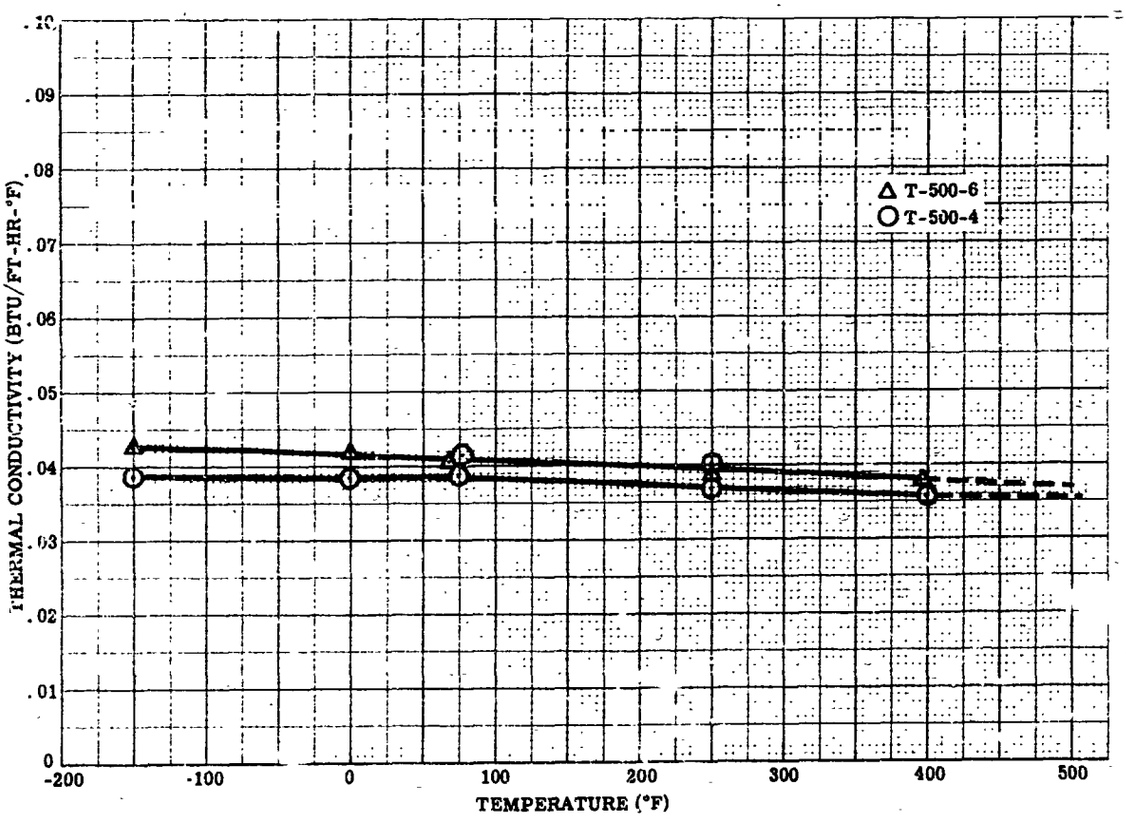

Figure 2-3. Thermal Conductivity of Charred "THERMO-LAG" T-500

performed at temperatures above and below standard laboratory values by the equation

$$C_{ps} = \frac{W_t C_{pt} (t_{t1} - t_{t2})}{W_s (t_{s2} - t_{s1})}$$

where:

C_{ps} = Specific heat of sample

W_t = Weight of toluene (immersion liquid)

W_s = Total weight of sample

t_{t1} = Initial temperature of toluene

t_{s1} = Initial temperature of sample

For $t_{s2} = t_{t2}$ there exists equilibrium temperatures between sample and toluene.

The results of the conducted tests are presented in Figures 2-4 and 2-5. Figure 2-4 shows plots of the mean specific heat of virgin "THERMO-LAG" materials, T-500-4 and T-500-6 as a function of temperature. The charred "THERMO-LAG" materials, T-500-4 and T-500-6, as a function of temperature are given in Figure 2-5. The trends of the plotted data are typical for the types of material tested.

DENSITY. Tests to measure the density of "THERMO-LAG" T-500 materials were performed in accordance with Method A of ASTM D792-50, using a laboratory gravitometer.

Twelve samples of each "THERMO-LAG" material, T-500-4 and T-500-6, were subjected to density testing at temperatures of -150°F to 400°F. The results of these tests are presented in Figure 2-6. Within the range of experimental accuracy, the densities of the two compounds correspond and vary in almost a straight line relationship from about 68 LB/FT^3 at -150°F to about 59 LB/FT^3 at 400°F.

COEFFICIENT OF THERMAL EXPANSION. These tests were performed on both virgin and charred "THERMO-LAG" T-500 in accordance with ASTM D-696-44. The apparatus utilized, the procedure followed to perform the test, and the material specimens tested were discussed in previous progress reports.

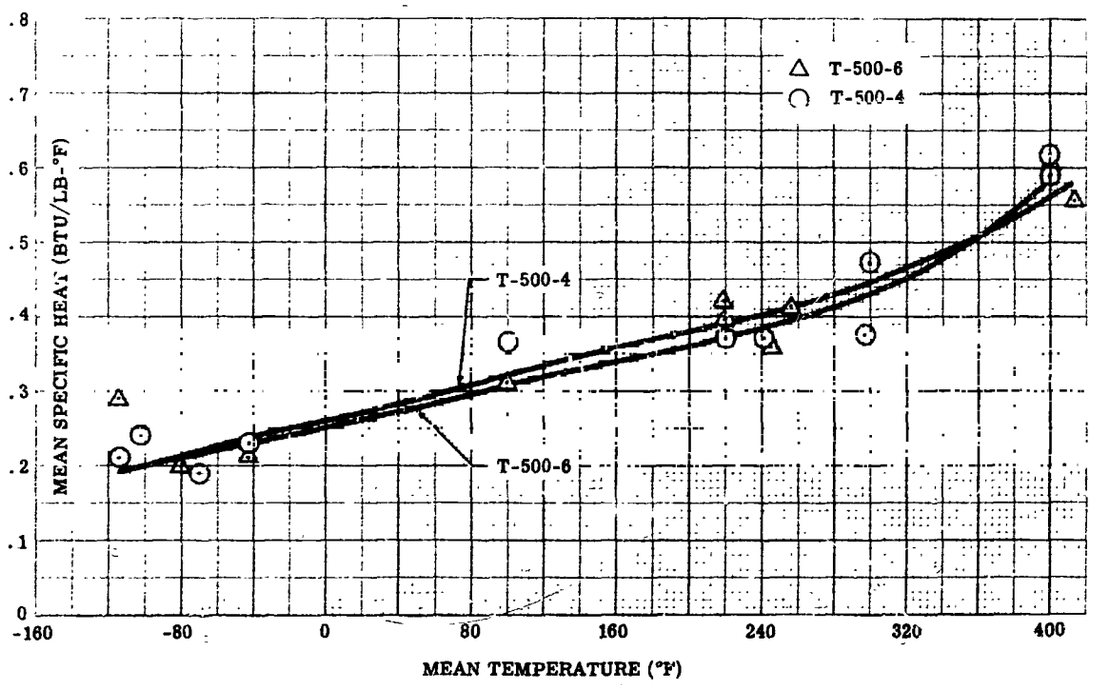

Figure 2-4. Mean Specific Heat of Virgin "THERMO-LAG" T-500 Versus Temperature

The coefficient of thermal expansion, α, (IN./IN.°C) was calculated between the test temperature and 30°C above and below test temperature using the equation

$$\alpha = \frac{\Delta L}{L \Delta T}$$

where:

ΔL = Average of three changes in length of the samples due to heating, (inches)

L = Length of test sample at test temperature, (inches)

ΔT = Temperature difference, °C, over which the changes in length of the specimen are measured

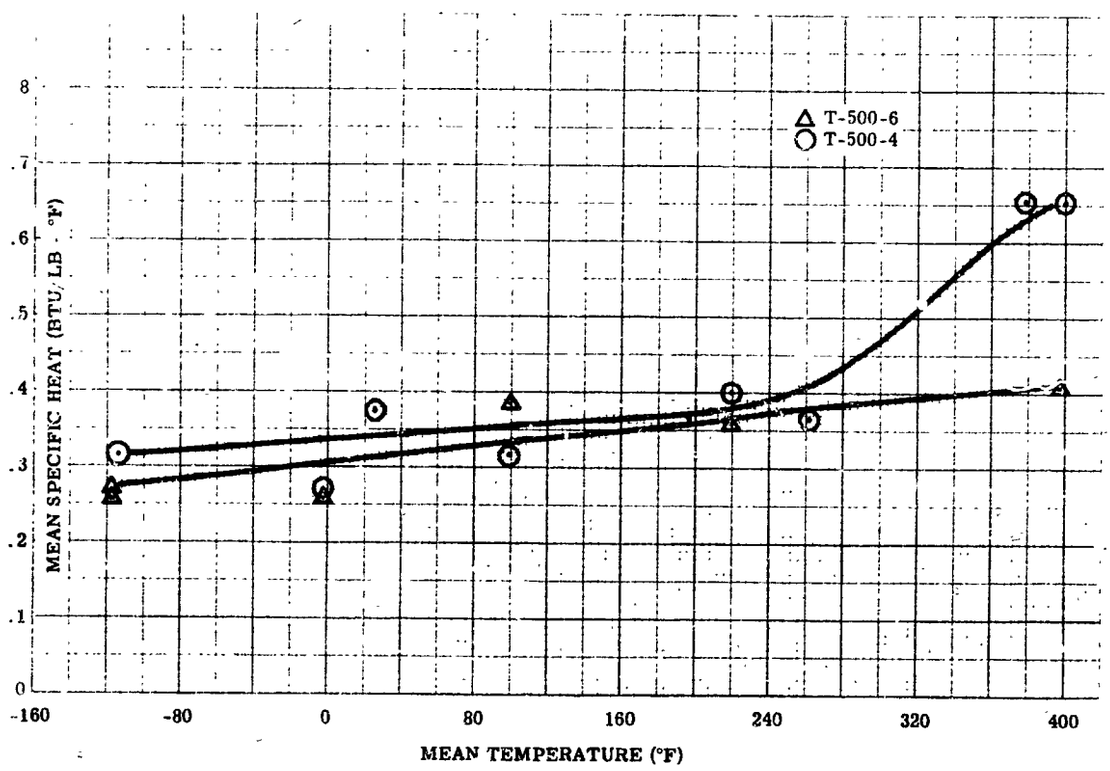

Figure 2-5. Mean Specific Heat of Charred "THERMO-LAG" T-500 Versus Temperature

Eight tests were performed on each of the virgin "THERMO-LAG" materials, T-500-4 and T-500-6. The results of these tests are illustrated in Figure 2-7. Study of the data indicates certain behavior characteristics of the two materials, i.e:

1. A phase transition from the glass to the elastic state in the temperature regime below room value for T-500-6.

2. The erratic behavior above 250°F indicates where T-500-4 began to behave as a viscous fluid.

For the charred "THERMO-LAG", ten tests were performed on each of the materials, T-500-4 and T-500-6. The results of the tests are shown in Figure 2-8.

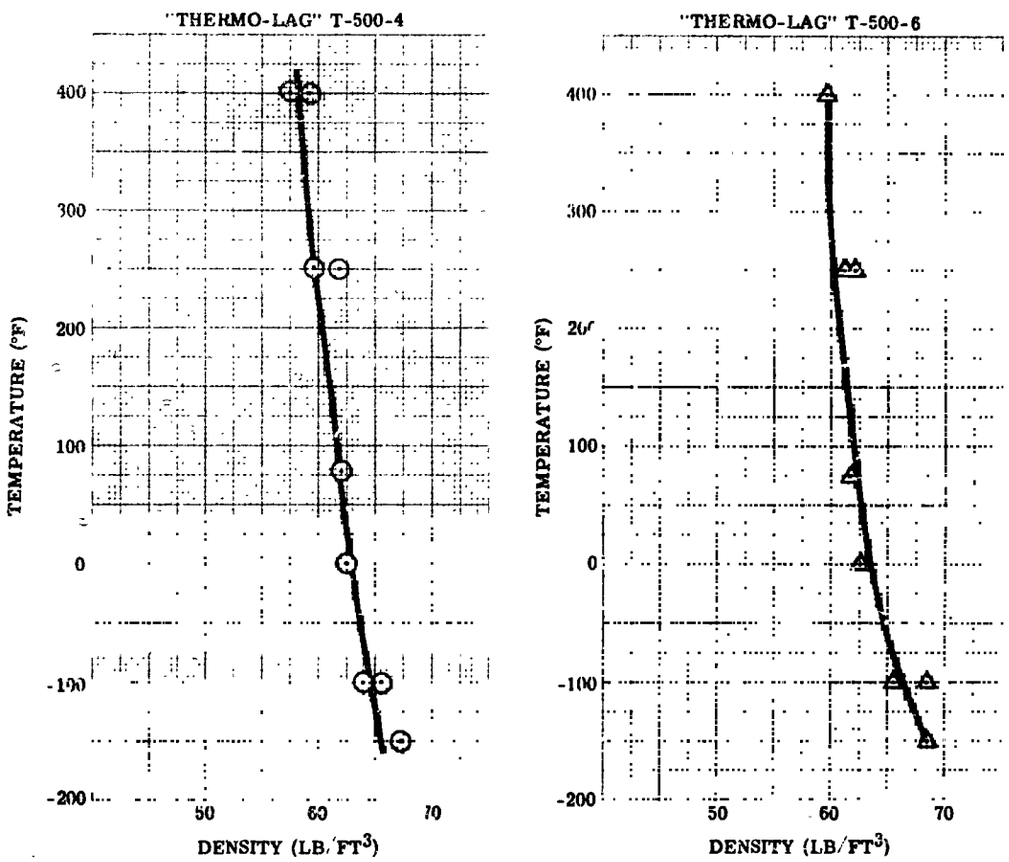

Figure 2-6. Density of "THERMO-LAG" T-500-4 and T-500-6

VACUUM EXPOSURE. The effect of very low pressure (5×10^{-5} mm Hg), equivalent to that realized at extreme altitude, on "THERMO-LAG" T-500-4 was investigated. The "THERMO-LAG" specimens one inch square and 3/8 inch thick were contained in flasks which were connected to a high vacuum system and evacuated to the desired vacuum. For the high temperature tests, the flasks containing the specimens were surrounded by a constant temperature bath.

The weight loss per unit area of the "THERMO-LAG" material for 48-hour periods of exposure, a given pressure, and for two temperatures was determined. The results of the tests are illustrated in Figure 2-9. A study of the recorded data indicates that a substantial portion of the total weight loss occurred within the first seven hours of exposure. A portion of this weight loss is attributed to loss of physically entrapped liquid volatiles.

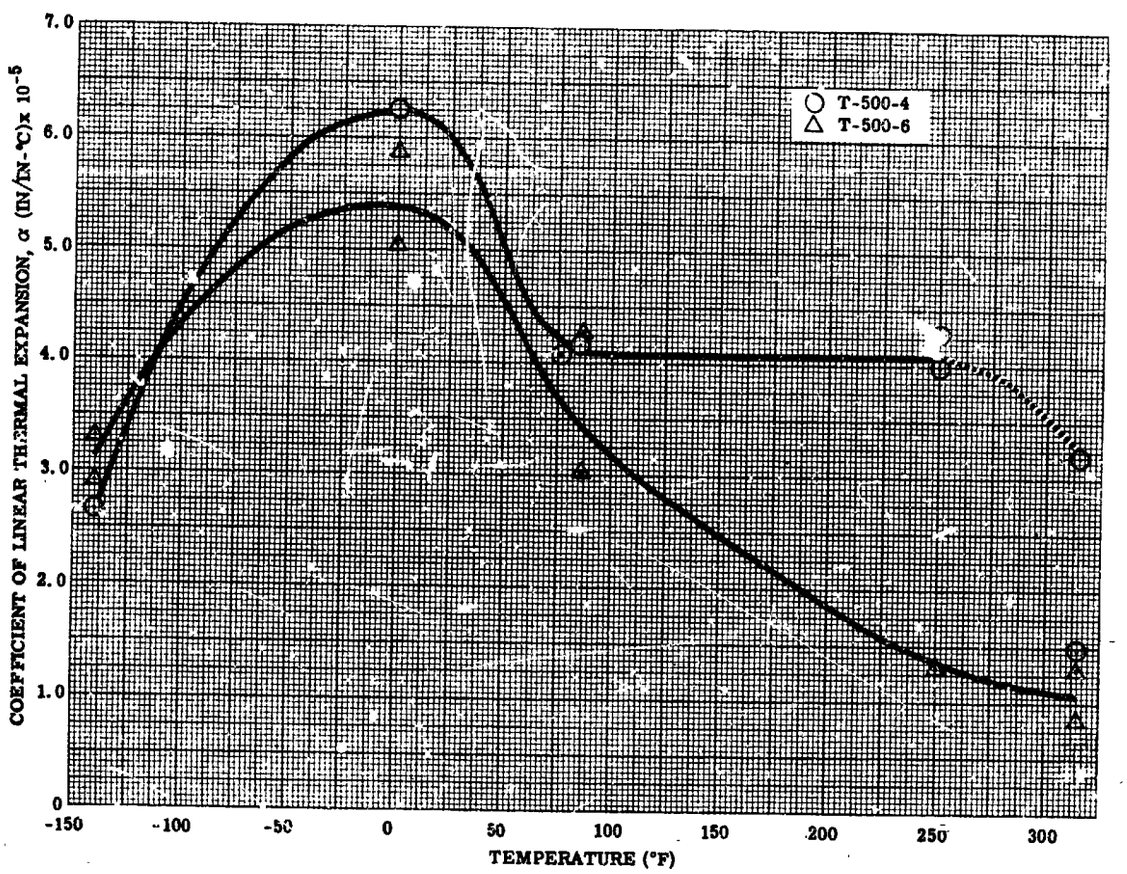

Figure 2-7. Coefficient of Thermal Expansion for Virgin "THERMO-LAG" T-500 Materials

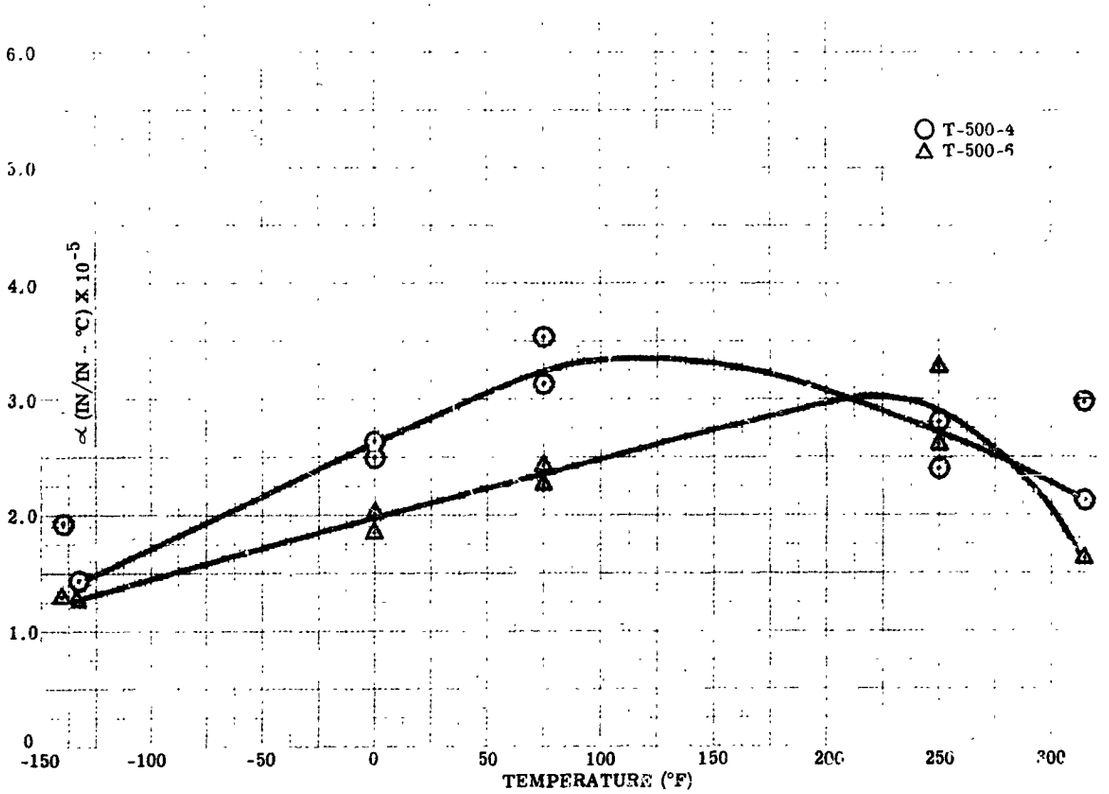

Figure 2-8. Coefficient of Thermal Expansion for Charred "THERMO-LAG" T-500 Materials

THERMAL-CHEMICAL CHARACTERISTICS.

PHASE CHANGE OF VIRGIN MATERIAL. A qualitative investigation using differential thermal analysis was continued to determine whether phase changes occur prior to sublimation; if the phase changes are endothermic or exothermic; and to determine the approximate temperature of sublimation. The apparatus used in the determination was a Deltatherm Differential Thermal Analyzer and an external furnace. Both "THERMO-LAG" T-500-4 and T-500-6 were analyzed, using approximately one gram of pulverized material for each test.

Differential thermal analysis compares the temperature rise of some standard with that of the specimen undergoing testing. When the sample absorbs more energy than the

Figure 2-14. Deltatherm Thermogravimetric Analyzer

Test tensile strength was determined by using the recorded data in the standard stress equations

$$\sigma_{ULT} = \frac{P_{ULT}}{A}$$

where:

σ_{ULT} = Tensile strength, (LB/IN.^{2})

P_{ULT} = Maximum load carried, (LB)

A = Cross-sectional area of sample, (IN.^{2})

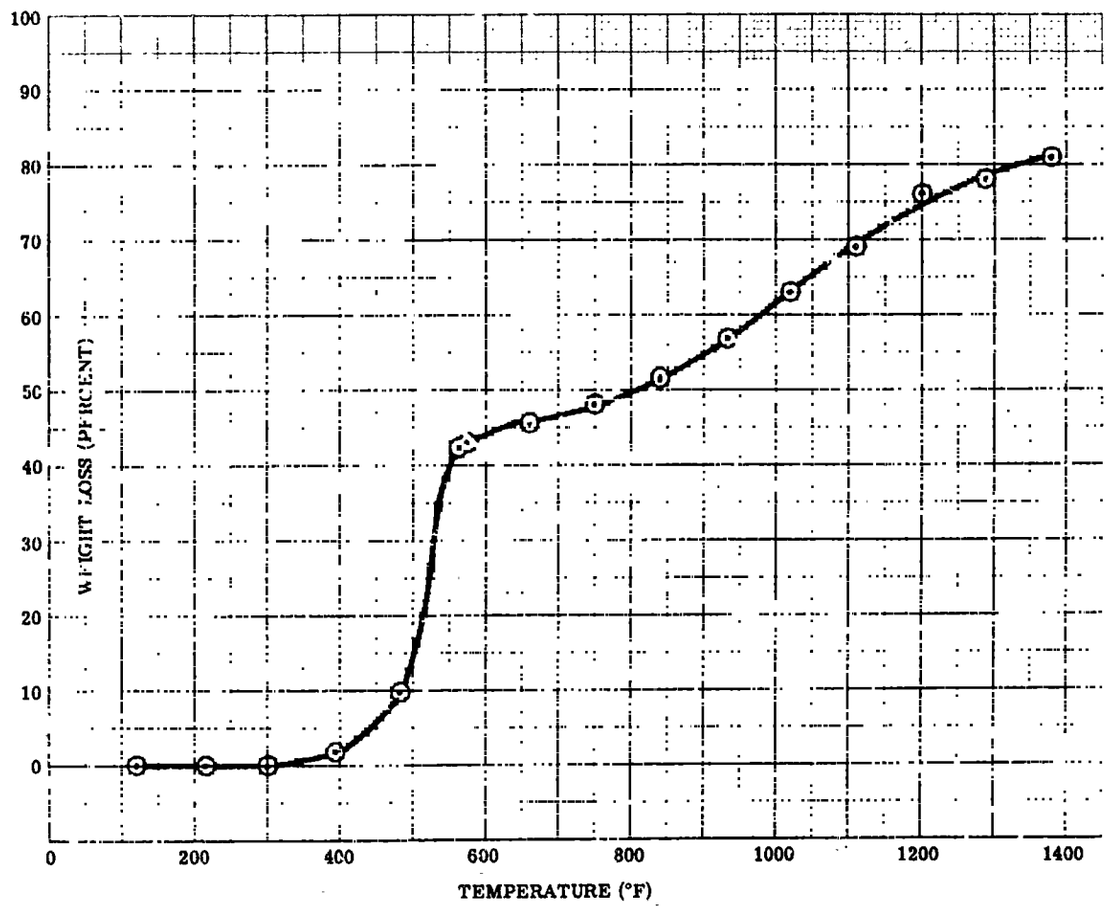

Figure 2-16. Thermogravimetric Analysis of "THERMO-LAG" T-500-4 at 5°C/Minute Heating Rate (2.62 MG Sample Weight)

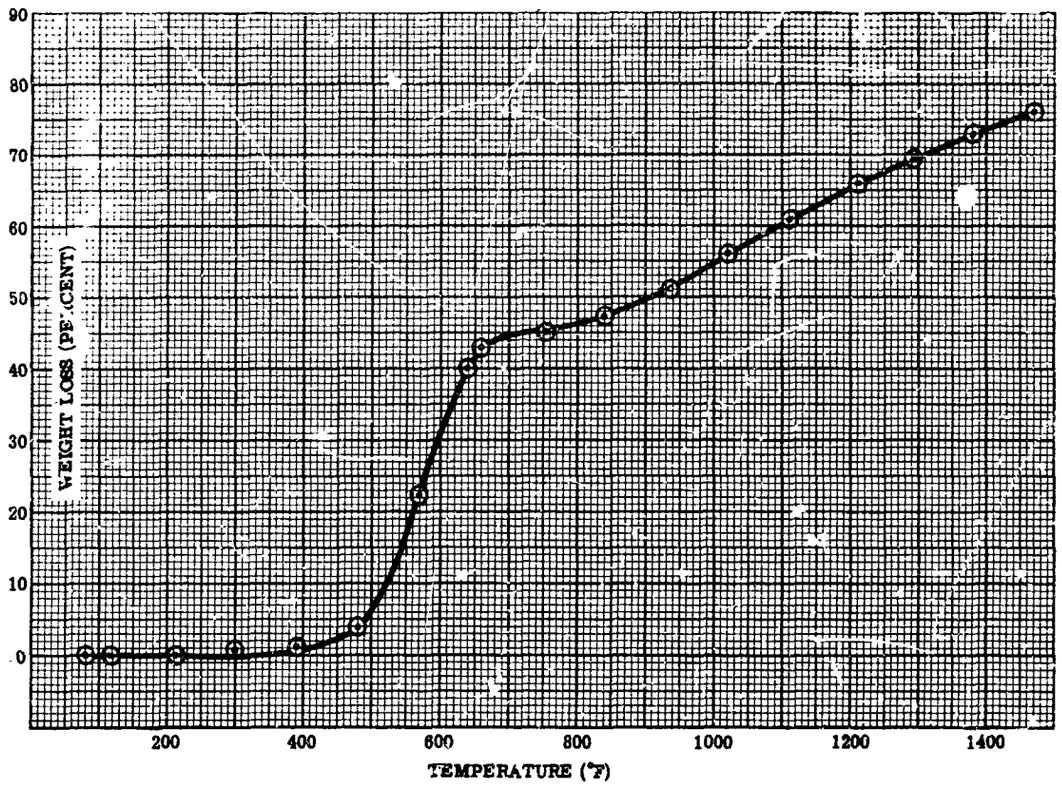

Figure 2-17. Thermogravimetric Analysis of "THERMO-LAG" T-500-4 at 10°C/Minute Heating Rate (4.73 MG Sample Weight)

The specimen to undergo testing, with a thermocouple attached for measuring its imposed temperature, was placed in a shear fixture in the oven. Temperature above room value was applied and stabilized for conditions of equilibrium, and the automatic programer of a cross-head travel of 0.05 inch/MIN was started. The deflection of the specimen resulting from the applied structural and temperature loads was plotted in the x-y recorder.

The punched shear stress was determined by using the recorded data in the standard stress equation

$$S = \frac{L}{A}$$

where:

S = Shear strength, (LB/IN.^{2})

L = Load carried, (LB)

A = Area of sheared edge, (FT^2)

Area of sheared edge = xc

c = Circumference of the punch tool (πd), where punch diameter was one inch

x = Thickness of specimen

Thirteen tests were performed on "THERMO-LAG" T-500-6, with six of these tests being at cryogenic temperatures of 0°F, -150°F, and -250°F. There were also thirteen tests conducted on the T-500-4 material. Seven of these tests were at the given cryogenic temperatures. The results of these tests for both materials are recorded as curves on Figure 2-28. The reported shear strength is higher for the T-500-6 material at room and elevated temperatures as the punched shear is in the direction normal to the laminated fibers.

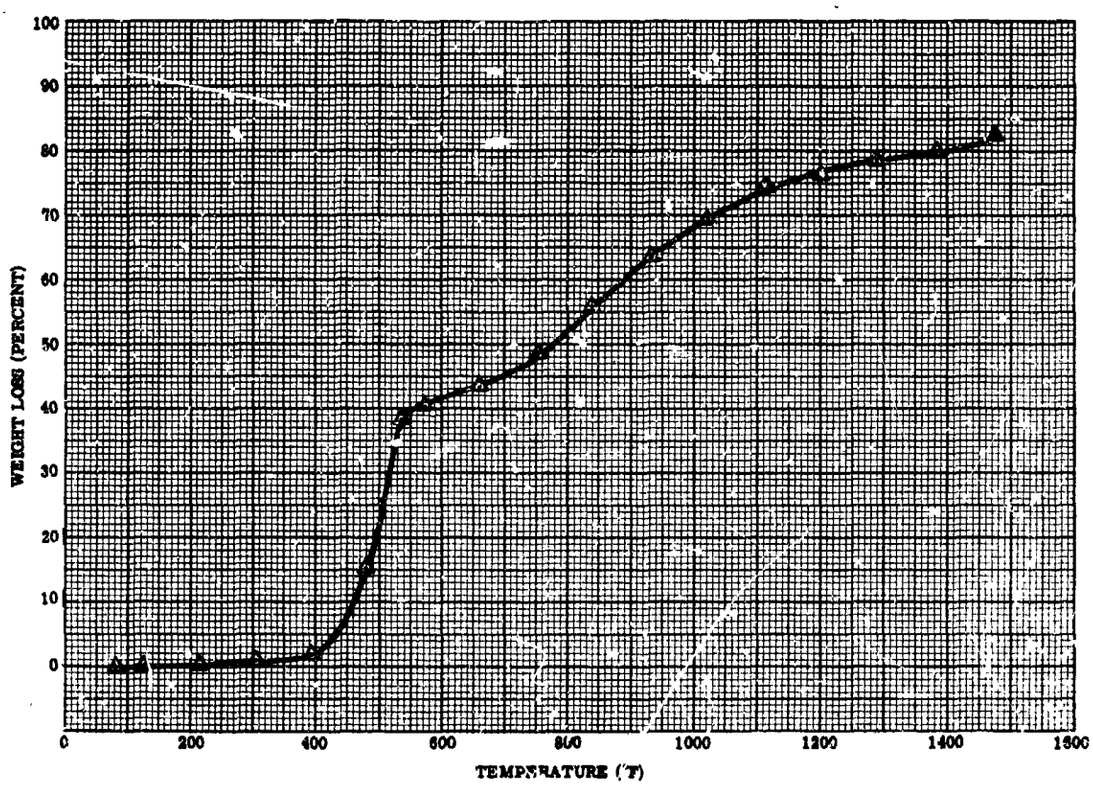

Figure 2-18. Thermogravimetric Analysis of "THERMO-LAG" T-500-6 at 2°C/Minute Heating Rate (3.3 MG Sample Weight)

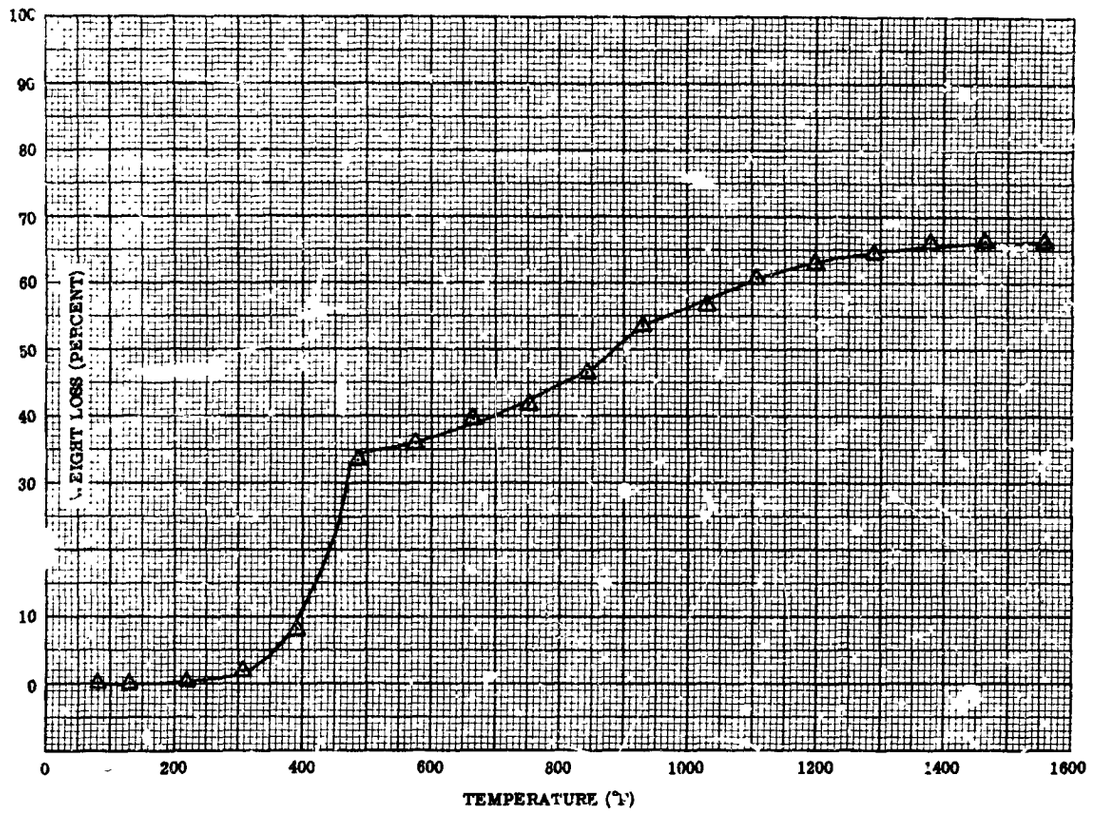

Figure 2-19. Thermogravimetric Analysis of "THERMO-LAG" T-500-6 at 5°C/Minute Heating Rate (3.9 MG Sample Weight)

For the range of temperatures tested, the results indicate that the T 500-6 material contains approximately the required percentage of laminated fibers. They contribute to its higher normal shear stress at elevated temperatures and cause only slightly lower values than the normal T-500 material at cryogenic temperatures. The shear stress tests normal to the structural fibers of the material simulate the approximate effect that normal impingement of micrometeorites, dust, and water particles may have on a heat shield material.

FLEXURAL STRENGTH. The flexural properties of "THERMO-LAG" T-500 were determined in accordance with ASTM D 790-61A. The equipment utilized for the performance of the tests consisted of a Research Inc. Material testing unit consisting of an hydraulically operated, automatically controlled, load frame, an X-Y recorder, and an

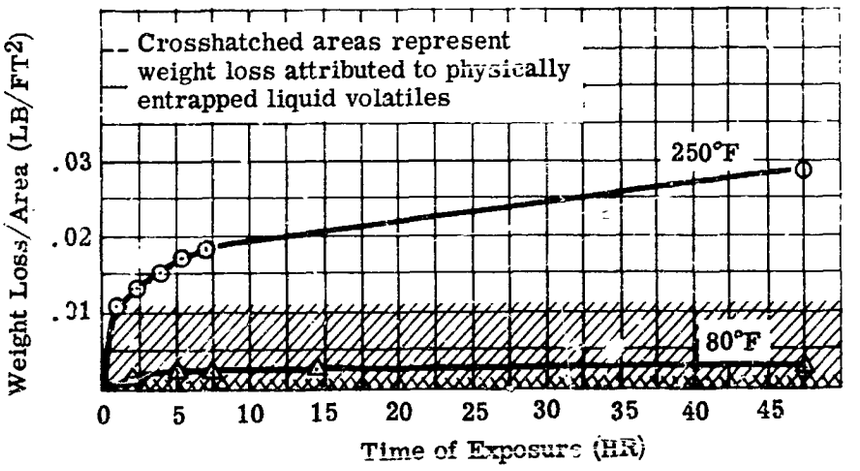

Figure 2-9. Effect of Temperature at Low Pressure on Weight Loss of "THERMO-LAG" T-500

standard, an endothermic process is recorded, and when the sample absorbs less energy than the standard, an exothermic process is recorded.

A summarized result of the analysis for "THERMO-LAG" T-500-4 and T-500-6 where rates of temperature rises of 2 and 5°C/MIN were imposed are illustrated in Figures 2-10 and 2-11. Both materials were analyzed in an inert atmosphere. A study of recorded data indicates that two distinct phase changes occurred for each test. The first endotherm indicates a phase change in the crystal structure of the subliming material. The second endotherm indicates the temperature of sublimation of the subliming material taken as the point at which the slope change is first observed. The sublimation temperature, as indicated in Figures 2-10 through 2-13 is, on the average, about 550°F for T-500-4, and 545°F for T-500-6.

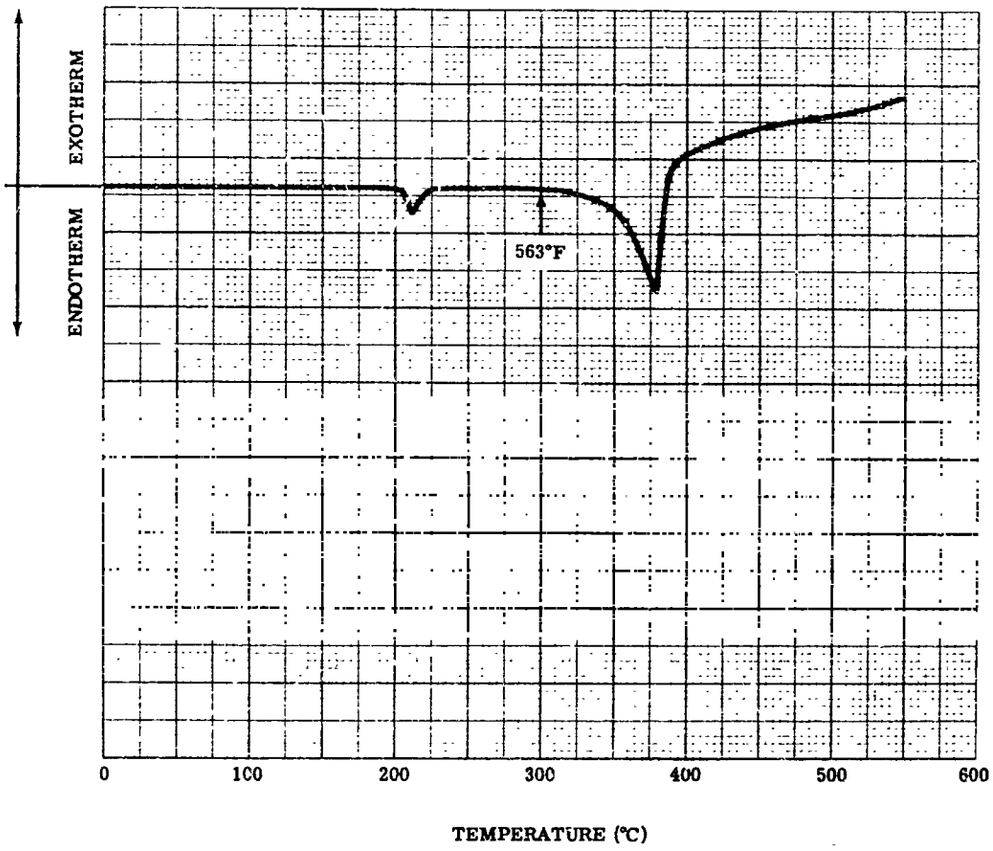

Figure 2-10. Differential Thermal Analysis of "THERMO-LAG" T-500-4 at 2°C/Minute Heating Rate (T_S = 563°F)

THERMOGRAVIMETRIC ANALYSIS. A qualitative investigation using thermogravimetric analysis was undertaken to determine the rates that "THERMO-LAG" T-500 material loses weight during the sublimation process at a constant temperature rise, and to determine the temperature range at which the maximum weight loss of "THERMO-LAG" T-500 occurs. The apparatus used in the determination was a Deltatherm Thermogravimetric Analyzer which incorporates an electronic balance and an oven as illustrated in Figure 2-14. Both "THERMO-LAG" T-500-4 and T-500-6 were analyzed using approximately three to four milligrams of pulverized material for each test.

Thermogravimetric analysis indicates the rate the material loses weight during the sublimation of the salt and the occurrence of polymer degradation in "THERMO-LAG" by recording the weight losses for the appropriate temperature range for a constant heated rate.

Seven thermogravimetric analyzer tests of two or more rates of temperature rises of 2, 5, and 10°C/MIN were performed on each T-500 material. Figures 2-15 through 2-20 are illustrative of the proposed heated rates of the performed tests. The plotted data indicate that the weight loss rates of "THERMO-LAG" T-500 materials during the sublimation phase are independent of the imposed heated rates. The only difference is a shift in the temperature scale for the sublimation phase.

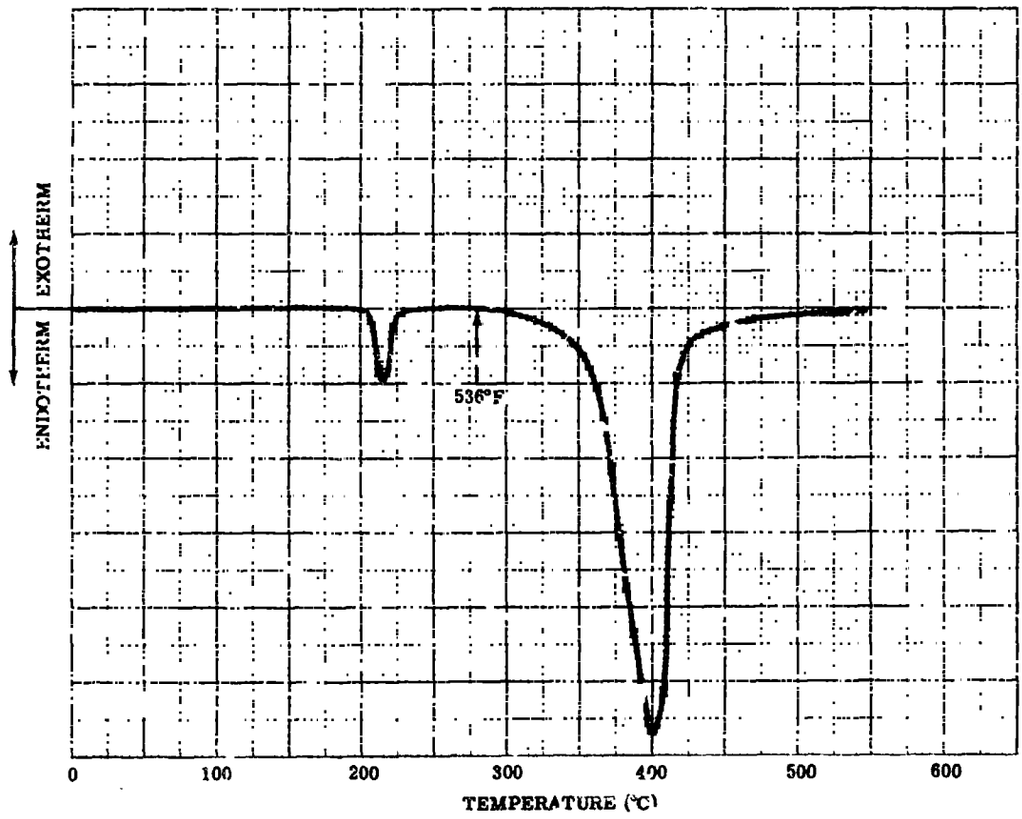

Figure 2-11. Differential Thermal Analysis of "THERMO-LAG" T-500-4 at 5°C/Minute Heating Rate (T_B = 536°F)

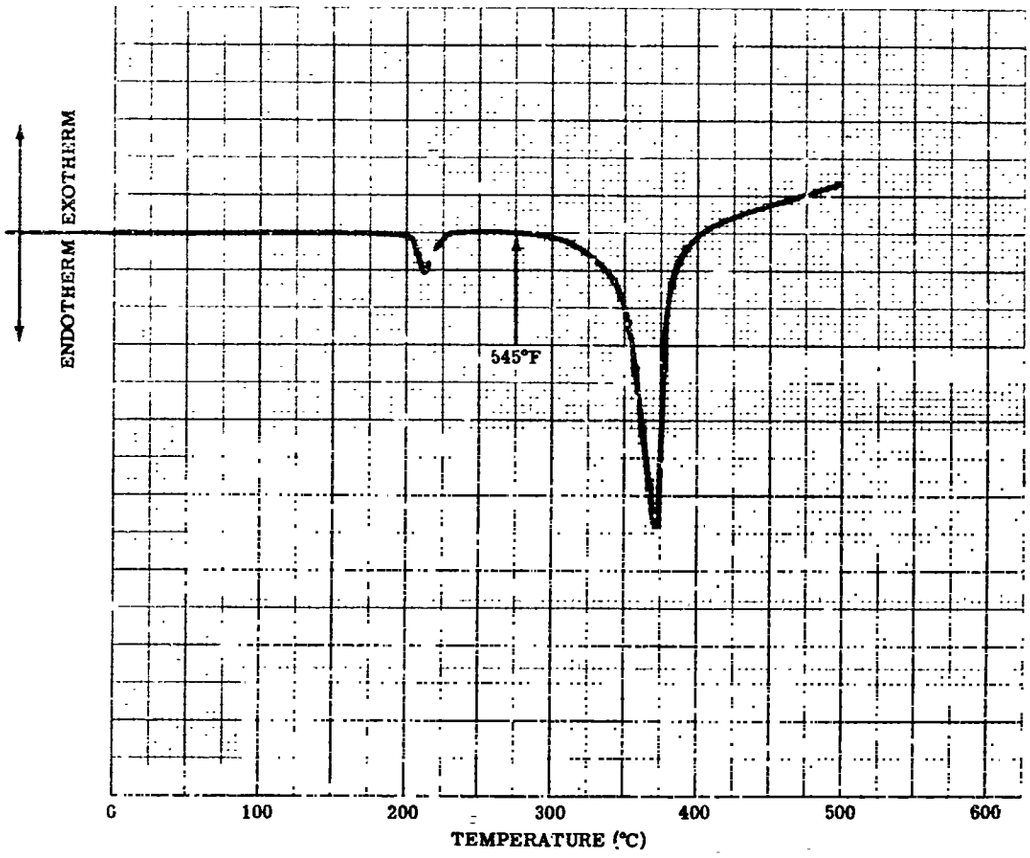

Figure 2-12. Differential Thermal Analysis of "THERMO-LAG" T-500-6 at 2°C/Minute Heating Rate (T_S = 545°F)

MECHANICAL PROPERTIES (PRECAST AND SPRAYED MATERIALS).

TENSILE STRENGTH. To facilitate testing at temperature extremes where utilization of conventional extensometers is not possible, tab-end specimens were used to determine the tensile properties of "THERMO-LAG" materials, T-500-4 and T-500-6. The material test specimen models are illustrated in Figure 2-21. The equipment used to conduct the tests consisted of the Research Inc. material testing unit. The equipment is shown in Figure 2-22. A specimen in position within the cryogenic chamber for tensile test at the low temperatures is shown in Figure 2-23.

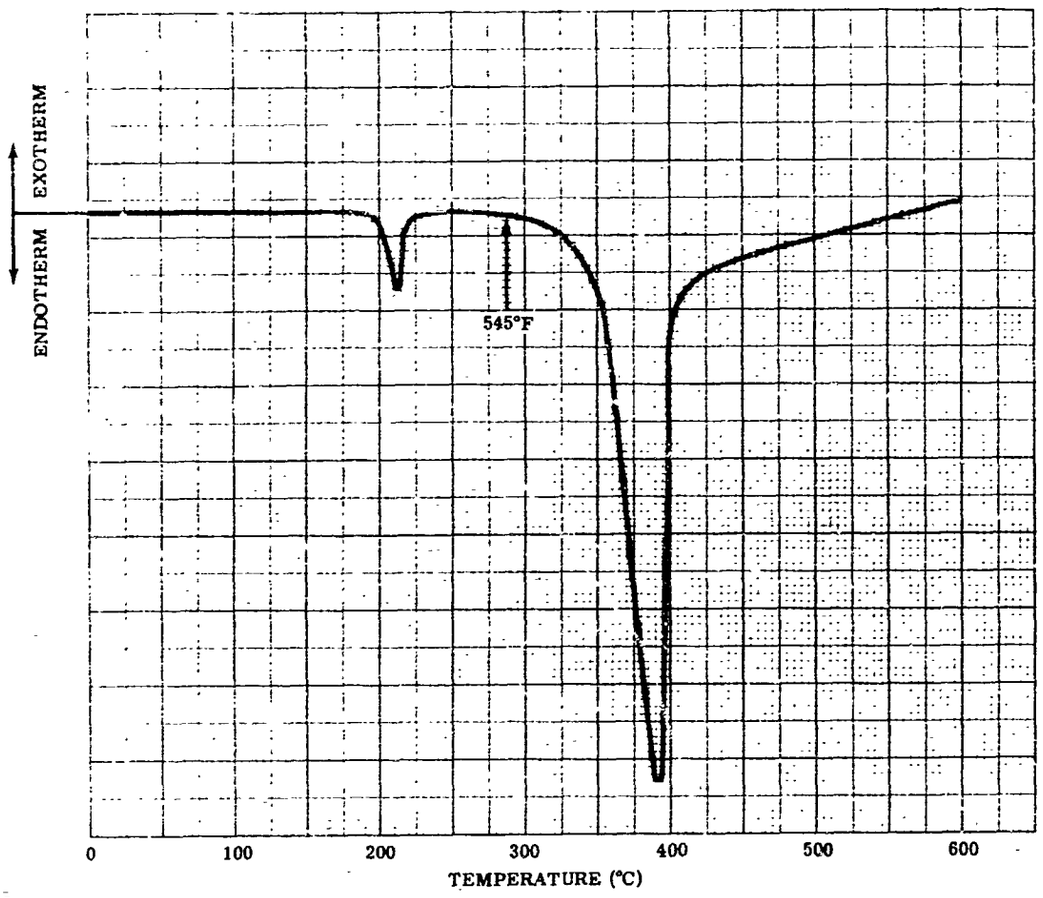

Figure 2-13. Differential Thermal Analysis of "THERMO-LAG" T-500-6 at 5°C/Minute Heating Rate (T_S = 545°F)

The low-temperature tests were conducted with a cryogenic chamber using liquid nitrogen to produce the low temperatures. The chamber being positioned between the load and stationary frame is the material testing unit of Research Inc. The unit consists of an inner and outer chamber.

The outer chamber is an oblate sphere 16-inches in diameter and 12-inches in height. The outer chamber is vacuumed to a low pressure. Specimen holders are connected through bellows to the stationary and load frames.

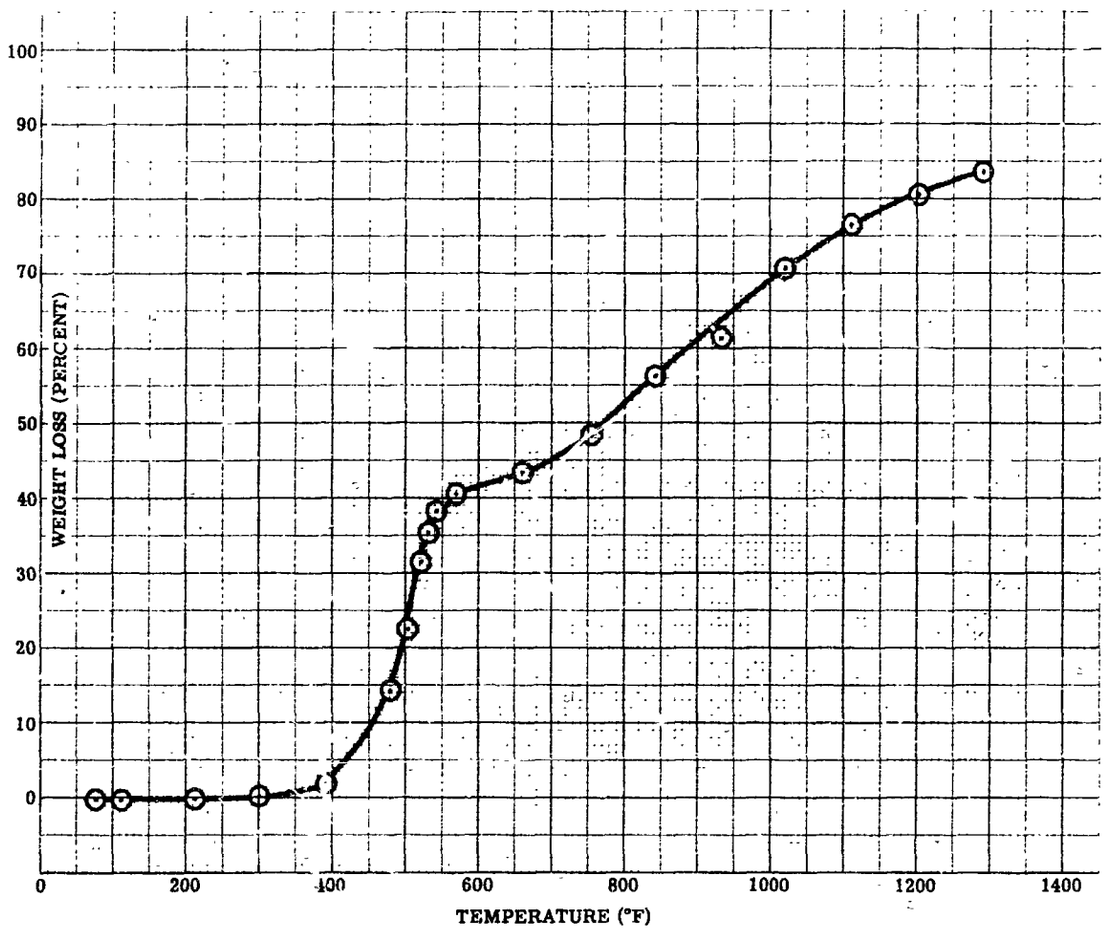

Figure 2-15. Thermogravimetric Analysis of "THERMO-LAG" T-500-4 at 2°C/Minute Heating Rate (3.78 MG Sample Weight)

The inner chamber is for testing and is cooled by passage of liquid nitrogen. It is an elongated sphere eight-inches in diameter and 10-inches in height. The inner walls have a high-absorptivity coating for the radiant heat transferred from the specimen. The outer surface wall of the chamber, to minimize radiant heat transfer from the outer chamber, is coated with a low-absorptivity gold paint. Glass windows in the chambers allow visual observation of tests. Precise and stabilized specimen temperatures are provided by two quartz lamps within the inner chamber. The lamps can be controlled automatically or manually.

The initial modulus stress was determined by using the recorded data in the equation

$$E = \frac{\sigma_E}{\epsilon_E}$$

where:

E = Initial modulus, (LB/IN.^{2})

σ_E = Stress at elastic limit, (LB/IN.^{2})

ϵ_E = Strain at elastic limit, (IN./IN.)

The elongation at the specimen, ϵ_{max} (IN./IN.) was determined from the equation

$$\epsilon_{max} = \frac{\Delta_{max}}{\text{Gage Length}}$$

where:

Δ_{max} = Total increase in length (IN.) of gage length

Twelve tests were performed on each of the "THERMO-LAG" materials, T-500-4 and T-500-6. The tests were evenly divided between elevated, and cryogenic temperatures. The results of these tests for both materials are recorded in Figures 2-24 through 2-26. The tensile strength of the materials, T-500-4 and T-500-6, are plotted in Figure 2-24. The data indicates the increase in tensile strength that laminated fibers contribute to the material. Figure 2-25 shows the initial modulus of the materials. The tensile elongations of the materials are shown on Figure 2-26. The data indicates the influence the laminated fibers, with low-ductile strength, have upon the elongation of the T-500-6 material.

The curves indicate that due to the metal tabs, there was a stress concentration at the ends of the "THERMO-LAG" specimens. At elevated temperatures, the materials were ductile enough to dissipate this effect and failures in the middle of the test specimens. At the cryogenic region of temperatures, the failures occurred in the bond between the specimen and the tab-end, which resulted in the low recorded values of tensile strength and elongation illustrated in Figures 2-24 and 2-26 respectively.

SHEAR STRENGTH. Shear stress properties in the direction normal to the flat face surface of "THERMO-LAG" T-500 were determined in accordance with ASTM D 732-46, using the punch-type shear tool. The equipment utilized to conduct the test consisted of the Research Inc. Material testing unit. For the cryogenic testing series, a cryogenic chamber using liquid nitrogen was used to produce the low temperatures. The desired temperatures were maintained by the quartz infrared lamp of the test facility. A specimen in position within the cryogenic chamber for testing at the low temperatures is shown in Figure 2-27.

The material test specimens were 0.25-inch thick blocks two inches square, with a 5/16-inch hole drilled in the center to accommodate the bolt on the shear tool.

infrared oven that contains the specimen. For the series of cryogenic tests, a cryogenic chamber using liquid nitrogen was used to produce the low temperatures. A specimen in position within the cryogenic chamber for testing at the low temperatures is shown in Figure 2-29.

The material test specimens were rectangular bars of 4.0 x 0.25 x 0.5 inches.

The specimen to undergo testing, with a thermocouple taped to one end, was placed in a holder supplied in the test chamber with the specimen span set at 2.678 inches. For elevated temperature tests, temperature was applied, and after it had reached the desired value and stabilized for conditions of equilibrium, the automatic rate-of-travel of the cross-head of 0.05 inch/MIN was started. For the low-temperature tests, the cryogenic chamber was used with liquid nitrogen as the coolant medium. The deflection of the specimen resulting from the applied structural and temperature loads was plotted on the x-y recorder.

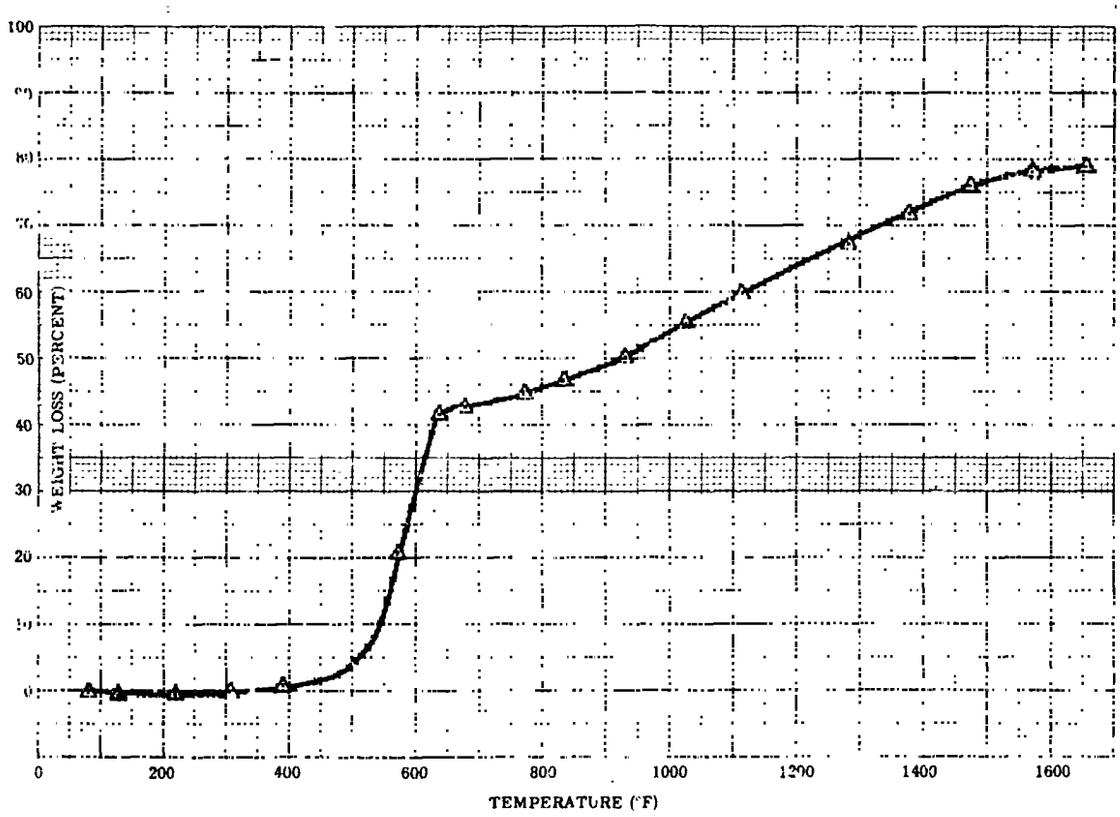

Figure 2-20. Thermogravimetric Analysis of "THERMO-LAG" T-500-6 at 10°C/Minute Heating Rate (4.3 MG Sample Weight)

The maximum flexural strength (σ) in the outer fiber was determined by using the recorded data in the standard stress equation

$$\sigma = \frac{3PL}{2bd^2}$$

where:

σ = Maximum flexural stress, (LB/FT^2)

P = Applied load, (LB)

L = Span of specimen (FT)

b = Width of specimen, (FT)

d = Depth of specimen, (FT)

Fourteen tests were performed on each of the "THERMO-LAG" materials, T-500-4 and T-500-6. Seven of these were cryogenic test series performed on each material. The results of all tests are recorded in Figure 2-30. As would be expected of the two materials, T-500-6 has the greater flexural strength for the entire range of test temperatures.

Also recorded in Figure 2-30 are the ultraviolet test data of T-500-4 and T-500-6. Three tests were performed on each material. The recorded data indicates no variation between these and data from normal tests at room temperatures.

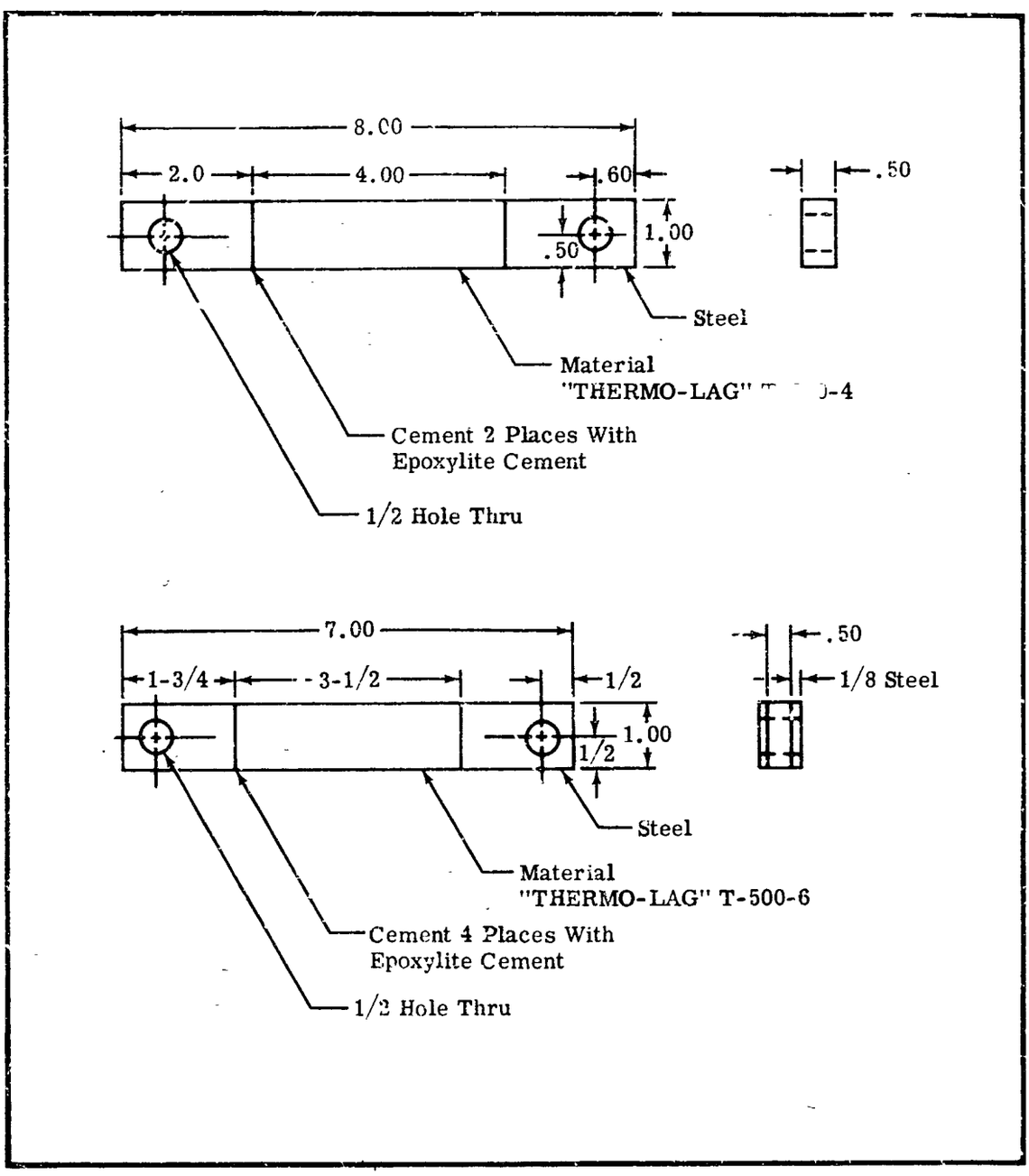

Figure 2-21. Tensile Strength and Elongation Models for "THERMO-LAG" T-500-4 and T-500-6

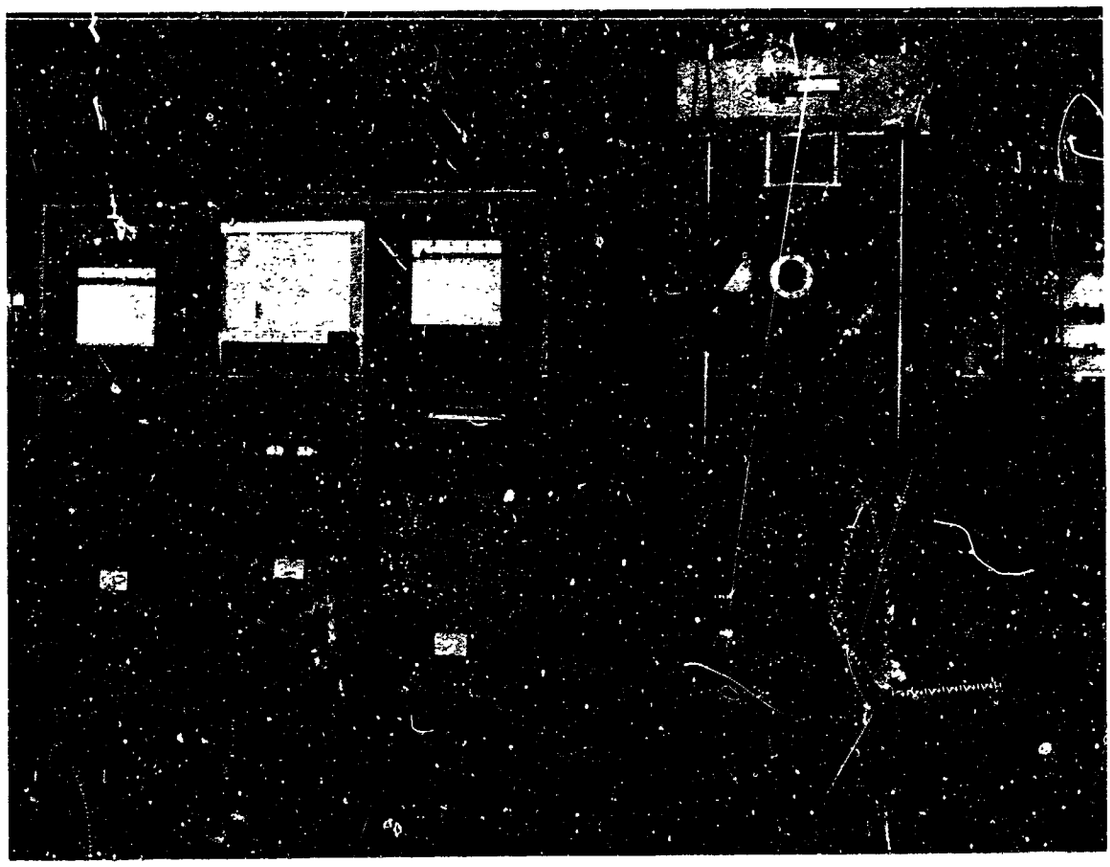

Figure 2-22. Research Inc. Material Testing Equipment

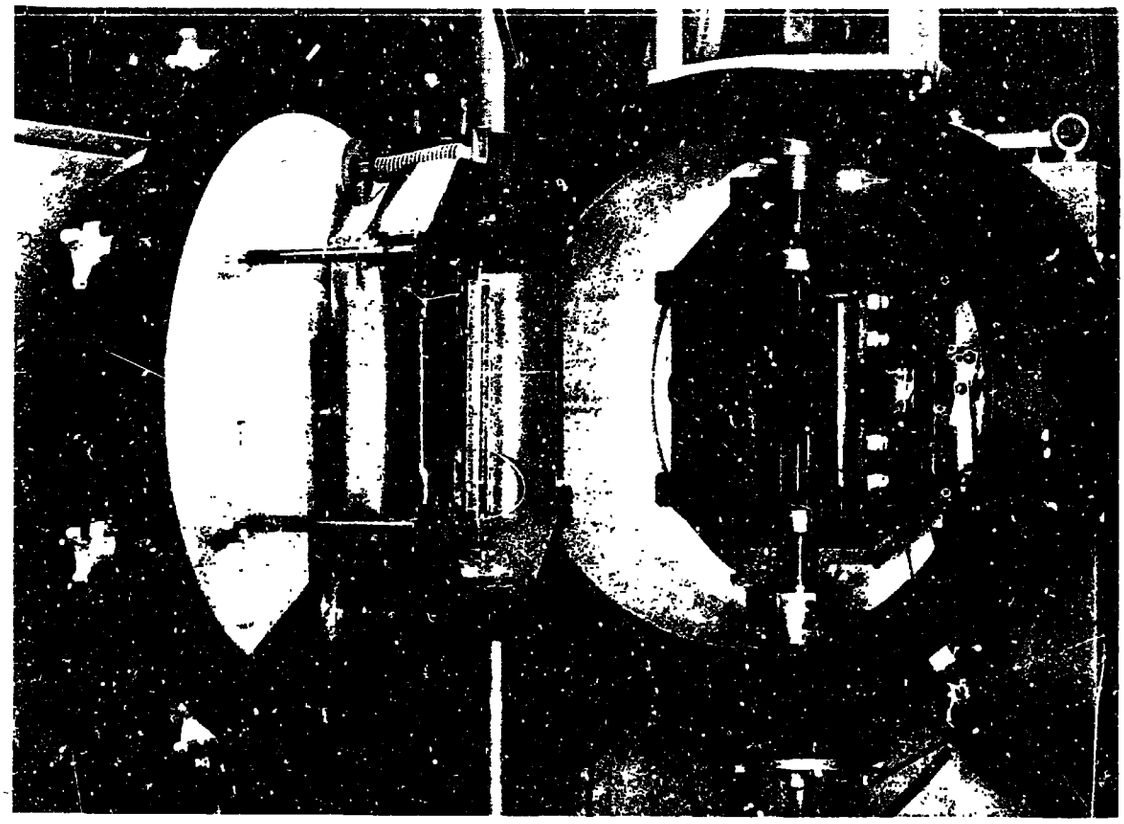

Figure 2-23. Specimen Held in Position for Tensile Test in the Cryogenic Chamber

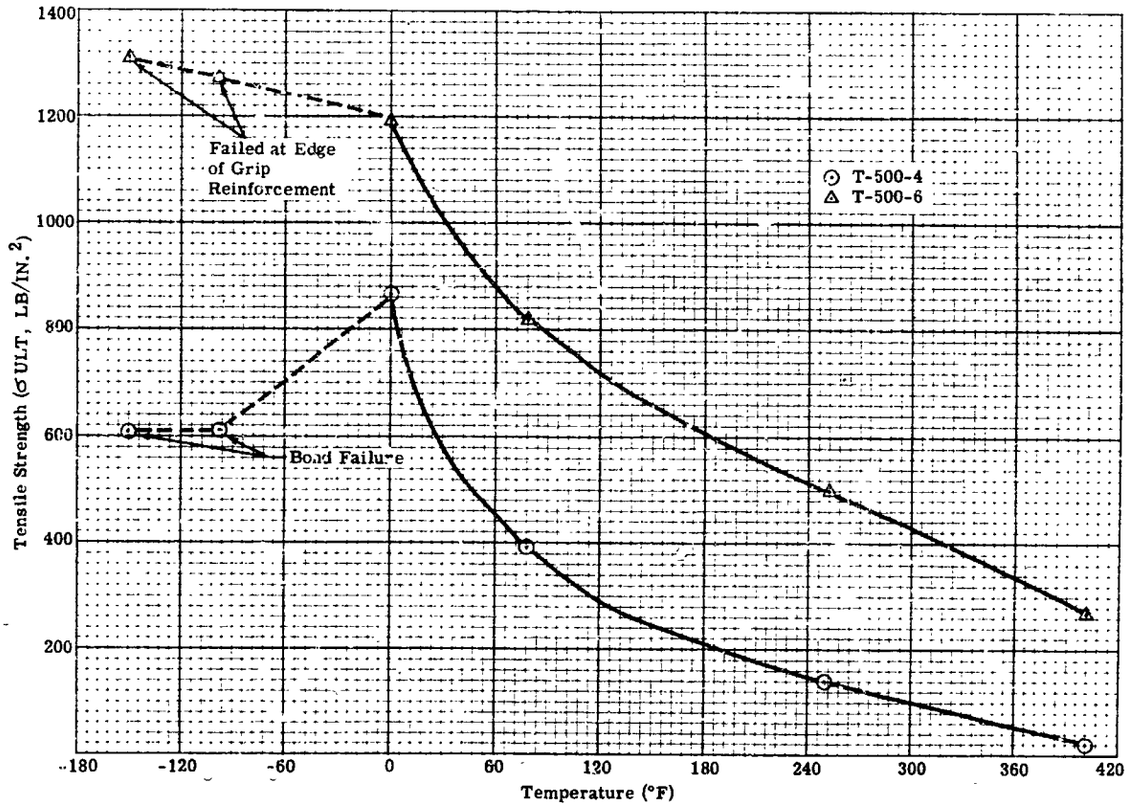

Figure 2-24. Tensile Strength of "THERMO-LAG" T-500-4 and T-500-6

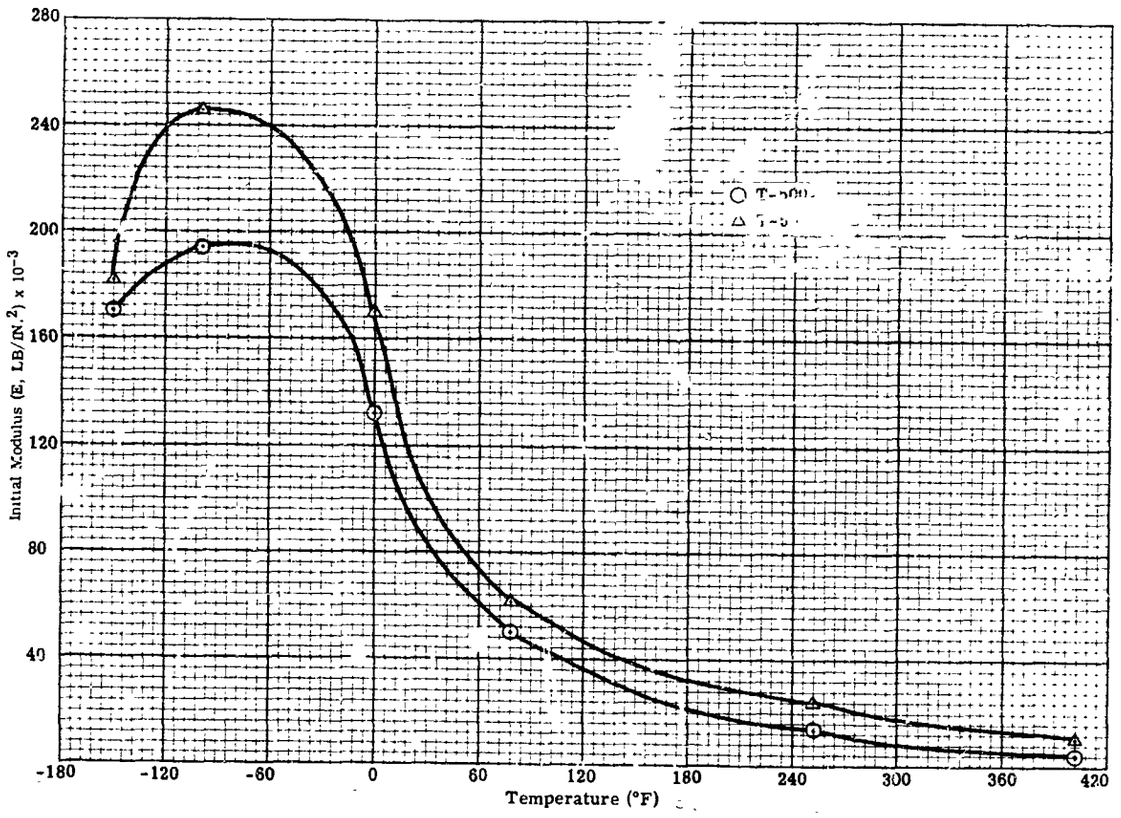

Figure 2-25. Initial Modulus of "THERMO-LAG" T-500-4 and T-500-6

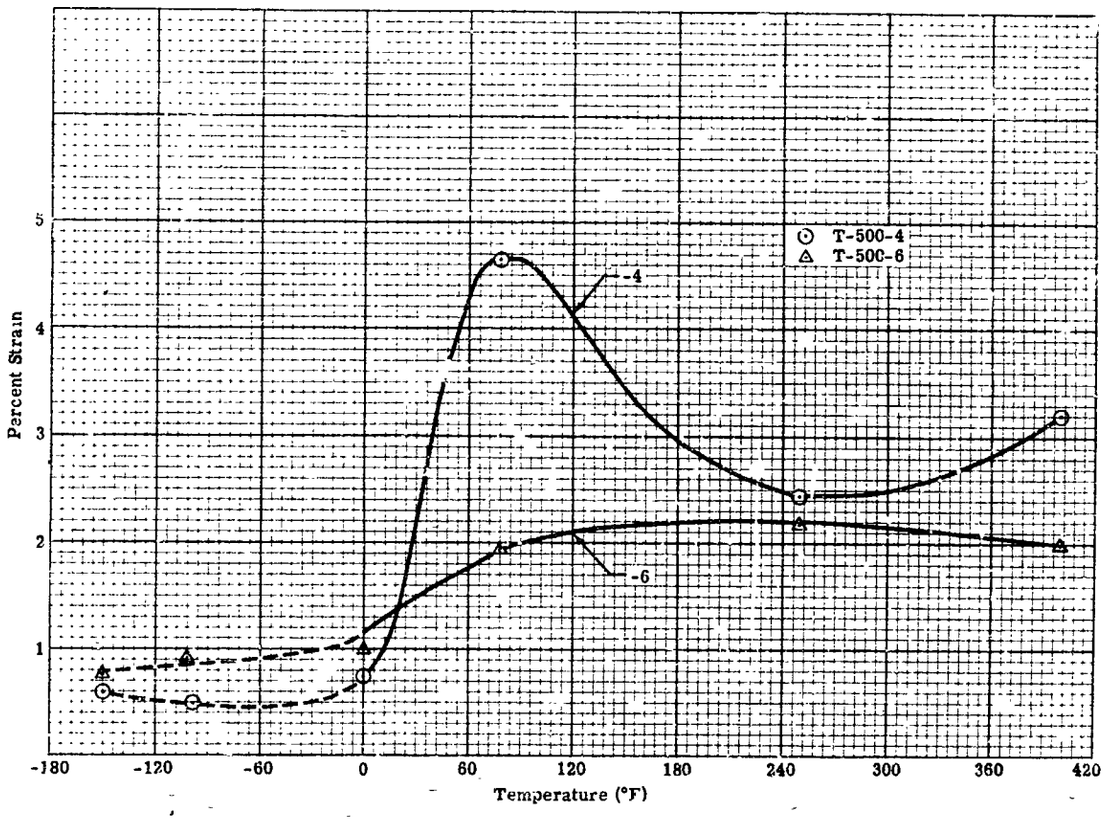

Figure 2-26. Tensile Elongation of "THERMO-LAG" T-500-4 and T-500-6

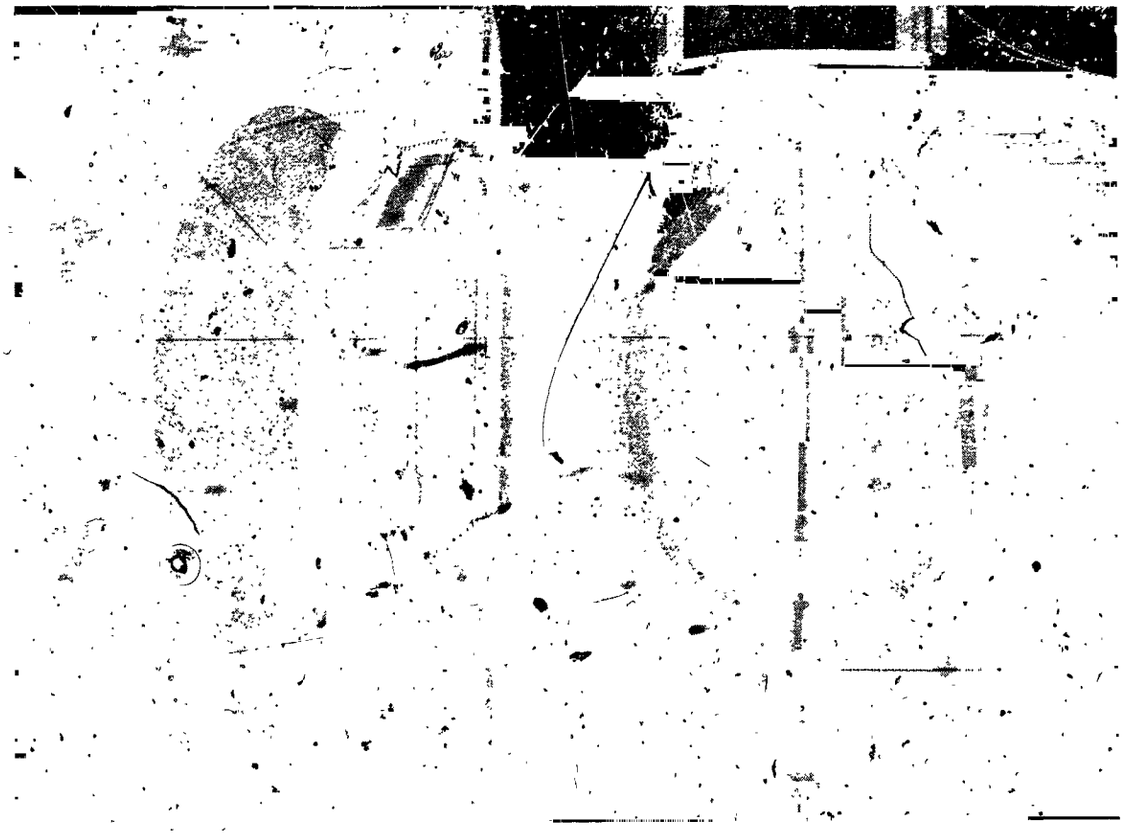

Figure 2-27. Specimen Held in Position for Shear Test in the Cryogenic Chamber

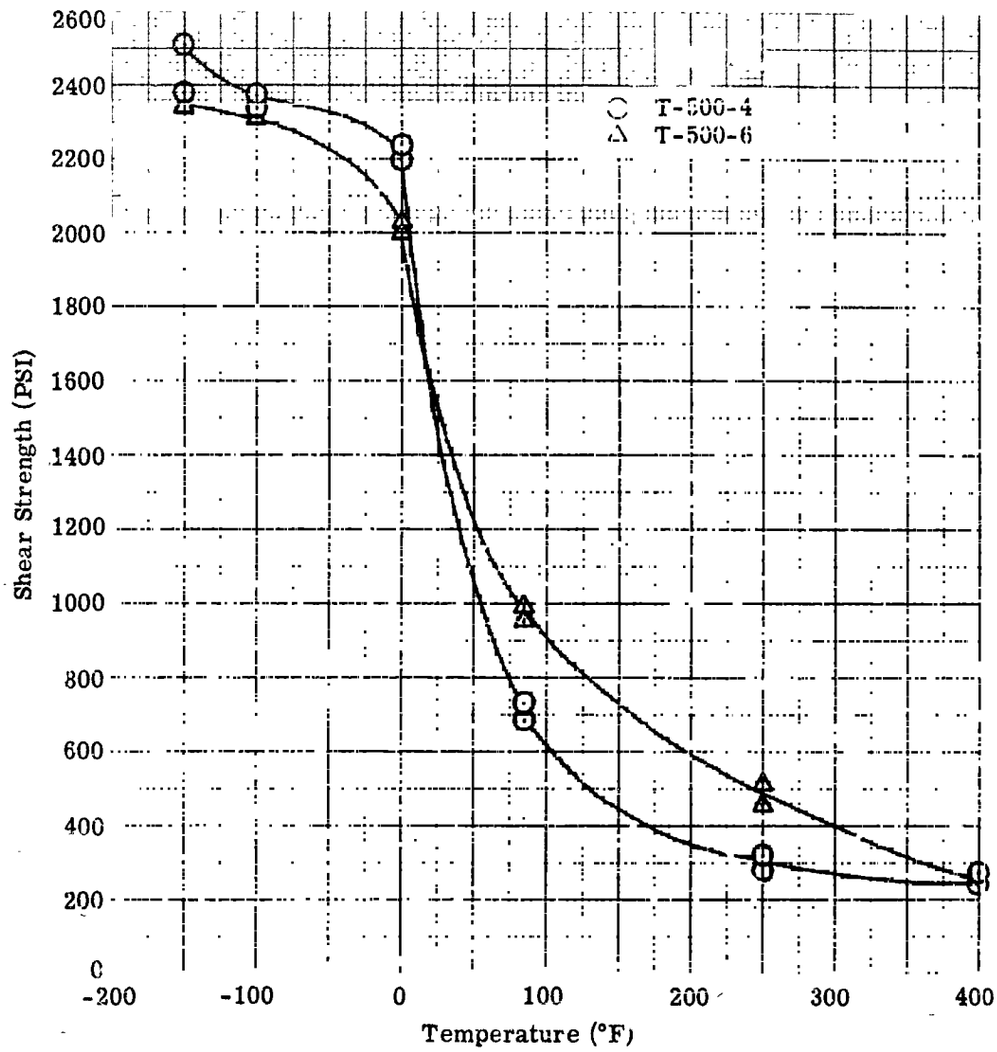

Figure 2-28. Shear Strength Results of "THERMO-LAG" T-500-4 and T-500-6

Figure 2-29. Specimen Held in Position for Flexural Strength Test in the Cryogenic Chamber

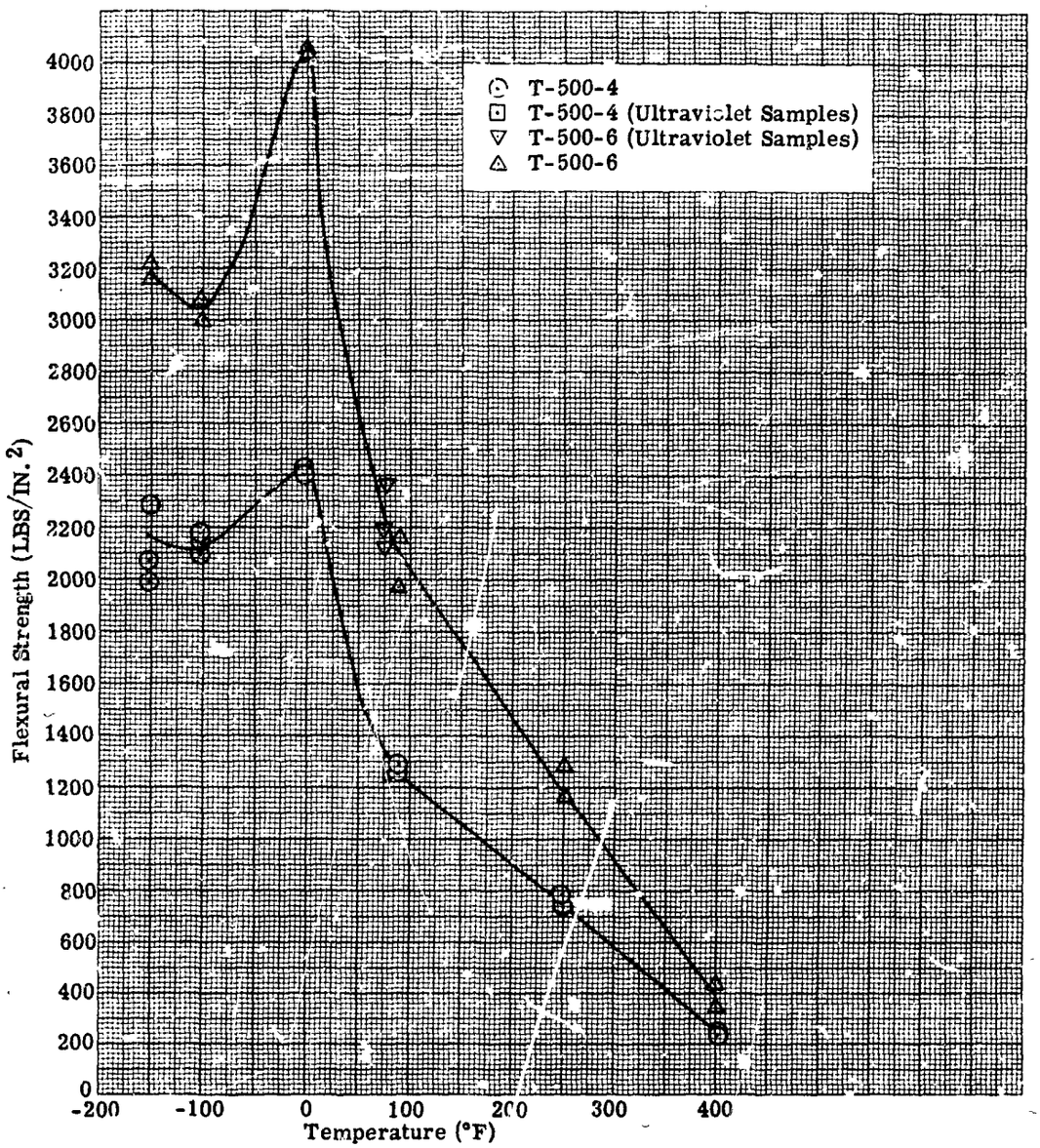

Figure 2-30. Flexural Strength Results of "THERMO-LAG" T-500-4 and T-500-6

BLANK PAGE

SECTION III

SPACE PERFORMANCE EVALUATION

REENTRY SIMULATION (CONVECTION AND RADIATION).

TEST DESIGN.

This test program was designed to use existing techniques for the evaluation of gross thermodynamic performance of "THERMO-LAG" T-500 material. Work progressed in this test program which was also designed to separate the different effects of the environment upon the material so that the test data could be correlated with theoretical predictions. The simulation tests conducted during the reporting period were:

1. Variation of oxygen concentration in the plasma stream.

2. Flight simulation for sidewall heating of Low Pressures.

3. Radiation-ablation performance under purely radiative heat loads.

VARIATION OF OXYGEN CONCENTRATION IN THE PLASMA STREAM. Tests were conducted to provide an order of magnitude estimate of the importance of debris layer-oxygen chemical kinetics upon the rate and extent of debris layer recession in relation to the variation of oxygen concentration in the plasma stream. The test matrix containing the condition and durations of tests performed and the model geometry are listed in Table 3-1.

Table 3-2 identifies each test and summarizes the preliminary results. The preliminary data reduction results which indicate the trends of parameter interdependency associated with an oxidizing debris are presented in Figures 3-1 and 3-2. The analysis and data reduction of the tests appears in Section IV of this report.

AIR-ARC FLIGHT SIMULATION TESTS. Flight Simulation Tests were conducted for selected portions of a super-orbital reentry trajectory. The test matrix containing the conditions, the durations of test runs, model geometry, measured material recession, and cold wall heat blockage is listed in Table 3-3.

Figures A-29 through A-58 illustrate some results of these tests (See Appendix A). The curves of the main body of the figures show the substrate temperature - time histories at the sidewalls of the models. The stagnation temperature of the corresponding model is plotted in the upper right-hand corner of each figure.

Test No.	Duration (SEC)	Test Point	Model NO.	Total Enthalpy (BTU/LB)	Nose Radius (IN.)	Cold Wall Stag. Heat Flux (BTU/FT^2 SEC)	Stagnation Pressure (ATM)
1	420	3	O-14	2,500	1	50	.026
2	420	4	O-15	2,500	1	50	.026
3	420	5	O-16	2,500	1	50	.026
4	300	8	O-9	5,000	1	110	.026
5	300	9	O-11	5,000	1	110	.026
6	300	10	O-13	5,000	1	110	.026
7	150	15	O-1	10,000	5/8	300	.0290
8	150	16	O-2	10,000	5/8	300	.0290
9	150	17	O-3	10,000	5/8	300	.0290
10	300	21	O-6	15,000	1	110	.00267
11	300	22	O-7	15,000	1	110	.00267
12	300	23	O-8	15,000	1	110	.00267

Table 3-1. Variation of Oxygen Concentration Tests

Figures 3-3 through 3-8 show the results of studies conducted on transient debris layer formation. Figure 3-3 shows results from previous data and is used for comparison purposes. The figures indicate that when the debris layer reaches a constant thickness, the heat blockage parameter

$$H_{eff} = \frac{\text{hot wall heat flux}}{\text{mass loss weight}}$$

likewise becomes constant. It should be noted therefore, that short duration will not yield results indicative of material performance where a constant mass loss rate is assumed.

RADIATION TEST. A series of tests were performed to determine the ablative performance under purely radiative heats. These tests to simulate the thermal environment of a

Model NO.	Nose Radius (IN.)	Run Duration (SEC)	Stagnation Enthalpy (BTU/LB)	Test Point NO.	Stagnation Cold Wall Heat Flux (BTU/FT^2-SEC)	Percent O2	Model Stagnation Pressure (ATM)	Recession to Debris Layer (IN.)	Debris Thickness (IN.)	Total Recession (IN.)	Surface Temp. = 0.9, (°F)	Enthalpy Difference (BTU/LB)	Hot Wall Heat Flux (BTU/FT^2-SEC)	Cold Wall Heat Blockage (BTU/LB)
0-1	5/8	150	9,897	15	297	15	.0291	.28	.08	.360	3,510	8,750	262	18,550
0-2	5/8	150	10,055	16	295	7	.0289	.117	.17	.287	3,300	9,000	265	23,300
0-3	5/8	150	10,165	17	301	0	.0291	.022	.20	.222	2,380	9,405	279	30,500
0-6	1	300	14,988	21	108	15	.00267	.268	.17	.438	3,180	13,968	101	11,100
0-7	1	300	15,185	22	105	7	.00265	.156	.25	.406	3,110	14,1[illegible]5	98.3	11,600
0-8	1	300	15,052	23	107	0	.00266	.063	.27	.333	3,050	14,077	100	14,450
0-9	1	300	4,965	8	109	15	.026	.068	.30	.368	2,910	4,035	88.7	13,350
0-11	1	300	5,000	9	107	7	.0258	.042	.30	.342	2,780	4,110	86	14,000
0-13	1	300	5,110	10	109	0	.026	.026	.31	.336	2,620	4,270	91	14,600
0-14	1	420	2,488	3	48.7	15	.0255	.035	.19	.225	2,010	1,843	36	13,650
0-15	1	420	2,510	4	46.8	7	.0258	.023	.19	.215	1,920	1,895	35.3	13,750
0-16	1	420	2,505	5	47.9	0	.0256	.009	.17	.179	1,780	1,925	36.8	16,900

Table 3-2. Stagnation Point Oxidation Results

vehicle in vacuum eliminate the transpiration cooling phenomenon. The heat blockage becomes a function of reradiation, sensible heating of gases in the debris layer, chemical reactions in the debris layer, and latent heat of sublimation of the compound.

Some tests designed to complement the plasma-arc test series were performed at heat fluxes of 7.4 and 9 BTU/FT^2-SEC. These radiant heat fluxes are within the scope of the aft body sidewall heat fluxes of a superorbital manned spacecraft. The results of the tests are recorded in Figures 3-9 and 3-10.

MODIFICATION OF CERTAIN REENTRY SIMULATION TESTS AND PARAMETER ANALYSES.

AIR-ARC GAP CONDITION TESTS. The effect of discontinuities in the ablative material surface that may result from assembly around observation windows, inspection hatches,

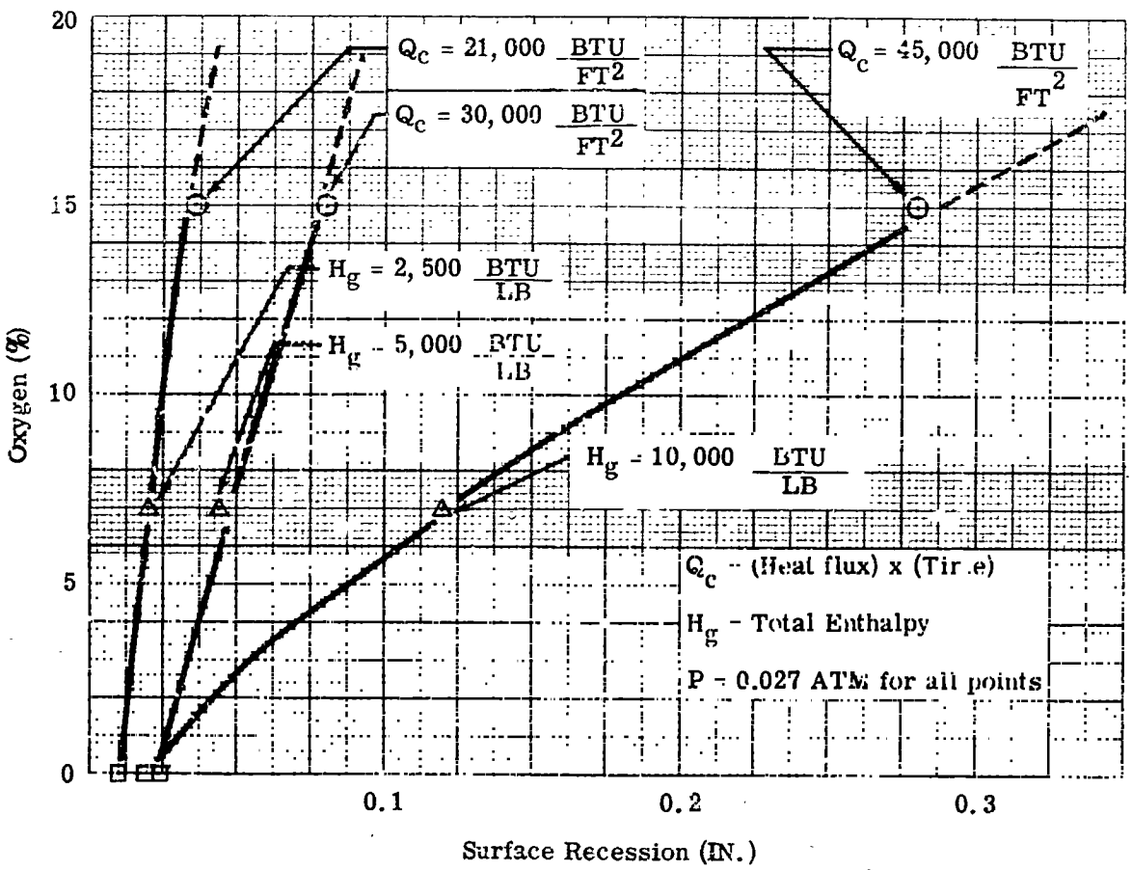

Figure 3-1. Percentage of Oxygen Versus Surface Recession for "THERMO-LAG" T-500

access doors, etc., are to be investigated by a series of gap tests. These tests will provide data which will determine the effect of gap width and depth of the thermal protection received by the substrate material from the "THERMO-LAG" T-500 material.

The body geometry of the models to be tested with gaps and their dimensions were reported in Emerson Electric's Quarterly Progress Report Number 1468. The model proposed was a hemispherical cylinder with three slots, each either normal or parallel to the flow field for evaluation. A revised conducted design analysis of the test program has resulted in the following modifications.

1. The gap model will be a two-dimensional body with a two-inch diameter cylindrical leading edge and a flatplate aft section (see Figure 3-11). The two-dimensional wing body will contribute to the establishment of a stable aerodynamic boundary layer and better correlation of flat plate heating analysis than the three-dimensional body.

2. To maintain an established heat flux over the test area, the leading edge geometry will be a water-cooled copper head.

3. Each flat face surface of a model will have a single gap. One will be normal to the flow stream with the other parallel to the flow stream. This modification will contribute to the control of the flow variables that influence the data reduction capability of test.

4. For the intended data reduction analysis, the thermocouples will be buried in a flat face surface at the following positions:

   a. At the substrate within the gap.
   b. Parallel to the gap measurement point under a smooth surface where the flow streams will not be influenced by the gap.
   c. Directly in line with the gap measurement point under a smooth surface where the flow streams will be influenced by the gap.

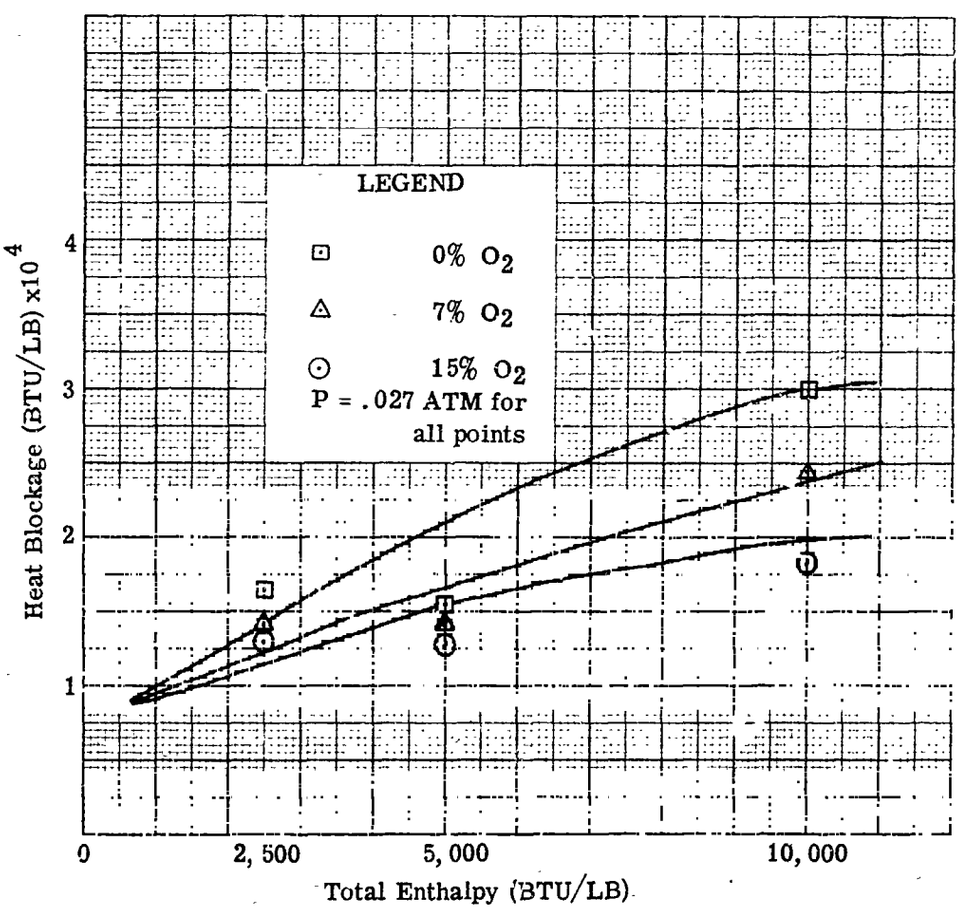

Figure 3-2. Heat Blockage Versus Total Enthalpy for "THERMO-LAG" T-500

Temperature histories of the substrate material, the ablative material at the undisturbed and disturbed flow stream region, will be recorded. The actual temperature histories will be compared to theoretical temperature histories. Theoretical transient analysis will be run on the IBM ablation program for cases where the material is continuous in a correspondent environment. An index of the loss of thermal protection will be determined. The substrate temperature history under the gap will be compared to those under the undisturbed surfaces for the position immediately adjacent to, and that removed from, the gap. The temperature history recorded for the undisturbed flow region will give an indication of the boundary layer characteristics for the heating analysis.

The revised gap test matrix is outlined in table 3-4.

Model NO.	Nose Radius (IN.)	Run Duration (SEC)	Stagnation Enthalpy (BTU/LB)	Test Point NO.	Stagnation Cold Wall Heat Flux (BTU/FT^2-SEC)	Percent O_2	Stagnation Pressure (ATM)	Recession to Debris Layer (IN.)	Debris Thickness (IN.)	Total Recession (IN.)	Surface Temperature = 0.9 (°F)	Enthalpy Difference (BTU/LB)	Hot Wall Heat Flux (BTU/FT^2-SEC)	Cold Wall Heat Blockage (BTU/LB)
N-64	1	420	2550	2	47.4	21	.021	.442	.253	.285	2440	1750	32.5	10140
N-15	1	420	3560	1	43.5	21	.015	.055	.30	.355	2570	2760	37.6	8550
N-36	1	420	5125	6	48	21	.0076	.139	.20	.339	2710	4280	40.1	8950
N-35	1	90	4950	6	48.5	21	.0076	.013	.092	.105	2570	4150	40.6	6240
N-53	1	30	5865	6	48	21	.0076	.001	.050	.051	2500	4265	40.5	4250
N-82	1	900	4890	6	48	21	.0076	.328	.319	.645	2770	4.25	39.6	10020
N-54	1	300	5100	7	105	21	.026	.047	.219	.266	2600	4070	87.5	17800
N-9	1	2260	4950	7	104	21	.026	.383	.579	.962	2660	4100	86.3	36800
N-30	1	300	5050	11	163	21	.059	.478	.078	.556	3110	4050	131	13200
N-48	1	45	10,120	13	162	21	.016	.097	.062	.159	3630	8920	141	7750
N-4[illegible]	1	465	9850	13	163	21	.016	1.173	.144	1.317	3630	8850	143	8680

Table 3-3. Preliminary Stagnation Point Results

Model NO.	Nose Radius (IN.)	Run Duration (SEC)	Stagnation Enthalpy (BTU/LB)	Test Point NO.	Stagnation Cold Wall Heat Flux (BTU/FT^2-SEC)	Percent O_2	Stagnation Pressure (ATM)	Recession to Debris Layer (IN.)	Debris Thickness (IN.)	Total Recession (IN.)	Surface Temperature = 0.9 (°F)	Enthalpy Difference (BTU/LB)	Hot Wall Heat Flux (BTU/FT^2-SEC)	Cold Wall Heat Blockage (BTU/LB)
N-105	5/8	150	10,085	14	278	21	.028	.584	.021	.605	3980	8585	238	10360
N-42	5/8	210	9950	14	280	21	.029	.733	.081	.814	3870	8650	243	10840
N-112	5/8F*	300	12,120	18	154	21	.023	.755	.076	.831	3850	10,820	137	8350
N-106	5/8	150	11,850	18	278	21	.023	.514	.091	.605	3960	10,550	247	10370
N-94	5/8	300	11,785	19	154	21	.0058	.430	.149	.579	3500	10,585	138	11920
N-21	1	300	15,170	20	105	21	.0027	.289	.156	.445	3240	14,100	98	10600
N-71	1F	300	17,480	25	174	21	.02	.675	.075	.750	4030	16,180	161	10420
N-29	1	150	17,650	25	317	21	.02	.514	.076	.590	4310	16,250	292	12100
N-110	5/8	300	17,480	28	278	21	.0106	.587	.118	.705	3720	16,230	258	17940
N-75	1	150	22,850	26	253	21	.0086	.342	.103	.445	4080	21,550	239	12780

Table 3-3. Preliminary Stagnation Point Results (Continued)

Model NO.	Nose Radius (IN.)	Run Duration (SEC)	Stagnation Enthalpy (BTU/LB)	Test Point NO.	Stagnation Cold Wall Heat Flux (BTU/FT^2-SEC)	Percent O_2	Stagnation Pressure (ATM)	Recession to Debris Layer (IN.)	Debris Thickness (IN.)	Total Recession (IN.)	Surface Temperature = 0.9 (°F)	Enthalpy Difference (BTU/LB)	Hot Wall Heat Flux (BTU/FT^2-SEC)	Cold Wall Heat Blockage (BTU/LB)
N-73	1F	100	23,050	27	251	21	.027	.055	.111	.166	3870	21,750	237	22800
N-65	1	270	23,000	27	457	21	.027	.785	.078	.863	4200	21,650	431	21400
N-26	1	150	23,330	27	453	21	.027	.435	.070	.505	4230	21,950	427	20200
N-2	1	90	23,100	27	455	21	.027	.21	.067	.277	4260	21,750	428	22200
N-11	1	42	23,250	27	457	21	.027	.096	.068	.164	4130	21,950	431	18800
N-6	1	30	22,900	27	456	21	.027	.063	.062	.125	4180	21,600	430	16400
N-22	1	15	23,500	27	455	21	.027	.019	.007	.026	3630	22,350	423	39500

Table 3-3. Preliminary Stagnation Point Results (Continued)

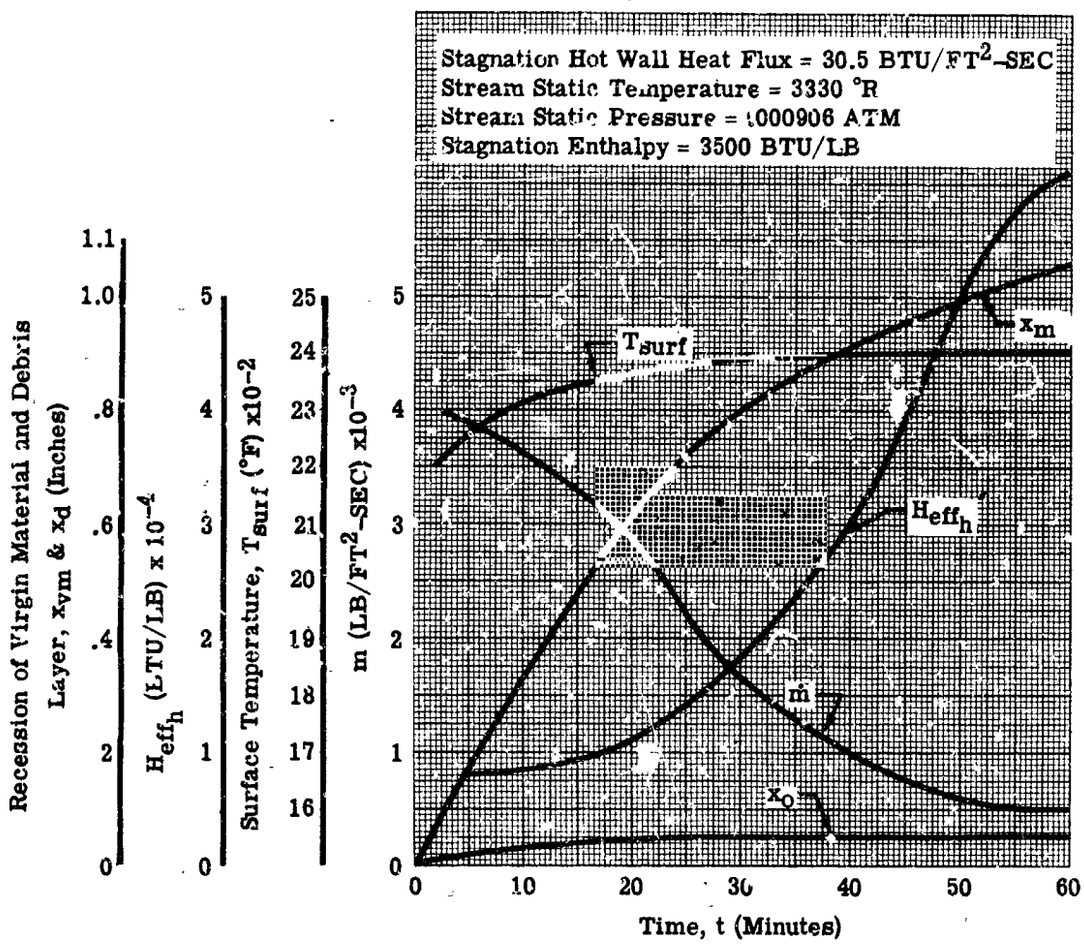

Figure 3-3. Transient Histories for Stagnation Heat Flux of 35 BTU/FT²-SEC

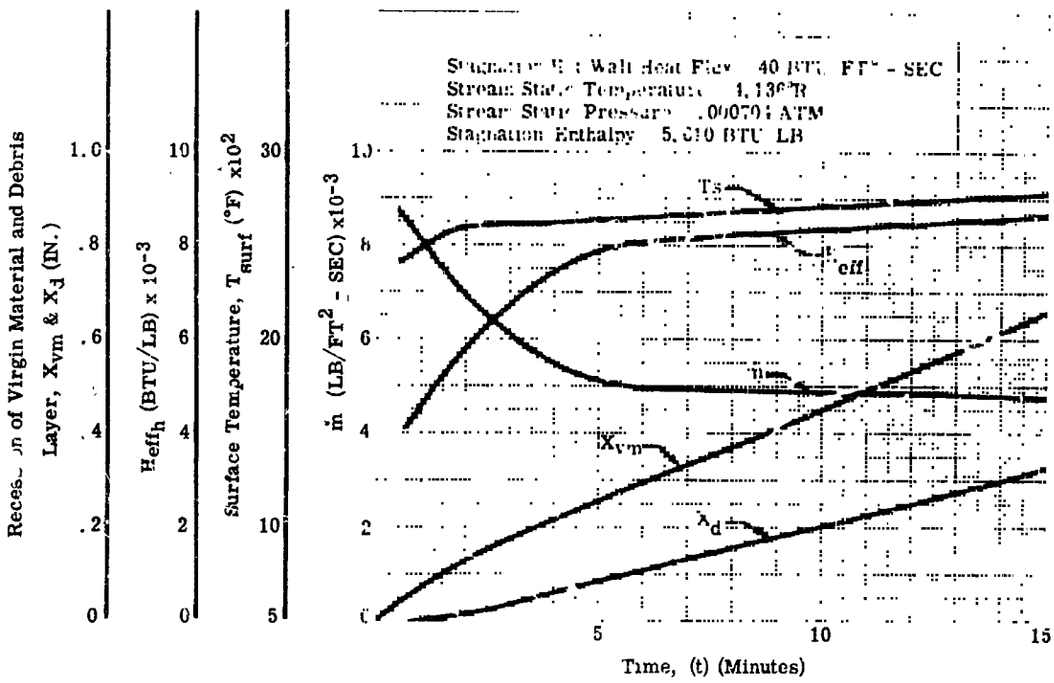

Figure 3-4. Transient Histories for Stagnation Heat Flux of 48 BTU/FT^2-SEC

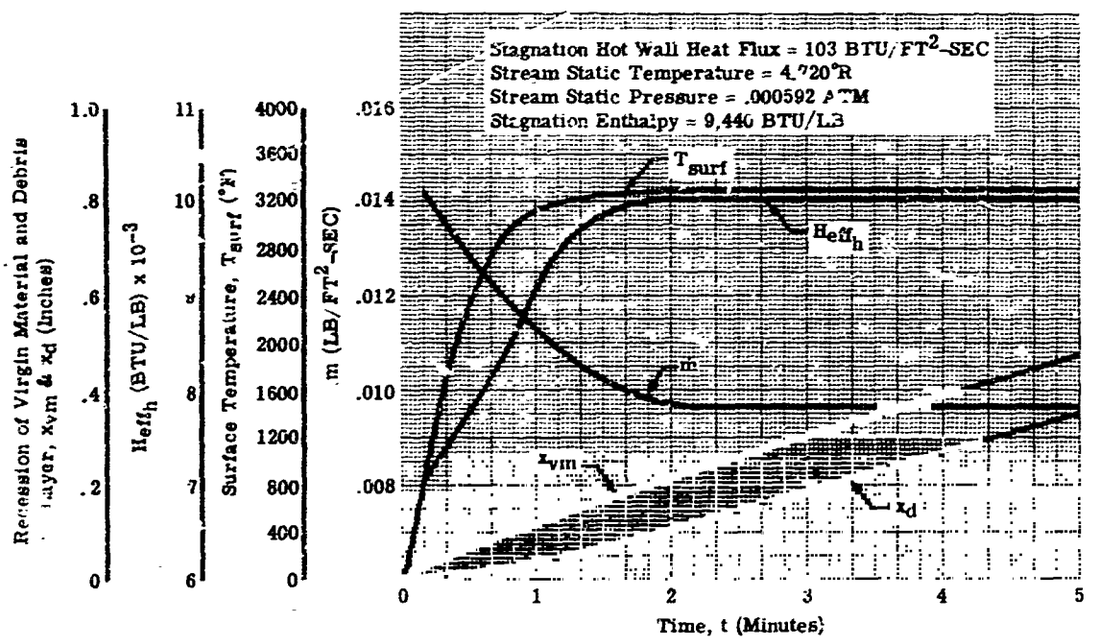

Figure 3-5. Transient Histories for Stagnation Heat Flux of 110 BTU/FT^2-SEC

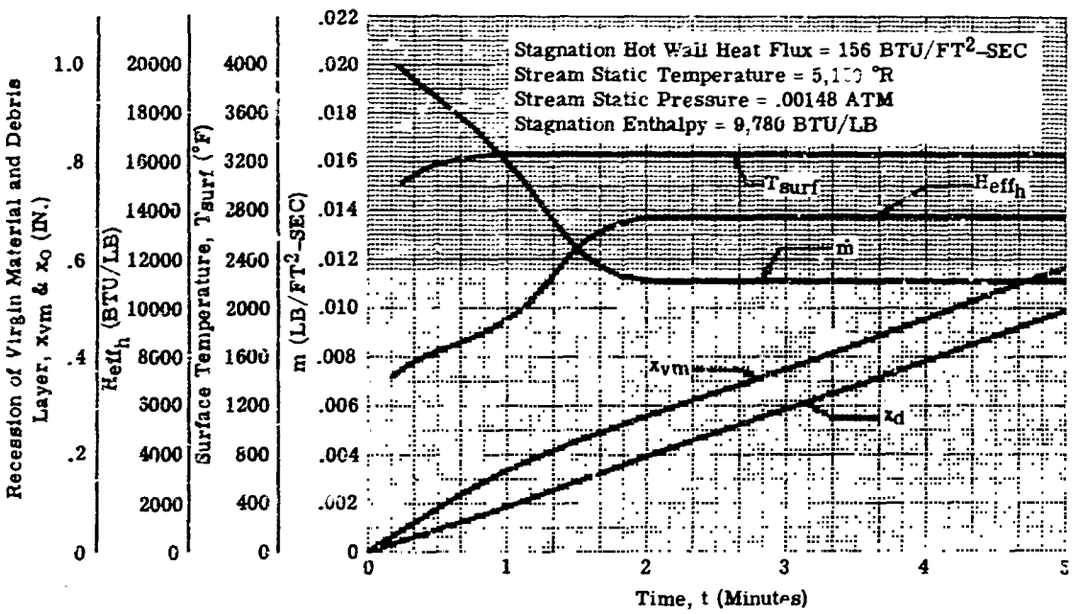

Figure 3-6. Transient Histories for Stagnation Heat Flux of 170 BTU/FT^2-SEC

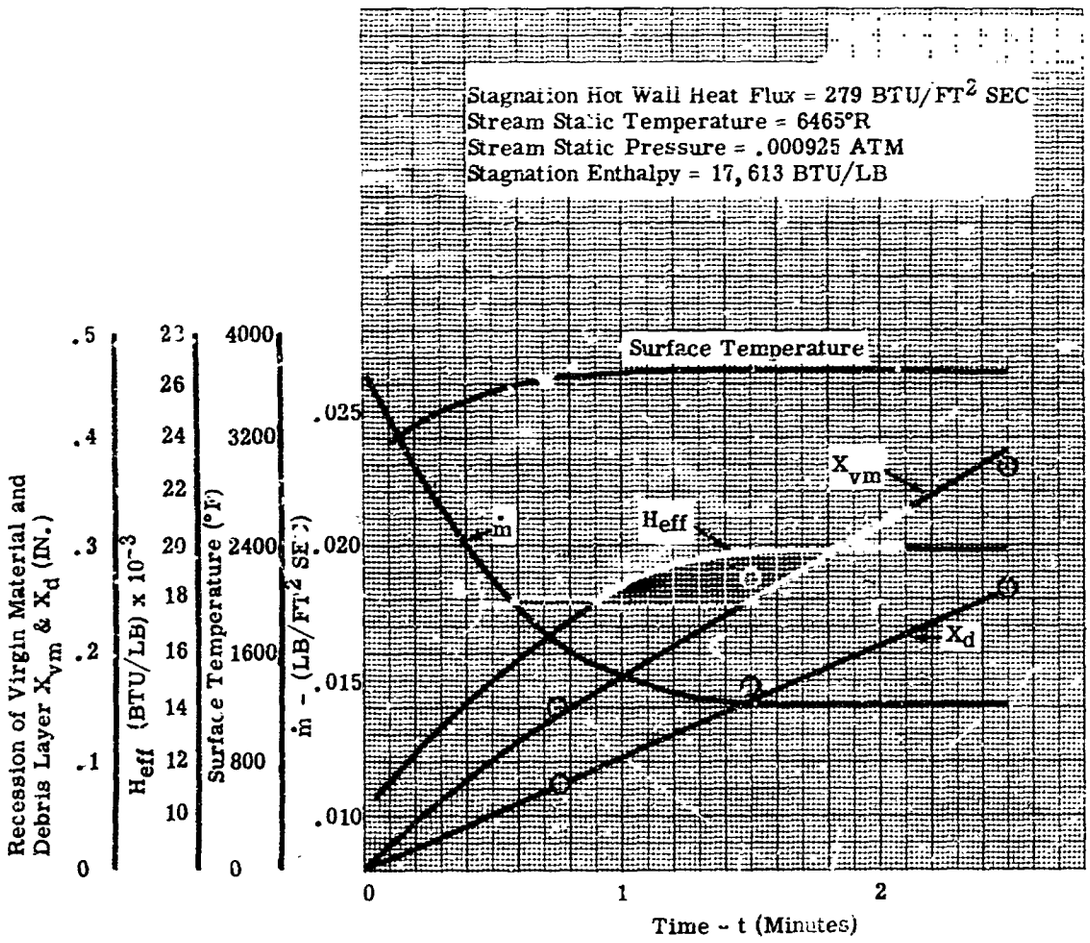

Figure 3-7. Transient Histories for Stagnation Heat Flux of 300 BTU/FT^2-SEC

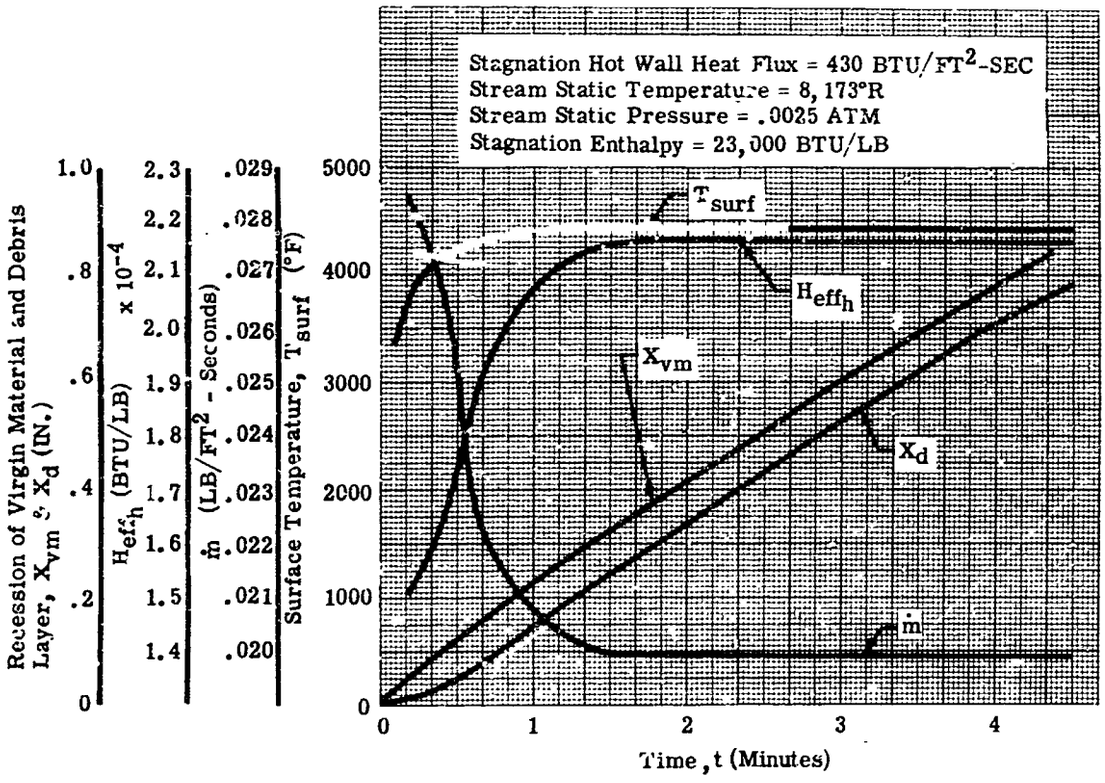

Figure 3-8. Transient Histories for Stagnation Heat Flux of 456 BTU/FT^2-SEC

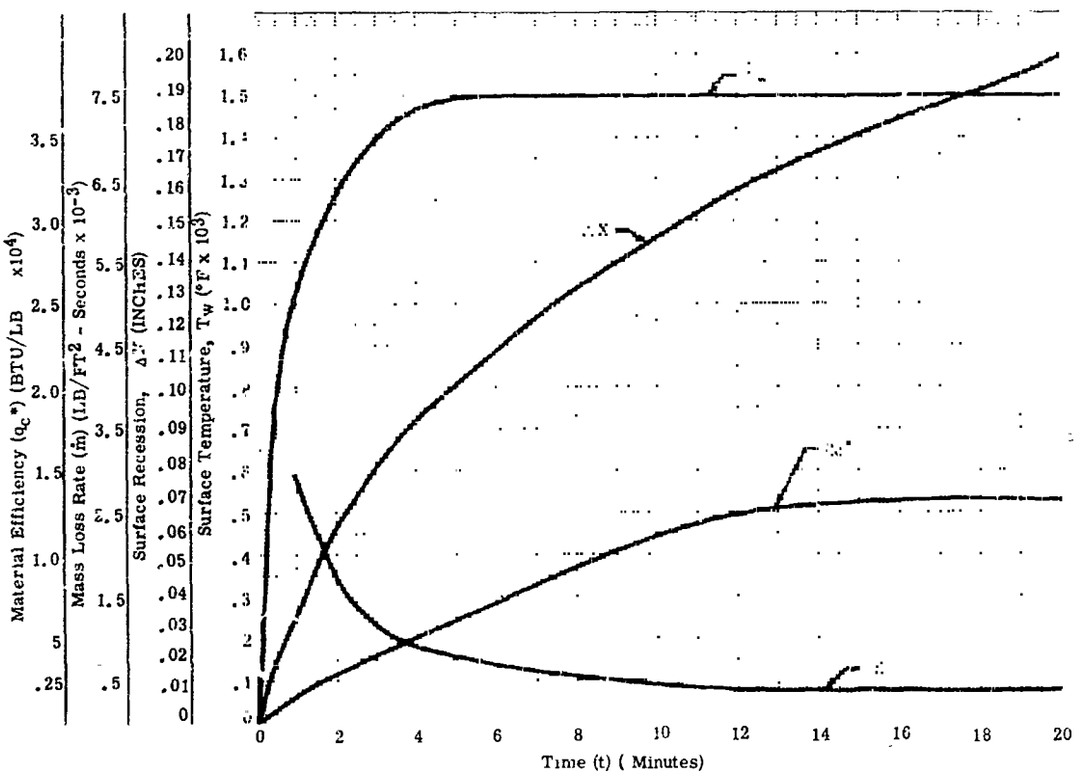

Figure 3-9. Composition - Radiation Ablation for Radiation Heat Flux of 7.4 BTU/FT^2-SEC

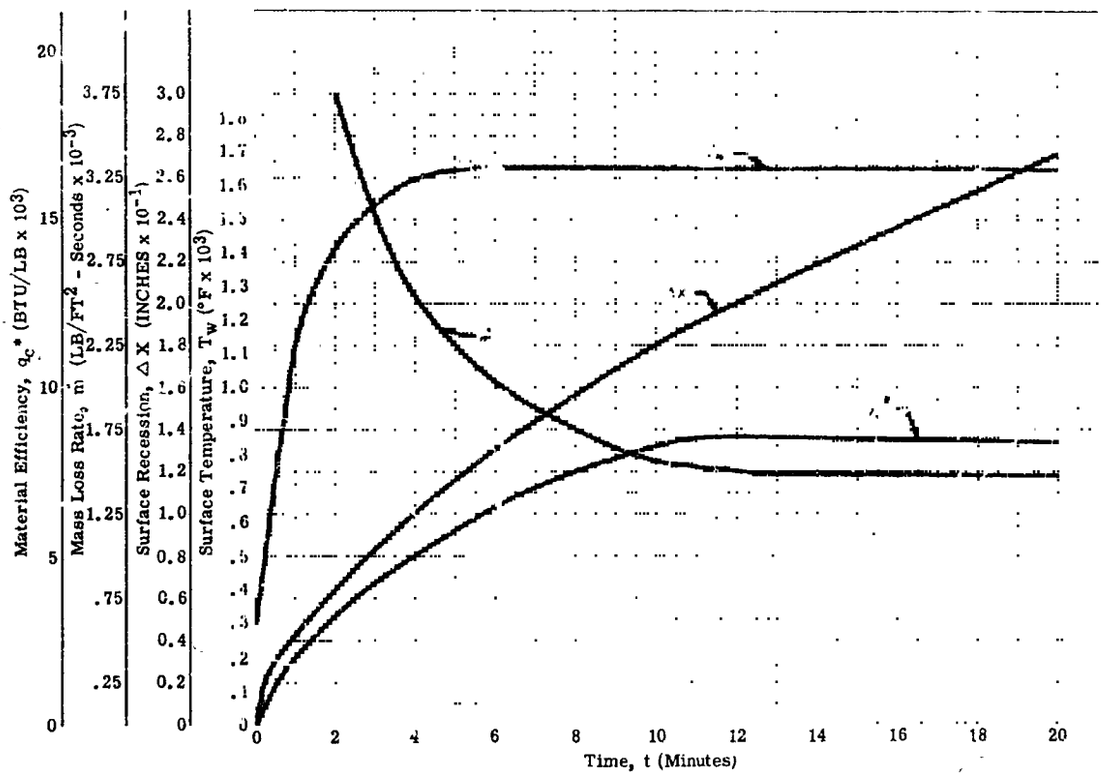

Figure 3-10. Composition - Radiation Ablation for Radiation Heat Flux of 9 BTU/FT^2-SEC

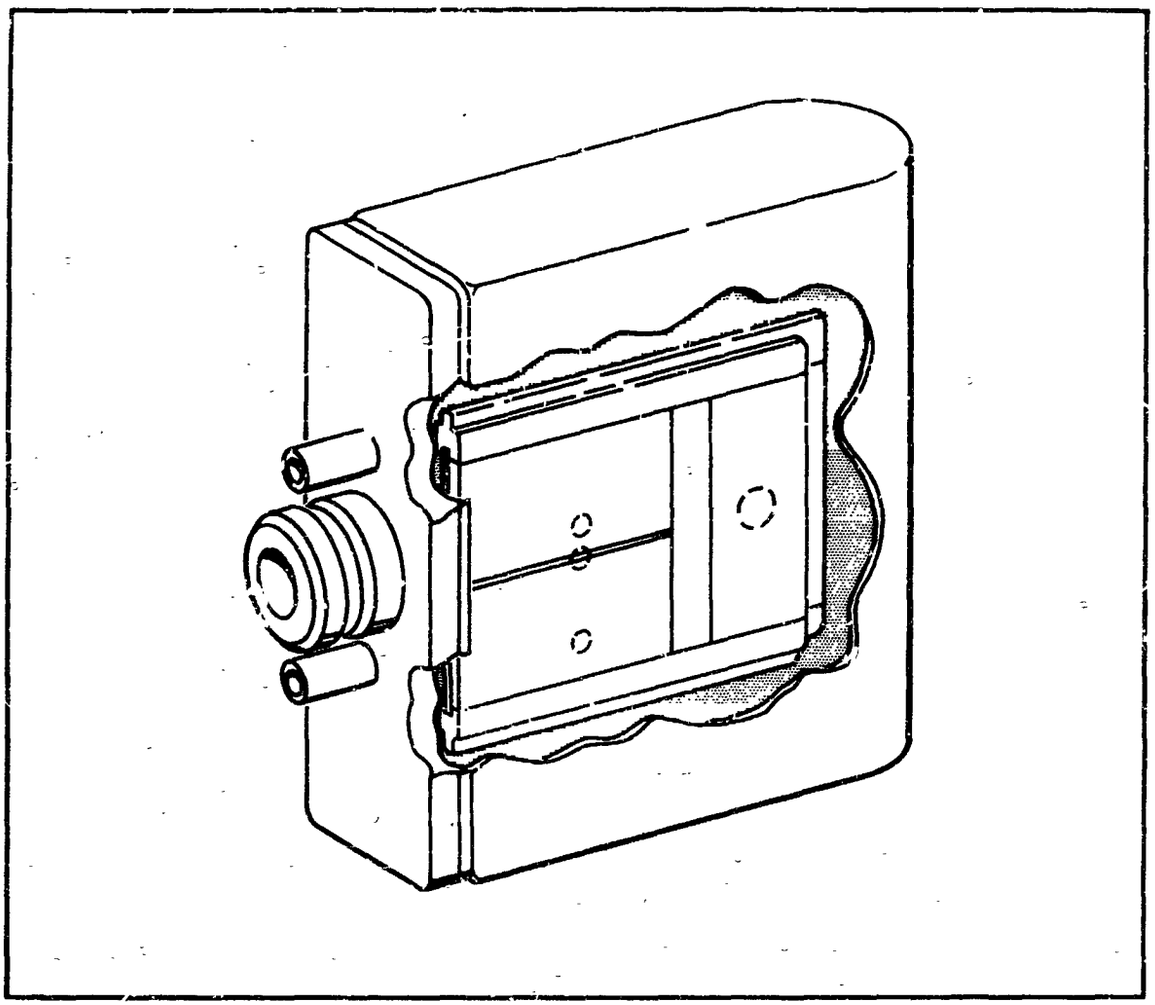

Figure 3-11. Test Gap Model

Plasmadyne Test Point	Stagnation Pressure (ATM)	Stagnation Heat Flux (BTU/FT^2-SEC)	Stagnation Enthalpy (BTU/LB)	Slot Depth (IN.)	Slot Gap (IN.)
12	0.007	110	10,000	0.125	0.02
12	0.007	110	10,000	0.125	0.05
12	0.007	110	10,000	0.125	0.1
12	0.007	110	10,000	0.06	0.02
12	0.007	110	10,000	0.06	0.05
12	0.007	110	10,000	0.06	0.1
12	0.007	110	10,000	0.02	0.02
12	0.007	110	10,000	0.02	0.05
12	0.007	110	10,000	0.02	0.1

Table 3-4. Revised Test Matrix - Air-Arc Gap Tests

BLANK PAGE

SECTION IV

PERFORMANCE ANALYSIS AND PREDICTION

DEBRIS LAYER RECESSION.

RESULTS OF THE ANALYSIS. To determine, by experimental analysis, the surface recession of a carbonaceous debris layer under the influence of a high energy fluid stream, consideration was given to:

1. Oxidation of carbon with oxygen in the fluid stream.

2. Erosion from shear stress exerted mostly by the stripped nitrogen.

The empirical expression would be a function of the carbon surface temperature. Experimental data indicates that recession by oxidation prevails at carbon surface temperatures approximately 4000°R and below, with erosion by shear stresses predominate at higher values.

Predicted values of the reaction rate are tabulated in Table 4-1. Table 4-2 records experimental data. Investigation of the tabulated test data indicates that only the rate controlling term of the Arrhenius equation was used to determine the values for R and n

A check of the analytical values was made from a cross plot of recession versus surface temperature as a function of test time. Variation of the parameter from 0 to 1, as the term R_I is independent of surface temperature, resulted in almost equivalent values of R_I. The values of R_I listed in Table 4-2 were predicted for the order of reaction, n = 0.25. The existing variations in the predicted reaction rate constants are 15 percent. A value of 100 for R_I gives 10 percent accuracy.

Temperature (°F)	$\log_{10} Kp_{CO}$	$\log_{10} Kp_{CO_2}$
1800	8.8	7.5
2500	7.5	5.
4000	6.3	2.5
5500	5.6	1.2

Table 4-1. Equilibrium Constants for CO and CO_2 at Elevated Temperature

Model NO.	Stag. Enthalpy BTU/LB	Partial Oxygen Pressure ATM	Surface TEMP °F	Recession Rate IN/SEC	Rate Constant R IN/SEC-ATM.^{25}	Order of Reaction n
0-1	10,000	.00435	3912	2.5×10^{-3}	100	.25
0-2	10,000	.00203	3912	2×10^{-3}	97	.25
0-1	10,000	.00435	3732	1.6×10^{-3}	101	.25
0-2	10,000	.00203	3732	1.2×10^{-3}	97	.25
0-1	10,000	.00435	3552	1.0×10^{-3}	102	.25
0-2	10,000	.00203	3552	$.8 \times 10^{-3}$	103	.25
0-1	10,000	.00435	3192	$.28 \times 10^{-3}$	94	.25
0-2	10,000	.00203	3192	$.22 \times 10^{-3}$	93	.25
0-6	15,000	.00039	3732	$.94 \times 10^{-3}$	107	.25
0-7	15,000	.00018	3732	$.71 \times 10^{-3}$	98	.25
0-6	15,000	.00039	3552	$.501 \times 10^{-3}$	95	.25
0-7	15,000	.00018	3552	$.46 \times 10^{-3}$	102	.25
0-6	15,000	.00039	3462	$.43 \times 10^{-3}$	103	.25
0-7	15,000	.00018	3462	$.33 \times 10^{-3}$	100	.25
0-9	5,000	.0039	3372	$.1 \times 10^{-3}$	100	.25
0-11	5,000	.0018	3232	$.20 \times 10^{-3}$	98	.25

Table 4-2. Experimental Data and Results of Oxidation Tests

Use of the predicted values for the terms n and R_I allows the rate controlling equation to be expressed in the generalized form

$$\frac{dx}{dt} = 100\,(P_{O_2})^{0.25}\, e^{-36200/T}$$

for the instantaneous reaction rate, and

$$\int_{x_i}^{x_2} dx = 100\,(P_{O_2})^{0.25} \int_{t_1}^{t_2} e^{-\frac{36200}{T_W(t)}}\, dt$$

for overall recession. The terms are expressed in inches, seconds, atmosphere of pressure, and °R. The range of variables at which the diffusion controlling and recession due to oxidation effect equations can be expected to give good correlation to measured recession rates are:

T_W(°F)	3000-4000
P_{O2}, stag (ATM)	0.0001-.006
Hg, stag (BTU/LB)	5000-15,000

For steady state conditions the generalized rate controlling equation can be used to predict virgin material recession rate because it has been observed that both recession rates are same and constant.

OXIDATION AND DIFFUSION MODEL AND ANALYSIS.

The rate of oxidation of carbon in a high energy air stream is contingent upon the rate of the following five processes:

1. Transport of oxygen to the surface.
2. Adsorption of oxygen impinging on the surface.
3. Chemical reaction between an oxygen molecule adsorbed on the surface and a carbon.
4. Desorption of the products CO from the surface.
5. Transport of CO away from the surface.

The adsorption process mentioned above is activated adsorption or chemisorption where definite electron bonds correspond to the formation of a product between the adsorbate and the surface.

Processes (1) and (3) are acknowledged as controlling actions, with (3) for the temperature range below 4000°R and (1) for temperatures at and above. Due to the kinetics at the herein considered temperatures, no consideration is given for formations of NO and NC in the analysis.

The analysis assumes that carbon is consumed mostly by surface oxidation, i.e., surface oxidation preceeds sublimation. Investigators have given the activation energy of surface oxidation at about 2,000 BTU/LB of carbon and the heat of sublimation of carbon at about 25,000 BTU/LB.

The main features of the analysis can be illustrated by a simple physicochemical model. The model in which partially dissociated air flows over a carbon surface is shown in Figure 4-1.

The event for each of the media are described by the accompanying reaction:

1. Debris Surface

$$C + O \longrightarrow CO$$

$$2C + O_2 \longrightarrow 2CO$$

$$C + CO_2 \longrightarrow 2CO$$

2. Gas-Phase Oxidation Zone

$$2CO + O_2 \rightleftharpoons 2CO_2$$

$$CO + \tfrac{1}{2} O_2 \rightleftharpoons CO_2$$

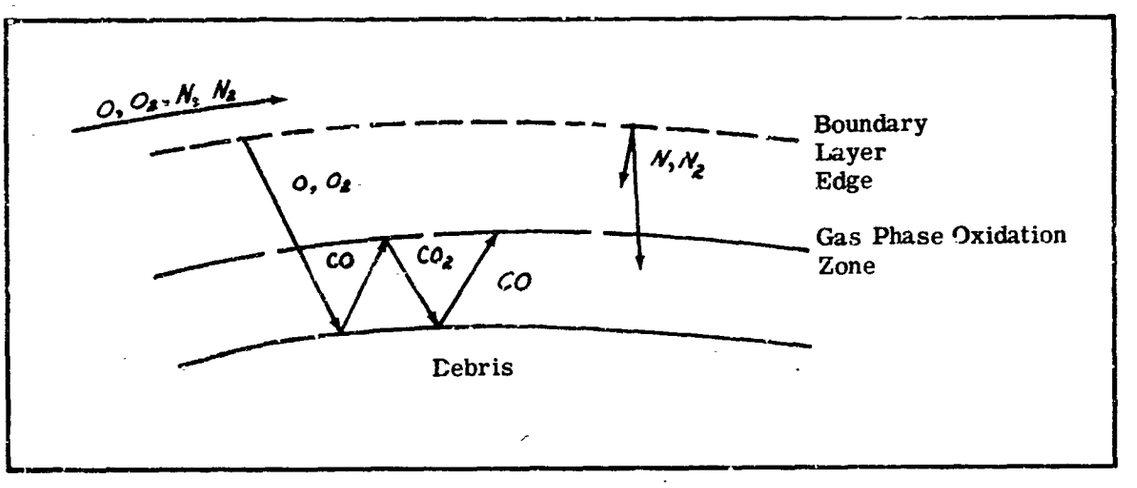

Figure 4-1. A Physicochemical Model of Partially Dissociated Air Flow Over a Carbon Surface

The reactions at the debris surface are limited to forward reactions. The chemical reaction rate of the high bond carbon monoxide molecule makes release of the oxygen atom and readsorption of the carbon atom improbable.

The limiting cases for the gas-phase oxidation zone are:

1. Where the zone is the carbon surface or very near to it.
2. Where the zone is at or very near to the edge of the boundary layer.

The first case will apply primarily to the non-porous carbon surface where mass injection from inside of the system into the boundary layer will be negligible, whe. as, the second case will apply to the porous carbon surface where mass injection will be maximum.

The equilibrium constants for formations of CO and CO_2 can be predicted by the following expressions:

$$\text{Log}_{10}\ K_{P_{CO}} = \frac{P_{CO}}{P_{O_2}^{1/2}}$$

$$\text{Log}_{10}\ K_{P_{CO_2}} = \frac{P_{CO_2}}{P_{CO} \cdot P_{O_2}^{1/2}}$$

The values predicted from the above expressions for rate formations of CO and CO_2 for elevated temperatures of interest are tabulated in Table 4-1.

The preceding analysis indicates that an increase in temperature increases the ratio CO/CO_2. Figuratively, this indicates that an increase in distance between the gas-phase reaction zone and material surface is accompanied by higher values of the ratio CO/CO_2. The resultant gas-phase oxidation product, CO_2, impinging on the debris surface will then be negligible compared to CO at the herein considered temperatures. Elimination of the CO_2 reaction allows the rate equation for the contributing reactions to be written by the expression of Arrhenius

$$R_I\ (P_{O_2})^n\ e^{-E/RT_w}$$

where the symbols appearing here and in remaining sections are defined:

R_I = reaction rate constant, IN./SEC-ATM^n

P_{O_2} = partial pressure of oxygen in the fluid stream, ATM

n = order of reaction, ($o < n < 1$)

E = activation energy, (40 Kcal/mole)

R = gas constant, 1.987 cal/mole - °K

T_w = wall temperature of substrate material, °K

For rate controlling regimes, reaction rates of surface oxidation is quite insensitive to boundary layer conditions. The provision being that the oxygen be sufficient in the boundary layer stoichiometrically.

The analysis is this point has dealt with controlling oxidation reaction by the chemical resistance at the surface. Emphasis will now be given to the controlling reaction of diffusional resistance of the stagnant gas film going away from the debris surface.

The thickness of the gas film depends on the velocity of gas past the surface. With increasing temperatures above 3500 °R, the chemical resistance at the surface decreases. At some temperatures then, the effect of chemical resistance will be in equilibrium with that of diffusional resistance. The event of still higher temperatures will result in diffusional resistance becoming the controlling reaction. The chemical - diffusional transition is characteristic of the heat transfer phenomena and is a function of the gas velocity. Indications are that the transition temperature is from 3500 to 4000 °R. The rate equation for the diffusion controlling regime can be expressed as

$$R_{II} \; (P_{O_2})^m V$$

where symbols not previously defined are:

R_{II} = diffusional rate constant IN./SEC-ATM^n

V = gas velocity IN./SEC

m = empirical diffusional constant

In the present treatment the contributions to the recession rate due to oxidation effects are superimposed in the following way:

$$\frac{dx}{dt} \quad R_I (P_{O_2})^n e^{-E/RT_w} + R_{II} (P_{O_2})^m V$$

The contribution of the chemical reaction is represented by the first term. The second term represents the contribution of the diffusional rate.

In the data reduction, the analysis did not consider the contribution of the diffusional term to surface recession. Additional tests made at higher temperatures should be able to determine its contributing content. The analysis indicates the controlling reactions are additive. There is also the probable indication that the diffusional term will contribute for close correspondence of predicted and measured recession rates.

MASS INJECTION.

SUMMARY AND INTRODUCTION. An ablative material that sublimes is recognized as an effective heat protection system for hypervelocity applications. For this reason the vapor injected into the boundary layer effectively blocks a large fraction of aerodynamic heat from

entering the skin surface. An effective application of a subliming heat shield could be its utilization for transpiration cooling techniques. Transpiration cooling would allow a coolant medium from within the interior of the vehicle to pass through the porous heat shield and out into the high temperature boundary layer of gas. Its effectiveness will be due to the following two conditions:

1. The large wetted area within the multitude of pores within the subliming heat shield results in a high heat exchange between the coolant and the skin.

2. The effect on the boundary layer of the injected medium will have a cooling aptitude to reduce the magnitude of heat reaching the vehicle skin surface.

The analysis illustrates the built-in attribute of the subliming heat shield for transpiration cooling technique. Investigations have correlated the transpiration cooling factor α with variables involved in a system. The term α is a measure of the degree of efficiency of gas injected into the boundary layer and will range from 0 to 1.0. It is commonly presented as a function of molecular weight as used in the analysis.

The theory of transpiration cooling is briefly discussed to present the requirements for an empirical equation to predict its effectiveness. It is known that cooling the boundary layer stabilizes the laminar flow. The effect on the downstream flow by the upstream mass injection is analyzed for the contribution of the transpiration cooling factor.

STAGNATION EFFECT.

For steady state ablation the heat transferred from the external stream to the ablating surface is equal to the sum of the rate of absorption of heat by the ablator and the radiation from the surface. Thus, considering a unit area of surface

$$ST_o P_\infty U_\infty (H_{aw} - H_w) = \dot{m} H + q_r$$

where:

ST = Stanton No.

P_∞ = free stream density

U_∞ = free stream velocity

H_{aw} = adiabatic wall enthalpy

H_w = wall enthalpy

$\dot{m}$ = mass injection rate

q_r = heat radiated

H = heat absorbed by mass injected

A nondimensional ablation rate can be written in the form.

$$\dot{m}/P_\infty U_\infty = ST \frac{\Delta H}{H} - \frac{q_r}{H P_\infty U_\infty}$$

also

$$q_o = ST_o P_\infty U_\infty (H_{aw} - H_w)$$

Therefore effective heat of ablation q^* is

$$q^* = H/\left(\frac{ST}{ST_o} - \frac{q_r}{q_o}\right)$$

where:

ST = Stanton No. with mass injection

ST_o = Stanton No. without mass injection

q_o = heat transfered without mass injection

The significance of the blocking ratio, $\frac{ST}{ST_o}$ is apparent in the study. This ratio is a function of Reynolds number, Mach number, rate of ablation, properties of ablating species, and type of flow field.

Since $h_o \Delta H \quad h \Delta H + \dot{m} \alpha \Delta H$

$$\alpha = \frac{1 - \frac{h}{h_o}}{\frac{\dot{m}}{h_o}}$$

where h = heat trans coeff, with mass injection

h_o = heat trans coeff, without mass injection

Smaller the h/h_o, higher the α.

The value of α of gases injected can be obtained by measuring the change in heat transfer coefficient or skin friction and the amounts of gases of known properties and composition through porous model surface.

Most of the experimental data available was reduced in the form shown in Figure 4-2.

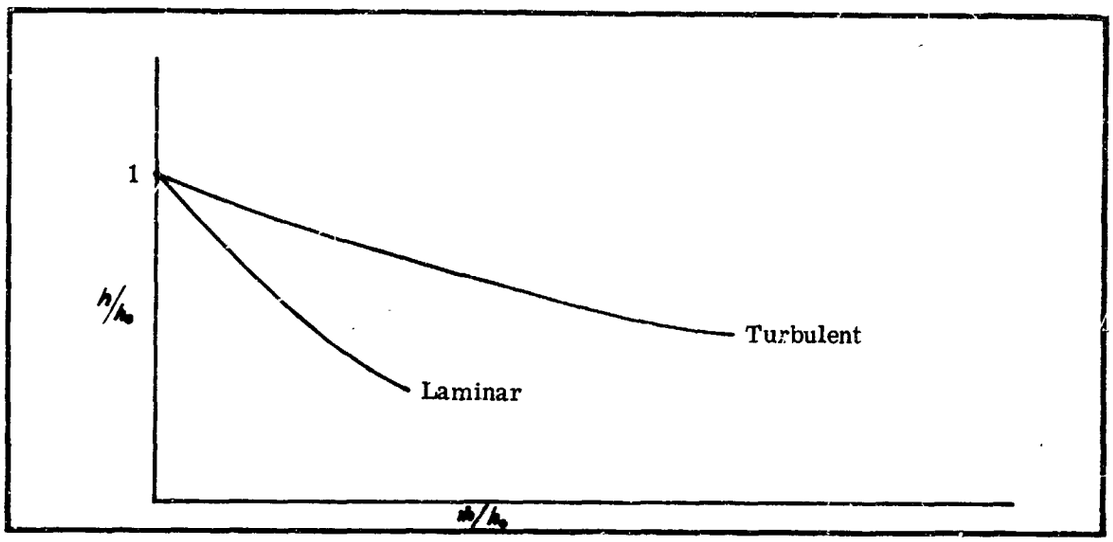

Figure 4-2. The Variation of h/h_0 With $\dot{m}/h_0$ for Boundary Layer Flow Conditions

There exist to date two empirical equations correlating with variables involved. Adams proposed the following:

For laminar boundary layer $\alpha_L = N(29/M_v)^a$

where

$0.67 \leq N \leq 0.72$

$0.25 \leq a \leq 0.4$

M_v is the molecular weight of gas injected
29 is the molecular weight of air

For turbulent boundary layer,

$$\alpha_T \approx \frac{1}{3}\alpha_L$$

It is seen from the laminar expression for α equation that the only variable considered is the molecular weight of the gas injected.

A second correlation for laminar was proposed by Faulder, and is related to h/h_0.

Derivation was based upon a vaporizing ablator where the term L is constant. The expression being,

$$\frac{h}{h_o} = \frac{1}{1 + 0.26[(29/M_V) + 2]^{0.84} \; \Delta H/L}$$

where:

M_V is the molecular weight of the gas injected

ΔH is the enthalpy difference across the boundary layer

L is the heat blockage by the system other than transpiration cooling

Whether the above equation could be applied to a plastic ablator where the debris has formed has not been correlated at present due in particular to the functional relationship between M_V and L with debris surface temperature.

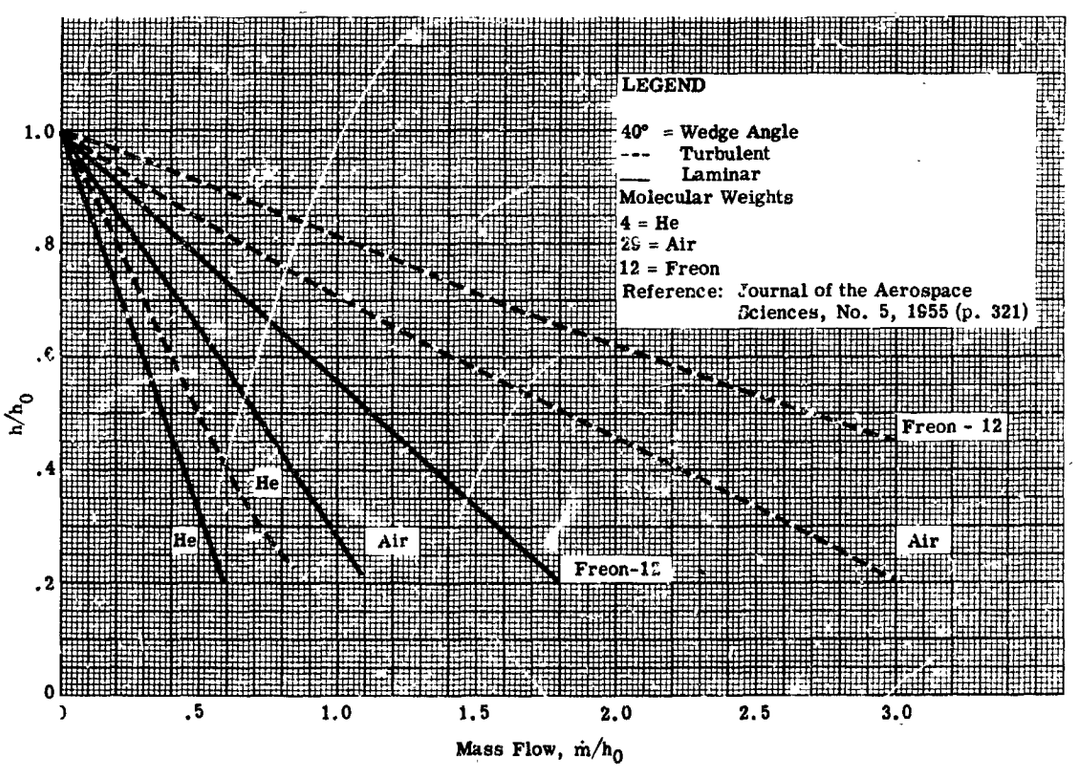

Figure 4-3. Effect of Molecular Weight of Gas Injected on Heat Transfer Coefficient

Figures 4-3, 4-4 and 4-5 illustrate effects of molecular weight of gas injected and flow conditions on heat transfer coefficients. No correlations on hemispherical models have been formed at the time of this article. However, it is reasonable to assume that same trend holds for the hemispherical models.

For laminar and turbulent cases, light gases are more effective than the heavy gases in reducing the coefficient, and a large reduction in coefficient results from rather small transpiration rates.

At high blowing rates from ablating surfaces the coefficients do not go to zero as indicated by a simple extrapolation. High blowing rates cause transition for laminar flow and appear to destroy boundary layer character for turbulent flow.

It therefore becomes difficult to make any general statements about the asymptotic values of the coefficient for very large blowing rates.

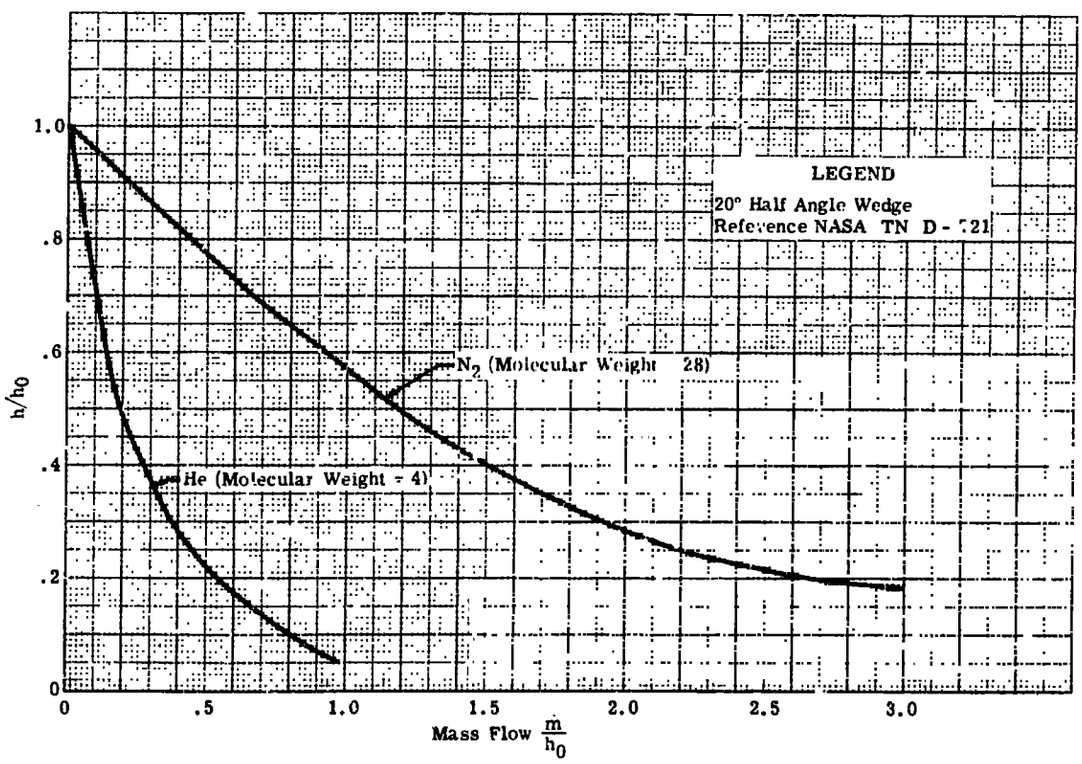

Figure 4-4. Effect of Weight of Gas Injected on Heat Transfer Coefficient

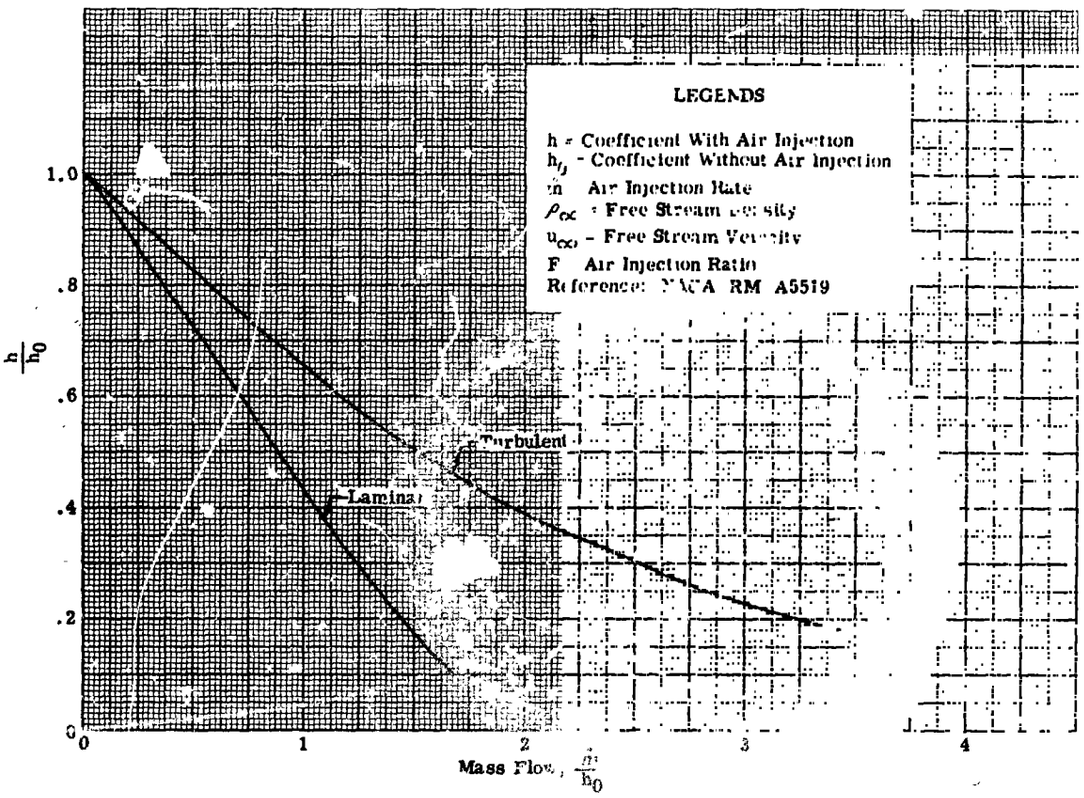

Figure 4-5. Effect of Transpiration of Air on Heat Transfer

DOWNSTREAM EFFECT.

Several studies have been made to determine the downstream effect upon stagnation-point mass injection. Experimental studies are limited, but a brief discussion can be given here.

Hoshizaki and Smith arbitrarily defined persistence factor

$$\alpha \equiv \left(\frac{A_t}{A_p}\right)\left(\frac{Q_p}{Q_t}\right)$$

where:

A_t is total protected surface area

A_p is the area of mass injection

Q_p is effective enthalpy on mass injection area

Q_t is total effective enthalpy of absorption.

It will be observed from the above expression that the more persistent the downstream effect of the coolant, the larger the Q_t will be and thus the smaller α will be. It is, however, considered a rather crude analysis.

Libby and Cresci made further studies using similarity parameters obtained from boundary layer analysis as defined below

$$N_1 \equiv (m_c / R_o \mu_{se}) \tilde{N}R_\infty^{-1/2}$$

$$N_2 \equiv N_{Nu} \tilde{N}R_\infty^{-1/2}$$

$$\bar{h}_c, \vartheta_w$$

where

m_c is mass flow of injected gas per unit time

R_o is nondimensionalizing length (hemisphere nose radius)

μ_{se} is viscosity coefficient of stream at external of the boundary layer

$\tilde{N}R_\infty$ is Reynolds number of free stream

N_u is Nasselt number

$\bar{h}_c$ is static enthalpy ratio of gas injected prior to injection

ϑ_w is T/T_{se} at wall

The above parameters permit the extrapolation of test results to other flow conditions provided that laminar flow prevails. Since the tests of Libby were carried out with a Mach number of 6.0, stagnation pressure of 600 PSIA it becomes questionable if the results can be applied to our simulation studies.

It is generally agreed that 20 ~ 30 times of mass injection at stagnation region is required to affect the downstream heat transfer to the magnitude that is obtained at stagnation region. Downstream heat flux will be increased when:

1. Mass injection at stagnation region causes turbulence at downstream.
2. Exothermic reactions in the boundary layer at downstream.
3. Turbulence caused by geometry of downstream.

BLANK PAGE

SECTION V

STRUCTURAL CONSIDERATIONS AND APPLICATIONS

STRUCTURAL APPLICATIONS.

DEVELOPMENT OF "THERMO-LAG" T-500 PUTTY FOR JOINT, GAP, AND EDGE FILLERS.

Development of techniques for the utilization of "THERMO-LAG" T-500 in the roles of joint, gap, and edge fillers were investigated to determine the optimum conditions for artificial curing. Successful application of "THERMO-LAG" for these purposes would qualify it for use in sealing gaps around the windows, hatches, and other orifices of a super-orbital vehicle. Techniques considered were those having utility under field conditions.

The T-500 used for the tests was compounded in the normal manner, and reduced to a doughlike or putty consistency by the addition of mothl ethyl ketone solvent. The test specimens were cylindrical patties, hand-shaped to a diameter of approximately two inches, and 5/8-inch thick.

Attainment of the desired degree of cure was determined by extracting unpolymerized solids from a vertical cross-section of the cured specimen through a predetermined procedure using methyl ethyl ketone. Evaporation of the solvent from the test specimen, induced by a thermonic heating device, left a residue of soluble solids. The percentage of solubles was calculated by determining differences in weight and the weight of the unextracted sample. The measured value was used as an index in determining the degree of cure attained by the "THERMO-LAG" T-500 putty. An inverse relationship existed between the percentage of solubles present and the degree of polymerization of the organic bonding agent, caused by the artificial cure technique.

INFRARED CURING.

This technique utilized a bank of four 375-watt, 115/125-volt Westinghouse infrared heat lamps. The uncured patties were exposed to these lamps for varying periods of up to eight hours. The specimens were placed in a horizontal position directly beneath the face of the lamps, thus assuring uniform exposure.

After exposure the degree of cure was determined by the method of extraction described previously. The data is presented in Table 5-1.

Exposure Time	Percent Solubles at 6-inch Exposure Distance	Percent Solubles at 12-inch Exposure Distance
0	24.9	24.9
1	19.8	24.1
2	7.3	18.9
3	9.2	9.2
4	8.2	6.6
5	4.9	-
6	-	7.5
7	4.4	-
8	5.9	9.1

Table 5-1. Degree of Artificially Induced Cure by Infrared Source

The presented data indicates that a more rapid cure was obtained at a 6-inch exposure distance. However, two disadvantages occurred at this exposure level, in that salt sublimation was observed, and some blistering occurred on the top surface of a few of the patties. At a 12-inch exposure distance, neither of these two phenomena were observed. The exposure distance, as a criteria, will be investigated if the infrared technique warrants continued study.

Patties cured for periods exceeding three hours displayed a small amount of salt in the evaporate. The formation caused an increase in the above calculated percentage values. For the 12-inch exposure distance, the tabulated data indicates a four hour period as adequate to cure the T-500 putty patties.

ELECTRICAL HEAT INDUCED CURING.

A resistance heating method to cure T-500 putty patties was investigated in the screening process. The conductive element was a graphite string obtained from a carbon fabric, 24 grams per square foot, manufactured by National Carbon Company, Union Carbide Corporation. The T-500 putty patty was sliced in half in a plane parallel to the two inch diameter dimension. The graphite string was sandwiched in between the putty slices in an 'S' shape to allow for a large heating area. The putty sandwich was kneaded together to form the original patty size. The carbon string was equidistant from both surfaces of the patty and

in a plane parallel to the two inch diameter dimension. The ends of the 'S' shaped graphite string were connected to a variable AC transformer with small battery clips. A given current was applied over a one hour period. Both current and voltage readings were recorded. The degree of cure was determined by the previously described extraction method. The data is presented in Table 5-2.

Exposure Time (Hr)	Amperes (AC)	Voltage (AC)	Percent Solubles
0	0.0	0.0	24.9
1	0.3	29.6	21.3
1	0.5	32.6	16.2

Table 5-2. Degree of Electrical Heat Induced Cure (Single Graphite String)

The above percentage solubles values indicate that little curing occurred. Application of current in excess of 0.5 amperes caused the carbon string to burn through. An examination of the interior of each patty indicated the presence of voids adjacent to the position occupied by the graphite strings. White salt accumulated on the surface of the voids at a heating current of 0.5 amperes. Some salt sublimation was observed at the point of entrance of the carbon string into the patty during the course of the experiments. The above phenomena can be contributed to high hot-spot temperatures.

An attempt to minimize the above disadvantages was made by embedding two graphite strings in a T-500 putty patty. For the test the patty was cut into thirds. Each graphite string was sandwiched between freshly cut surfaces in the shape of an 'S'. The 'S' shapes were arranged so that one laid cross-ways on top of the other with a one-third section of putty in between. The ends of the graphite strings were connected together to form an 'S' shaped parallel circuit. Current was applied in the same manner as described above. Voltage and current readings were taken and the degree of cure determined by the selected method. The data is presented in Table 5-3.

The tabulated solubility values indicate that little curing took place. In general, the same observations were noted as described for the single carbon string system. However, the size of the voids was observed to have decreased and no salt accumulation was visible. The conductive element technique does not warrant continued study as a method to cure T-500 putty.

CHEMICALLY ACCELERATED CURING.

The choice of a chemical accelerator was investigated as a method of curing T-500 putty. The technique involves the addition of chemical accelerators to the uncured T-500 putty.

The accelerator catalyzes and/or reacts with the organic bonding agent in the putty to cause polymerization or curing.

To date, three accelerators were tested in T-500 putty. The quantities used were obtained from published formulations on Hycar Polymers. Those used were:

1. Accelerator 808, a condensation product of butyraldehyde and aniline.

2. Thiuram M, tetramethylthiuram disulfide.

3. Accelerator 833, a condensation product of butyraldehyde and butylamine.

The above three are manufactured by E. I. DuPont De Nemours and Company, Elastomer Chemicals Department, Wilmington, Delaware.

The accelerators were mixed in the putty with a pestle until a uniform, homogeneous mix occurred. The mix was shaped by hand into cyclindrical patties of the previously described dimensions. The shaped patties were allowed to age in the laboratory at room temperature for definite time intervals. After aging, vertical cross-sections of each patty were extracted with methyl ethyl ketone to determine the degree of cure. The data is presented in Table 5-4.

The tabulated results indicate that Accelerator 808 and Thiuram M had no effect on curing. The first row of data, for no additive, is given for comparison. Accelerator 833 appeared to aid curing, but only after aging for 79.5 hours.

The process of selecting an optimum artificial curing technique for T-500 putty, facilitating its intended application, will continue into the next quarterly reporting period.

ATTACHMENT TECHNIQUES.

Species selection studies were performed to determine the bonding technique most suitable over the 0°F - 300°F temperature range. Five general catagories of surface treatment

Exposure Time (Hr)	Amperes (AC)	Voltage (AC)	Percent Solubles
0	0.0	0.0	24.9
4	0.3	12.0	19.8
4	0.4	17.0	17.7

Table 5-3. Degree of Electric Heat Induced Cure (Double Graphite Strings)

Additive	Quantity Present*	Aging Time (Hours)	Percent Solubles
0	0	0	24.9
Accelerator 808	2	20.5 80.0	20.8 20.6
Thiuram M	3.5	20.0 79.5	20.5 19.9
Accelerator 833	2	20.5 79.5	19.6 12.6

*Parts/100 parts rubber (Based on rubber in organic binder used in T-560 putty formulation).

Table 5-4. Degree of Chemically Accelerated Cure

were studies, and were reported, together with their application proc[illegible], in the Progress Reports for the months of January and February, 1963.

Of the catagories, three were mineral acids, reverse etch treated. The mineral acids used were chromic acid, sulphuric acid, and sulphuric acid plus phosphoric acid. Although a previous test using a nitric or sulphuric concentrate gave better adhesion, such treatment involves the risk of excessive hydrogen and the embrittlement of the steel. The mineral acids were tested at temperatures of 77°F, 150°F, and 300°F.

The results of some bond shear strength tests are presented in Figure 5-1.

Further study of the methods of surface treatment indicate the desirability of sandblast treatment.

Results of bond, shear, and tensile tests performed on sprayed "THERMO-LAG" T-500, using the mineral acid reverse etch, sandblast, and clean treatment techniques are presented in Figures 5-2 through 5-11.

SECONDARY BONDING.

Studies to determine the adhesive most suitable to meet the conditions imposed by the temperature environment which varies from -150°F to 300°F were conducted on five general catagories of adhesives. The results of these studies, together with their surface treatment techniques, were contained in the Progress Report for the month of January 1963. The entities tested were flexible materials of a rubber nature such as polysulfides and

silicones, semiflexible materials such as urethanes, and rigid, almost glassy, materials such as epoxies and phenolics.

These materials were subjected to preliminary screening tests using aluminum "T"'s scratched on 1-7/8" x 2" surface specimens. The adhesives were then plentifully applied to both faces of the "T" by brush. The initial cure was at 300°F for one-half hour. Some specimens required higher curing temperatures, as recorded.

The selection process eliminated Epoxylite 810, requiring the choice of another rubber adhesive. During this process three phenolics, one silicone-phenolic, one epoxy-phenolic, two epoxies, and one polysulfide were checked. The epoxies appear to be of questionable value at temperatures below 0°F.

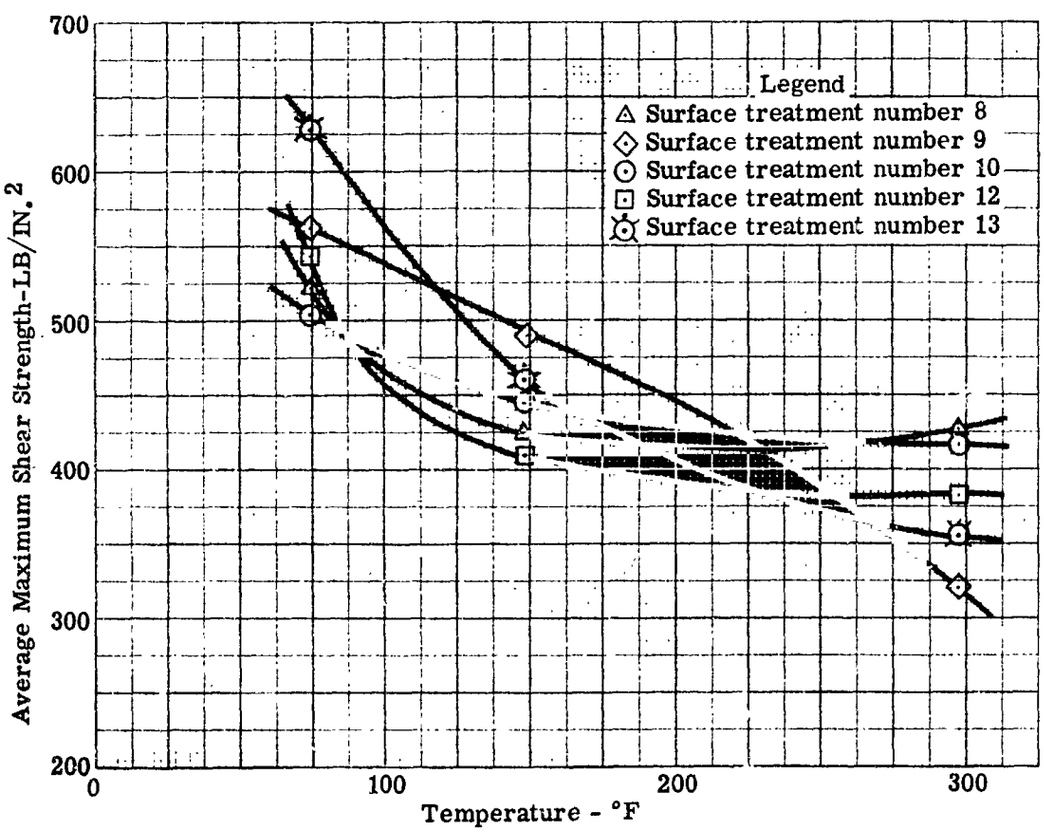

Figure 5-1. Effect of Surface Treatment on Bond Shear Strength

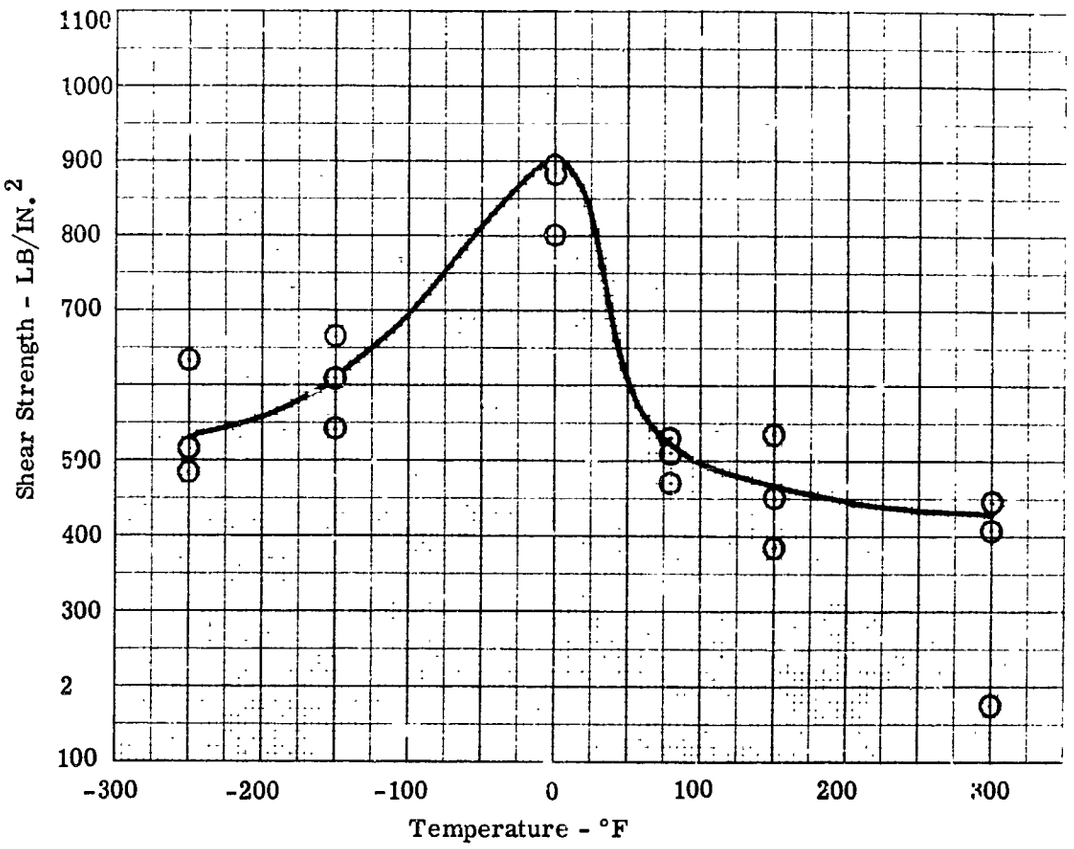

Figure 5-2. Bond Shear Test for Mineral Acid CrO_3 Surface Treatment

During the next quarterly reporting period screening efforts will be continued on the cementing of molybdenum steel, PH-15-7, to the aluminum "T"'s, and also on the cementing of the preformed "THERMO-LAG" material to the steel specimens for the bond shear and tensile tests.

STRUCTURAL ANALYSIS.

STRUCTURAL MODEL. An analysis is presented of slab stresses encountered in air-free infinite composite plates subjected to a single-dimensional heat flow normal to the plate. It is proposed that a truss network be substituted for the material in order to facilitate the calculation of discontinuity of stresses to compensate for the effects of local contour and bond flexibility on heat shield analysis.

Substantiation for this proposed substitution is supplied by the problem of an elestic slab bonded to a rigid base, and subjected to a constant temperature change, and analyzed by the methods of minimum potential energy and complementary energy. The potential energy method was chosen to show the displacements occuring in the truss, while the complementary energy method was chosen for the stresses. Thus, it is evident that if acceptable results are produced through incorporation of the truss analogy, then the extension of the same analogy to problems involving varying temperatures and material properties would be indicated.

A number of truss analysis results are included together with the analysis of the structural model. Included in the study were single and double diagonal truss networks, and networks of varying stiffness ratio members.

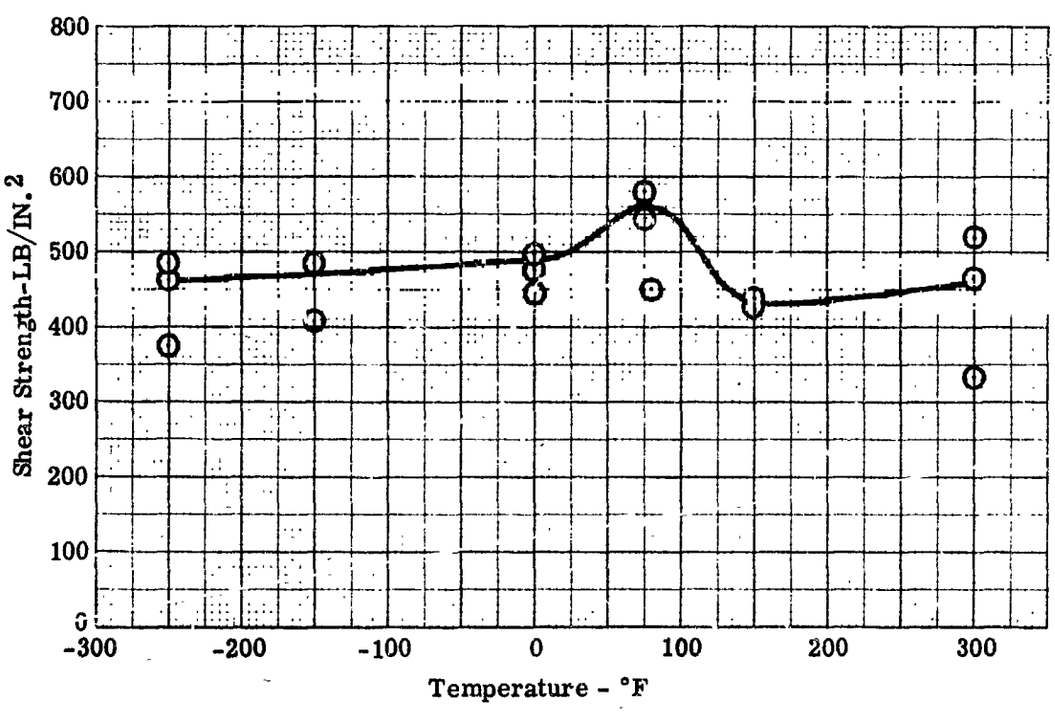

Figure 5-3. Bond Shear Test for Mineral Acid H_2SO_4 Surface Treatment

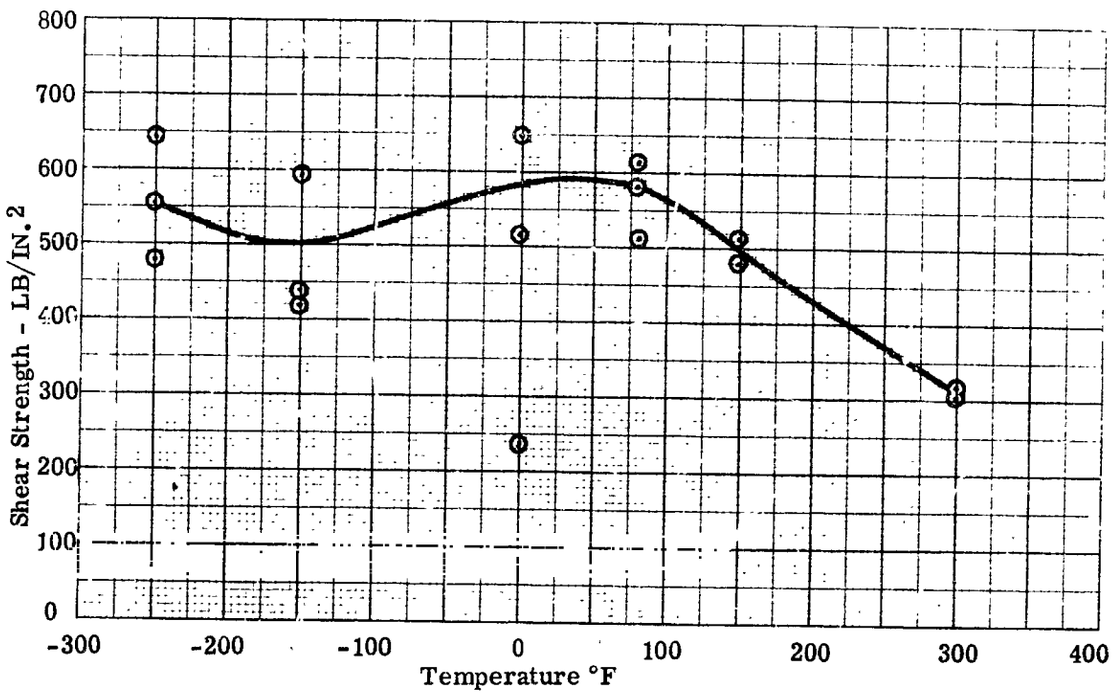

Figure 5-4. Bond Shear Test for Mineral Acid $H_3PO_4 \cdot H_2SO_4$ Surface Treatment

RESULTS OF TRUSS ANALYSIS.

The following paragraphs contain the results of the truss analysis of an elastic slab bonded to a rigid substructure.

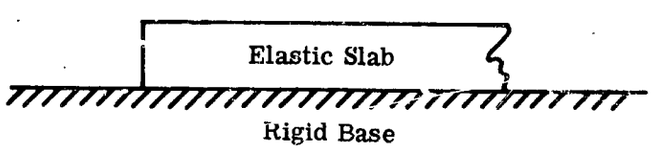

The elastic slab was assumed to be subjected to a constantly changing temperature and the resultant surface stresses were calculated.

A general method of analysis of the stresses developed in an elastic panel bonded to a honeycomb substructure and subjected to a varying temperature environment through its thickness is evolved. This method permits the material properties to vary as a function of the thickness. The model considers a free, infite composite plate. Due to its utilization as an aft body substructure, the analysis considers the honeycomb structure.

The truss solutions presented make it possible to investigate the stiffness ratios of a single diagonal truss network versus a double diagonal truss network, and a 2 x 4 matrix truss network versus a 2 x 5 matrix truss network.

Included in the considerations are comparisons of the external displacements of the elastic slab as calculated by the single diagonal network and by the single diagonal network methods versus a solution determined by the potential energy analysis method.

DISCUSSION OF ANALYSES AND CONCLUSION. An elastic, homogeneous heat shield bonded to a rigid substructure and subjected to a constantly changing temperature was analyzed through the application of the principles of minimum potential energy and minimum complementary energy. These solutions furnished a basis for comparison with the results derived from the truss network simplification of the same problem. If a relatively accurate evaluation of the stresses and deformations can be accomplished through application of the truss solution, conservation of time can be achieved in the calculations of more complex bonding and material combinations.

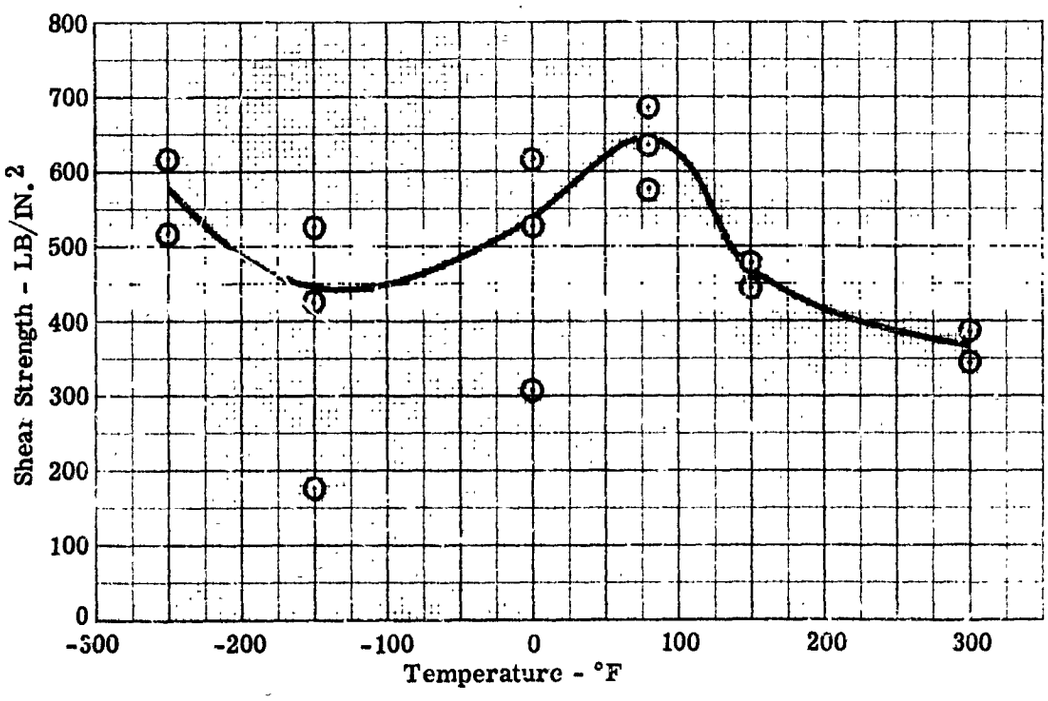

Figure 5-5. Bond Shear Test for Sandblasted Surface Treatment

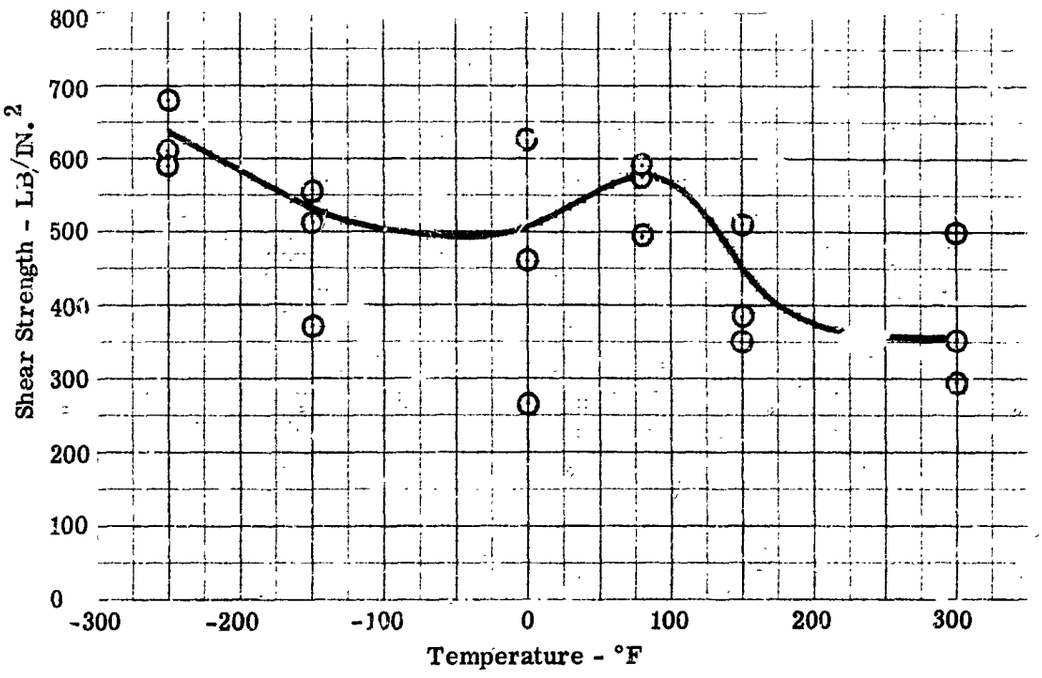

Figure 5-6. Bond Shear Test for Chemically Cleaned Surface Treatment

The more rigorous energy methods can become extremely complex in problems involving mixed stresses and strain boundary conditions. In addition, since the solutions in such cases require a systematic improvement in approximate values until a relatively unchanging solution is achieved, it becomes extremely difficult to utilize generalized geometrical variations and material properties in their solution. Due to these factors, the simplified truss solution becomes increasingly attractive as a method for evaluating more complex systems. However, it was felt that to proceed with the truss network method without knowledge of its applicability would not represent good engineering practice. Therefore it was felt imperative to expend the time and effort required to achieve a comparison of the truss solution of this particular problem with a solution obtained through the application of the standard techniques.

Both the interface stresses and the external displacements of the slab were calculated by the energy methods. These are shown in Figures 5-12 through 5-15. The principle of complementary energy was used for the approximate calculation of the interface stresses, the principle of potential energy for the external displacements.

In applying the principle of minimum potential energy through the use of the Rayleigh-Ritz method, it became necessary to select displacement functions which satisfied the given displacement boundary conditions of the problem, but contained some arbitrariness which allowed the energy to be minimized. By varying the degree of arbitrariness while maintaining a form similiar to the displacement functions, the final solution was obtained upon stabilization of the potential energy. Fourteen unknowns were required to achieve a stationary potential energy value.

A two term solution employing the complementary energy method has been completed but was not exact enough for an evaluation. Consequently, a comparison of these stresses with those obtained from the truss analogy are not shown in the results.

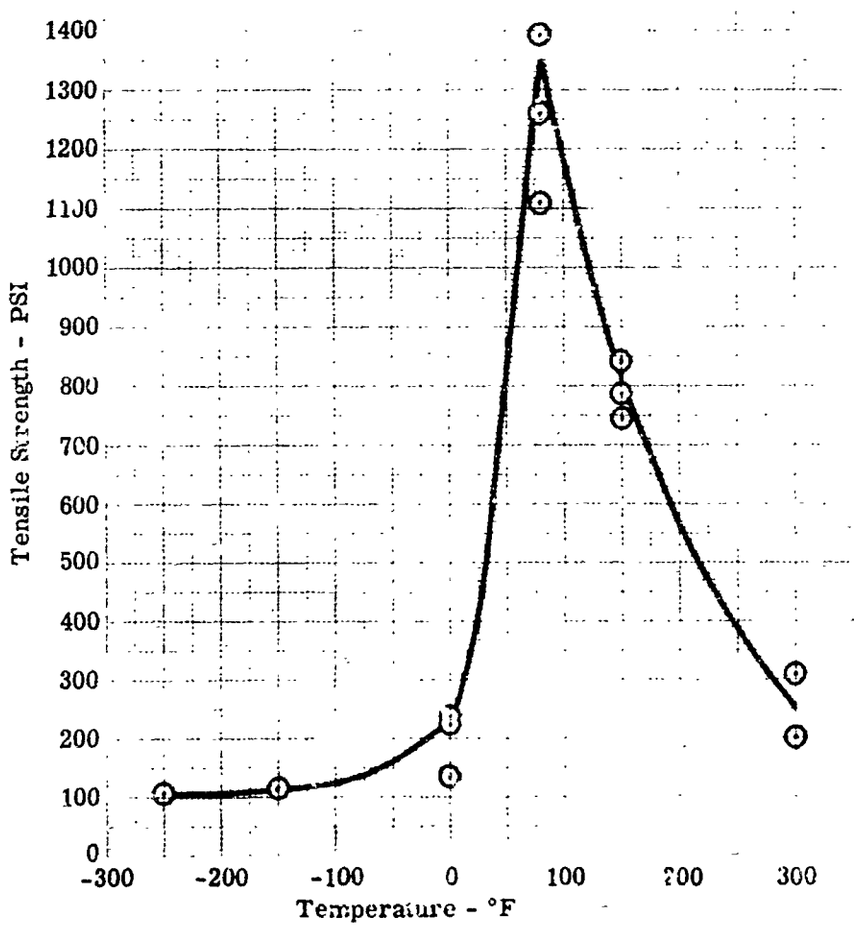

Figure 5-7. Tensile Test for Mineral Acid CrO_3 Surface Treatment

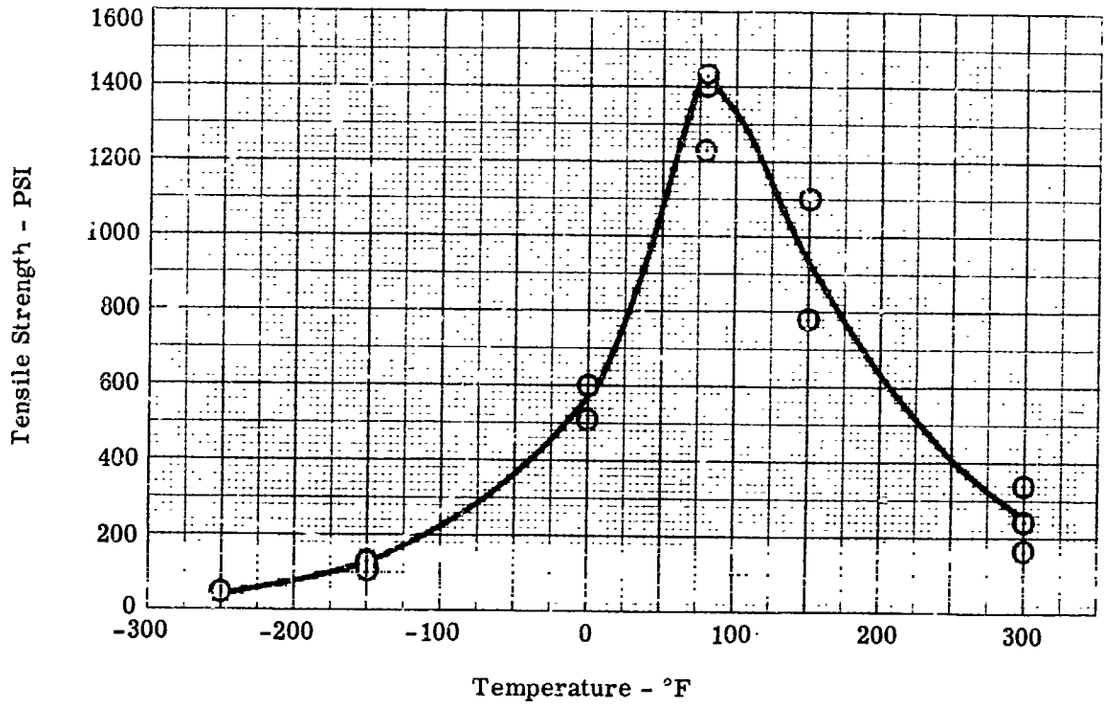

Figure 5-8. Tensile Test for Mineral Acid H_2SO_4 Surface Treatment

A comparison of displacements of both the single and double diagonal truss network with the potential energy solution is illustrated in Appendix A. As shown in Appendix A, the double diagonal truss solution produces the more realistic displacements and, for such a coarse truss network, the results were surprisingly good. The double diagonal truss network will probably be considered exclusively in future work.

The information in Appendix A also compares interface stresses for various truss networks. Increasing a single diagonal truss network to a double diagonal network reduces peak stresses. Maintaining the same geometry but varying the stiffness of the members has little effect on interface stresses. This indicates that Poisson's Ratio has very little influence on this problem. This will be further confirmed by varying Poisson's Ratio in the energy solutions and noting the results.

It should be noted that complete agreement of the truss analogy and the energy methods will not provide sufficient evidence of the validity of the truss analogy since the energy methods are only approximate. For future study, consideration will be given to comparison of the truss network with either a classical solution such as a plate with a hole, subjected to an axial load, or a Lame Network.

ANALYSIS OF THE STRUCTURAL MODEL.

The problem of an elastic, homogeneous slab bonded to a rigid substructure and subjected to a constant temperature change was analyzed by applying the principle of minimum potential energy and the principle of minimum complementary energy. A more detailed description of these theorems can be found in Sokolnikoff's, "Mathematical Theory of Elasticity", and in Report No. P-61-17 by Gerald F. Gillis for Rohm and Haas Company. An important application of these energy principles relates to their use in obtaining approximate solutions.

The energy principles were applied through use of the Rayleigh-Ritz method. This method assumes that a nearly true solution can be represented by a set of functions involving a limited number of constants. These constants are then obtained by minimizing the energy.

The Rayleigh-Ritz method was applied to the principle of minimum potential energy by specifying displacements as a function of undertermined constants such that the displacement boundary conditions were satisfied. Continuity of the assumed displacements guarantees

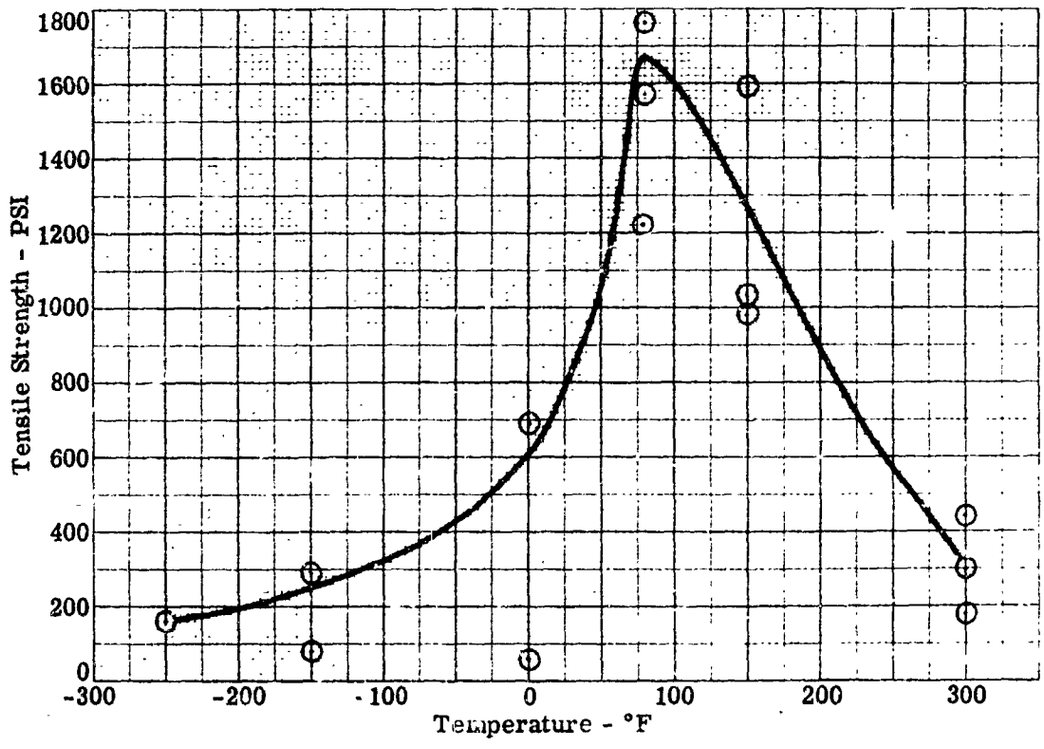

Figure 5-9. Tensile Test for Mineral Acid H_3PO_4. H_2SO_4 Surface Treatment

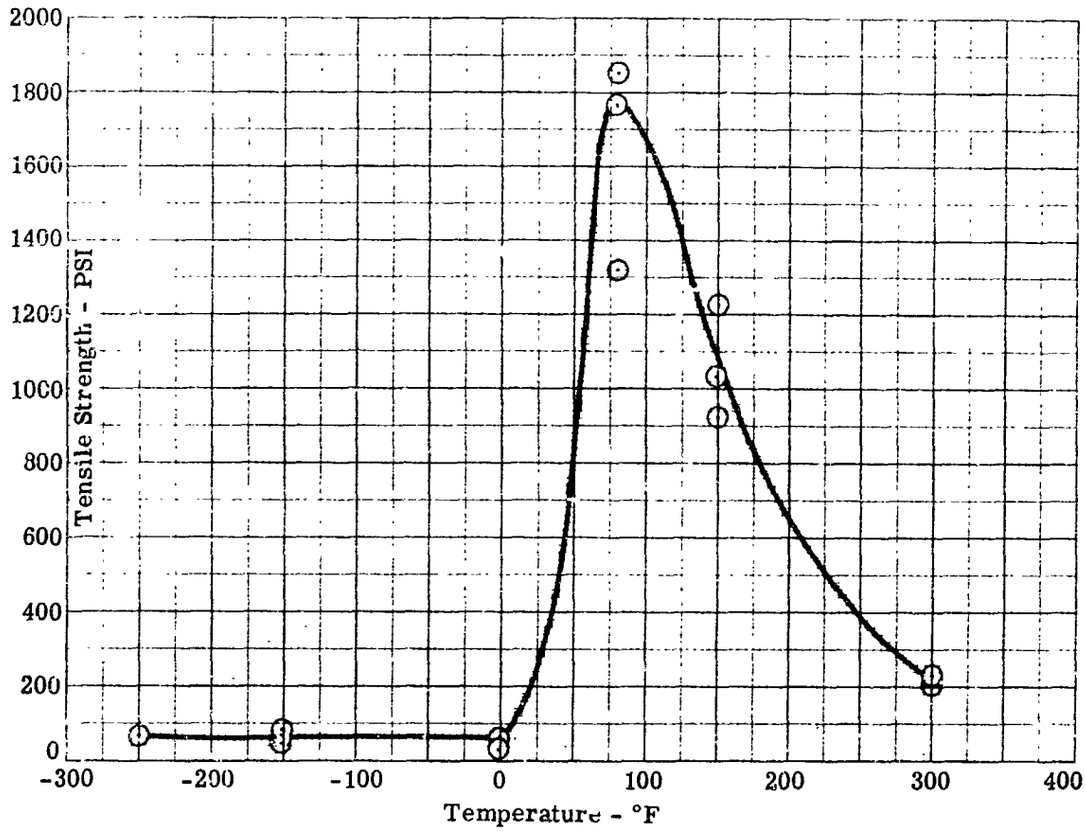

Figure 5-10. Tensile Test for Sandblasted Surface Treatment

satisfaction of the compartibility equations. These displacements were then substituted into the potential energy expression and the constants were determined by minimizing the energy. The displacements obtained by substituting the values of these constants into the assumed functions will not, in general, exactly satisfy the equilibrium equations. However, even though the accuracy of the associated stresses is likely to be poor, this method can provide a good approximation to the displacements.

In applying the Rayleigh-Ritz method to the principle of minimum complementary energy, the stresses were assumed to be functions of undertermined constants such that the equilibrium equations and stress boundary conditions were identically satisfied. The stresses were then substituted in the complementary energy expression and the unknown constants were evaluated by minimizing the energy. These stresses would approximately satisfy the compatibility equations but, since these equations were not exactly satisfied, the accuracy of any displacements subsequently determined from such a solution would be inadequate.

To summarize the two energy principles, the theorem of minimum potential energy was applied in cases where displacements and strains were required and the theorem of minimum complementary energy was best suited for the determination of stresses.

A method was developed for calculating the stresses occurring in the center of a large, unrestrained composite plate consisting of an elastic slab on a honeycomb substructure, subjected to a varying temperature differential through its thickness. The material properties were allowed to vary as a function of the temperature. Since it was assumed that plane sections remained plane throughout the temperature change, the strain could consequently be written in the following manner: $\epsilon = \epsilon_{\cdot} + Kz$

where $\epsilon_{\cdot}$ and K are constants and z is the distance normal to the plate. The unknowns could be determined thru Hooke's Law and the fact that no net load or moment can occur through a cross section. The stress at any point appears as $\sigma = E(\epsilon_{\cdot} + Kz)$

where E is the modulus associated with z . The symbols appearing here and in the following equations may be found in Appendix B.

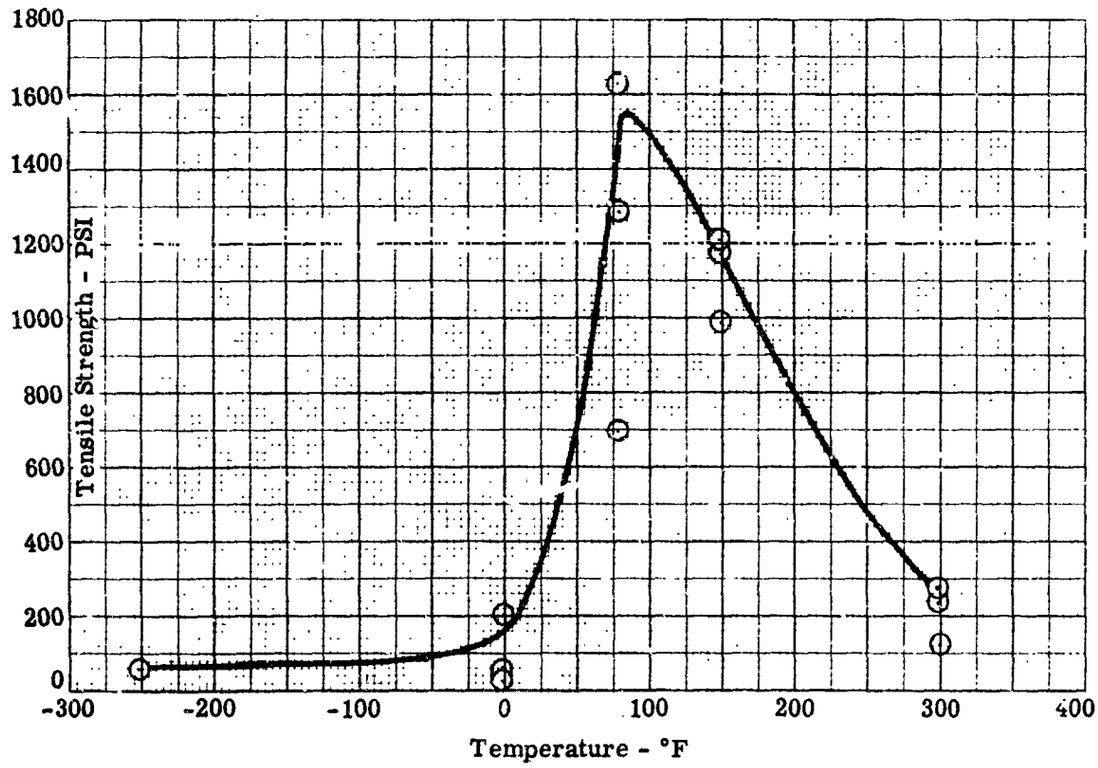

Figure 5-11. Tensile Test for Chemically Cleaned Surface Treatment

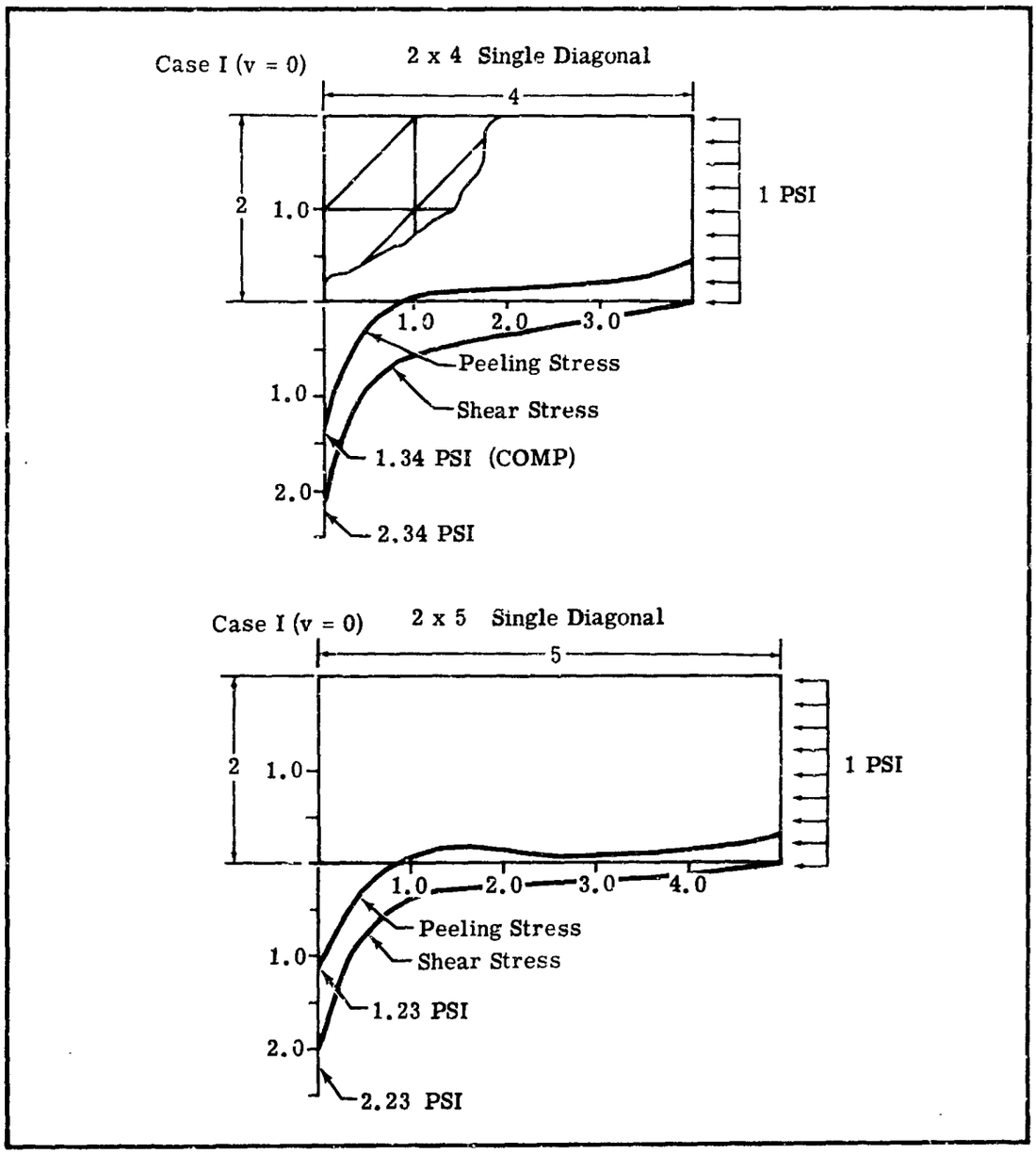

Figure 5-12. Comparison of Stresses (Sheet 1 of 2)

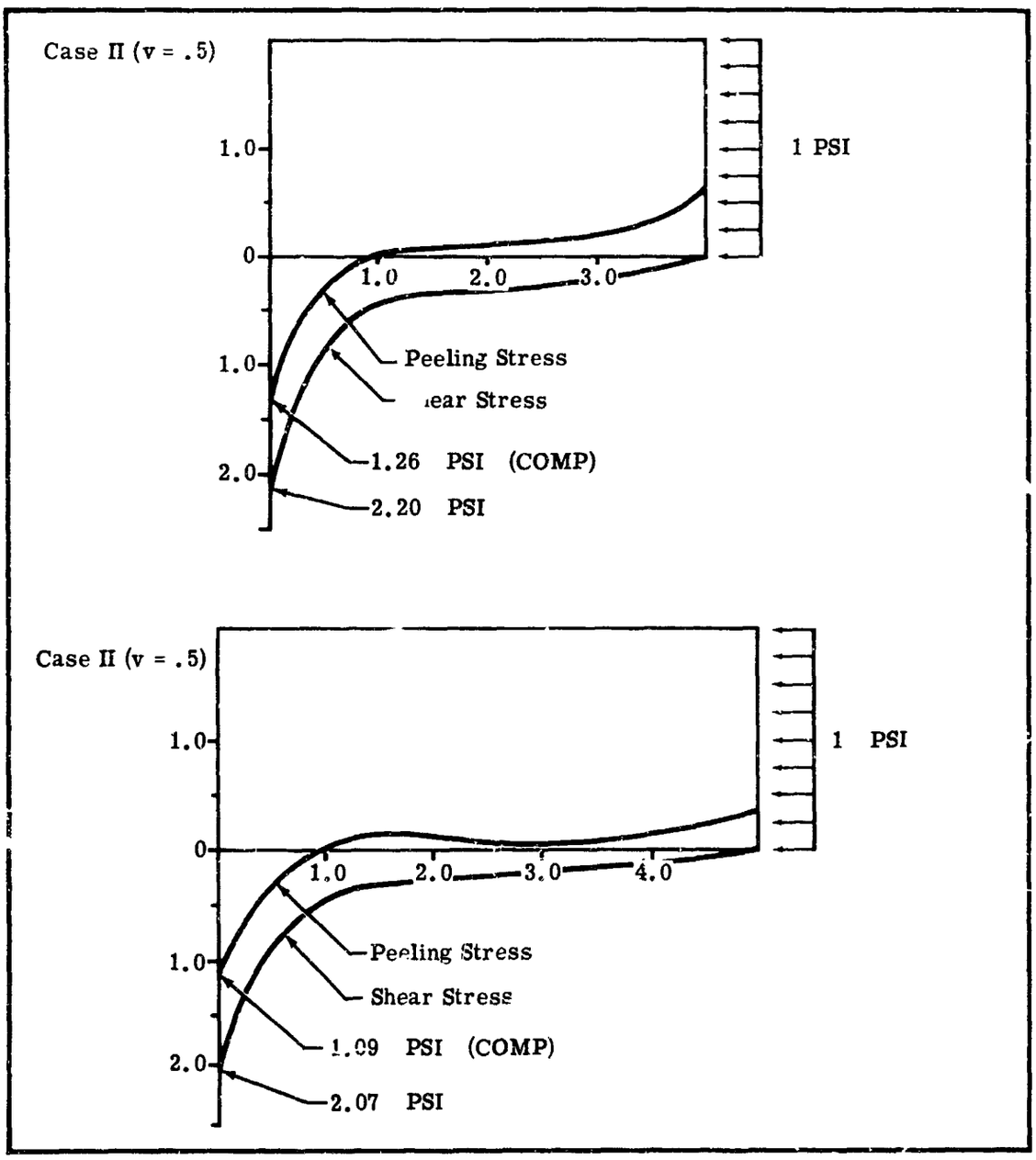

Figure 5-12. Comparison of Stresses (Sheet 2 of 2)

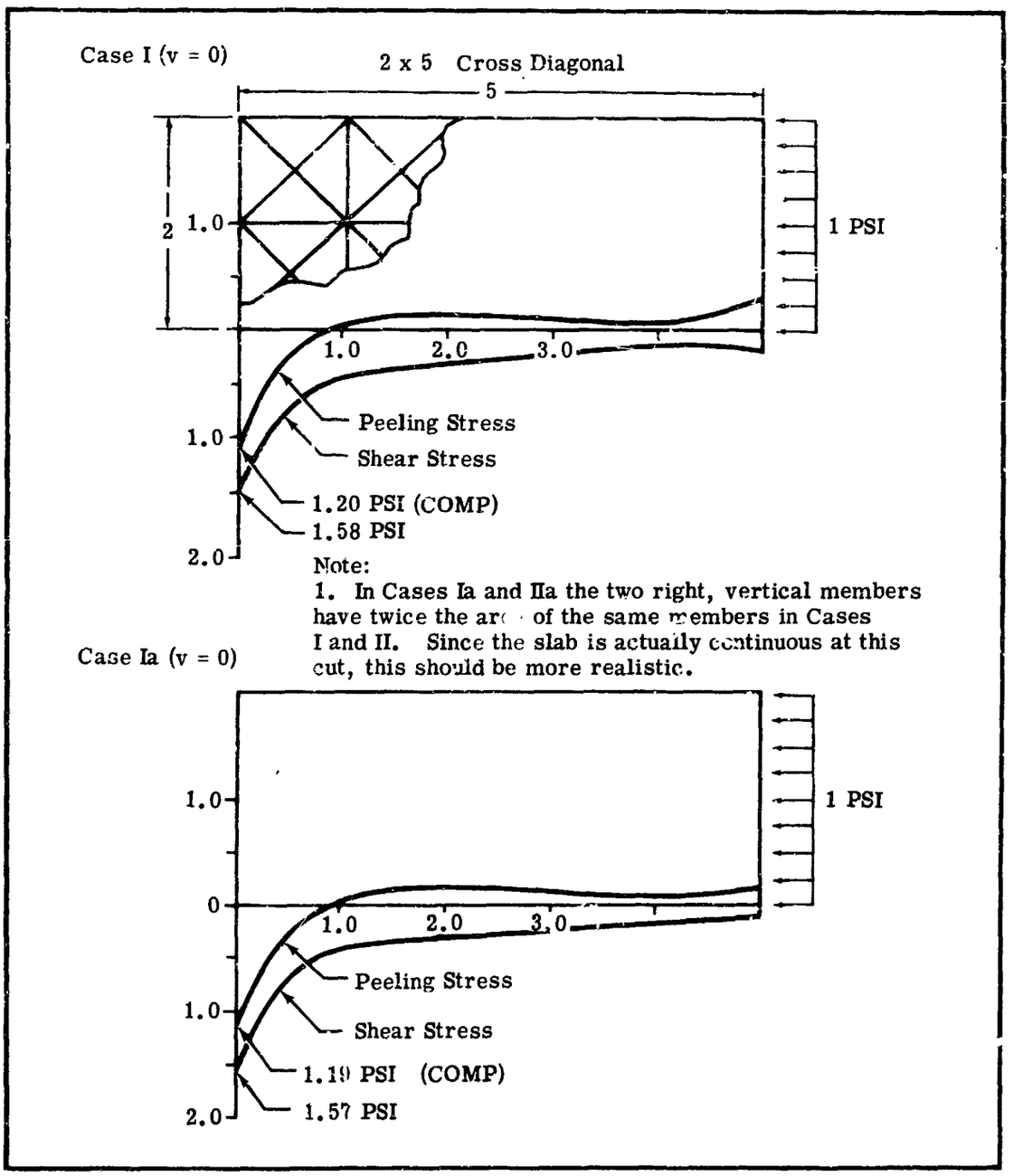

Figure 5-13. Comparison of Stresses (Sheet 1 of 2)

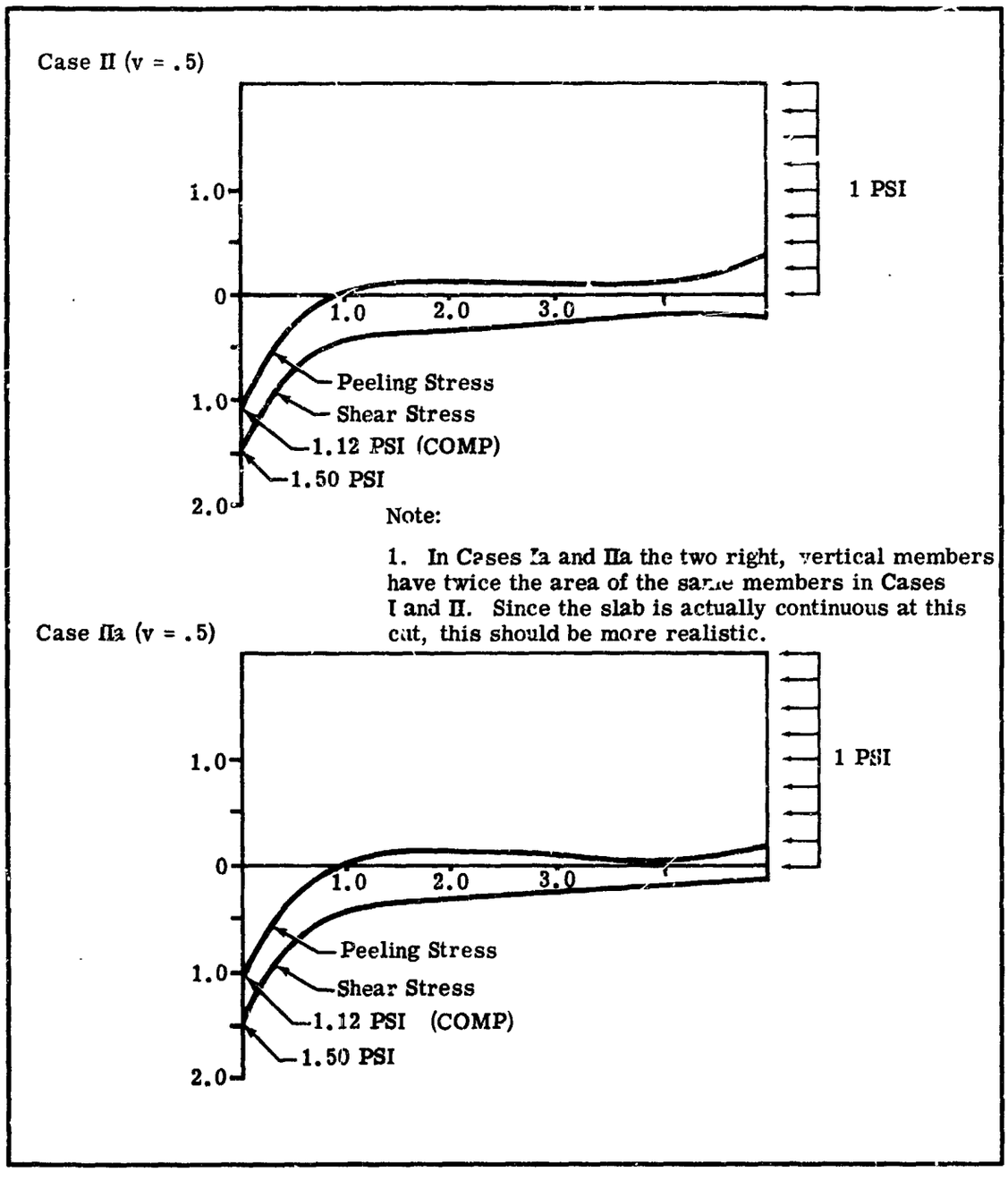

Figure 5-13. Comparison of Stresses (Sheet 2 of 2)

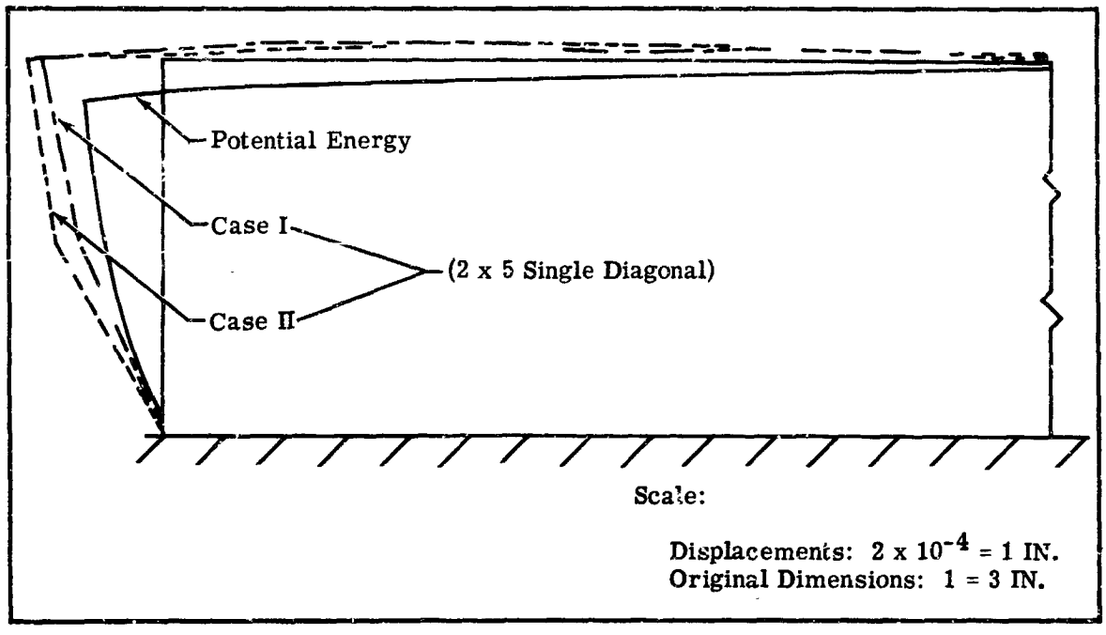

Figure 5-14. Comparison of Displacements

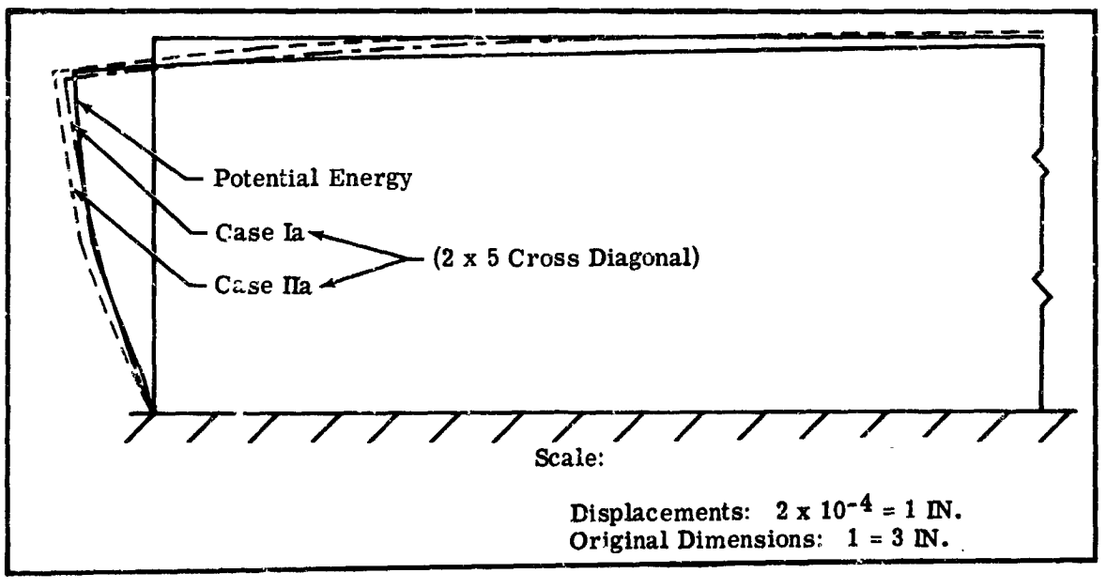

Figure 5-15. Comparison of Displacements

RELATIVE STIFFNESS OF TRUSS MEMBER FOR CROSS DIAGONAL.

In order to achieve a better simulation of the material continuum of the elastic slab, a cross diagonal truss network was considered in place of the single diagonal, referenced in the first Quarterly Report. In the cross diagonal truss it became necessary to also determine the relative areas of the diagonals to the horizontal and vertical members. These areas were determined by matching the shear properties of the truss to the material continuum tensile properties. Matching of both shear and tensile properties for all values of Poisson's Ratio was not feasible. Since this primarily represents a problem of shearing the load into the substructure, the shear properties of the truss were made equal to those of the material continuum.

It was then possible to apply a shear load to both the truss and an element from the elastic slab, giving,

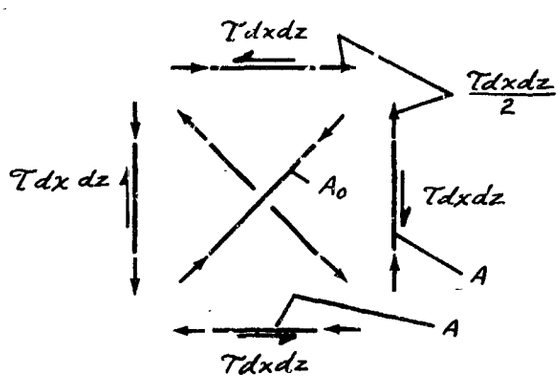

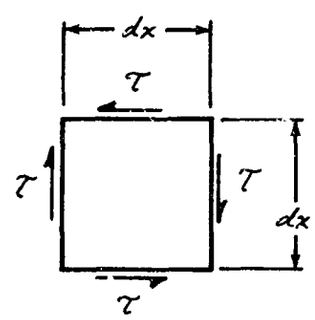

dz Thick

The displacement across the corners of a square element is: $\Delta_E = \frac{\sqrt{2}(1+\nu)\tau dx}{E}$

The displacement of one of the diagonals of the truss network may be calculated as follows:

$$\Delta_T = \frac{P_L}{\Delta_E}$$

where this would be the displacement of a diagonal,

$$\Delta_T = \frac{\left(\frac{\sqrt{2}\,\tau dx dz}{2}\right)\left(\sqrt{2}\, dx\right)}{A_0 E} = \frac{\tau dx^2 dz}{A_0 E}$$

Equating the displacement of the truss diagonal to that of the homogeneous element,

$$\Delta_E = \Delta_T$$

$$\frac{\sqrt{2}\,(1+\nu)Tdx}{E} = \frac{Tdx^2dz}{A_0E}$$

$$A_0 = \frac{dxdz}{\sqrt{2}(1+\nu)}$$

At this phase it becomes necessary to define $dxdz$ in terms of A of the truss. To determine the loads in the truss members for an axial pull, the following use of the schematic was made,

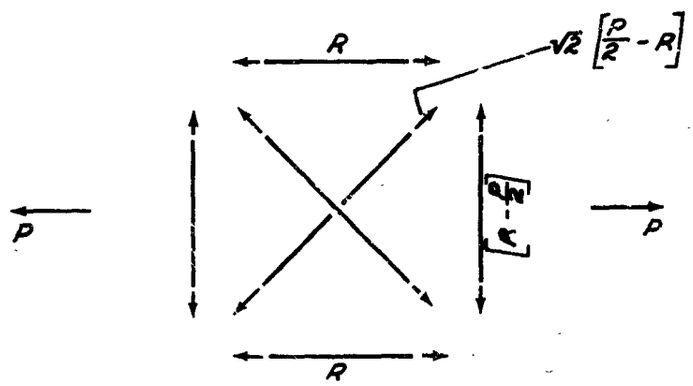

The internal strain energy of the system is, $U = \Sigma \frac{P^2L}{2AE}$

where P is the load in any member and L, A and E are the length, area and modulus of elasticity, respectively.

$$U = 2\left[\frac{R^2dx}{2AE}\right] + 2\left\{\frac{\left[R - \frac{P}{2}\right]^2 dx}{2AE}\right\}$$

$$+ 2\left\{\frac{\left[\sqrt{2}\left(\frac{P}{2} - R\right)\right]^2 \sqrt{2}\,dx}{2A_0E}\right\}$$

Minimizing the energy with respect to the unknown:

$$\frac{\partial U}{\partial R} = 0 = \frac{2Rdx}{AE} + \frac{2\left(R - \frac{P}{2}\right)dx}{AE} + \frac{4\left(\frac{P}{2} - R\right)(-\sqrt{2})dx}{A_0E}$$

Solving for R, $$R = \left[\frac{A_0 + 2\sqrt{2}A}{4(A_0+\sqrt{2}A)}\right]P$$

With the above expression for R the displacement in the direction of the load P could be determined and comparision made with a similar displacement for a homogeneous element, making use of the following diagrams:

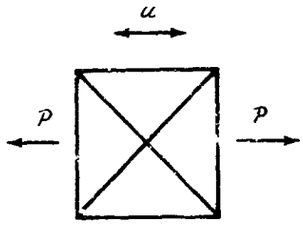

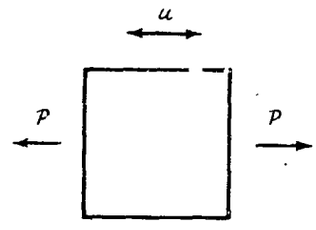

$$u = \frac{\left[\frac{A_0+2\sqrt{2}A}{4(A_0+\sqrt{2}A)}\right]Pdx}{AE} \qquad u = \frac{Pdx}{dxdzE}$$

Equating u's, $$dxdz = \frac{4\Delta(A_0+\sqrt{2}\Delta)}{A_0+2\sqrt{2}A}$$

The experssion was substituted into the previous experssion for A_0, giving

$$A_0 = \frac{dxdz}{\sqrt{2}(1+\nu)} = \frac{4A(A_0+\sqrt{2}A)}{(A_0+2\sqrt{2}A)\sqrt{2}(1+\nu)}$$

Solving explicitly for A_0 in terms of A, we have

$$A_0 = 2A\left[\frac{-\nu+\sqrt{\nu^2+2(1+\nu)}}{\sqrt{2}(1+\nu)}\right]$$

SIMULATING A HONEYCOMB WITH A CAP AND SHEAR WEB STRUCTURE.

In the analysis of an elastic slab on a flexible base (sandwich construction) it was necessary to simulate the sandwich construction (considered a honeycomb) by an analogous structure. In simulating honeycomb construction, it was felt that a cap and shear web type structure would provide an ideal analogy. The horizontal caps were analogous to the face material,

the shear webs to the honeycomb and the vertical caps to the compressive strength of the honeycomb. The properties of the honeycomb are assumed as follows:

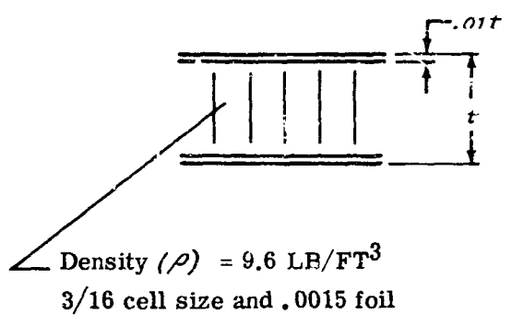

NOTE

The honeycomb sandwich is stainless steel throughout.

In determining the analogous cap and shear web structure for the sandwich honeycomb structure, the following program was followed:

Cap and shear web:

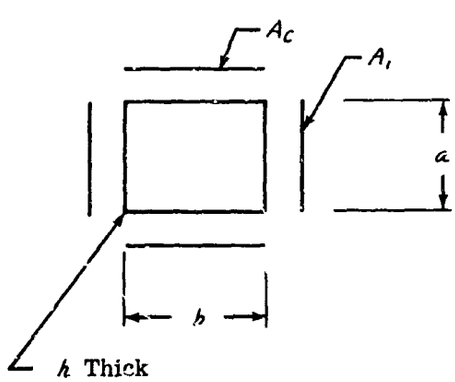

Honeycomb dz thick: $A_c = (.01t)dz = .010\,dz$

A_1 was made equivalent to solid material per unit of honeycomb.

Honeycomb area: $= \frac{b}{2} dz$

Density honeycomb: $(\rho_H) = .00556\ LB/IN^2$

Density steel: $(\rho_S) = .283\ LB/IN^3$

$$\frac{\rho_H}{\rho_S} = \frac{.00556}{.283} = .0196$$

$$A_1 = \left[\frac{b}{2} dz\right] .0196 = .98\left(\frac{b}{a}\right) A_C$$

Since $\frac{b}{a}$ would be known, A_1 was taken as a direct function of A_C. The shear web area would be determined also by the consideration of relative densities.

$$h = .0196\ dz$$

$$h = \frac{1.96}{a} A_C$$

To determine A_C for the cap and shear web as a function of A of the truss, the following analysis was made:

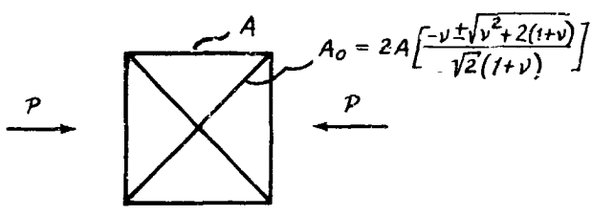

Elastic slab

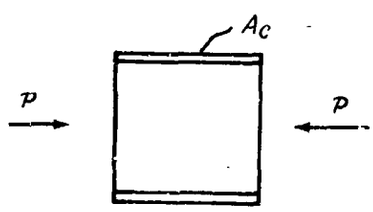

Cap and shear web

The load in the horizontal member of the cross diagonal truss would be,

$$R_T = \left[\frac{A_o + 2\sqrt{2}A}{4(A_o + \sqrt{2}A)}\right] P$$

Substituting for A_0,

$$R_T = \frac{1}{4}\left[\frac{2A\left(-\nu \pm \sqrt{\nu^2+2(1+\nu)}\right)+4(1+\nu)A}{2A\left(-\nu \pm \sqrt{\nu^2+2(1+\nu)}\right)+2(1+\nu)A}\right]P$$

$$R_T = \frac{1}{4}\left[\frac{2+\nu+\sqrt{\nu^2+2(1+\nu)}}{1+\sqrt{\nu^2+2(1+\nu)}}\right]P$$

Displacement

$$u_T = \frac{PL}{AE_T} = \frac{PL}{4AE_T}\left[\frac{2+\nu+\sqrt{\nu^2+2(1+\nu)}}{1+\sqrt{\nu^2+2(1+\nu)}}\right]$$

The displacement in the horizontal member of the cap and shear web being,

$$u_C = \frac{\frac{P}{2}L}{A_C E_C} = \frac{PL}{2A_C E_C}$$

The two displacements can be rated according to the displacements in the actual materials. The displacements were calculated as follows:

Elastic slab:

$$u_S = \frac{PL}{(dz\,dx)E_S}$$

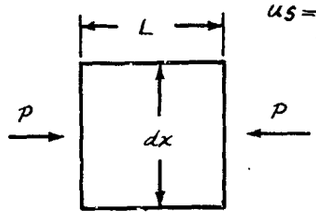

dz Thick

Honeycomb:

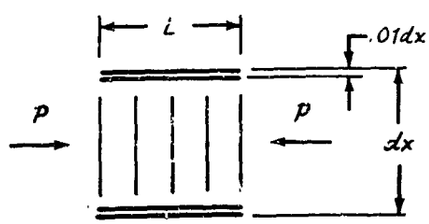

dz Thick

$$u_H = \frac{\frac{P}{2}L}{(.01dx\,dz)E_H}$$

Therefore, equating P's, $$\frac{u_S\, dz\, dx\, E_S}{L} = \frac{u_H \cdot .02\, dx\, dz\, E_H}{L}$$

$$\frac{u_H}{u_S} = 50\,\frac{E_S}{E_H}$$

The displacements for the idealized structures were then substituted in the equation, giving,

$$50\,\frac{E_S}{E_H} = \frac{u_H}{u_S} = \frac{u_C}{u_T} = \frac{\dfrac{PL}{2A_C E_C}}{\dfrac{PL}{4AE_T}\left[\dfrac{2+\nu+\sqrt{\nu^2+2(1+\nu)}}{1+\sqrt{\nu^2+2(1+\nu)}}\right]}$$

$$\frac{E_T}{E_C} = \frac{E_S}{E_H}$$

$$50 = \frac{2A\left(1+\sqrt{\nu^2+2(1+\nu)}\right)}{A_C\left(2+\nu+\sqrt{\nu^2+2(1+\nu)}\right)}$$

or,

$$A_C = \frac{A\left(1+\sqrt{\nu^2+2(1+\nu)}\right)}{25\left(2+\nu+\sqrt{\nu^2+2(1+\nu)}\right)}$$

The energy stored in a shear web can be visualized by use of the diagram:

t Thick

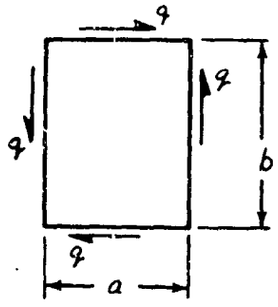

$$U = \frac{q^2}{2tG}\,ab$$

The energy stored in a beam loaded in the following manner can be presented by the expression:

$$U = \int_0^L \frac{\left(P - \frac{P}{L}x\right)^2 dx}{2AE} = \int_0^L \frac{P^2\left(1 - \frac{x}{L}\right)^2 dx}{2AE}$$

$$U = \frac{P^2}{2AE}\left[x - \frac{x^2}{L} + \frac{x^3}{3L^2}\right]_0^L = \frac{P^2}{2AE}\left[L - L + \frac{L}{3}\right]$$

$$U = \frac{P^2 L}{6AE}$$

MINIMUM POTENTIAL ENERGY METHOD APPLIED TO AN ELASTIC SLAB ON A RIGID BASE.

In order to help substantiate the previous work done with the truss analogy, the same problem was analyzed by the method of minimum potential energy. This method was used as a check on displacements only and should not be employed for the calculation of stresses. The particular analysis based on plane strain; the problem being presented by the stress diagram,

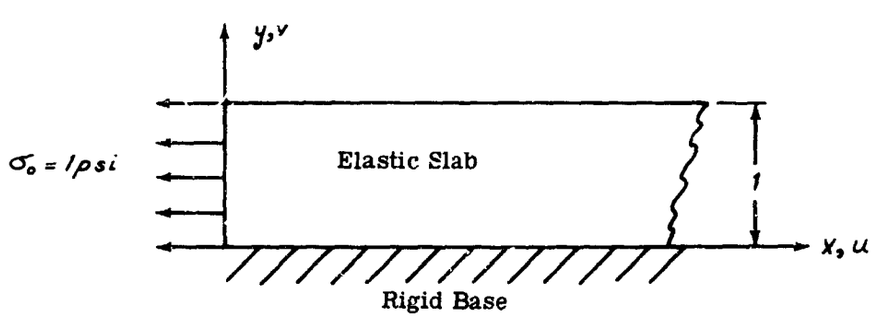

The slab has a unit thickness in the Z direction normal to the paper and is in a state of plane strain.

The above stress distribution shown on the slab was based on a constant temperature change throughout the thickness of the slab.

For the particular problem the potential energy V was defined as:

$$V=\int_0^1\int_0^\infty W\,dy\,dx-\int_0^1 Tu\,dy$$

where,
$$W=\tfrac{1}{2}\lambda(\epsilon_x+\epsilon_y)^2+G(\epsilon_x^2+\epsilon_y^2)+\tfrac{1}{2}G(\gamma_{xy}^2)$$

The symbol T, is the surface traction moving through the displacement u at $x=0$. In the problem $T=-1$.

It was stated previously that the displacements were chosen such that displacement boundary conditions were satisfied in an arbitrary manner by choosing the displacements as continuous functions of the condition of continuity of the material was satisfied.

The displacement boundary conditions became, $u=0$ and $v=0$ at $y=0$ and $x=0\to\infty$

The displacement functions chosen to satisfy this boundary condition are:

$$u=\left(\sum_0^2 A_i y^{i+1}\right)e^{-\alpha_1 x}+\left(\sum_0^2 B_i y^{i+1}\right)e^{-\alpha_2 x}$$

$$v=\left(\sum_0^2 C_i y^{i+1}\right)e^{-\alpha_1 x}+\left(\sum_0^2 D_i y^{i+1}\right)e^{-\alpha_2 x}$$

These two functions contain fourteen degrees of freedom. From these functions the strains became:

$$\epsilon_x=\frac{\partial u}{\partial x}=-\alpha_1\left(\sum_0^2 A_i y^{i+1}\right)e^{-\alpha_1 x}-\alpha_2\left(\sum_0^2 B_i y^{i+1}\right)e^{-\alpha_2 x}$$

$$\epsilon_y=\frac{\partial v}{\partial y}=\left[\sum_0^2 C_i(i+1)y^i\right]e^{-\alpha_1 x}+\left[\sum_0^2 D_i(i+1)y^i\right]e^{-\alpha_1 x}$$

$$\gamma_{xy}=\frac{\partial u}{\partial y}+\frac{\partial v}{\partial x}=\left[\sum_0^2 A_i(i+1)y^i\right]e^{-\alpha_1 x}+\left[\sum_0^2 B_i(i+1)y^i\right]e^{-\alpha_2 x}$$

$$-\alpha_1\left(\sum_0^2 C_i y^{i+1}\right)e^{-\alpha_1 x}-\alpha_2\left(\sum_0^2 D_i y^{i+1}\right)e^{-\alpha_2 x}$$

The derived strains were substituted into the internal strain energy expression and the displacement, u, at $x = 0$ was substituted into the external work expression. The resulting expression for the potential energy being,

$$
\begin{aligned}
V = \int_0^1\int_0^\infty \Bigg\{ & \frac{\lambda}{2}\Bigg\langle\Bigg[\sum_0^2 C_i(i+1)y^i - \alpha_1\sum_0^2 A_i y^{i+1}\Bigg]e^{-\alpha_1 x} \\
& + \Bigg[\sum_0^2 D_i(i+1)y^i - \alpha_2\sum_0^2 B_i y^{i+1}\Bigg]e^{-\alpha_2 x}\Bigg\rangle^2 \\
& + G\Bigg\langle\Bigg[-\Bigg(\alpha_1\sum_0^2 A_i y^{i+1}\Bigg)e^{-\alpha_1 x} - \Bigg(\alpha_2\sum_0^2 B_i y^{i+1}\Bigg)e^{-\alpha_2 x}\Bigg]^2 \\
& + \Bigg[\sum_0^2 C_i(i+1)y^i e^{-\alpha_1 x} + \sum_0^2 D_i(i+1)y^i e^{-\alpha_2 x}\Bigg]^2\Bigg\rangle \\
& + \frac{G}{2}\Bigg\langle\sum_0^2 A_i(i+1)y^i e^{-\alpha_1 x} + \sum_0^2 B_i(i+1)y^i e^{-\alpha_2 x} \\
& - \alpha_1\sum_0^2 C_i y^{i+1} e^{-\alpha_1 x} - \alpha_2\sum_0^2 D_i y^{i+1} e^{-\alpha_2 x}\Bigg\rangle^2\Bigg\} dy\,dx \\
& - \int_0^1 (-1)\Bigg[-\sum_0^2 A_i y^{i+1} - \sum_0^2 B_i y^{i+1}\Bigg]dy
\end{aligned}
$$

where $\nu = 4.8$ and $E = 10^6$ PSI for the particular problem under consideration.

The potential energy, V, was then integrated between the indicated limits, and the resulting expression for V was minimized by taking partials of V with respect to each of the unknowns. The resulting expression contains fourteen nonlinear equations in fourteen unknowns. The fourteen simultaneous equations were programmed using the 1620 computer of Saint Louis University. The results are:

$\alpha_1 = .2276$ $\qquad$ $\alpha_2 = .8858$

SUB-SCRIPTS	A	B	C	D
0	2.262×10^{-7}	-31.52×10^{-7}	$.3682 \times 10^{-7}$	-1.455×10^{-7}
1	-8.175×10^{-7}	33.48×10^{-7}	$-.4275 \times 10^{-7}$	-8.468×10^{-7}
2	4.681×10^{-7}	-13.83×10^{-7}	$.0630 \times 10^{-7}$	3.078×10^{-7}

$V = -4.24 \times 10^{-7}$

Substitution of these results into the initial equations for displacements, there will occur at the forward edge where $x = 0$ and $y = 0 \rightarrow 1$, the expressions:

$$u = (-29.258y + 25.305y^2 - 9.149y^3) \times 10^{-7}$$

$$v = (-1.0868y - 8.8955y^2 + 3.141y^3) \times 10^{-7}$$

The displacements of the top surface of the slab at $y = 1$ and $x = 0 \rightarrow \infty$ were,

$$u = -1.232 \times 10^{-7} e^{-.2276x} - 11.81 \times 10^{-7} e^{-.8858x}$$

$$v = .0037 \times 10^{-7} e^{-.2276x} - 6.845 \times 10^{-7} e^{-.8858x}$$

A plot of these displacements are shown below. The scale factor being:

Displacements	$2 \times 10^{-6} = 1$ IN.
Original Dimensions	1 = 3 IN.

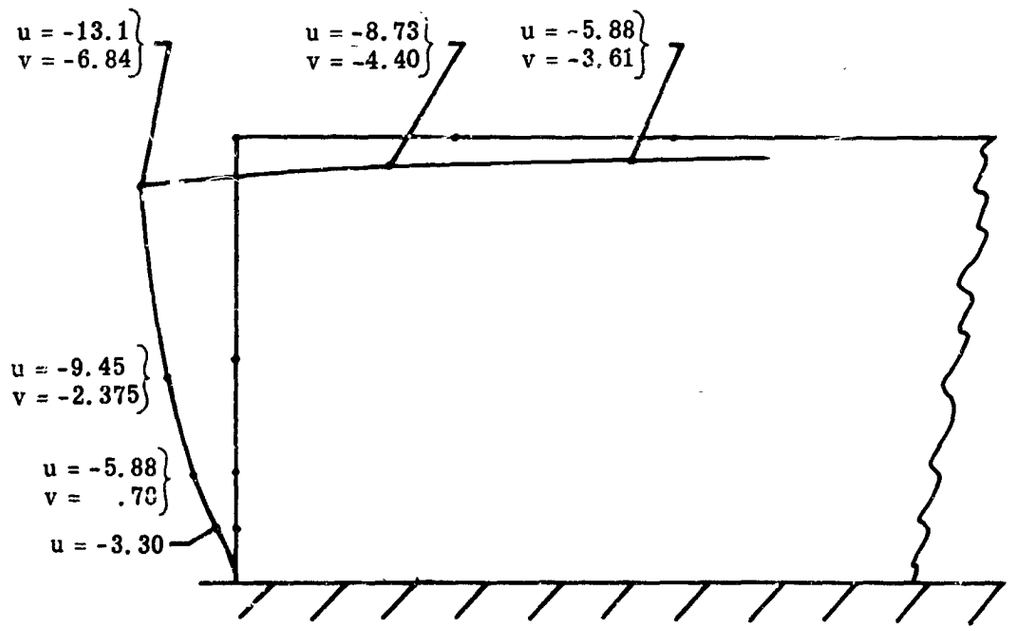

NOTE:

All displacements are at 10^{-7} in.

Upon substituting the results from the previous relationship into the general equations, we have,

$$\epsilon_x = -(.2276)(2.262y - 8.175y^2 + 4.681y^3) \times 10^{-7} e^{-.2276x}$$

$$-(.8858)(-31.52y + 33.48y^2 - 13.83y^3) \times 10^{-7} e^{-.8858x}$$

$$\epsilon_y = (.3682 - .8550y + .1890y^2) \times 10^{-7} e^{-.2276x}$$

$$+(-1.455 - 16.936y + 4.234y^2) \times 10^{-7} e^{-.8858x}$$

$$\gamma_{xy} = \left[(2.262 - 16.350y + 14.043y^2) - .2276(.3682y - .4275y^2 + .063y^3)\right] \times 10^{-7} e^{-.2276x}$$

$$+\left[(-31.52 + 66.96y - 41.49y^2) - .8858(-1.455y - 8.468y^2 + 3.078y^3)\right] \times 10^{-7} e^{-.8858x}$$

From these strains the stresses were determined and the interface forces calculated in order to check the overall balance. The forces being:

Σ of forces in x direction $(y = 0)$ $\qquad -1 = \int_0^\infty G\gamma\, dx$

$$-1 = \int_0^\infty G\left[2.262 \times 10^{-7} e^{-.2276x} - 31.52 \times 10^{-7} e^{-.8858x}\right] dx$$

$$-1 = G\left[\frac{2.262}{-.2276} \times 10^{-7} e^{-.2276x} - \frac{31.52}{-.8858} \times 10^{-7} e^{-.8858x}\right]_0^\infty$$

or $\qquad -1 = .338 \times 10^{6}\left[\frac{2.262}{.2276} - \frac{31.52}{.8858}\right] \times 10^{-7} = -.866$

These expressions indicate that the interface sheat was low about 13 percent.

The stress in the y direction at the interface being at $y = 0$,

$$\sigma_y = \frac{\nu E}{(1+\nu)(1-2\nu)}(\epsilon_x + \epsilon_y) + \frac{E}{1+\nu}\epsilon_y$$

$$\sigma_y = \frac{.48 \times 10^6}{(1.48)(.04)}\left(.3682 \times 10^{-7} e^{-.2276x} - 1.455 \times 10^{-7} e^{-.8858x}\right)$$

$$+ \frac{10^6}{1.48}\left(.3682 \times 10^{-7} e^{-.2276x} - 1.455 \times 10^{-7} e^{-.8858x}\right)$$

Σ of forces in y direction, was

$$0=\int_0^\infty \sigma_y dx=\int_0^\infty\left[\frac{.48}{.04}+1\right]\left(\frac{1}{14.8}\right)\left(.3682e^{-.2276x}-1.455e^{-.8858x}\right)dx$$

$$0=\frac{.52}{(.04)(14.8)}\left(-\frac{.3682}{.2276}e^{-.2276x}+\frac{1.455}{.8858}e^{-.8858x}\right)\Bigg|_0^\infty$$

$$0=\frac{.52}{(.04)(14.8)}\left(\frac{.3682}{.2276}-\frac{1.455}{.8858}\right)=-.0175$$

The vertical loads show values reasonably well in balance.

To determine Σ of the moments about the forward face, the following expression was solved:

$$.5=\int_0^\infty \sigma_y x dx$$

$$.5=\int_0^\infty\left(\frac{.52}{.04(14.8)}\right)\left(.3682xe^{-.2276x}-1.455xe^{-.8858x}\right)dx$$

$$.5=\frac{.52}{(.04)(14.8)}\left(\frac{.3682}{(+.2276)^2}-\frac{1.455}{(+.8858)^2}\right)$$

$$.5=4.61$$

The moments appear considerably out of balance, indicating being that the original assumptions for displacements do not satisfy the equilibrium equations. However, this is not to say that the original equations were completely incorrect concerning the displacements.

The previously presented problem assumed the original displacements in terms of fourteen unknowns. The analysis would correspond to fourteen degrees of freedom. To make the problem move tractable, eight of the unknowns were set equal to zero. The problem then reduces to six nonlinear equation with six unknowns. The displacement equations were then presented in the form

$$u=A_0ye^{-\alpha_1 x}+B_0ye^{-\alpha_2 x}$$

$$v=C_0ye^{-\alpha_1 x}+D_0ye^{-\alpha_2 x}$$

Incorporating these displacements in the equation for potential energy, V, and minimizing with respect to each unknown, the value of the unknowns became,

$\alpha_1 = .2277$

$\alpha_2 = .8858$

$A_0 = -2.577\times10^{-7}$

$B_0 = -6.483\times10^{-7}$

$C_0 = -.1509\times10^{-7}$

$D_0 = -2.990\times10^{-7}$

$V = -2.265\times10^{-7}$

The computed values makes it possible to present the displacements of the forward surface of the slab in the following form:

$$u = -2.577 \times 10^{-7} y - 6.483 \times 10^{-7} y = -9.06 \times 10^{-7} y$$

$$v = -.1509 \times 10^{-7} y - 2.99_0 y = -3.141 \times 10^{-7} y$$

and displacements of the top surface of the slab as

$$u = -2.577 \times 10^{-7} e^{-.2277x} - 6.483 \times 10^{-7} e^{-.8858x}$$

$$v = -.1509 \times 10^{-7} e^{-.2277x} - 2.99_0 \times 10^{-7} e^{-.8858x}$$

The displacements were plotted as shown below. The same scale given in the previous analysis applies.

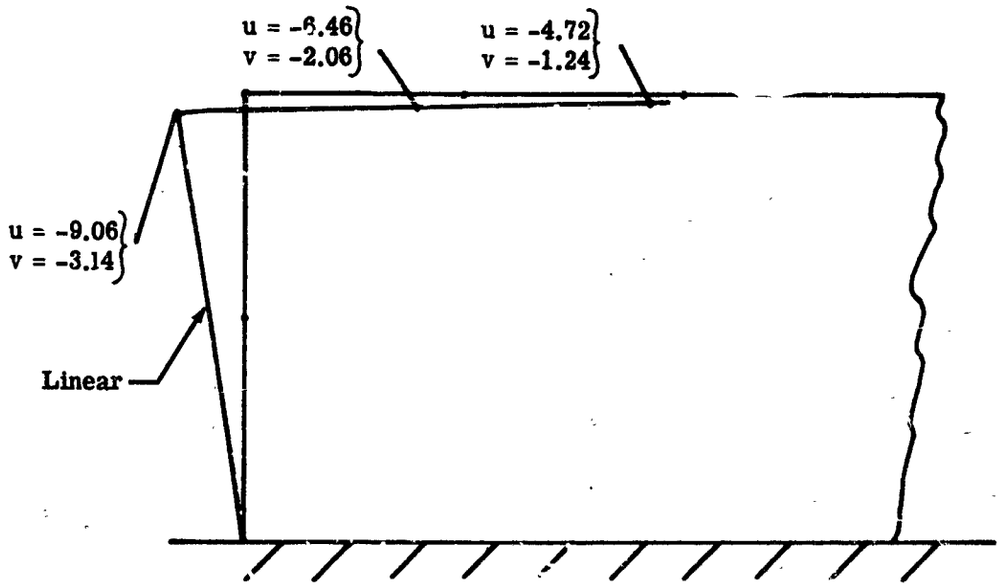

The two previously presented problems assumed the original displacements in terms of ten and fourteen unknowns. It is now the intended to solve the problem with four of the unknowns set equal to zero. The displacements equations would be, of the following form

$$u = (A_{oy} + A_1 y^2) e^{-\alpha_1 x} + (B_{oy} + B_1 y^2) e^{-\alpha_2 x}$$

$$v = (C_{oy} + C_1 y^2) e^{-\alpha_1 x} + (D_{oy} + D_1 y^2) e^{-\alpha_2 x}$$

Incorporating the preceding displacements into the equation for potential energy, V, and minimizing with respect to each unknown, the value of the unknowns became,

$\alpha_1 = .2276$

$\alpha_2 = .8858$

$A_0 = -1.19 \times 10^{-7}$

$A_1 = 1.97 \times 10^{-8}$

$B_0 = -2.144 \times 10^{-6}$

$B_1 = 9.18 \times 10^{-7}$

$C_0 = 2.72 \times 10^{-8}$

$C_1 = -2.76 \times 10^{-8}$

$D_0 = -2.02 \times 10^{-7}$

$D = -4.54 \times 10^{-7}$

$V = -4.096 \times 10^{-7}$

It does not appear necessary to show a plot of the external displacement. However, a plot of energy versus number of unknowns is in order. If it is shown that the energy achieved a stationary value, the potential energy solution presents a tractable solution.

Figure 5-16 shows that the potential energy approaches a stationary value, which lends assurance that the solution involving fourteen unknowns presents, the tractable solution for the original assumption of displacements.

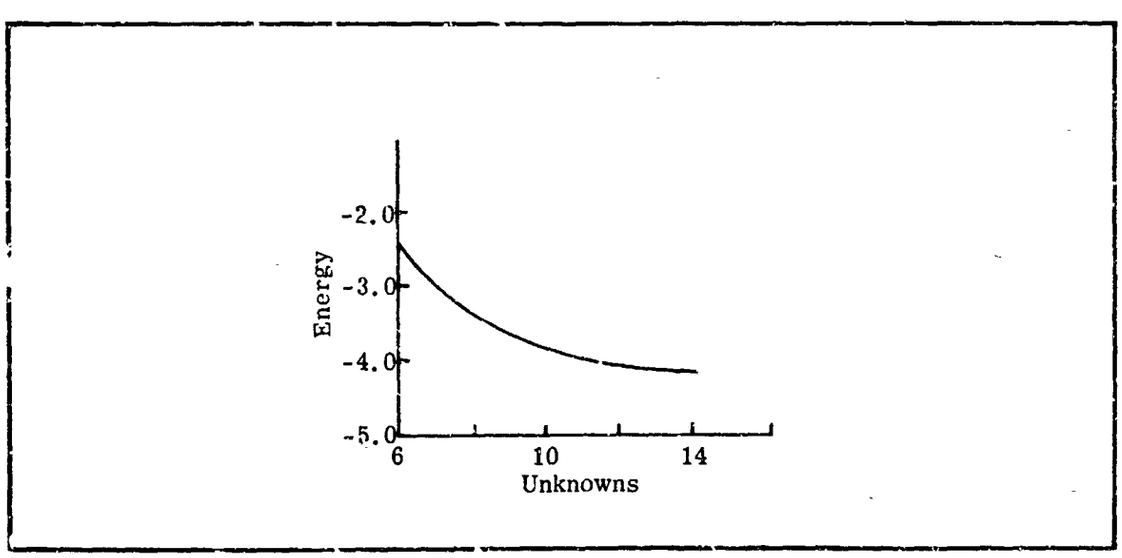

Figure 5-16. Potential Energy Curve

MINIMUM COMPLEMENTARY ENERGY ANALYSIS OF AN ELASTIC SLAB ON A RIGID BASE.

The problem to be considered is that of an elastic slab on a rigid base as shown in the diagram.

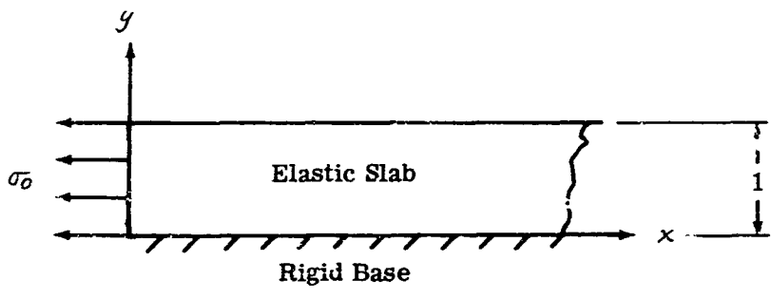

The analysis was based on plane stress with the stress components chosen in the following form:

$$\sigma_y = f(y)e^{-\alpha_1 x} + g(y)e^{-\alpha_2 x}$$

$$\sigma_x = \frac{f''}{\alpha_1^2} e^{-\alpha_1 x} + \frac{g''}{\alpha_2^2} e^{-\alpha_2 x}$$

$$\tau_{xy} = \frac{f'}{\alpha_1} e^{-\alpha_1 x} + \frac{g'}{\alpha_2} e^{-\alpha_2 x}$$

The above equations identically satisfy the equilibrium equations of elasticity:

$$\frac{\partial \sigma_x}{\partial y} + \frac{\partial \tau_{xy}}{\partial x} = 0$$

$$\frac{\partial \sigma_y}{\partial y} + \frac{\partial \tau_{xy}}{\partial x} = 0$$

The functions $f(y)$ and $g(y)$ are of the following form:

$$f(y) = A + By + Cy^2; \quad g(y) = D + Ey + Fy^2$$

The constants A thru C were chosen such that the following boundary conditions would be satisfied:

$$\sigma_y = 0 \quad @ \quad y = 1 \quad \text{and} \quad x = 0 \to \infty$$

$$\tau_{xy} = 0 \quad @ \; y = 1 \quad \text{and} \quad x = \to \infty$$

$$\sigma_x = \sigma_0 \quad @ \quad y = 0 \to 1 \quad \text{and} \quad x = 0$$

$$\tau_{xy} = 0 \quad @ \; y = 0 \to 1 \quad \text{and} \quad x = 0$$

For these conditions to be satisfied, the following must be true:

$$@ \; y = 1 \quad \text{and} \quad x = 0 \to \infty$$

$$A + B + C = 0$$

$$D + E + F = 0$$

$$\frac{B + 2C}{\alpha_1} = 0 \; ; \quad \frac{E + 2F}{\alpha_2} = 0$$

$$@ \; y = 0 \to 1 \quad \text{and} \quad x = 0$$

$$\frac{2C}{\alpha_1^2} + \frac{2F}{\alpha_2^2} = \sigma_0 \quad ; \quad \frac{B + 2Cy}{\alpha_1} + \frac{E + 2Fy}{\alpha_2} = 0$$

Since it is not desired that the constants be functions of y, the following relationships must hold:

$$\frac{B}{\alpha_1} = -\frac{E}{\alpha_2} \; ; \; \frac{2C}{\alpha_1} = -\frac{2F}{\alpha_2}$$

$$\frac{2}{\alpha_1^2}\left(-\frac{F\alpha_1}{\alpha_2}\right) + \frac{2F}{\alpha_2^2} = \sigma_0$$

$$F\left(\frac{\alpha_1 - \alpha_2}{\alpha_1 \alpha_2}\right) = \frac{\alpha_2}{2}\sigma_0$$

$$F = \frac{\alpha_1 \alpha_2^2 \sigma_0}{2(\alpha_1 - \alpha_2)}$$

$$\frac{2C}{\alpha_1^2} + \frac{\alpha_1 \sigma_0}{\alpha_1 - \alpha_2} = \sigma_0$$

$$C = \left(\sigma_0 - \frac{\alpha_1 \sigma_0}{\alpha_1 - \alpha_2}\right)\frac{\alpha_1^2}{2} = \left(\frac{\alpha_1 - \alpha_2 - \alpha_1}{\alpha_1 - \alpha_2}\right)\frac{\alpha_1^2}{2}\sigma_0$$

$$C = -\frac{\alpha_1^2 \alpha_2 \sigma_0}{2(\alpha_1 - \alpha_2)}$$

$$\frac{B}{\alpha_1} + \frac{2}{\alpha_1}\left(-\frac{\alpha_1^2 \alpha_2 \sigma_0}{2(\alpha_1 - \alpha_2)}\right) = 0$$

$$B = \frac{\alpha_1^2 \alpha_2 \sigma_0}{(\alpha_1 - \alpha_2)}$$

$$\frac{E}{\alpha_2} + \frac{2}{\alpha_2}\left(\frac{\alpha_1 \alpha_2^2 \sigma_0}{2(\alpha_1 - \alpha_2)}\right) = 0$$

$$E = -\frac{\alpha_1 \alpha_2^2 \sigma_0}{\alpha_1 - \alpha_2}$$

$$A = -\frac{\alpha_1^2 \alpha_2 \sigma_0}{(\alpha_1 - \alpha_2)} + \frac{\alpha_1^2 \alpha_2 \sigma_0}{2(\alpha_1 - \alpha_2)}$$

$$A = -\frac{\alpha_1^2 \alpha_2 \sigma_0}{2(\alpha_1 - \alpha_2)}$$

$$D = \frac{\alpha_1 \alpha_2^2 \sigma_0}{\alpha_1 - \alpha_2} - \frac{\alpha_1 \alpha_2^2 \sigma_0}{2(\alpha_1 - \alpha_2)}$$

$$D = \frac{\alpha_1 \alpha_2^2 \sigma_0}{2(\alpha_1 - \alpha_2)}$$

The complementary energy relationship becomes

$$V^* = \int_V W dV - \int_{S_u} T_i u_i dS$$

The term, S_{u_i} is that part of the surface over which displacements were prescribed. In the particular case $u_i = 0$, which allows the expression,

$$V^* = \int_0^\infty \int_0^1 W dx dy$$

where,

$$W = \frac{1}{2E}(\sigma_x^2 + \sigma_y^2) - \frac{\nu}{E}[\sigma_x \sigma_y] + \frac{1}{2G}(\tau_{xy})^2$$

$$V^* = \int_0^1 \int_0^\infty \left\{ \frac{1}{2E}\left[\frac{(f'')^2}{\alpha_1^4} e^{-2\alpha_1 x} + \frac{(g'')^2}{\alpha_2^4} e^{-2\alpha_2 x} + \frac{2f''g''}{\alpha_1^2 \alpha_2^2} e^{-(\alpha_1 + \alpha_2)x} \right.\right.$$

$$+f^2e^{-2\alpha_1 x}+g^2e^{-2\alpha_2 x}+2fge^{-(\alpha_1+\alpha_2)x}\Big]-\frac{\nu}{E}\Big[\frac{ff''}{\alpha_1^2}e^{-2\alpha_1 x}$$

$$+\frac{f''g}{\alpha_1^2}e^{-(\alpha_1+\alpha_2)x}+\frac{fg''}{\alpha_2^2}e^{-(\alpha_1+\alpha_2)x}+\frac{gg''}{\alpha_2^2}e^{-2\alpha_2 x}\Big]$$

$$+\frac{1}{2G}\Big[\frac{(f')^2}{\alpha_1^2}e^{-2\alpha_1 x}+\frac{(g')^2}{\alpha_2^2}e^{-2\alpha_2 x}+\frac{2f'g'}{\alpha_1\alpha_2}e^{-(\alpha_1+\alpha_2)x}\Big]dydx$$

Integrating the equation for V^* gives

$$V^*=\int_0^l\Big\{\frac{1}{2E}\Big[\frac{(f'')^2}{2\alpha_1^5}+\frac{(g'')^2}{2\alpha_2^5}+\frac{2f''g}{\alpha_1^2\alpha_2^2(\alpha_1+\alpha_2)}+\frac{f^2}{2\alpha_1}+\frac{g^2}{2\alpha_2}$$

$$+\frac{2fg}{(\alpha_1+\alpha_2)}\Big]-\frac{\nu}{E}\Big[\frac{ff''}{2\alpha_1^3}+\frac{f''g}{\alpha_1^2(\alpha_1+\alpha_2)}+\frac{fg''}{\alpha_2^2(\alpha_1+\alpha_2)}+\frac{gg''}{2\alpha_2^3}\Big]$$

$$+\frac{1}{2G}\Big[\frac{(f')^2}{2\alpha_1^3}+\frac{(g')^2}{2\alpha_2^3}+\frac{2f'g'}{\alpha_1\alpha_2(\alpha_1+\alpha_2)}\Big]\Big\}dy$$

$$V^*=\Big\{\frac{1}{2E}\Big[\frac{4C^2}{2\alpha_1^5}+\frac{4F^2}{2\alpha_2^5}+\frac{4CF}{\alpha_1^2\alpha_2^2(\alpha_1+\alpha_2)}+\frac{A^2+AB+\frac{2}{3}AC+\frac{B^2}{3}+\frac{BC}{2}+\frac{C^2}{5}}{2\alpha_1}$$

$$+\frac{D^2+DE+\frac{2}{3}DF+\frac{E^2}{3}+\frac{EF}{2}+\frac{F^2}{5}}{2\alpha_2}+\frac{2AD+BD+AE+\frac{2}{3}(DC+BE+AF)+\frac{CE+BF}{2}+\frac{2CF}{5}}{(\alpha_1+\alpha_2)}\Big]$$

$$-\frac{\nu}{E}\Big[\frac{2AC+BC+\frac{2}{3}C^2}{2\alpha_1^3}+\frac{2CD+CE+\frac{2}{3}CF}{\alpha_1^2(\alpha_1+\alpha_2)}+\frac{2AF+BF+\frac{2}{3}CF}{\alpha_2^2(\alpha_1+\alpha_2)}$$

$$+\frac{2DF+EF+\frac{2}{3}F^2}{2\alpha_2^3}\Big]+\frac{1}{2G}\Big[\frac{B^2+2BC+\frac{4}{3}C^2}{2\alpha_1^3}+\frac{E^2+2FE+\frac{4}{3}F^2}{2\alpha_2^3}$$

$$+\frac{2BE+2CE+2BF+\frac{8}{3}CF}{\alpha_1\alpha_2(\alpha_1+\alpha_2)}\Big]\Big\}$$

The above equation was simplified by expressing B and C in terms of A, and E and F in terms of D, giving,

$$C=A \qquad E=-2D$$

$$B=-2A \qquad F=D$$

$$V^* = \left\{ \frac{1}{2E}\left[\frac{A^2}{\alpha_1^5} + \frac{2D^2}{\alpha_2^5} + \frac{4AD}{\alpha_1^2\alpha_2^2(\alpha_1+\alpha_2)} + \frac{A^2}{10\alpha_1}\right.\right.$$

$$\left. + \frac{D^2}{10\alpha_2} + \frac{2AD}{5(\alpha_1+\alpha_2)}\right] - \frac{\nu}{E}\left[\frac{A^2}{3\alpha_1^3} + \frac{2AD}{3\alpha_1^2(\alpha_1+\alpha_2)} + \frac{2AD}{3\alpha_2^2(\alpha_1+\alpha_2)}\right.$$

$$\left.\left. + \frac{D^2}{3\alpha_2^3}\right] + \frac{1}{2G}\left[\frac{2A^2}{3\alpha_1^3} + \frac{2D^2}{3\alpha_2^3} + \frac{8AD}{3\alpha_1\alpha_2(\alpha_1+\alpha_2)}\right]\right\}$$

Substituting for A and D gives,

$$V^* = \left\{ \frac{1}{2E}\left[\frac{\alpha_2^2\sigma_0^2}{2\alpha_1(\alpha_1-\alpha_2)^2} + \frac{\alpha_1^2\sigma_0^2}{2\alpha_2(\alpha_1-\alpha_2)^2} - \frac{\alpha_1\alpha_2\sigma_0^2}{(\alpha_1-\alpha_2)(\alpha_1^2-\alpha_2^2)}\right.\right.$$

$$\left. + \frac{\alpha_1^3\alpha_2^2\sigma_0^2}{40(\alpha_1-\alpha_2)^2} + \frac{\alpha_1^2\alpha_2^3\sigma_0^2}{40(\alpha_1-\alpha_2)^2} - \frac{\alpha_1^3\alpha_2^3\sigma_0^2}{10(\alpha_1^2-\alpha_2^2)(\alpha_1-\alpha_2)}\right]$$

$$- \frac{\nu}{E}\left[\frac{\alpha_1\alpha_2^2\sigma_0^2}{12(\alpha_1-\alpha_2)^2} - \frac{\alpha_1\alpha_2^3\sigma_0^2}{6(\alpha_1-\alpha_2)(\alpha_1^2-\alpha_2^2)} - \frac{\alpha_1^3\alpha_2\sigma_0^2}{6(\alpha_1-\alpha_2)(\alpha_1^2-\alpha_2^2)}\right.$$

$$\left. + \frac{\alpha_1^2\alpha_2\sigma_0^2}{12(\alpha_1-\alpha_2)^2}\right] + \frac{1+\nu}{E}\left[\frac{\alpha_1\alpha_2^2\sigma_0^2}{6(\alpha_1-\alpha_2)^2} + \frac{\alpha_1^2\alpha_2\sigma_0^2}{6(\alpha_1-\alpha_2)^2}\right.$$

$$\left.\left. - \frac{2\alpha_1^2\alpha_2^2\sigma_0^2}{3(\alpha_1-\alpha_2)(\alpha_1^2-\alpha_2^2)}\right]\right\}$$

Combining terms of the equation gives,

$$V^* = \left\{ \frac{\sigma_0^2}{4E}\left[\frac{\alpha_2^3+\alpha_1^3}{\alpha_1\alpha_2(\alpha_1-\alpha_2)^2}\right]\right.$$

$$+ \frac{\sigma_0^2}{60E}\left[\frac{-(30\alpha_1\alpha_2+3\alpha_1^3\alpha_2^3+40\alpha_1^2\alpha_2^2)+\nu(10\alpha_1\alpha_2^3+10\alpha_1^3\alpha_2-40\alpha_1^2\alpha_2^2)}{(\alpha_1-\alpha_2)(\alpha_1^2-\alpha_2^2)}\right]$$

$$+\frac{\sigma_0^2}{240E}\left[\frac{(3\alpha_1^3\alpha_2^2+3\alpha_1^2\alpha_2^3+40\alpha_1\alpha_2^2+40\alpha_1^2\alpha_2)}{(\alpha_1-\alpha_2)^2}\right]$$

$$\left.+\frac{\sigma_0^2\nu}{240E}\left[\frac{(-20\alpha_1\alpha_2^2-20\alpha_1^2\alpha_2+40\alpha_1\alpha_2^2+40\alpha_1^2\alpha_2)}{(\alpha_1-\alpha_2)^2}\right]\right\}$$

In order to have a minimum energy expression for this particular form of the stress components, the following conditions must hold:

$$\frac{\partial V^*}{\partial \alpha_1}=0 \qquad \frac{\partial V^*}{\partial \alpha_2}=0$$

The stresses were then written in the following form:

$$\sigma_y=-\sigma_0\left[\frac{\alpha_1^2\alpha_2}{2(\alpha_1-\alpha_2)}\left(1-2y+y^2\right)e^{-\alpha_1 x}\right.$$

$$\left.-\frac{\alpha_1\alpha_2^2}{2(\alpha_1-\alpha_2)}\left(1-2y+y^2\right)e^{-\alpha_2 x}\right]$$

$$\sigma_x=-\sigma_0\left[\frac{\alpha_2}{(\alpha_1-\alpha_2)}e^{-\alpha_1 x}-\frac{\alpha_1}{(\alpha_1-\alpha_2)}e^{-\alpha_2 x}\right]$$

$$\tau_{xy}=-\sigma_0\left[\frac{\alpha_1\alpha_2}{(\alpha_1-\alpha_2)}\left(-1+\frac{y}{2}\right)e^{-\alpha_1 x}-\frac{\alpha_1\alpha_2}{\alpha_1-\alpha_2}\left(-1+\frac{y}{2}\right)e^{-\alpha_2 x}\right]$$

The solution to the previous two equations, as determined on the 1620 computer, was,

$\alpha_1=7.718; \quad \alpha_2=.762$

Use of these terms reduces the experssion for the stresses at the interface $(y=0)$ to:

$$\sigma_y=-\sigma_0\left[3.26e^{-7.718x}-.32e^{-.762x}\right]$$

$$\sigma_x=-\sigma_0\left[.110e^{-7.718x}-1.11e^{-.762x}\right]$$

ANALYSIS OF STRESSES IN AN ELASTIC SLAB WITH A HONEYCOMB SUBSTRUCTURE.

The problem of an elastic beam on a honeycomb substructure is given schematically by the following diagram:

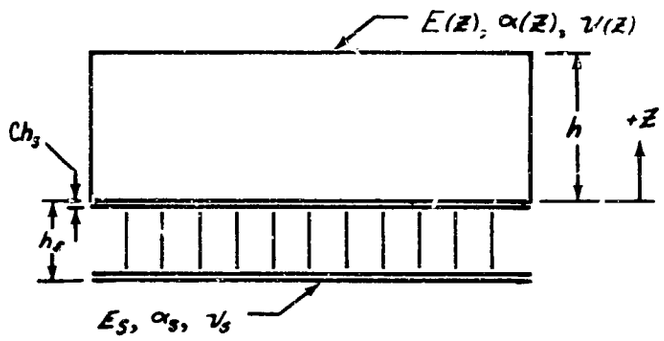

The assumption considered were:

1. Temperature, T, coefficient of thermal expansion, α, modulus of elasticity, E, and Poisson's Ratio, ν, of the heat shield material are functions of height z.

2. Temperature, T, and mechanical properties of steel remain uniform.

3. Thickness of steel plates, Ch_s, is small in comparison with height h_s.

4. Plane sections remain plane.

The boundary conditions being:

Initially: $(\epsilon = 0)$

$$\sigma_x = \alpha E T \quad 0 \le z \le h$$

For the faces: $\sigma_s = \alpha_s E_s T_o \qquad \sigma = \epsilon E = (\epsilon_o + Kz)E$

Forces:

$$2Ch_s\sigma + \int_0^h \sigma\, dz = \int_0^h E\alpha T\, dz + 2E_s\alpha_s T_o Ch_s$$

$$Ch_s(E_1)E_s + Ch_s[\epsilon_o + K(-h_s)]E_s + \int_0^h (\epsilon_o + Kz)E\, dz = \int_0^h E\alpha T\, dz + 2E_s\alpha_s T_o Ch_s$$

$$\epsilon_o\left[2Ch_s E_s + \int_0^h E\, dz\right] + K\left[-Ch_s^2 E_s + \int_0^h Ez\, dz\right] = \int_0^h E\alpha T\, dz + 2E_s\alpha_s T_o Ch_s$$

Moments:

$$-Ch_s^2\sigma + \int_0^h \sigma z\,dz = \int_0^h E\alpha T z\,dz - E_s\alpha_s T_0 Ch_s^2$$

$$-Ch_s^2[\epsilon_0 + K(-h_s)]E_s + \int_0^h (\epsilon_0 + Kz)Ez\,dz = \int_0^h E\alpha T z\,dz - E_s\alpha_s Ch_s^2$$

$$\epsilon_0\left[-Ch_s^2E_s + \int_0^h Ez\,dz\right] + K\left[+Ch_s^3E_s + \int_0^h Ez^2\,dz\right] = \int_0^h E\alpha T z\,dz - E_s\alpha_s T_0 Ch_s^2$$

Simultaneous solution of equations (1) and (2) yields:

$$K = \frac{\left[\int_0^h E\alpha T dz + 2E_s\alpha_s T_0 Ch_s\right]\left[-Ch_s^2E_s + \int_0^h Ez\,dz\right] - \left[2Ch_sE_s + \int_0^h E\,dz\right]\left[\int_0^h E\alpha T z\,dz - E_s\alpha_s T_0 Ch_s^2\right]}{\left[-Ch_s^2E_s + \int_0^h Ez\,dz\right]\left[-Ch_s^2E_s + \int_0^h Ez\,dz\right] - \left[2Ch_sE_s + \int_0^h E\,dz\right]\left[+Ch_s^3E_s + \int_0^h Ez^2\,dz\right]}$$

$$\epsilon_0 = \frac{-N\left[-Ch_s^2E_s + \int_0^h Ez\,dz\right] + D\left[\int_0^h E\alpha T dz + 2E_s\alpha_s T_0 Ch_s)\right]}{D\left[2Ch_sE_s + \int_0^h Ez\,dz\right]}$$

The terms N and D are the numerator and denominator respectively of the preceding equation for K. The resulting stresses being:

$\sigma_{HS} = (\epsilon_0 + KZ)E - \alpha TE$ (Heat shield)

$\sigma_S = (\epsilon_0 - Kh_s)E_S - \alpha_S T_0 E_S$ (Bottom plate)

$\sigma_S = \epsilon_0 E_S - \alpha_S T_0 E_S$ (Top plate)

ANALYSIS OF PLANE STRAIN STRESSES IN AN ELASTIC SLAB ON A HONEYCOMB PLATE.

The problem of an elastic beam on a honeycomb plate, given by the following schematic, was considered.

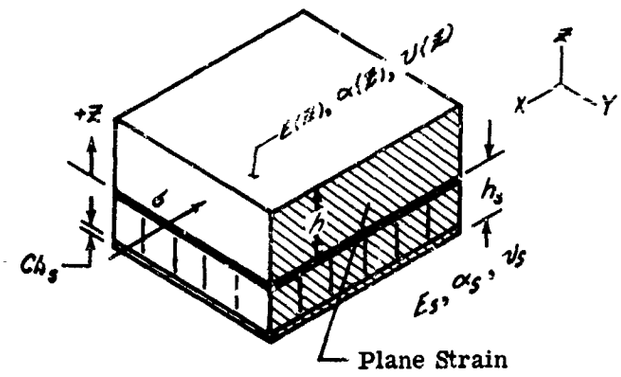

The plane stress solution of an elastic beam on a honeycomb beam can be resolved into a plane strain solution for an elastic slab on a honeycomb plate by making the following substitutions:

$$E = \frac{E}{1-\nu^2} \qquad E_S = \frac{E_S}{1-\nu_S^2}$$

$$\nu = \frac{\nu}{1-\nu} \qquad \nu_S = \frac{\nu_S}{1-\nu_S}$$

$$\alpha = (1+\nu)\alpha \qquad \alpha_S = (1+\nu_S)\alpha_S$$

$$K = \frac{\left[\int_0^h \frac{E\alpha T}{1-\nu}dz + 2\frac{E_S\alpha_S T_0}{1-\nu_S^2}Ch_S\right]\left[-Ch_S^2\frac{E_S}{1-\nu_S^2} + \int_0^h \frac{E}{1-\nu^2}z\,dz\right] - \left[2Ch_S\frac{E_S}{1-\nu_S^2} + \int_0^h \frac{E}{1-\nu^2}dz\right]\left[\int_0^h \frac{E\alpha T z}{1-\nu}dz - \frac{E_S\alpha_S T_0}{1-\nu_S}Ch_S^2\right]}{\left[-Ch_S^2\frac{E_S}{1-\nu_S^2} + \int_0^h \frac{E}{1-\nu^2}z\,dz\right]\left[-Ch_S^2\frac{E_S}{1-\nu_S^2} + \int_0^h \frac{E}{1-\nu^2}z\,dz\right] - \left[+2Ch_S\frac{E_S}{1-\nu_S^2} + \int_0^h \frac{E}{1-\nu^2}dz\right]\left[Ch_S^2\frac{E_S}{1-\nu_S^2} + \int_0^h \frac{E}{1-\nu^2}z\,dz\right]}$$

$$\epsilon_0 = \frac{-N\left[-Ch_S^2\frac{E_S}{1-\nu_S^2} + \int_0^h \frac{E}{1-\nu^2}z\,dz\right] + D\left[\int_0^h \frac{E\alpha T}{1-\nu}dz + 2\frac{E_S\alpha_S T_0}{1-\nu_S}Ch_S\right]}{D\left[2Ch_S\frac{E_S}{1-\nu_S^2} + \int_0^h \frac{E}{1-\nu^2}dz\right]}$$

The terms N and D are the numerator and denominator stresses respectively, of the preceding equation for K.

The results being:

$\sigma_{H.S} = (\epsilon_0 + KZ)\frac{E}{1-\nu^2} - \frac{\alpha T E}{1-\nu}$ (Heat shield)

$\sigma_S = \frac{\epsilon_0 E_S}{1-\nu_S^2} - \frac{\alpha_S T_0 E_S}{1-\nu_S}$ (Bottom plate)

$\sigma_S = (\epsilon_0 - Kh_S)\frac{E_S}{1-\nu_S^2} - \frac{\alpha_S T_0 E_S}{1-\nu_S}$ (Top plate)

ELASTIC SLAB ON HONEYCOMB PLATE.

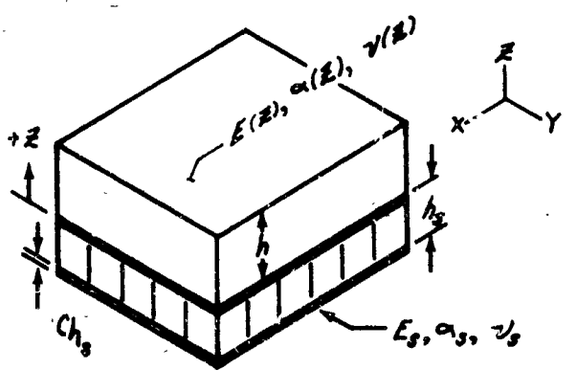

Consider the case of an elastic slab on an element of honeycomb plate as shown by the above schematic, the assumptions for the honeycomb beam being still valid:

Initially $\epsilon_x = \epsilon_y = 0$

$$\sigma_x = \sigma_y = \frac{-\alpha TE}{1-\nu}$$

Force equations:

$$2Ch_s\sigma + \int_0^h \sigma dz = \int_0^h \frac{\alpha TE}{1-\nu} dz + \frac{2E_s\alpha_s}{1-\nu_s} T_o Ch_s$$

$$\frac{Ch_s(\epsilon_o)E_s}{1-\nu_s} + \frac{Ch_s[\epsilon_o + K(-h_s)]E_s}{1-\nu_s} + \int_0^h \frac{(\epsilon_o + KZ)Edz}{1-\nu} = \int_0^h \frac{\alpha TE}{1-\nu} + \frac{2E_s\alpha_s}{1-\nu_s} T_o Ch_s$$

$$\epsilon_o\left[\frac{2Ch_sE_s}{1-\nu_s} + \int_0^h \frac{Edz}{1-\nu}\right] + K\left[\frac{-Ch_s^2E_s}{1-\nu_s} + \int_0^h \frac{Ezdz}{1-\nu}\right. = \int_0^h \frac{\alpha TE}{1-\nu} + \frac{2E_s}{1-\nu_s}\alpha_s T_o Ch_s$$

Moment equations:

$$-Ch_s^2\sigma + \int_0^h \sigma zdz = \int_0^h \frac{\alpha TE}{1-\nu} zdz - \frac{E_s\alpha_s}{1-\nu_s} T_o Ch_s^2$$

$$-\frac{Ch_s^2(\epsilon_o - Kh_s)}{1-\nu_s}E_s + \int_0^h \frac{(\epsilon_o + Kz)Ezdz}{1-\nu} = \int_0^h \frac{\alpha TEzdz}{1-\nu} - \frac{E_s\alpha_s T_o}{1-\nu_s} Ch_s^2.$$

$$\epsilon_o\left[\frac{-Ch_s^2E_s}{1-\nu_s} + \int_0^h \frac{Ezdz}{1-\nu}\right] + K\left[\frac{+Ch_s^3E_s}{1-\nu_s} + \int_0^h \frac{Ez^2dz}{1-\nu}\right] = \int_0^h \frac{\alpha TEzdz}{1-\nu} - \frac{E_s\alpha_s}{1-\nu_s} T_o Ch_s^2$$

$$K = \frac{\left[\int_0^h \frac{\alpha TE}{1-\nu}dz + \frac{2E_s\alpha_s}{1-\nu_s} T_o Ch_s\right]\left[\frac{-Ch_s^2E_s}{1-\nu_s} + \int_0^h \frac{Ezdz}{1-\nu}\right] - \left[\int_0^h \frac{\alpha TEzdz}{1-\nu} - \frac{E_s\alpha_s T_o}{1-\nu_s} Ch_s\right]\left[\frac{2Ch_sE_s}{1-\nu_s} + \int_0^h \frac{Edz}{1-\nu}\right]}{\left[-\frac{Ch_s^2E_s}{1-\nu_s} + \int_0^h \frac{Ezdz}{1-\nu}\right]\left[\frac{Ch_s^2E_s}{1-\nu_s} + \int_0^h \frac{Ezdz}{1-\nu}\right] - \left[\frac{2Ch_sE_s}{1-\nu_s} + \int_0^h \frac{Edz}{1-\nu}\right]\left[\frac{+Ch_s^3E_s}{1-\nu_s} + \int_0^h \frac{Ez^2dz}{1-\nu}\right]}$$

$$\epsilon_o = \frac{-N\left[-\frac{Ch_s^2E_s}{1-\nu_s} + \int_0^h \frac{Ezdz}{1-\nu}\right] + D\left[\int_0^h \frac{\alpha TE}{1-\nu}dz + \frac{2E_s\alpha_s}{1-\nu_s} T_o Ch_s\right]}{D\left[\frac{2Ch_sE_s}{1-\nu_s} + \int_0^h \frac{Edz}{1-\nu}\right]}$$

The terms N and D are the numerator and denominator respectively, of the preceding equation of K, the resulting stress being:

$$\sigma_{x_{H.S.}} = \sigma_{y_{H.S.}} = \left(\epsilon_o + \frac{Kz}{1-\nu}\right)E - \frac{\alpha TE}{1-\nu} \quad \text{(Heat shield)}$$

$$\sigma_{x_s} = \sigma_{y_s} = \frac{(\epsilon_0 - K h_s) E_s}{1 - \nu_s} - \frac{\alpha_s T_0 E_s}{1 - \nu_s} \quad \text{(Bottom plate)}$$

$$\sigma_{x_s} = \sigma_{y_s} = \frac{\epsilon_0 E_s}{1 - \nu_s} - \frac{\alpha_s T_0 E_s}{1 - \nu_s} \quad \text{(Top plate)}$$

$$\tau_{xy} = -\sigma_0 \left[-.846 e^{-1.716x} + .846 e^{-.762x} \right]$$

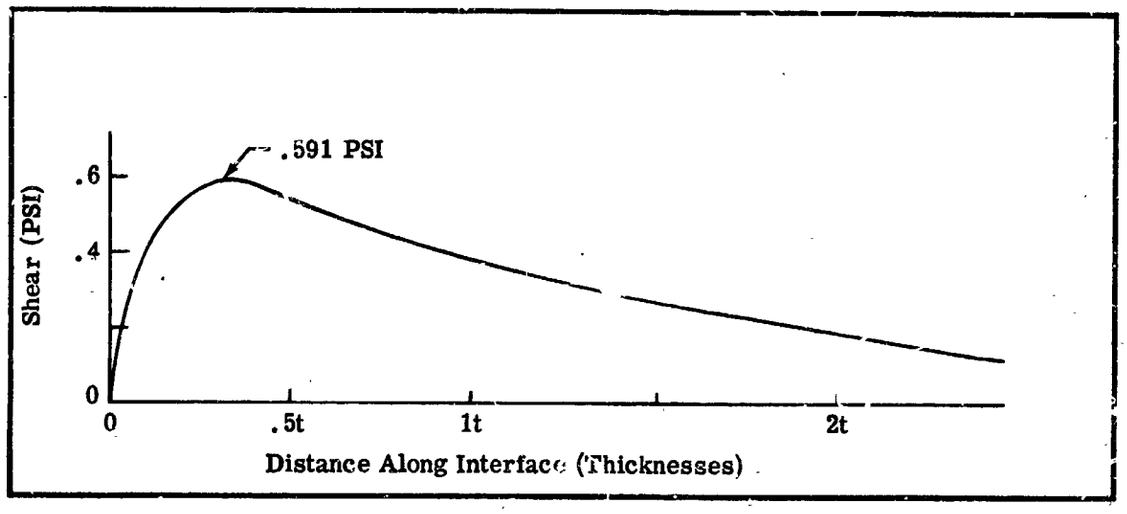

Figure 5-17. Shear Stress Versus X

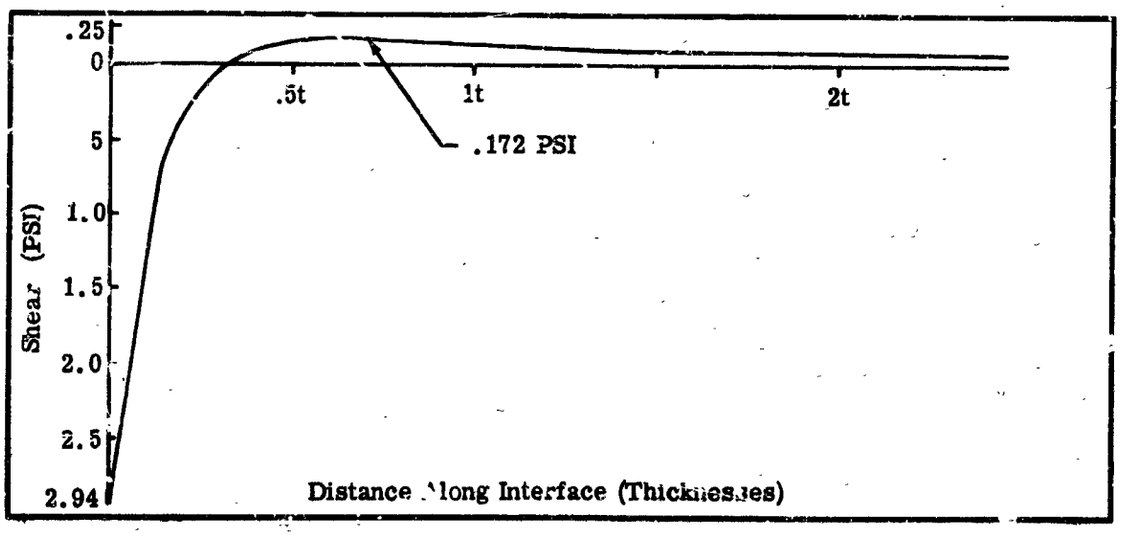

Figure 5-18. Peeling Stresses Along X Axis

BLANK PAGE

SECTION VI
BIBLIOGRAPHY

1. ASTM Standards. Part 6, 1955; Part 5, 1961; Part 9, 1961. American Society for Testing Materials.
2. Bernicker, R.P. "Downstream Effects of Transpiration Cooling." Journal of the Aerospace Sciences, Volume 29, No. 2 (August 1962), 658-659.
3. Bolon, R.L. "Differential Thermal Analysis of Explosives and Propellants Under Controlled Atmospheres." Analytical Chemistry, Volume 33, No. 10 (September 1961), 1452-1453.
4. Boley, B.A., and Weiner, J.H. "Theory of Thermal Stresses." New York: John Wiley and Sons, 1960.
5. Carslaw, H.S. and Jaeger, J.C. "Conduction of Heat in Solids." 2nd ed. London: Oxford Press, 1959.
6. Churchill, R.V. "Fourier Series and Boundary Value Problems." New York: McGraw Hill, 1941.
7. Cresci, R.J. and Libby, P.A. "The Downstream Influence of Mass Transfer at the Nose of a Slender Cone." Journal of the Aerospace Sciences, Volume 29, No. 2 (July 1962), 815-824.
8. Denbigh, K.G. "The Principles of Chemical Equilibrium." London: Cambridge Press, 1955.
9. Eckert, E.R.G., and Livingood, N.B. "Comparison of Effectiveness of Convection-, Transpiration-, and Film-Cooling Methods With Air as Coolant." NACA TN 3010, 1953.
10. Eckert, E.R.G. "Survey of Heat Transfer at High Speeds." WADC Technical Report 54-70, 1954.
11. Eshbach, O.W. et al. "Handbook of Engineering Fundamentals." 2nd ed. New York: John Wiley and Sons, 1952.
12. Faulders, C.R. "Heat Transfer in the Laminar Boundary Layer With Ablation of Vapor of Arbitrary Molecular Weight." Journal of the Aerospace Sciences, Volume 29, No. 1 (January 1962), 76-86.
13. Fay, J.A. and Riddell, F.R. "Theory of Stagnation Point Heat Transfer in Dissociated Air." Journal of the Aeronautical Sciences, Volume 25, No. 1 (February 1958), 73-85.
14. Garn, P.D. "Thermal Analysis." Analytical Chemistry, Volume 33, No. 9 (August 1961), 1247-1251.
15. Gatewood, B.E. "Thermal Stresses." New York: McGraw Hill, 1957.
16. Gollnick, A.F. Jr. "Thermal Effects on a Transpiration Cooled Hemisphere." Journal of the Aerospace Sciences, Volume 29, No. 1 (May 1962), 583-595.
17. Hansen, C.F. "Approximations for the Thermodynamics and Transport Properties of High-Temperature Air." NASA TR R-50, 1959.
18. Horton, W.S., "Oxidation Kinetics of Pyrolytic Graphite," General Electric Co., G.E.L. Document No. 60 GL 218, January 1961.

19. Hoshijaki, H., and Smith, H.J., "Axisymmetric Stagnation Point Mass - Transfer Cooling." Lockheed Missiles & Space Division LMSD-48379, December 17, 1958.
20. Hougen, O.A., and Watson, K.M., "Chemical Process Principles" Volume III, New York: John Wiley & Sons, 1955.
21. Importance of Correlating Ablation Performance in Terms of Basic Parameters, Emerson Electric Manufacturing Company, Technical Note 10562.
22. Instruction Manual, Deltatherm Model D2000, Part 9, Technical Equipment Corporation, Denver, Colorado.
23. Jakob, M. "Heat Transfer." Volumes 1 and 2. New York: John Wiley and Sons, 1956.
24. Kemp, N.H., Rose, P.H., and Detra, R.W. "Laminar Heat Transfer Around Blunt Bodies in Dissociated Air." Journal of the Aerospace Sciences. Volume 26, No. 1 (July 1959), 421-430.
25. Khitrin, L.N., "Fundamental Principles of Carbon Combustion and Factors Intensifying the Burning of Solid Fuels," Sixth Symposium on Combustion, New York: Reinhold Corporation, 1956.
26. Kivel, B. "Radiation From Hot Air and Stagnation Heating." Avco Corporation Research Report No. 79, October 1959.
27. Lange, N.A., et al. "Handbook of Chemistry." 8th ed. Ohio: Handbook Publishers, Inc., 1952.
28. Libby, P.A., and Cresci, R.J. "Experimental Investigation of the Downstream Influence of Stagnation-Point Mass Transfer." Journal of the Aerospace Sciences, Volume 28, No. 1 (January 1961), 51-64.
29. Libby, P.A. "The Homogeneous Boundary Layer at an Axisymmetric Stagnation Point With Large Rates of Injection." Journal of the Aerospace Sciences, Volume 28, No. 1 (January 1961), 48-60.
30. Libby, P.A., and Cresci, R. J., "The Downstream Influence of Mass Transfer at the Nose of a Slender Cone." Journal of the Aerospace Sciences, July 1962.
31. McAdams, W.H. "Heat Transmission." 3rd ed. New York: McGraw-Hill, 1954.
32. Mickley, H.S., et al. "Heat, Mass and Momentum Transfer for Flow Over a Flat Plate With Blowing and Suction." NASA TN 3208, July 1958.
33. Moore, J.A., and Zlotnick, M., "Combustion of Carbon in an Air Stream," ARS Journal, October 1961.
34. Moore, W.J. "Physical Chemistry." 2nd ed., New Jersey: Prentice-Hall, 1956.
35. Muki, R. and Sternberg, E. "On Transient Thermal Stresses in Viscoelastic Materials With Temperature Dependent Properties." Journal of Applied Mechanics, Volume 28, Series E, No. 2 (June 1961), 193-207.
36. Ness, N. "Foreign-Gas Injection Into a Compressible Turbulent Boundary Layer on a Flat Plate." Journal of the Aerospace Sciences, Volume 28, No. 2 (August 1961), 645-654.
37. Nolan, E.J., and Scala, S.M., "Aerothermodynamic Behavior of Phrolytic Graphite during Sustained Hypersonic Flight," ARS Journal, January 1962.
38. Pappas, C.C., and Okuno, A.F., "Measurements of Skin Friction of the Compressible Turbulent Boundary Layer on a Cone with Foreign Gas Injection." Journal of the Aerospace Science. May 1961.
39. Performance Evaluation of "THERMO-LAG" Material for Entry Heat Protection of

Advanced Manned Spacecraft, Emerson Electric Manufacturing Company, Quarterly Progress Report 1468, April 1963.
40. Perry, J. H., et al. "Chemical Engineer's Handbook." 3rd ed. New York: McGraw Hill, 1950.
41. Probstein, R.F. "Shock Wave and Flow Field Development in Hypersonic Re-Entry." ARS Journal, Volume 31, No. 2 (February 1961), 185-194.
42. Progress Report, Emerson Electric Manufacturing Company, St. Louis. NASA Contract NAS 9-877, October 1 to November 1, 1962.
43. Progress Report, Emerson Electric Manufacturing Company, St. Louis. NASA Contract NAS 9-877, November 1 to December 1, 1962.
44. Progress Report, Emerson Electric Manufacturing Company, St. Louis. NASA Contract NAS 9-877, December 1, 1962 to January 1, 1963.
45. Properties of "THERMO-LAG" T-500 EX 167 Subliming Compound, Emerson Electric Manufacturing Company, Report Number 1139.
46. Rashis, B. "Exploratory Investigation of Transpiration Cooling of a 40° Double Wedge Using Nitrogen and Helium As Coolants at Stagnation Temperatures From 1295°F to 2910°F." NASA TN D-721, May 1961.
47. Roehrig, J.R., and Simons, J.C., Jr. Accurate Calibration of Vacuum Gauges to 10^{-9} TORR." Presented at the Second International Congress of the I.O.V.S.T., October, 1961.
48. Rubesin, M.W. "The Influence of Surface Injection on Heat Transfer and Skin Friction Associated With the High-Speed Turbulent Boundary Layer." NACA RM A55L13, December, 1957.
49. Rubesin, M.W., Pappas, C.C., and Okuno, A.F., "The Effect of Fluid Injection on the Compressible Turbulent Boundary Layer - Preliminary Tests on Transpiration Cooling of a Flat Plate at M - 2.7 with Air as the Injected Gas." NACA RM A55119, September, 1957.
50. SAE Aerospace Applied Thermodynamics Manual, Section 3, Part G, Society of Automotive Engineers, Inc., Committee A-9, January, 1962.
51. Scala, S.M., and Gilbert, L.M., "Thermal Degradation of a Char-Forming Plastic During Hypersonic Flight." ARS Journal (June 1962), 917-924.
52. Schlichting, H. "Boundary Layer Theory." 4th ed. New York: McGraw-Hill, 1960.
53. Schmidt, D.L. "Ablation of Plastics." WADC Technical Report No. ASD-TR-61-650, Wright-Patterson AF Base, Ohio, Aeronautical Systems Division, February 1962.
54. Smith, J.M. "Introduction to Chemical Engineering Thermodynamics." New York: McGraw-Hill, 1949.
55. Sokolnikoff, I.S. "Mathematical Theory of Elasticity." New York: McGraw-Hill, 1956.
56. Tendeland, I., and Okuno, A.F. "The Effect of Fluid Injection on the Compressible Turbulent Boundary Layer - The Effect on Skin Friction of Air Injected Into the Boundary Layer of a Cone at M = 2.7." NACA RM A56D05, April 1958.
57. Thermal Protection of Structural Propulsion, and Temperature-Sensitive Materials For Hypersonic and Space Flight, WADD Technical Report 59-366, Part III, December 1960.
58. Timoshenko, S., and Goodier, J. N., "Theory of Elasticity." 2nd ed. New York: McGraw-Hill, 1951.

BLANK PAGE

APPENDIX A

TEST RESULTS

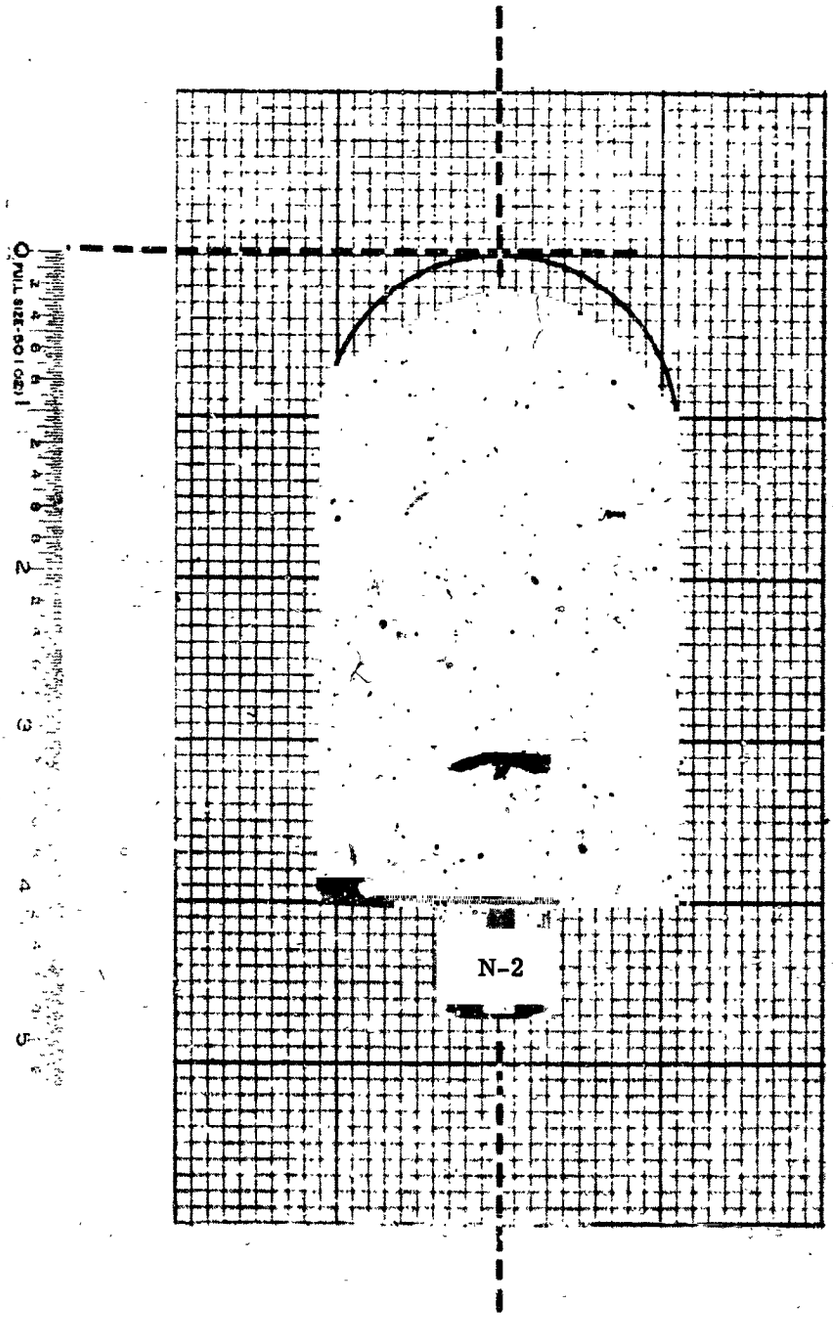

Figure A-1. Sectioned Model N-2 - After Test

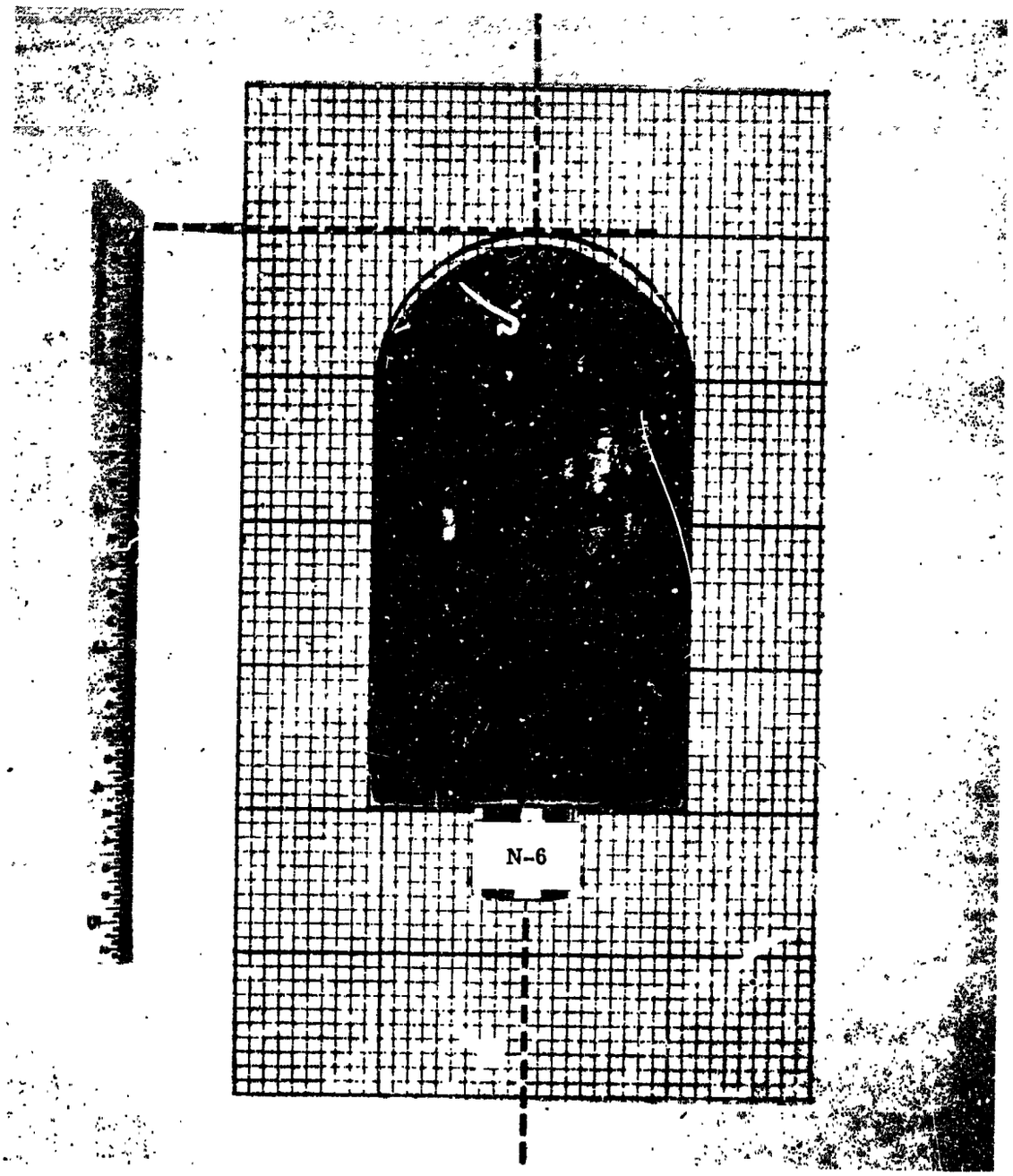

Figure A-2. Sectioned Model N-6 - After Test

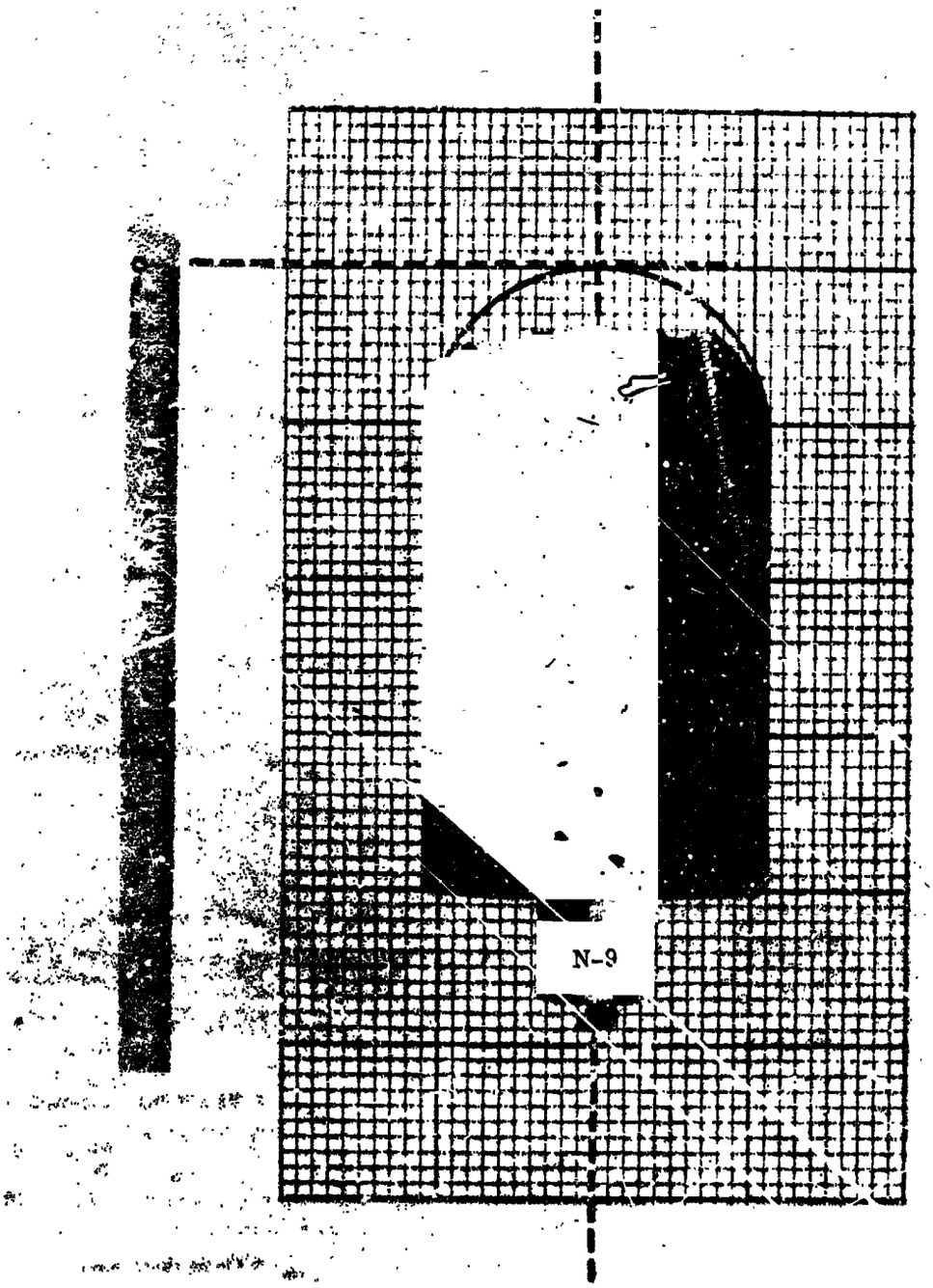

Figure A-3. Sectioned Model N-9 - After Test

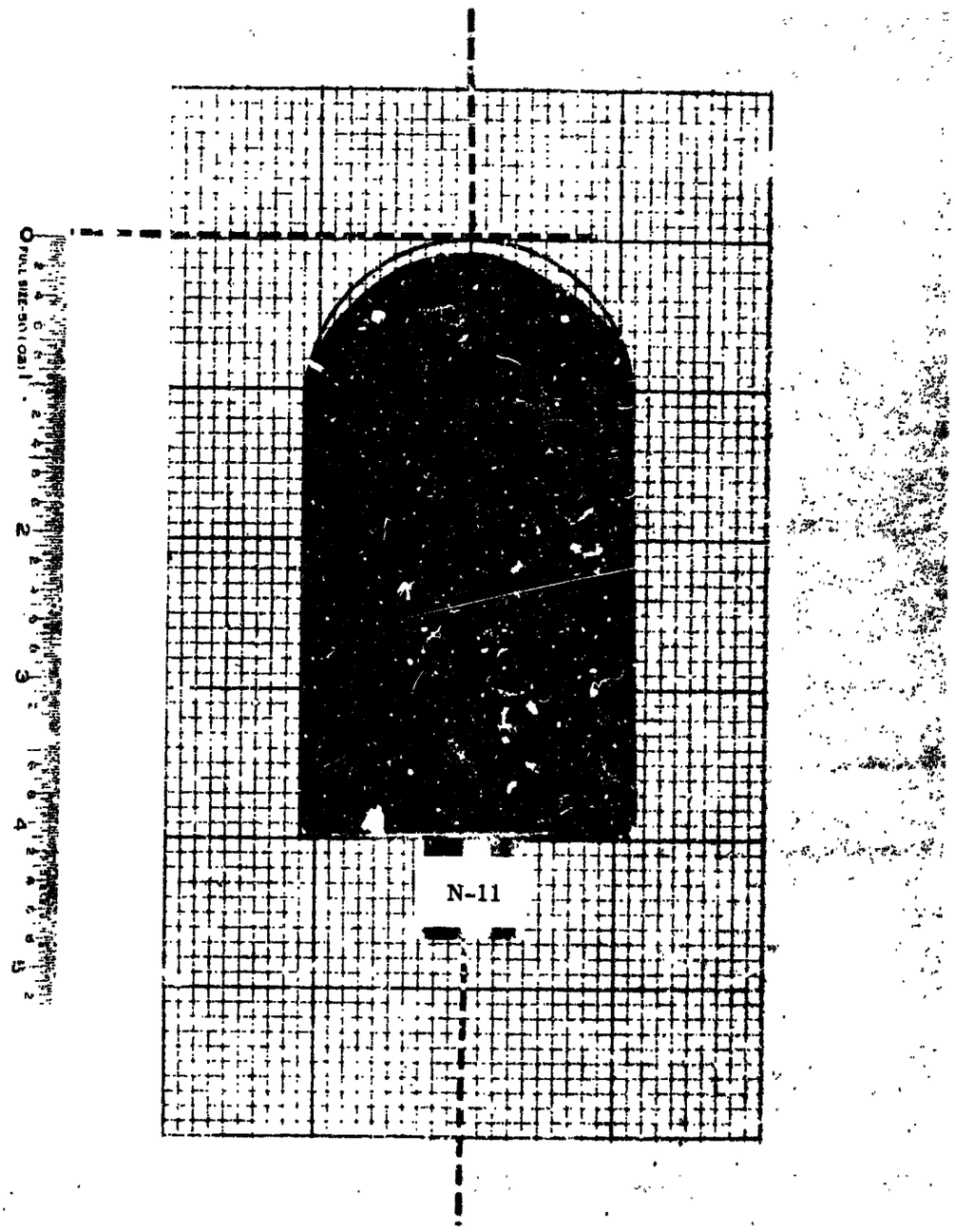

Figure A-4. Sectioned Model N-11 - After Test

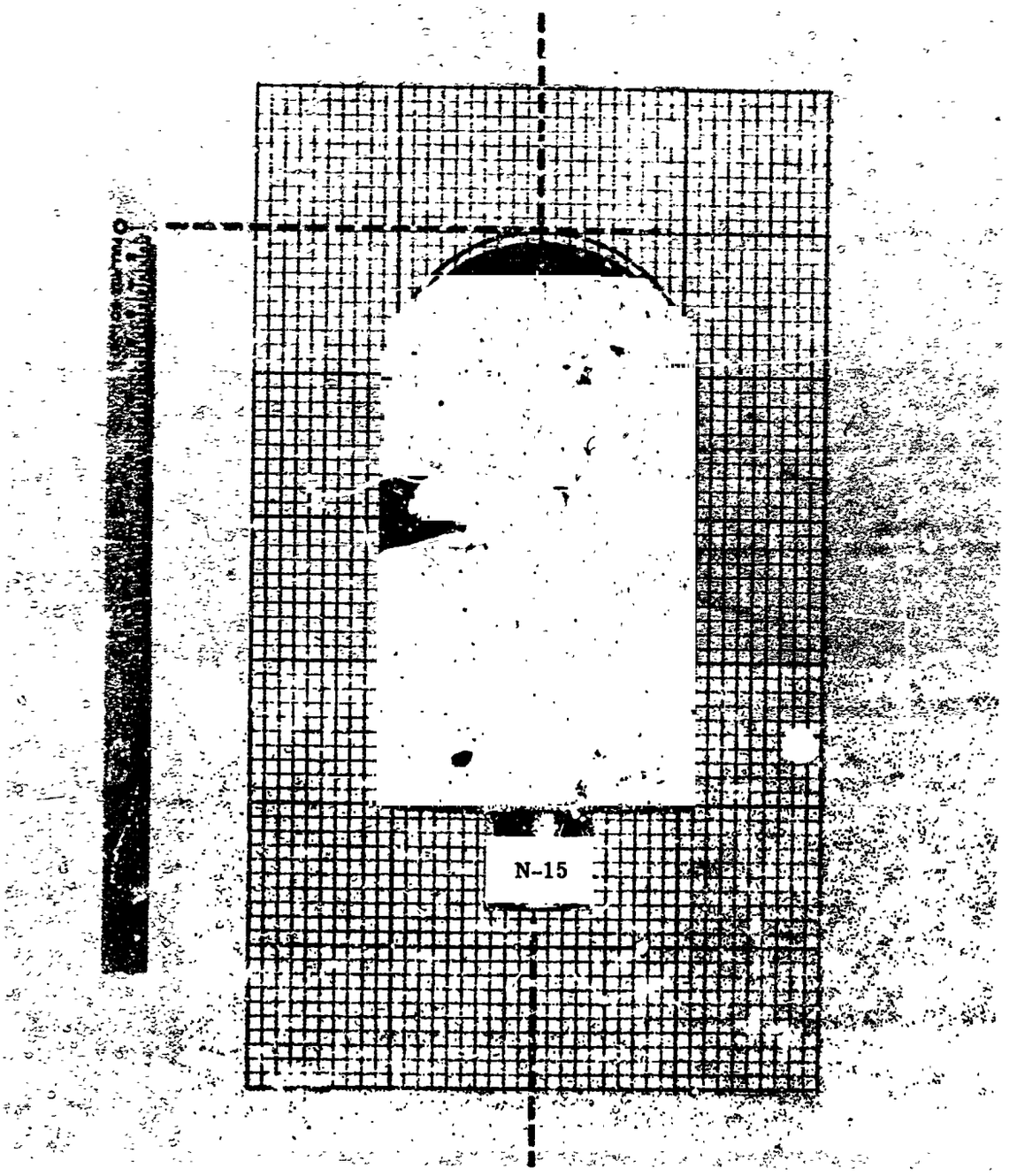

Figure A-5. Sectioned Model N-15 - After Test

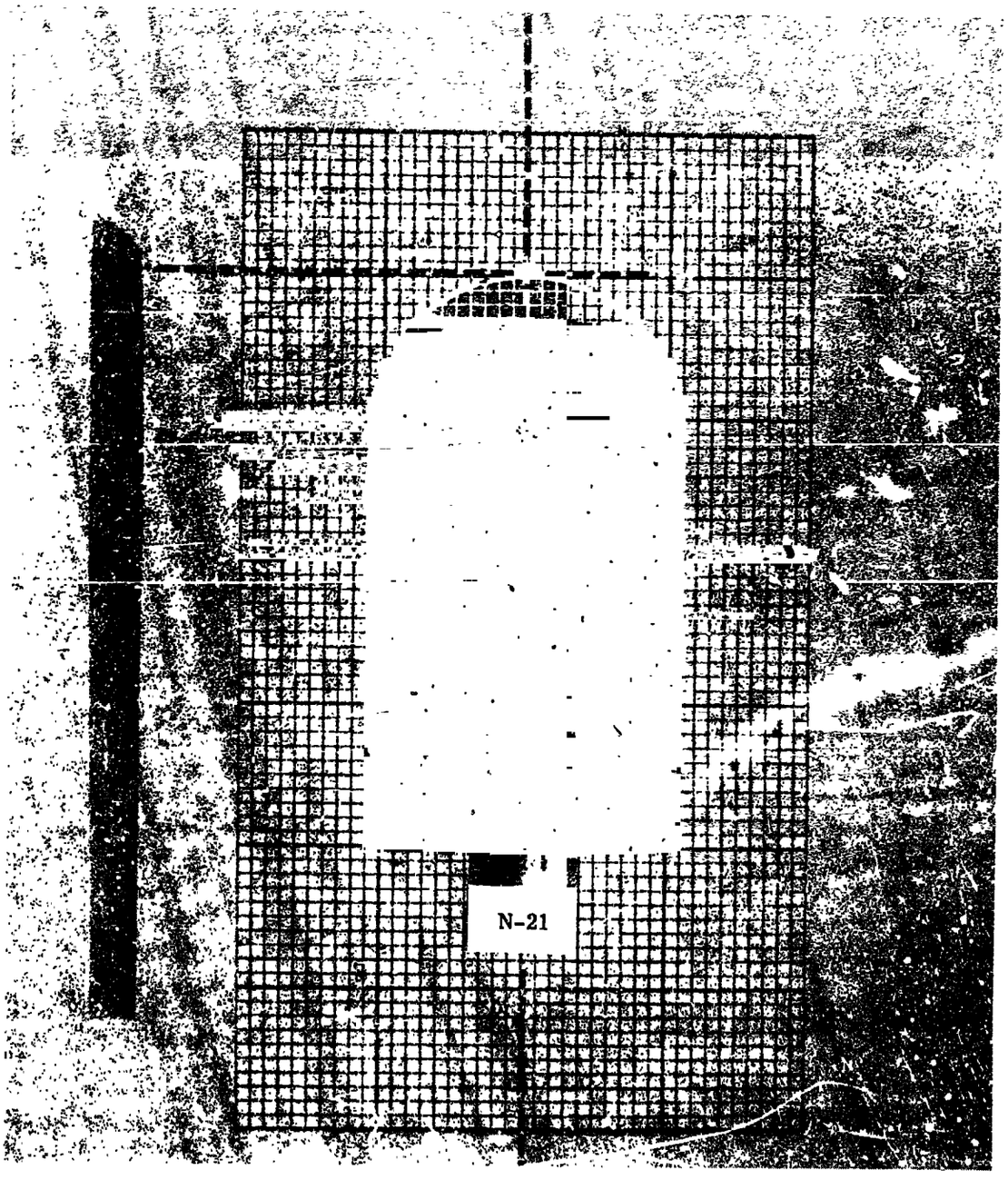

Figure A-6. Sectioned Model N-21 - After Test

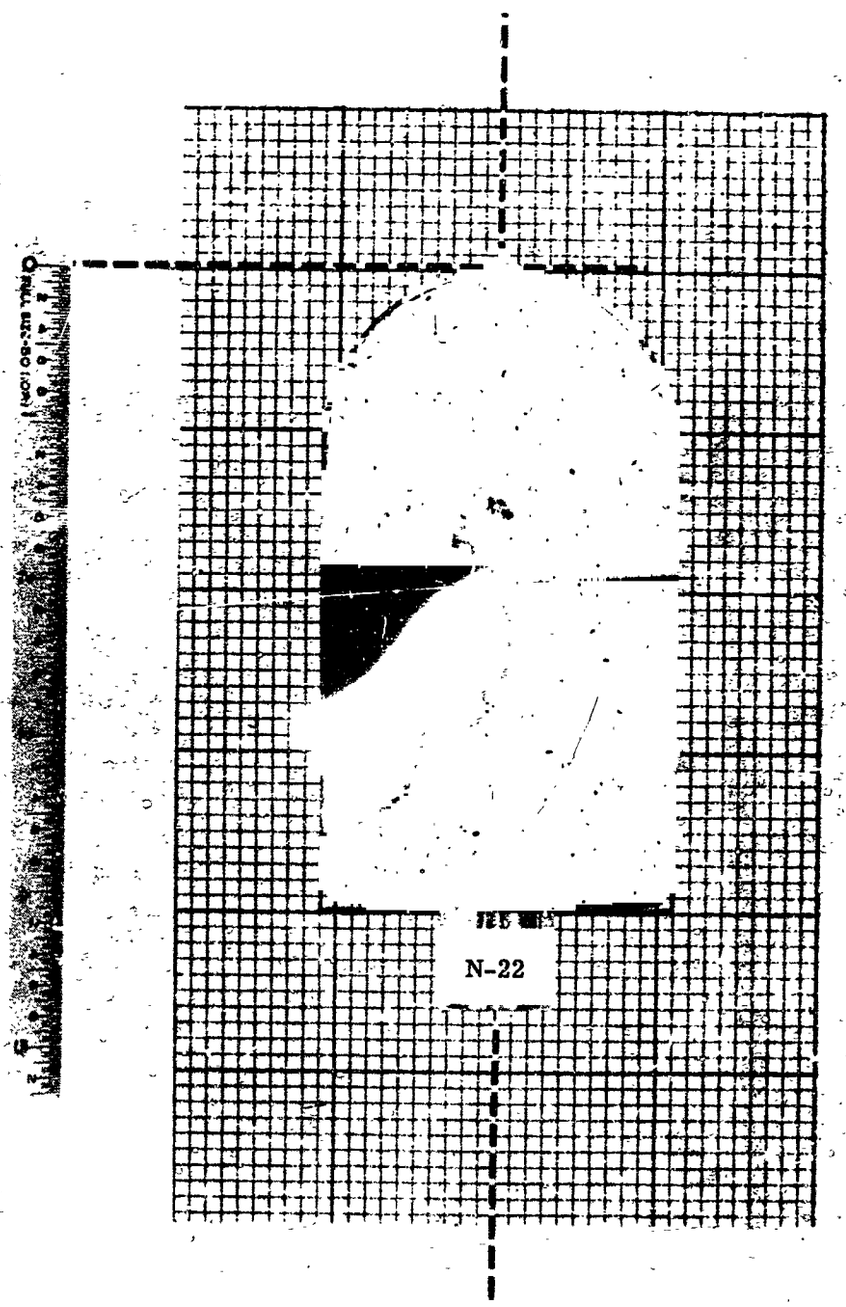

Figure A-7. Sectioned Model N-22 - After Test

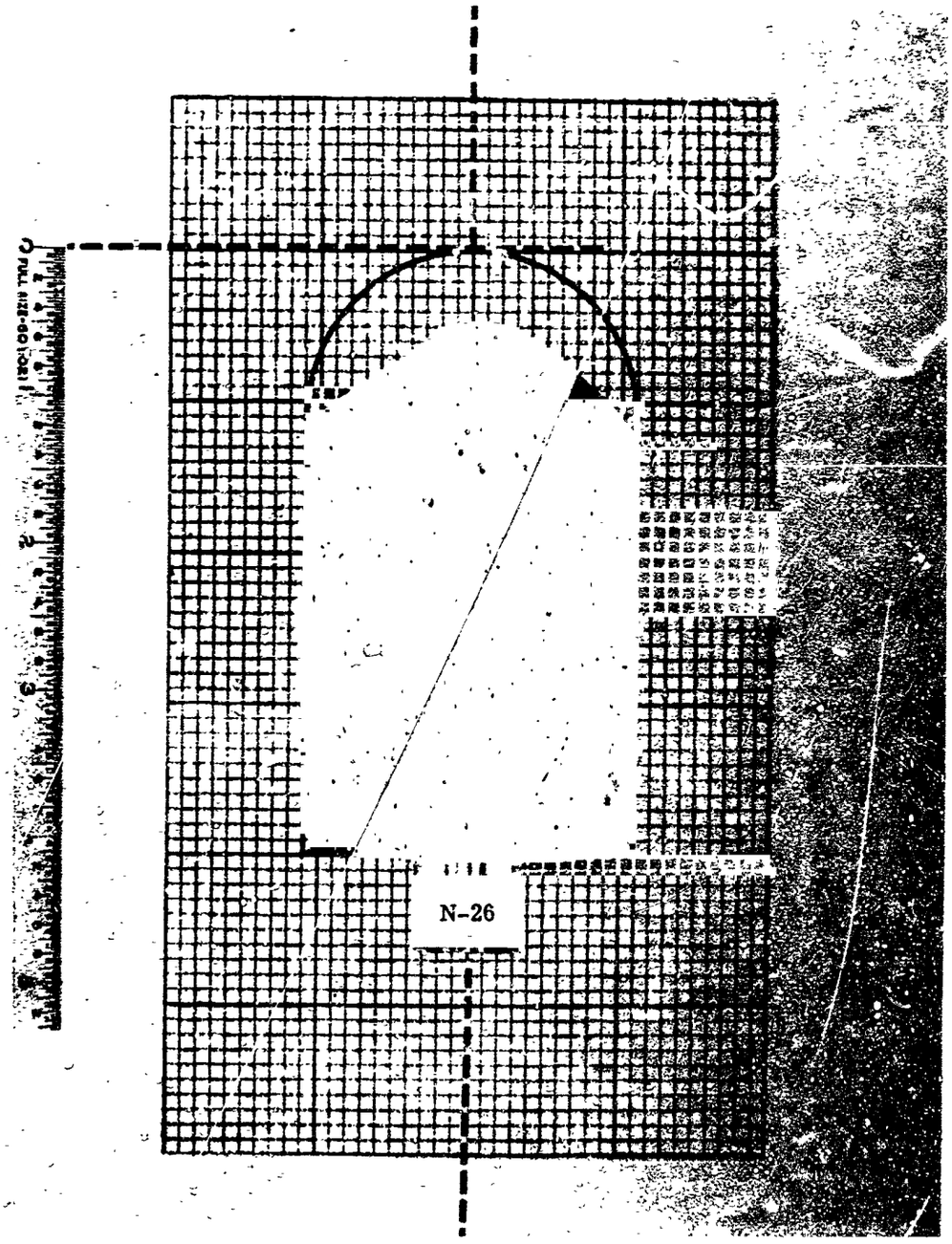

Figure A-8. Sectioned Model N-26 - After Test

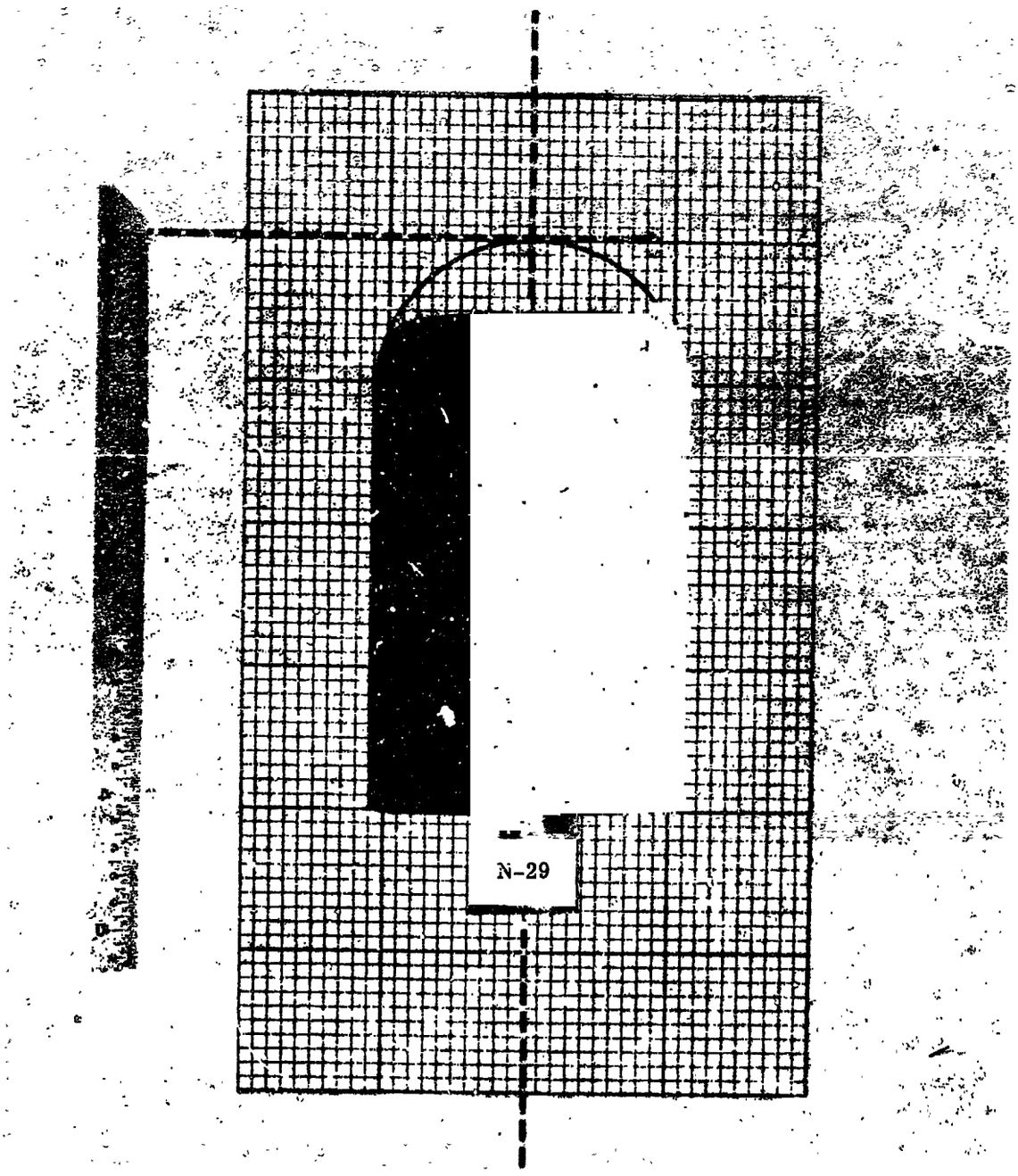

Figure A-9. Sectioned Model N-29 - After Test

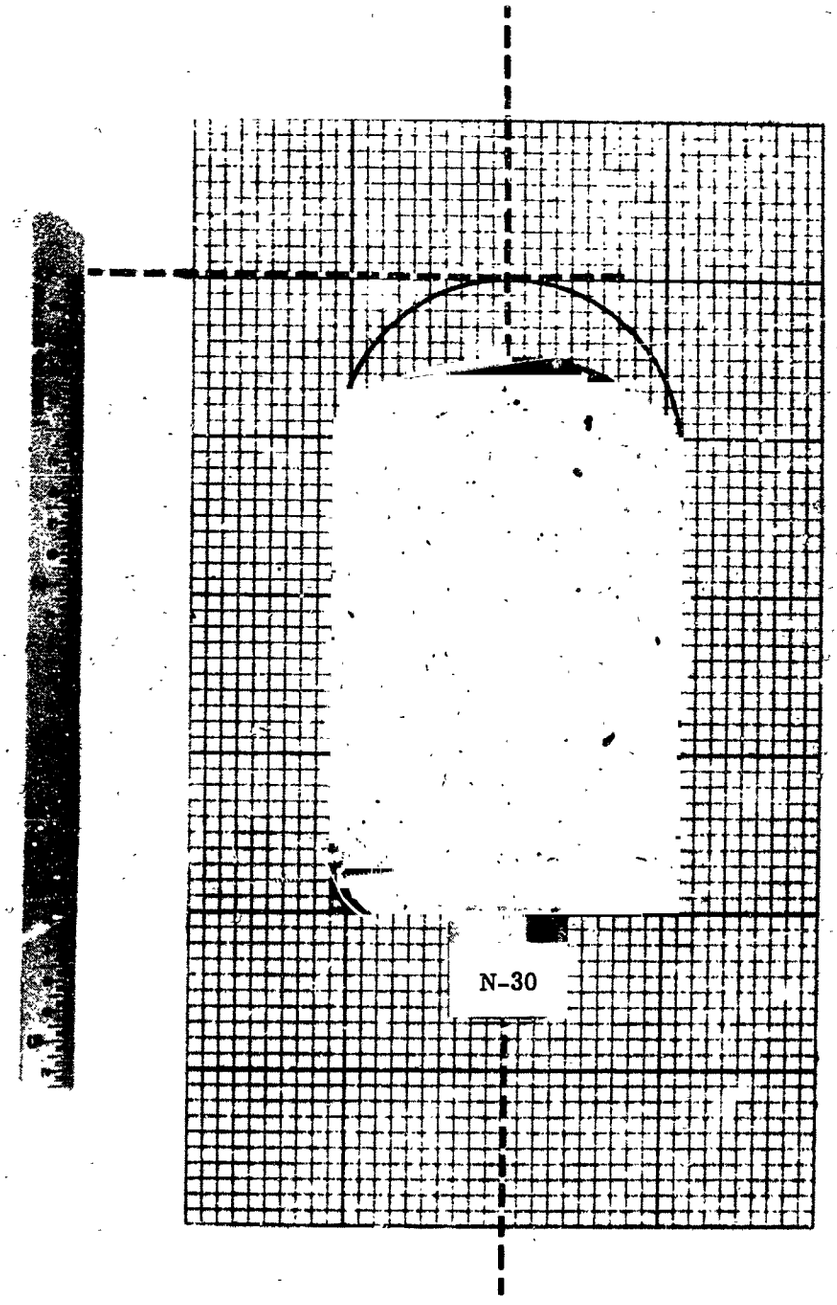

Figure A-10. Sectioned Model N-30 - After Test

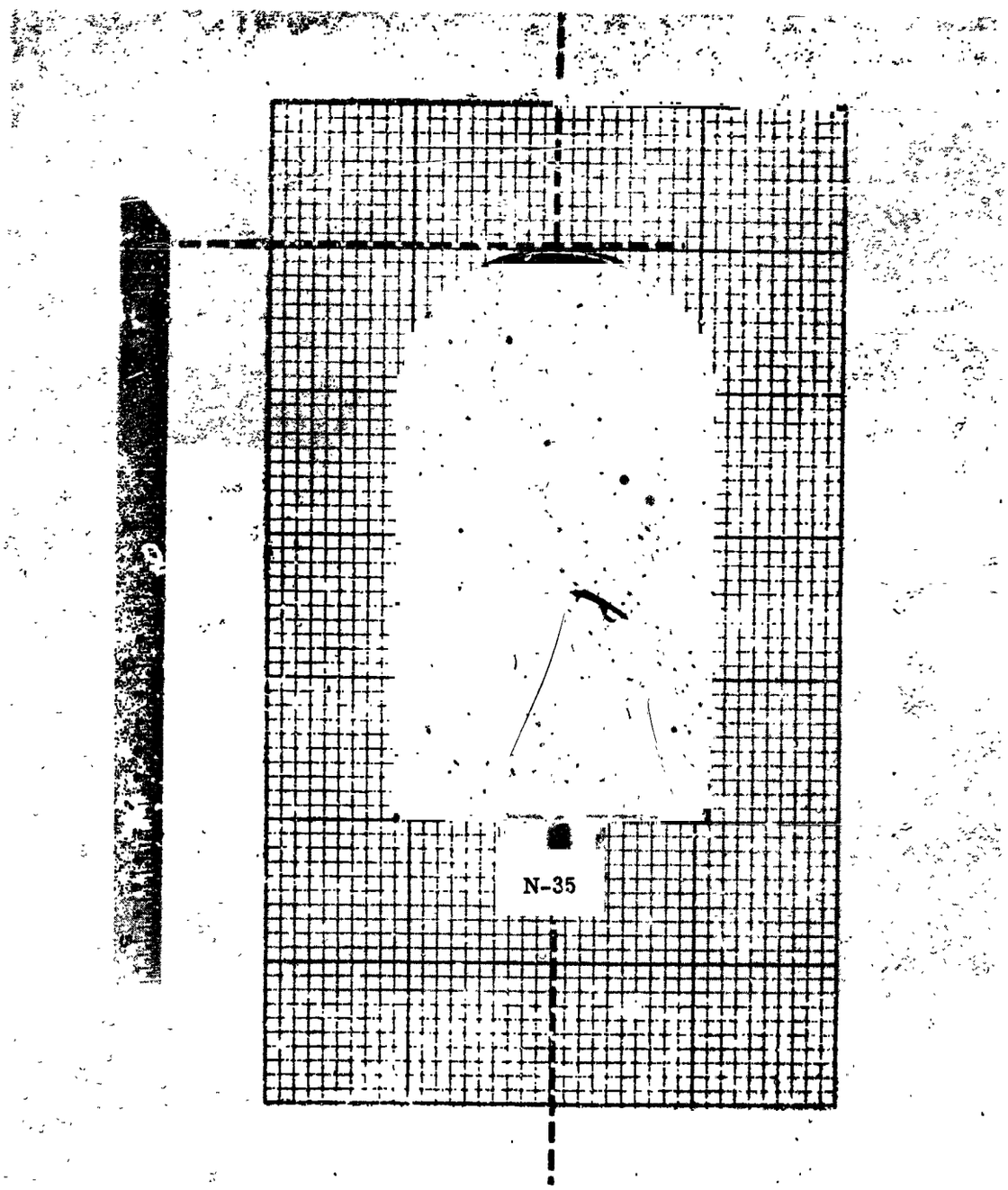

Figure A-11. Sectioned Model N-35 - After Test

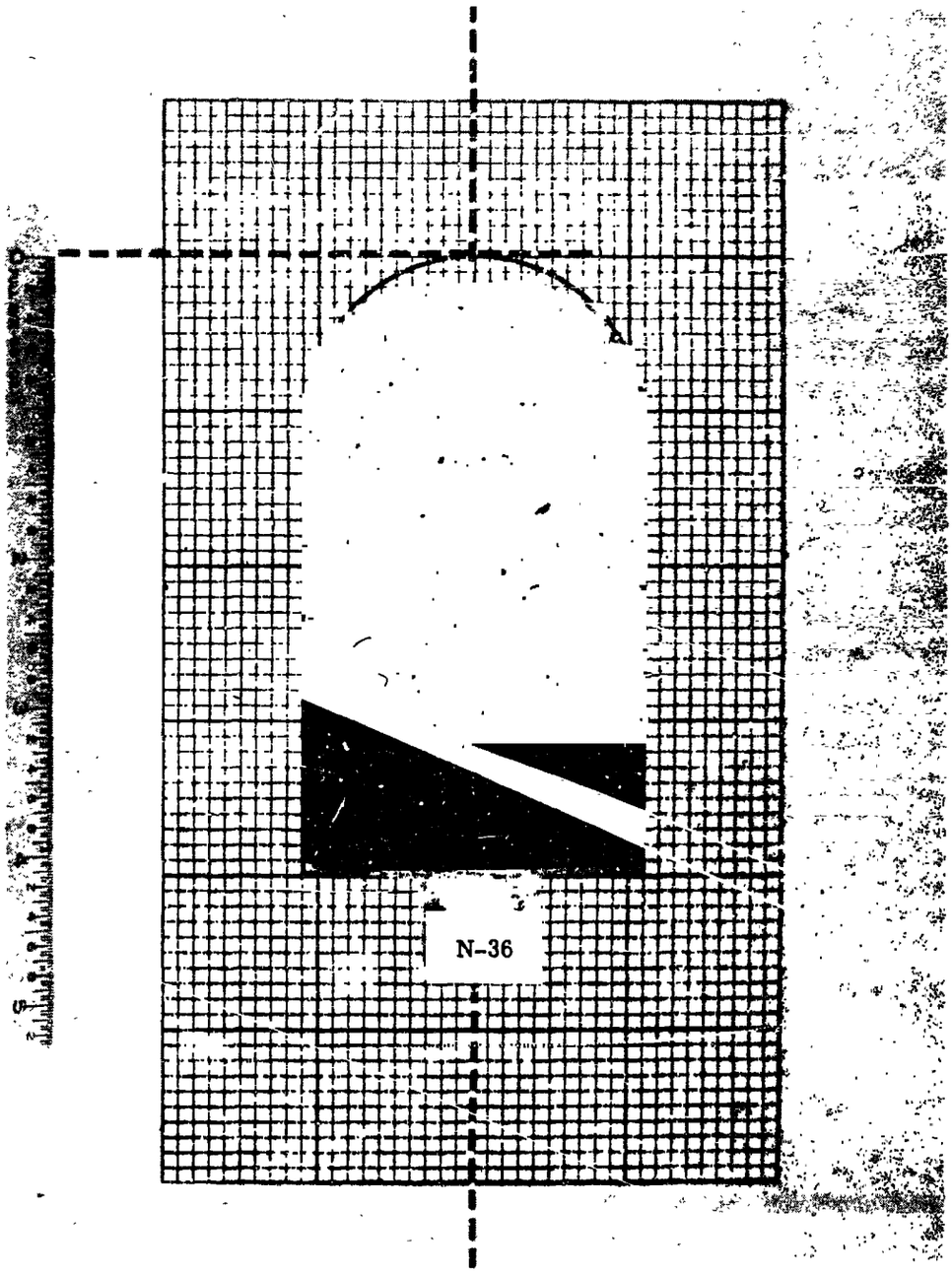

Figure A-12. Sectioned Model N-36 - After Test

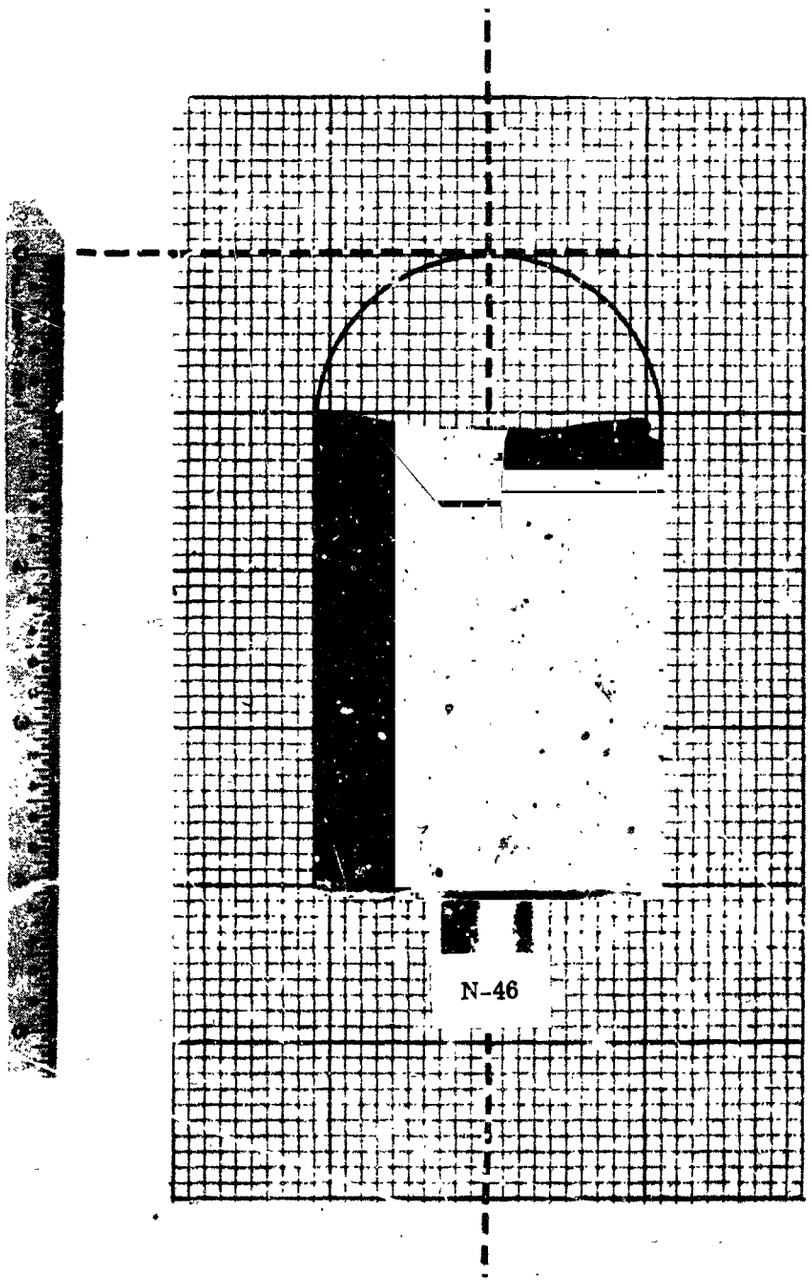

Figure A-13. Sectioned Model N-46 - After Test

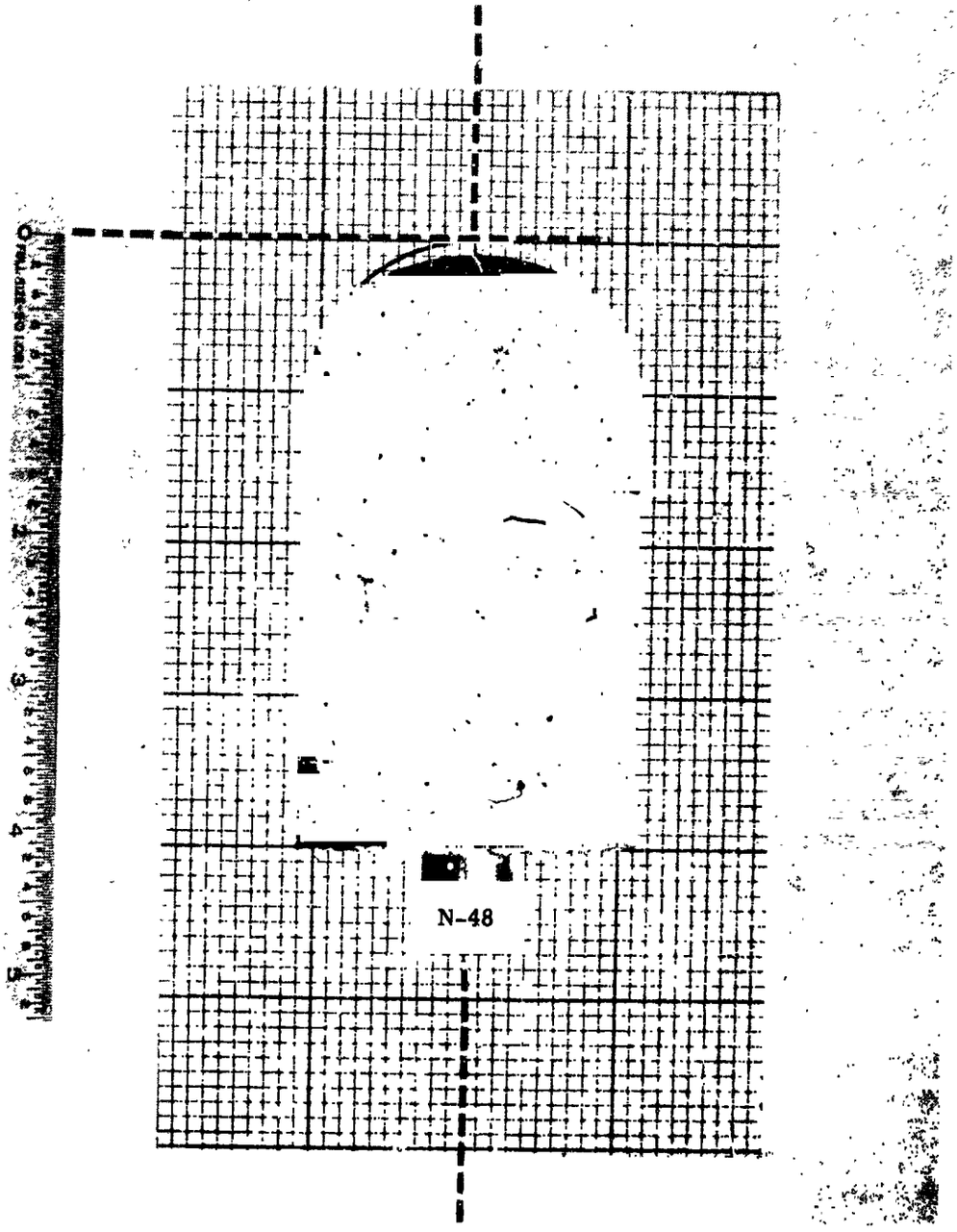

Figure A-14. Sectioned Model N-48 - After Test

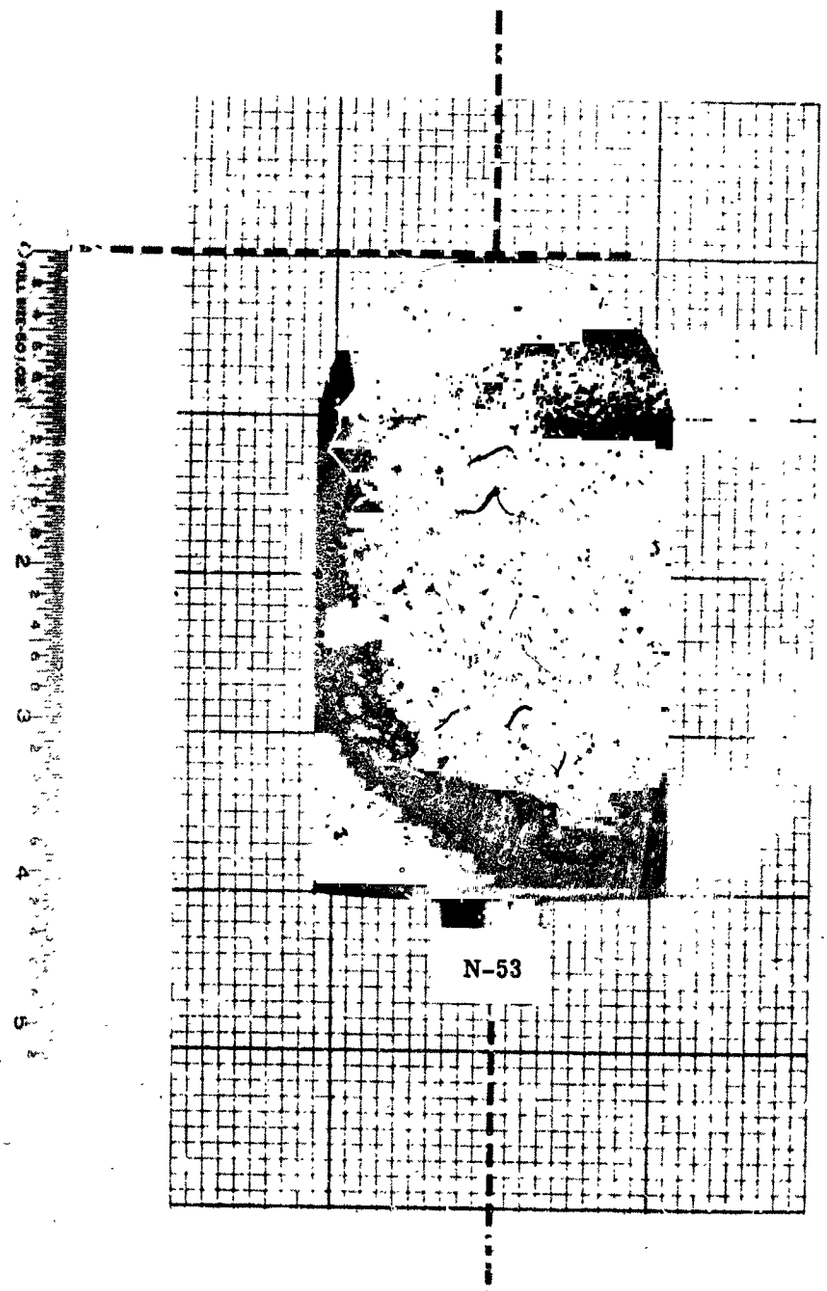

Figure A-15. Sectioned Model N-53 - After Test

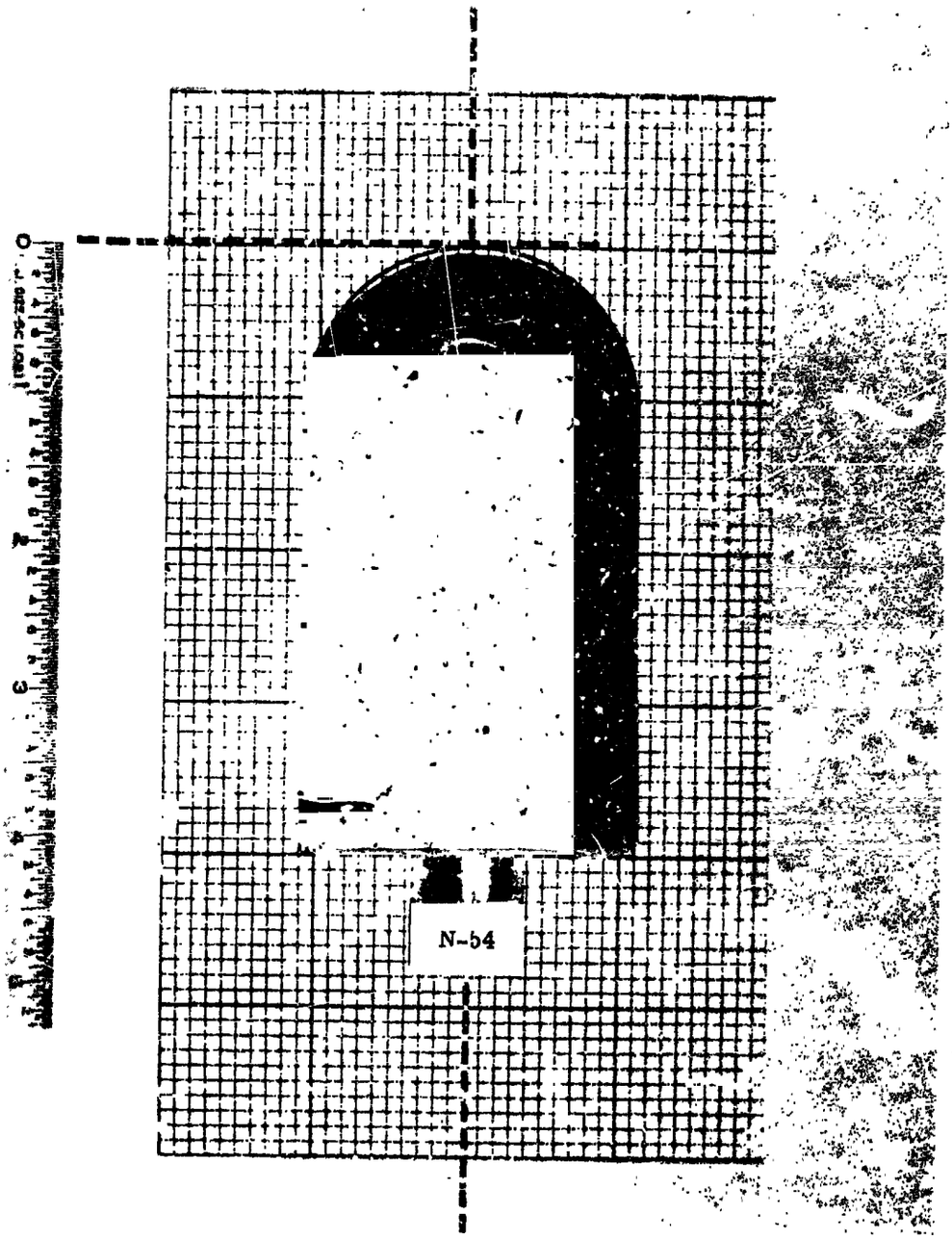

Figure A-16. Sectioned Model N-54 - After Test

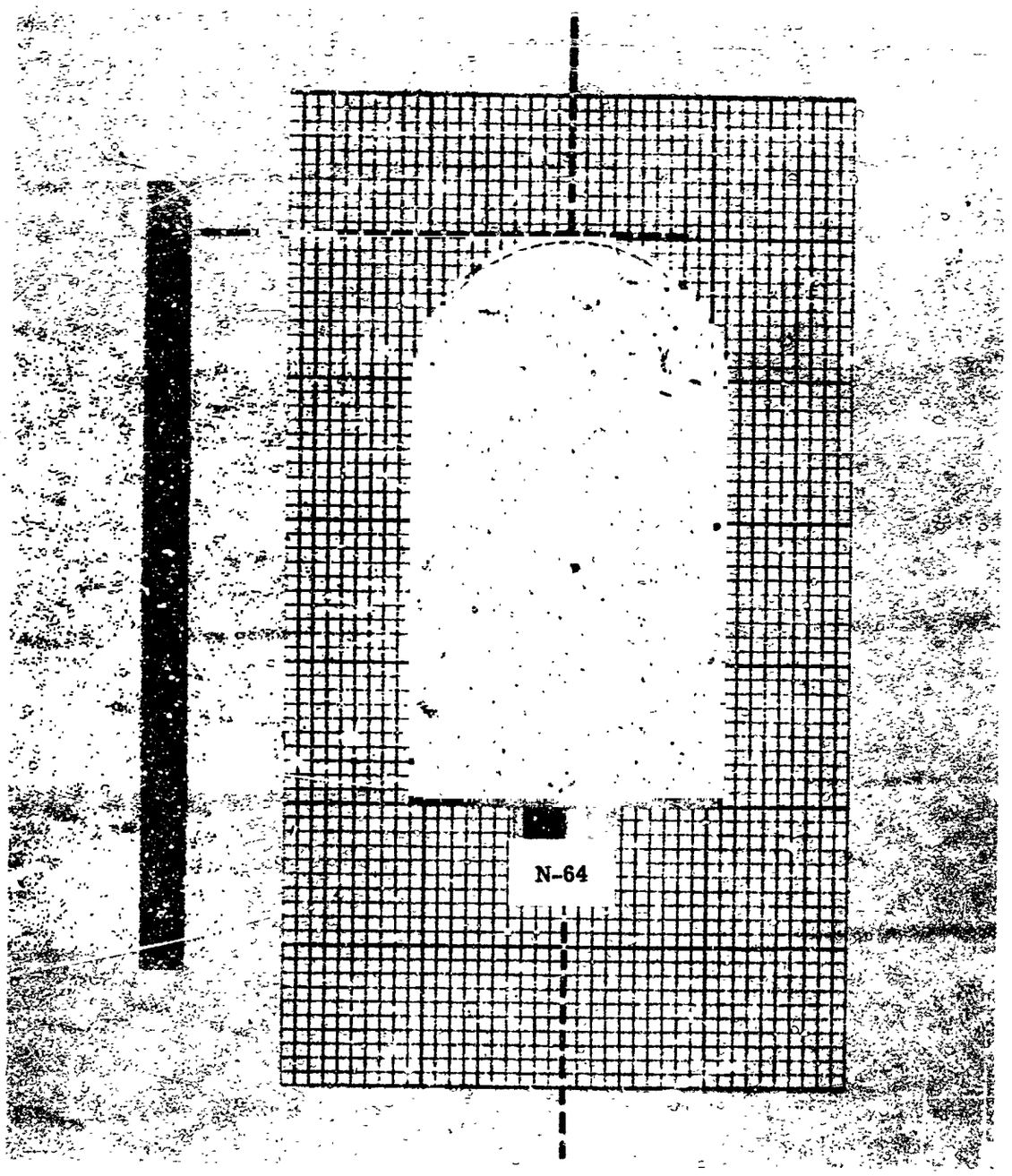

Figure A-17. Sectioned Model N-64 - After Test

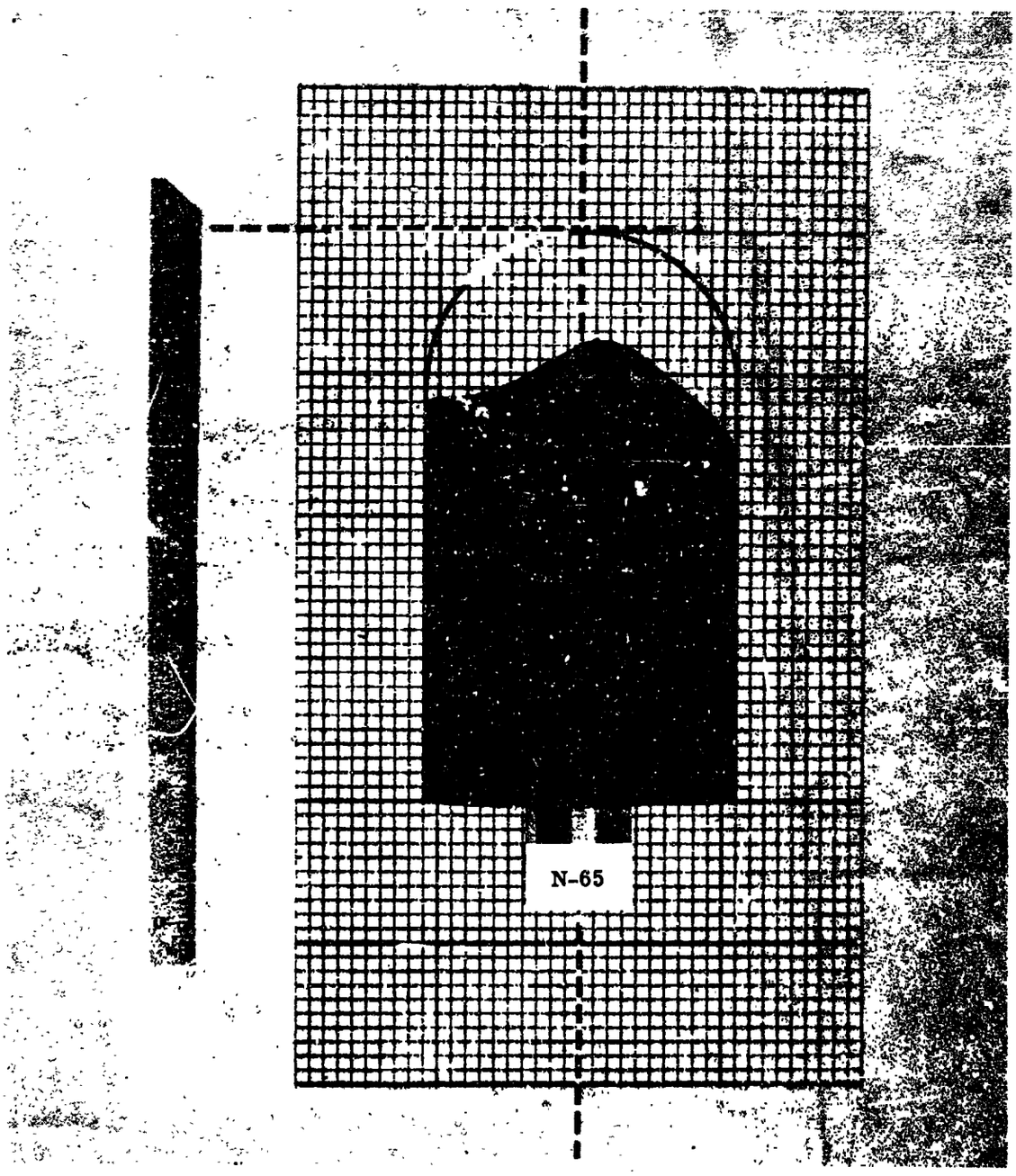

Figure A-18. Sectioned Model N-65 - After Test

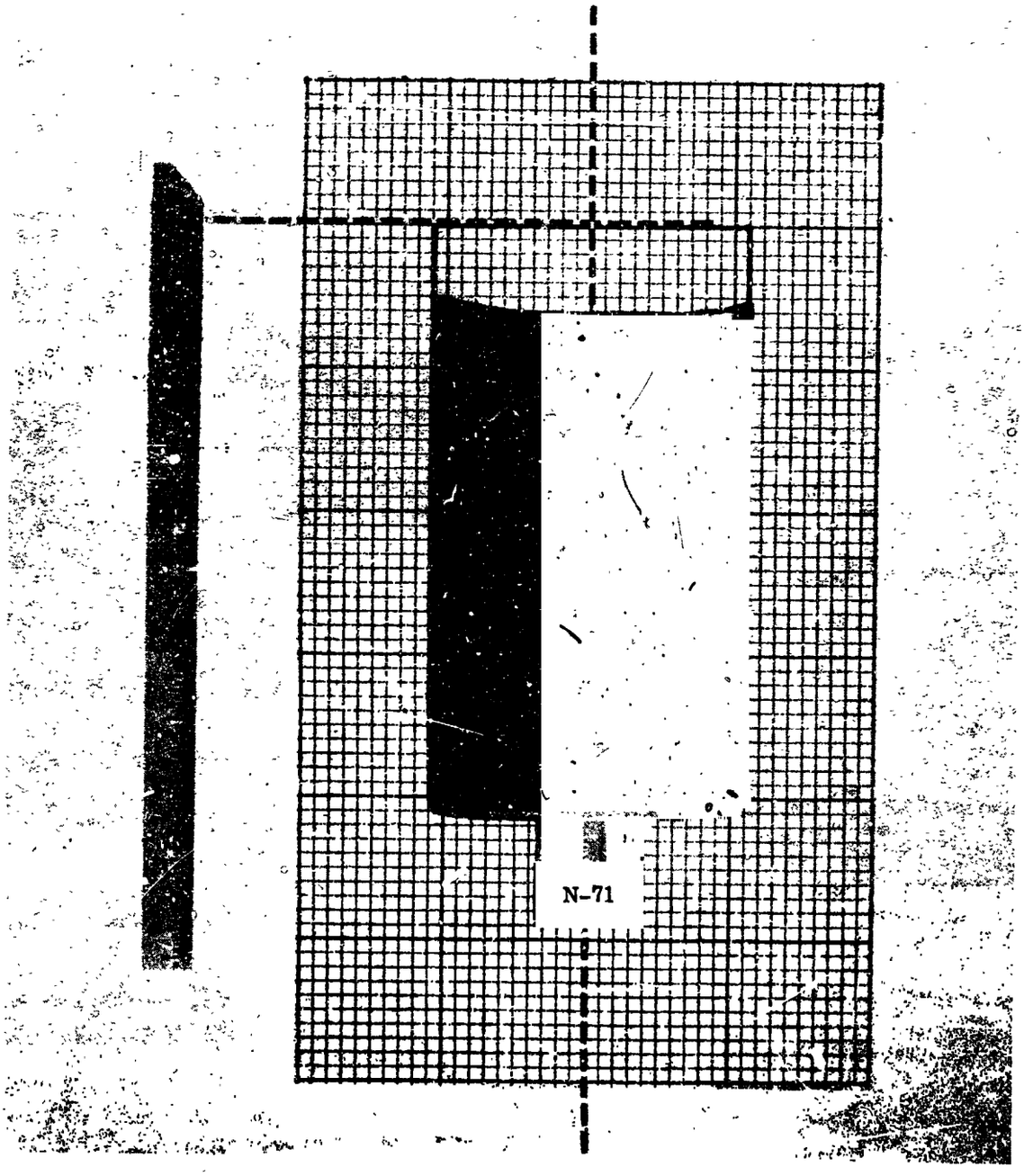

Figure A-19. Sectioned Model N-71 - After Test

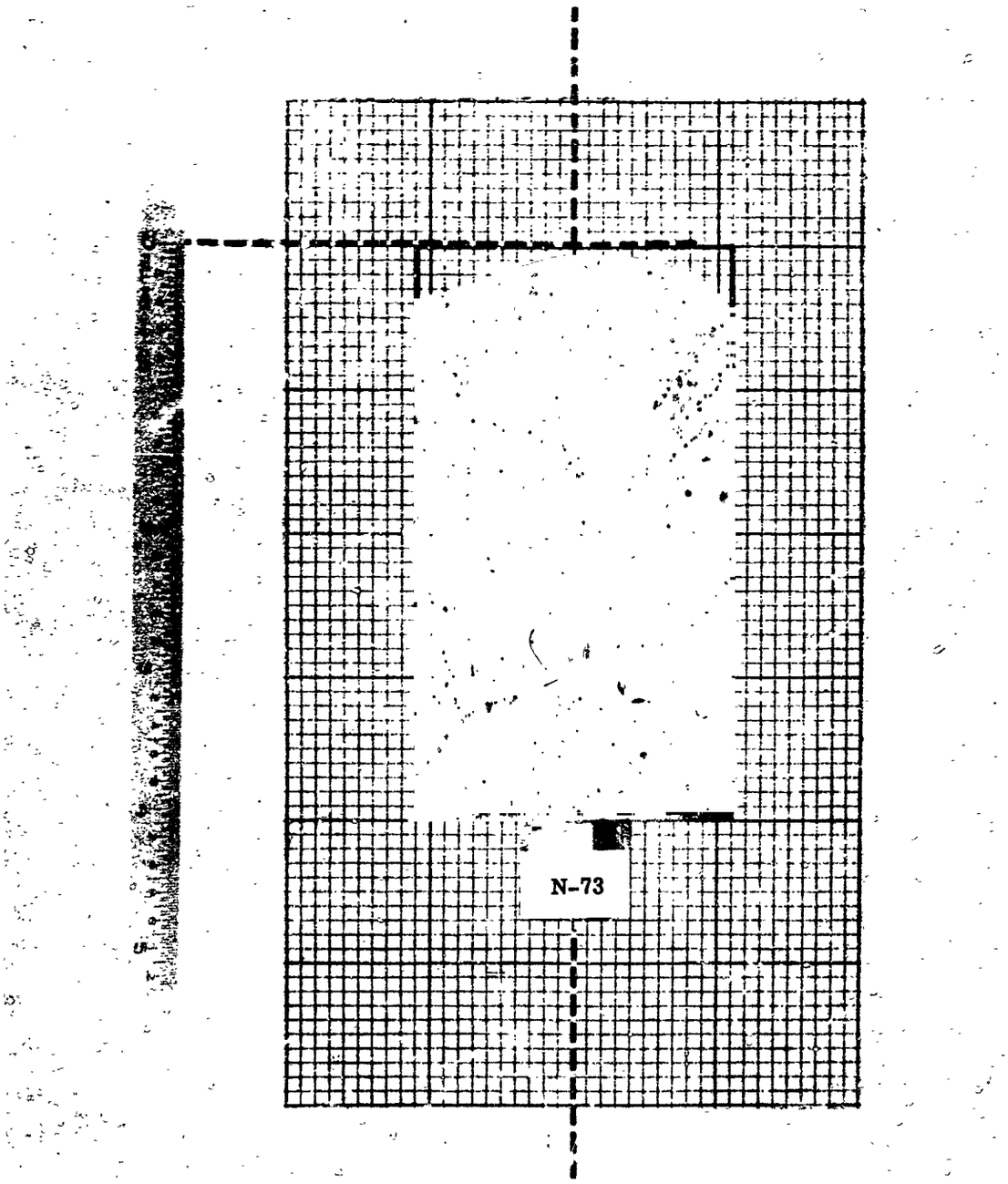

Figure A-20. Sectioned Model N-73 – After Test

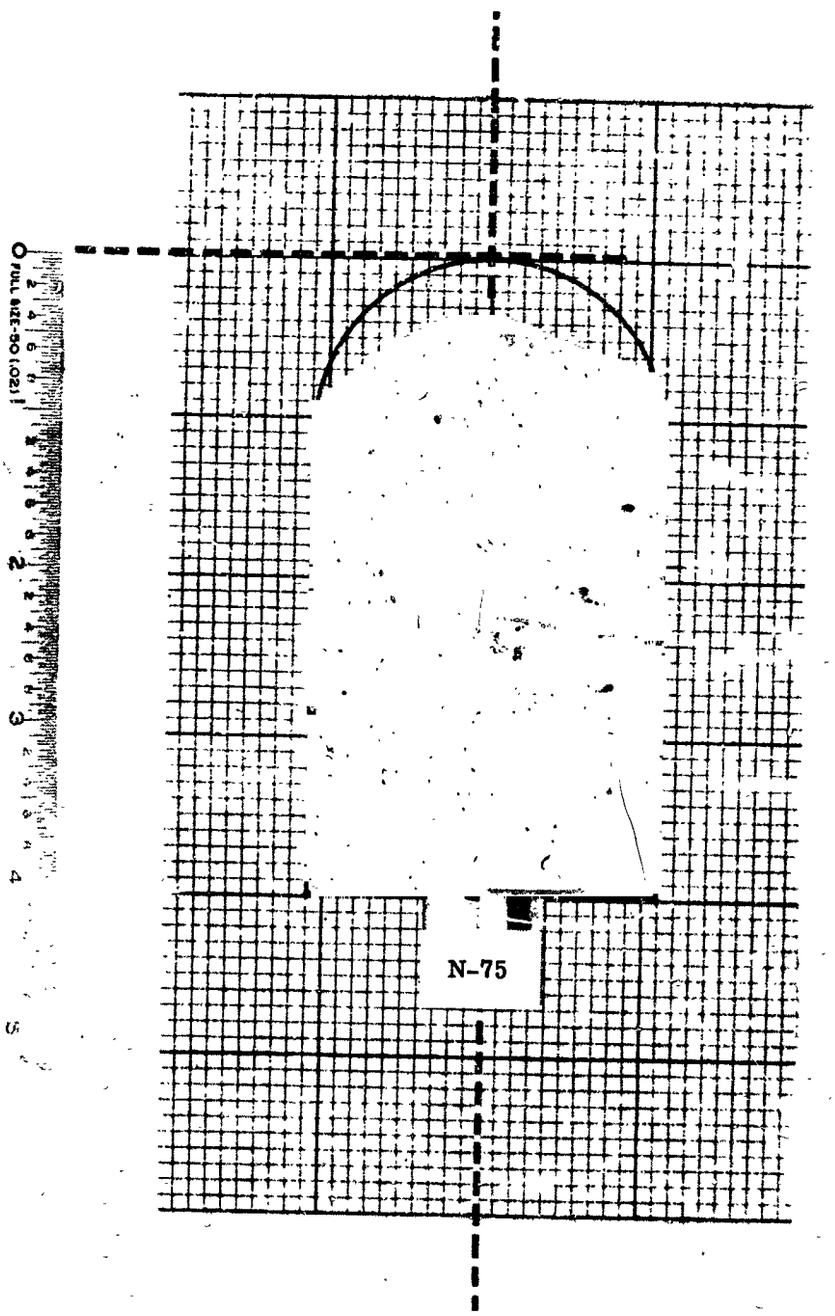

Figure A-21. Sectioned Model N-75 - After Test

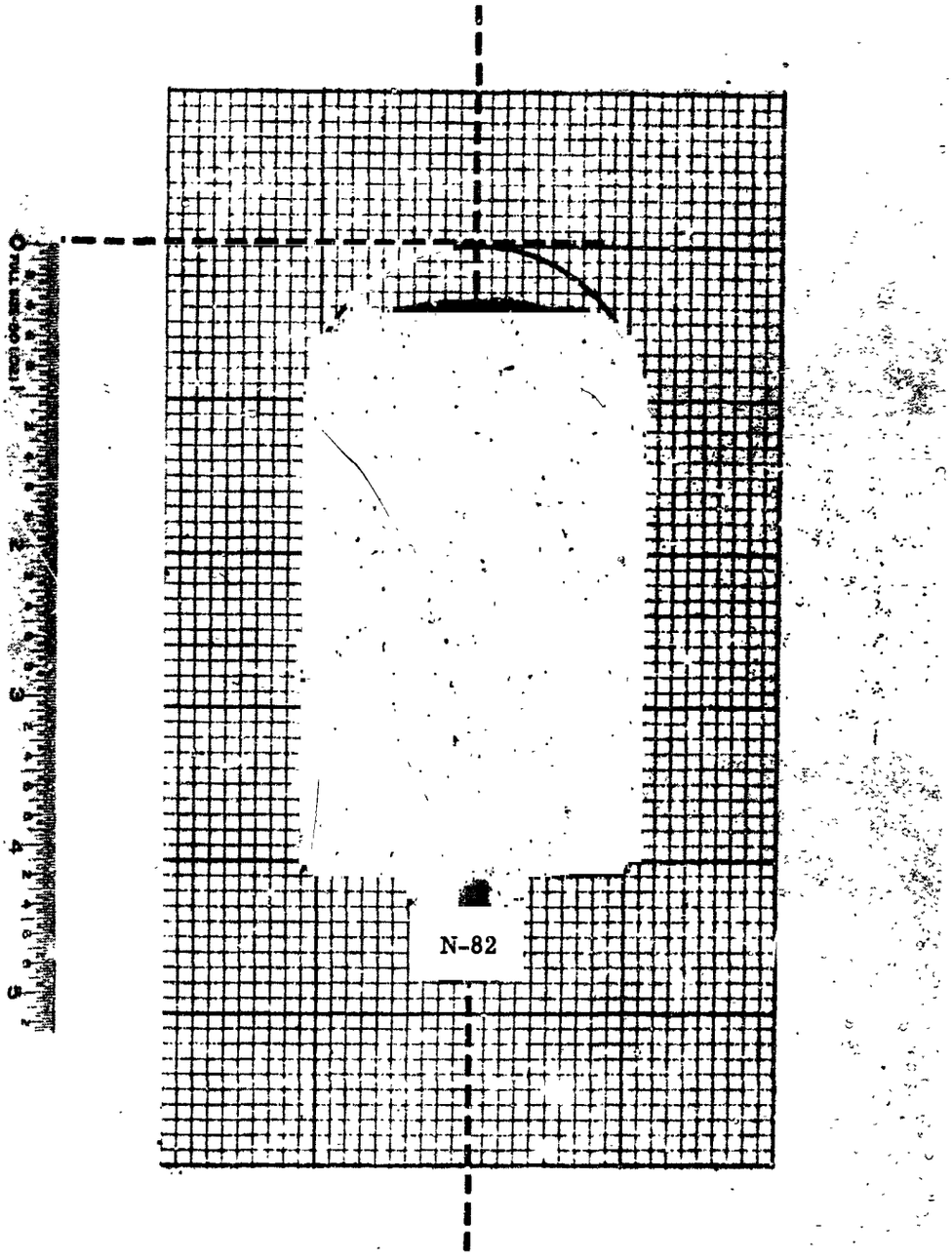

Figure A-22. Sectioned Model N-82 - After Test

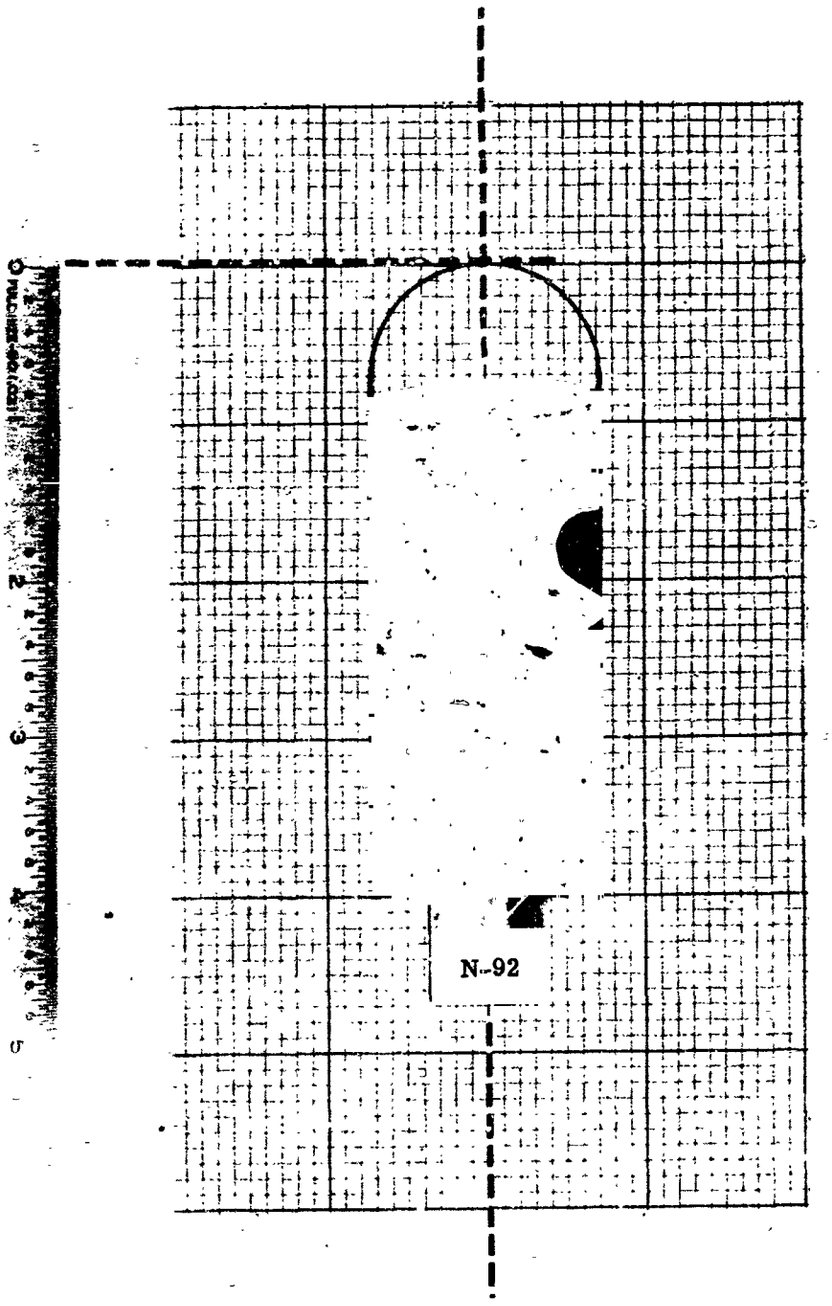

Figure A-23. Sectioned Model N-92 - After Test

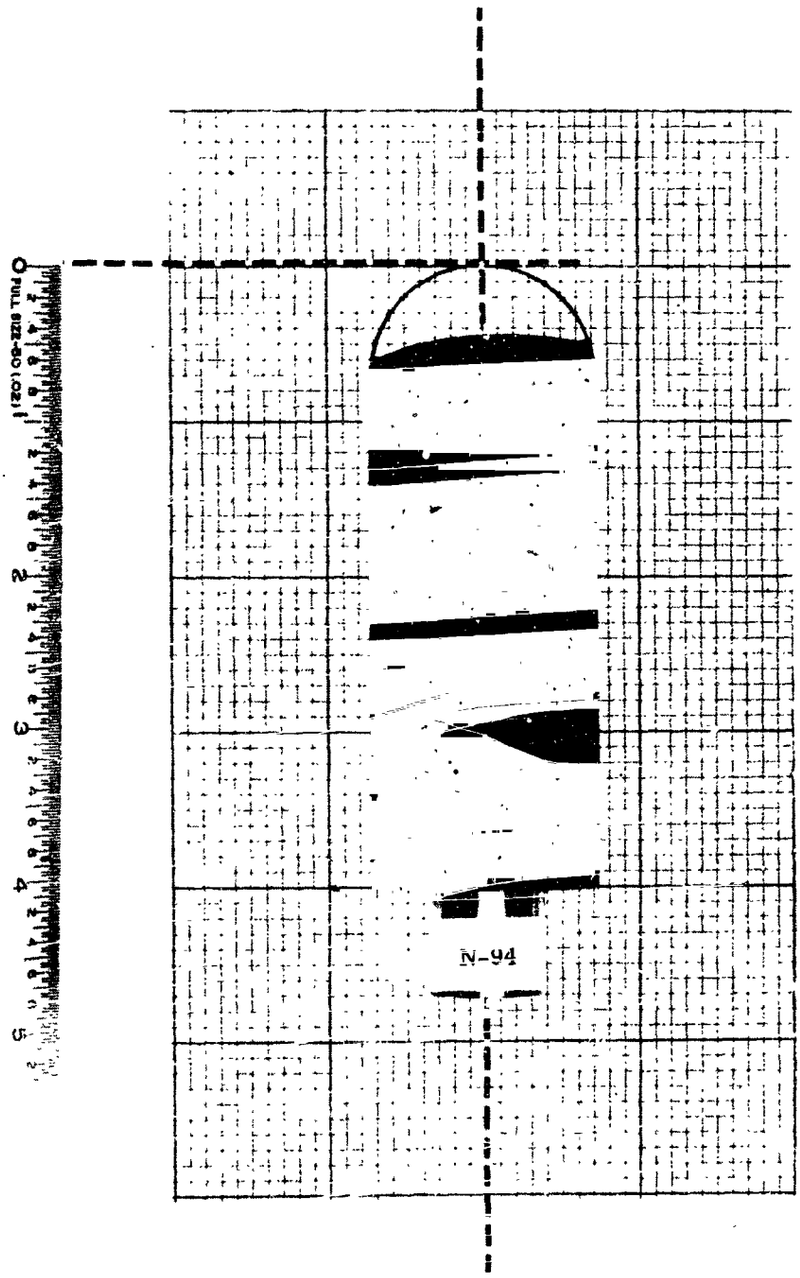

Figure A-24. Sectioned Model N-94 - After Test

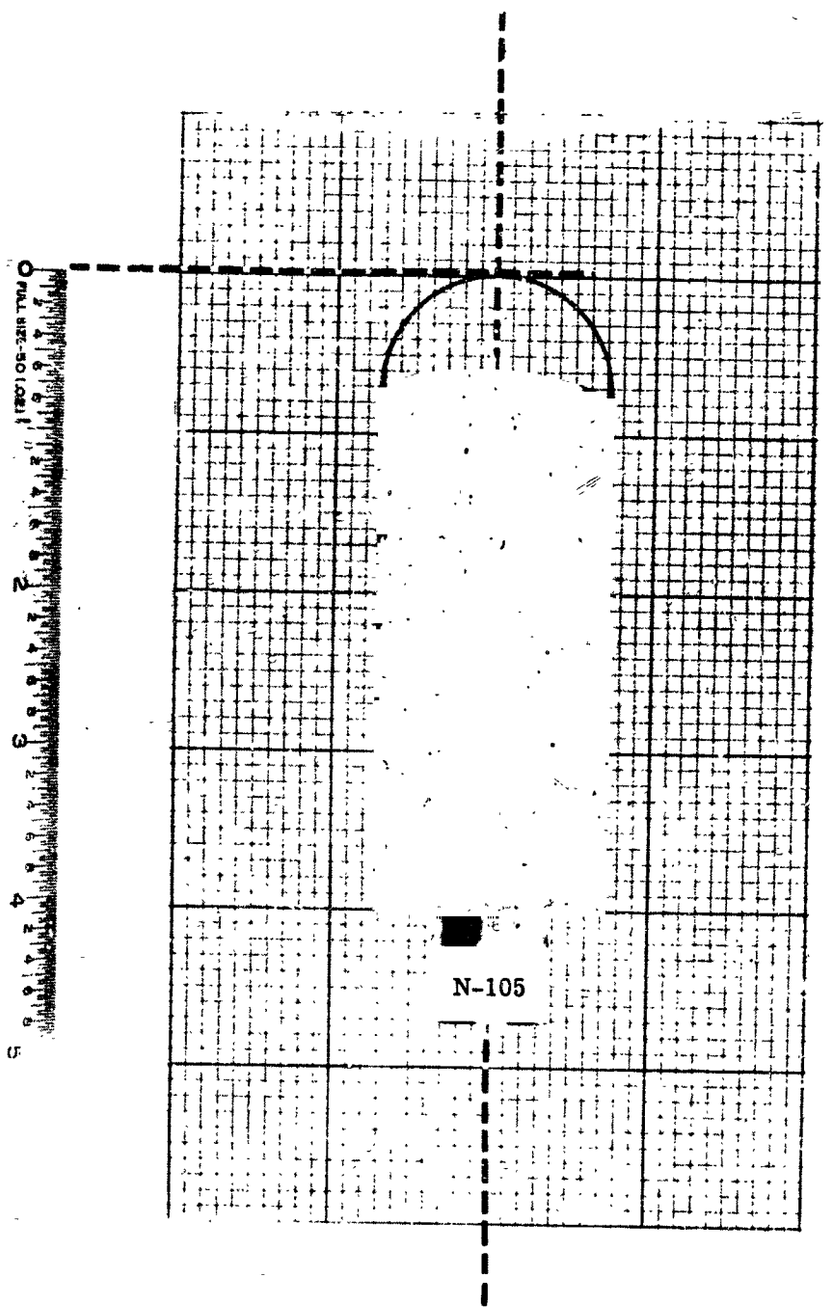

Figure A-25. Sectioned Model N-105 - After Test

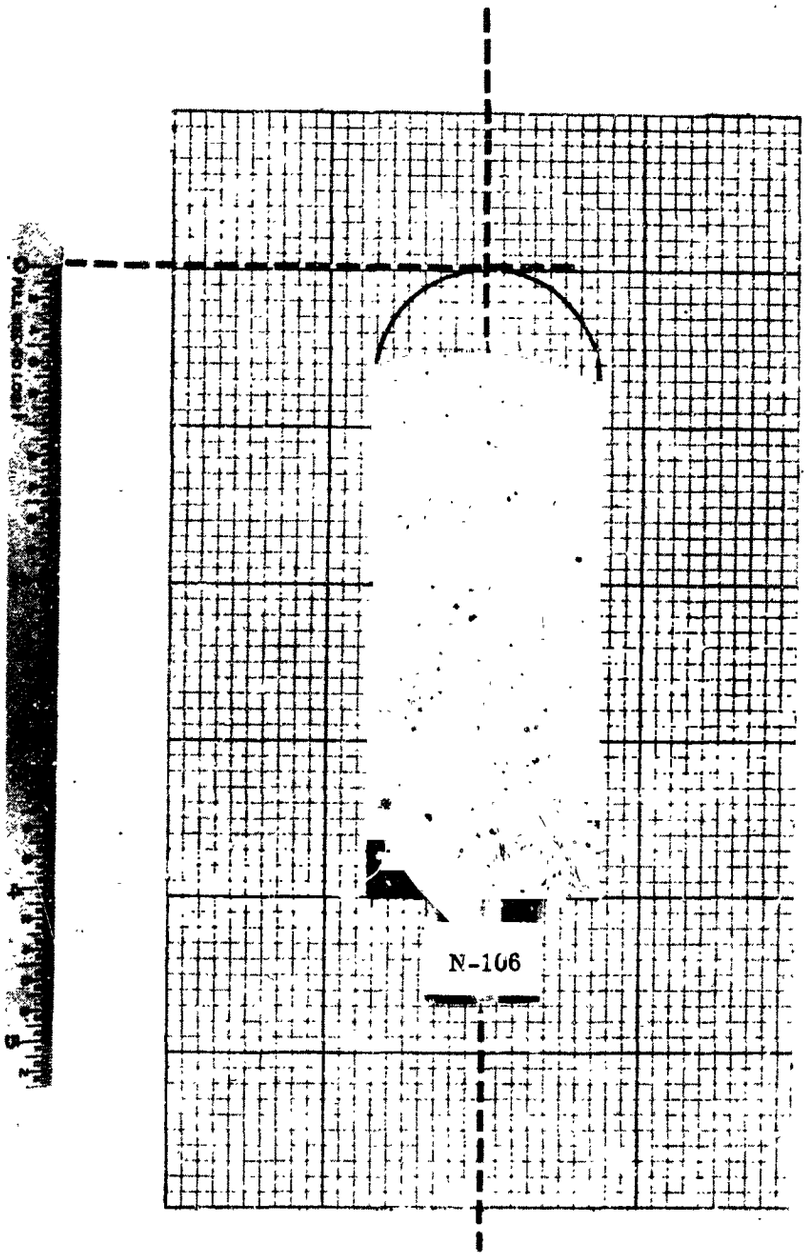

Figure A-26. Sectioned Model N-106 - ıter Test

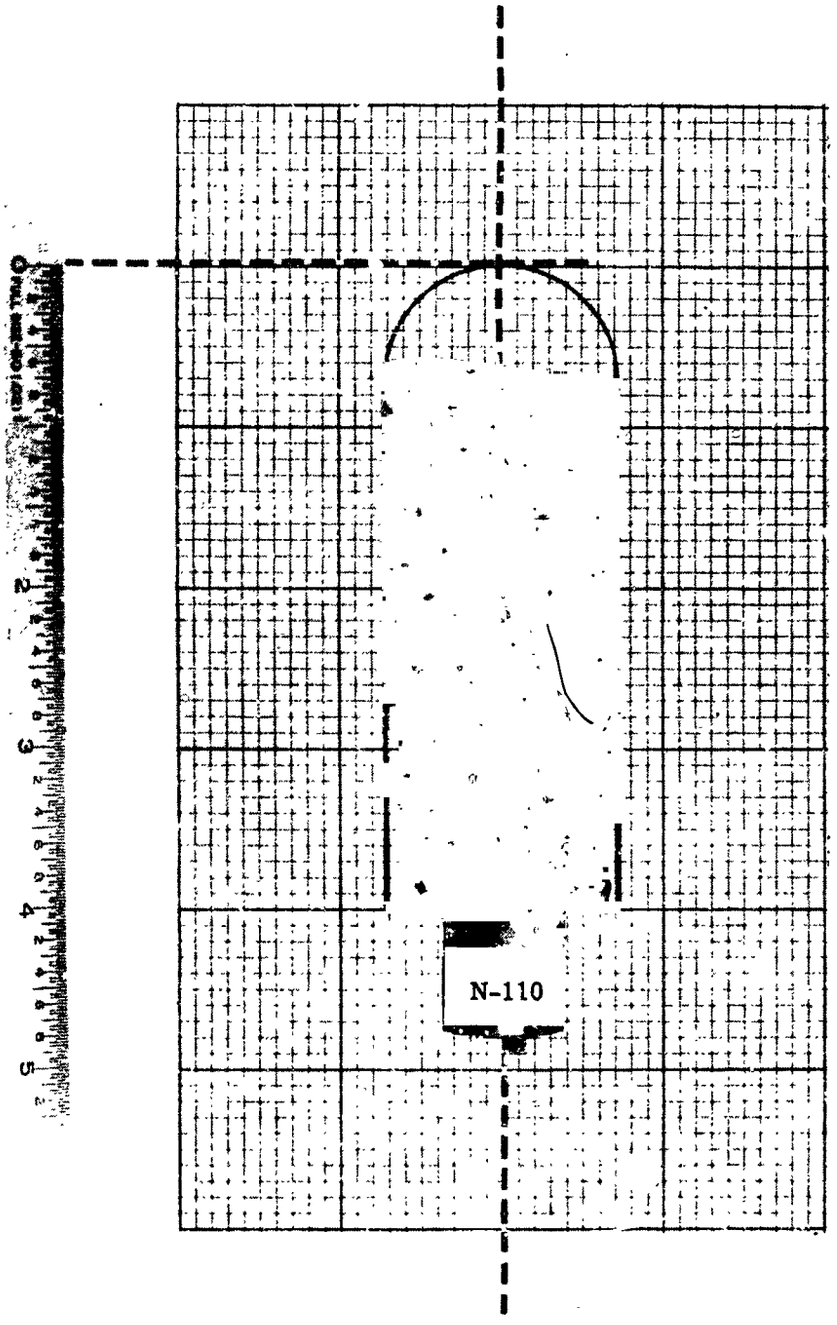

Figure A-27. Sectioned Model N-110 - After Test

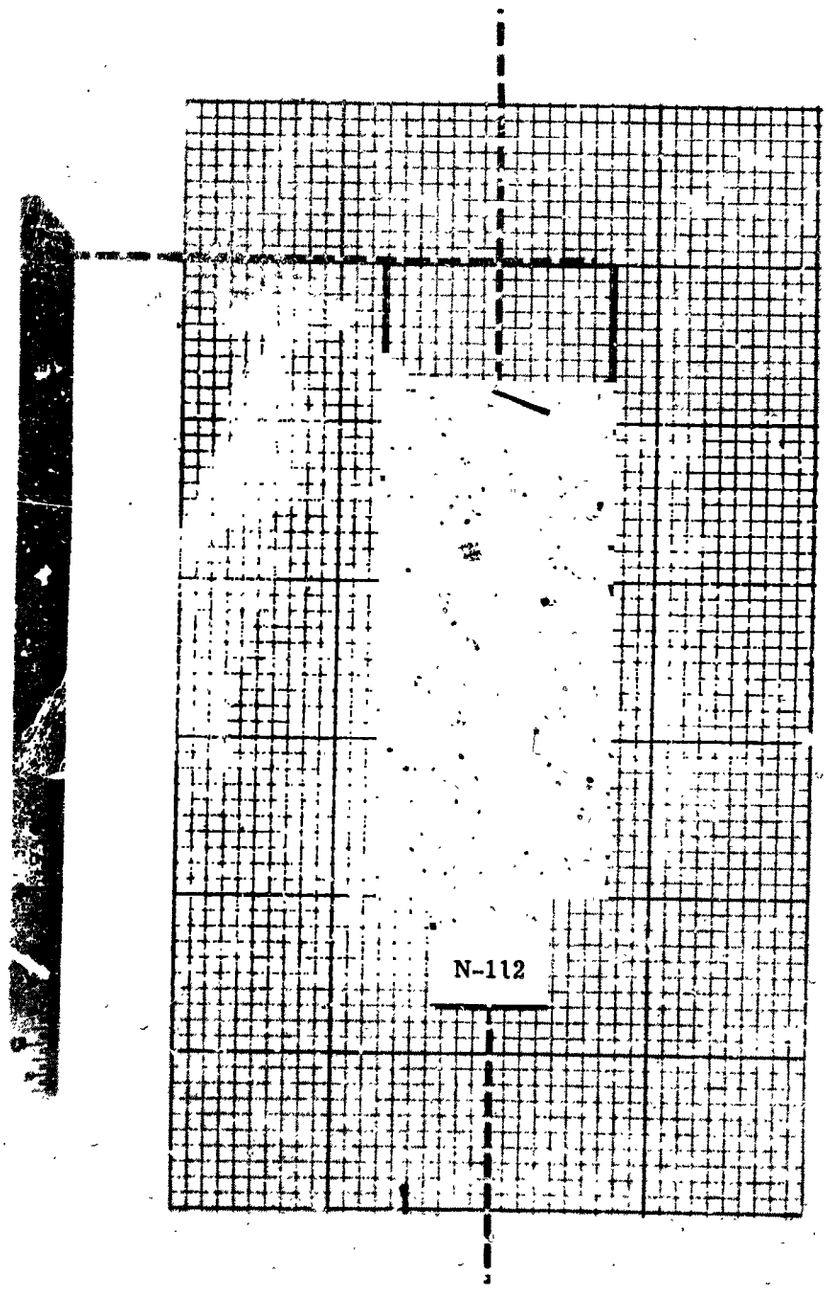

Figure A-28. Sectioned Model N-112 - After Test

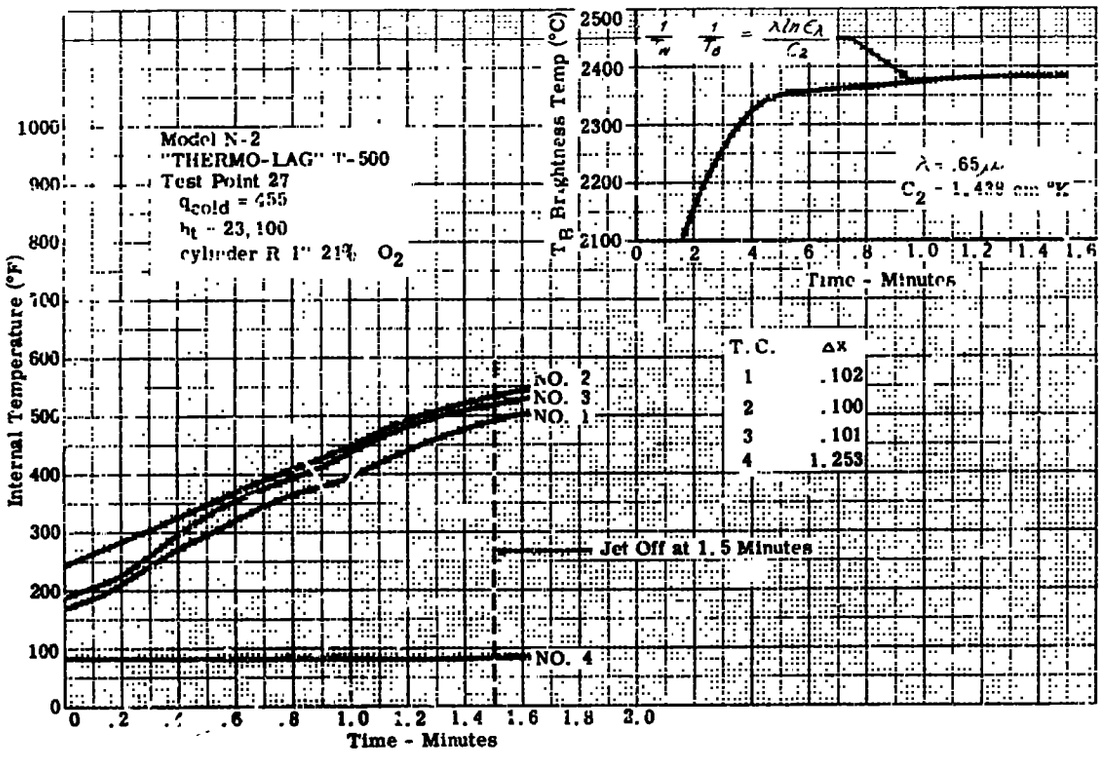

Figure A-29. Temperature - Time History of Model N-2

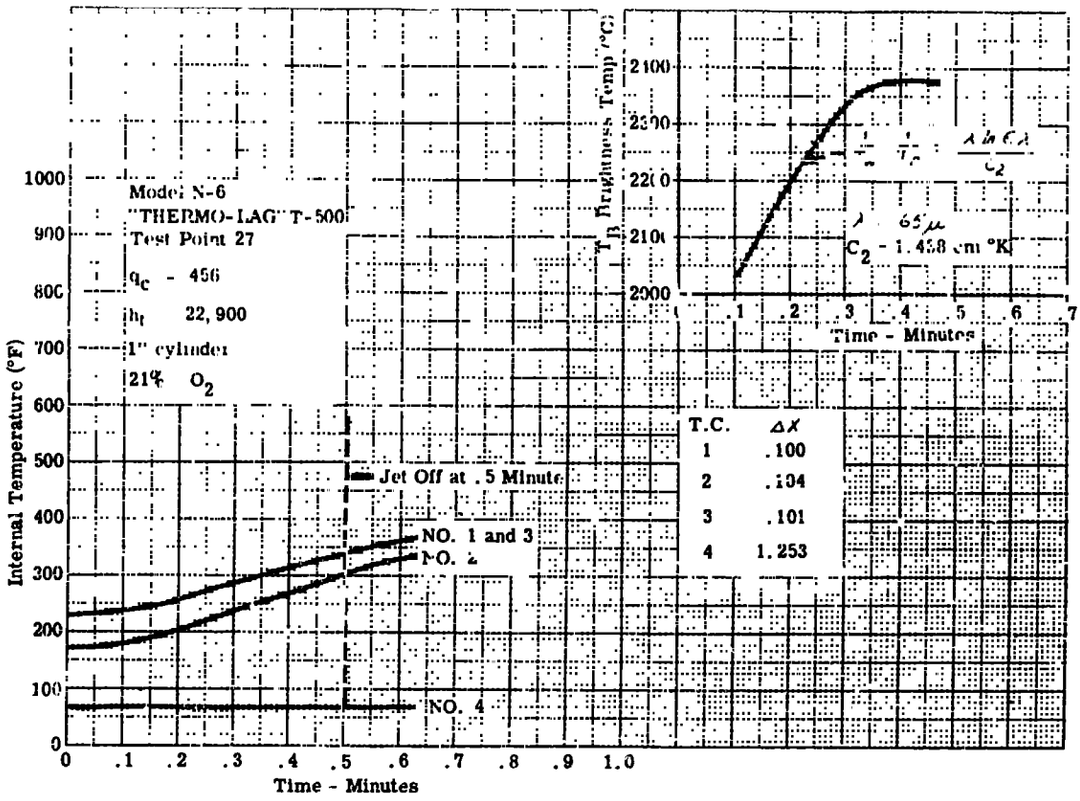

Figure A-30. Temperature - Time History of Model N-6

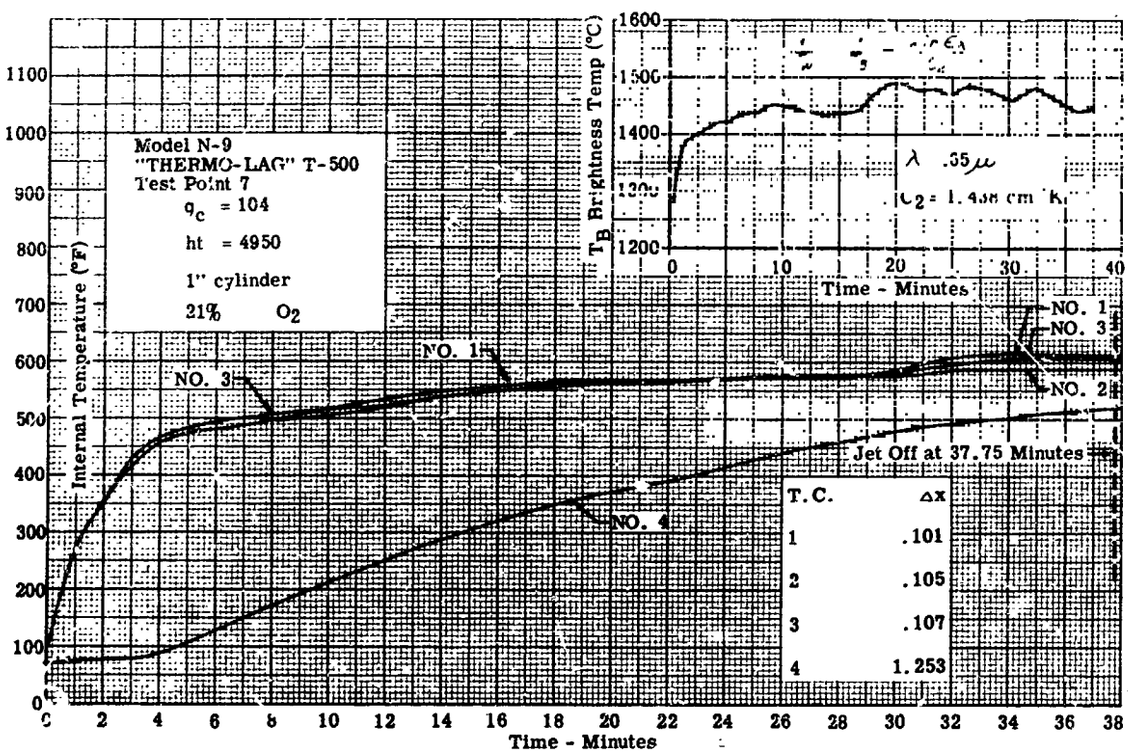

Figure A-31. Temperature - Time History of Model N-9

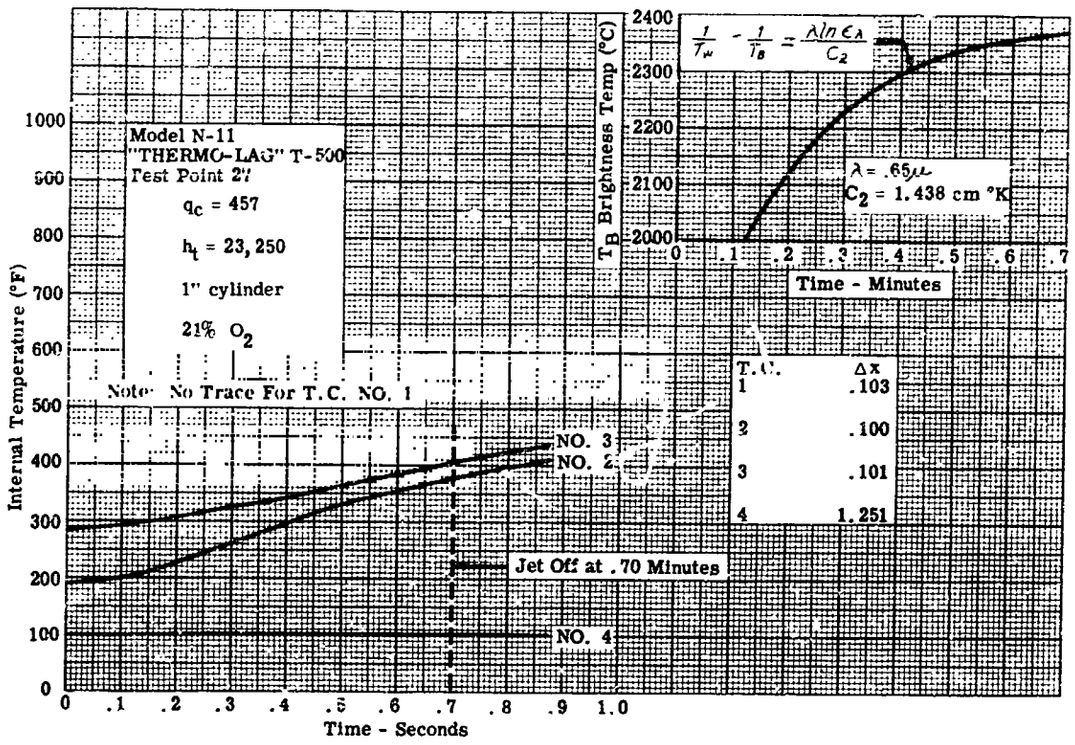

Figure A-32. Temperature - Time History of Model N-11

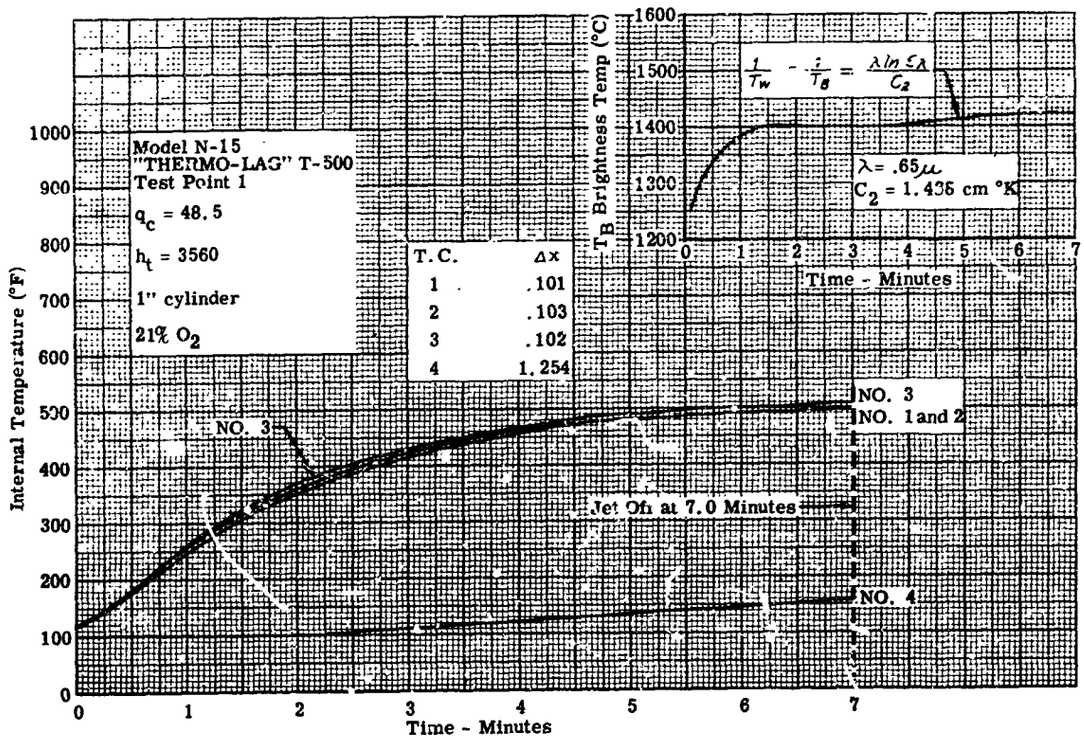

Figure A-33. Temperature - Time History of Model N-15

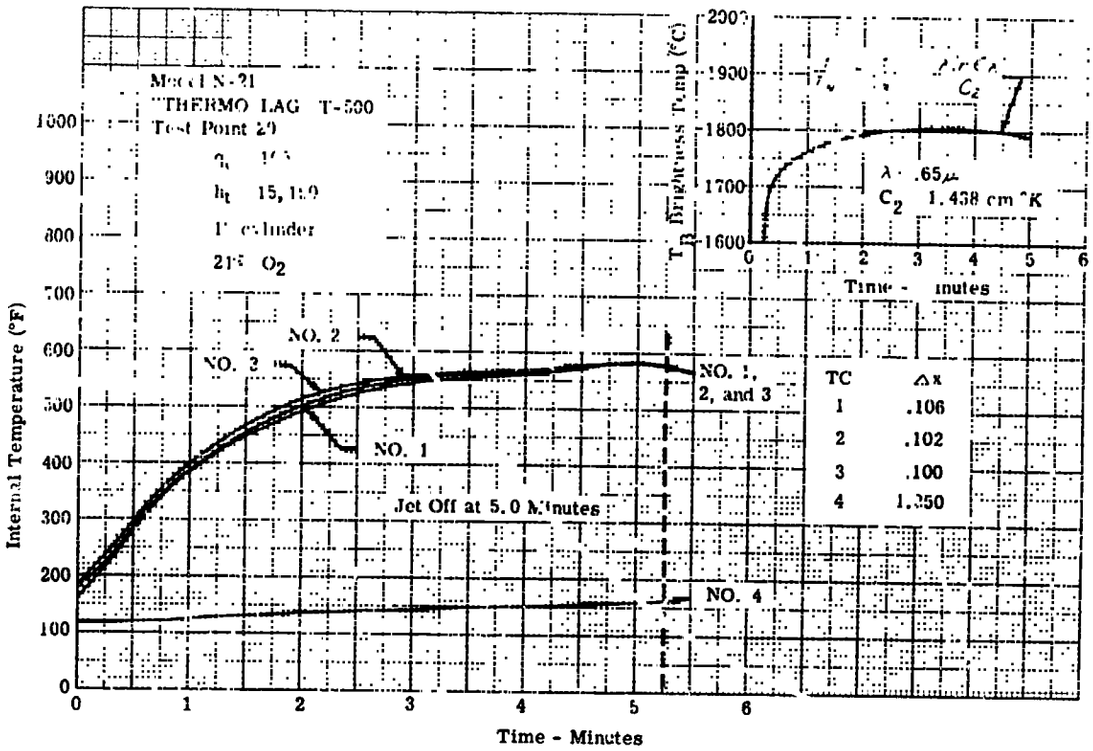

Figure A-34. Temperature - Time History of Model N-21

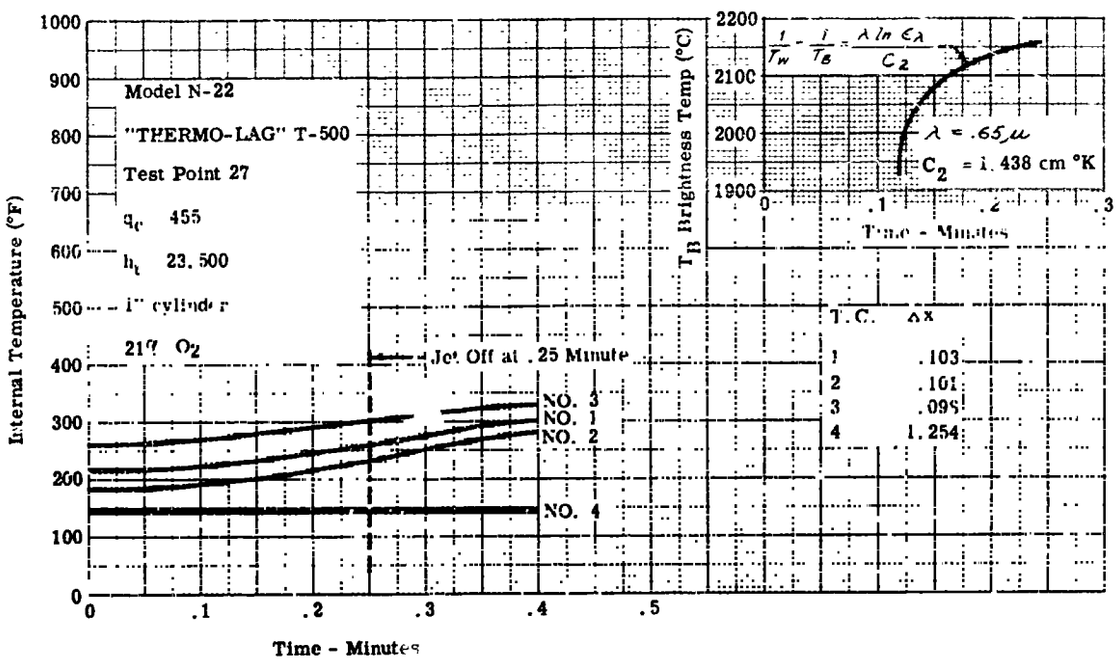

Figure A-35. Temperature - Time History of Model N-22

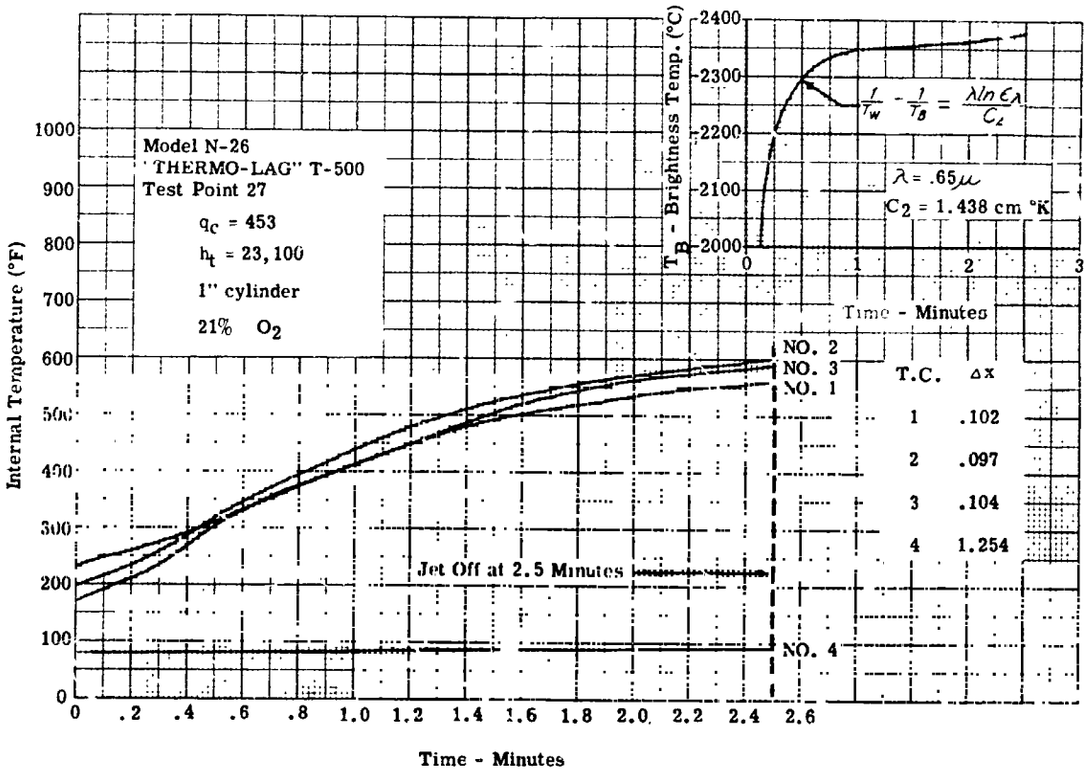

Figure A-36. Temperature - Time History of Model N-26

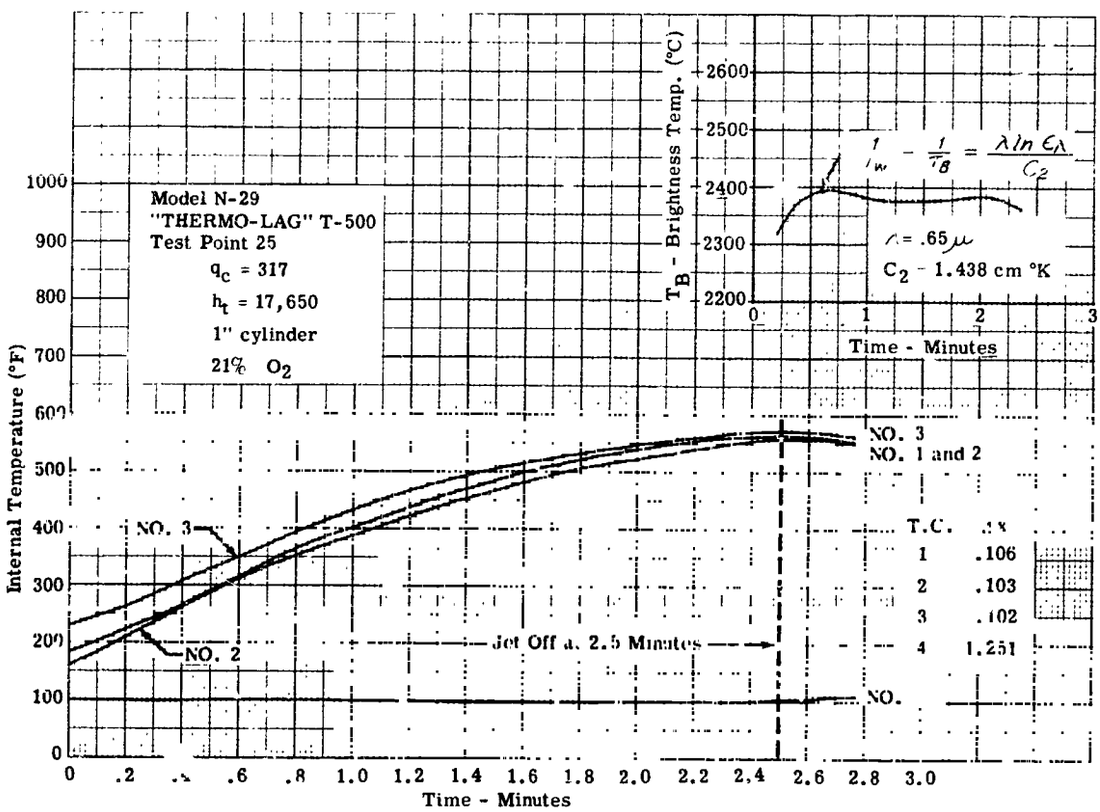

Figure A-37. Temperature - Time History of Model N-29

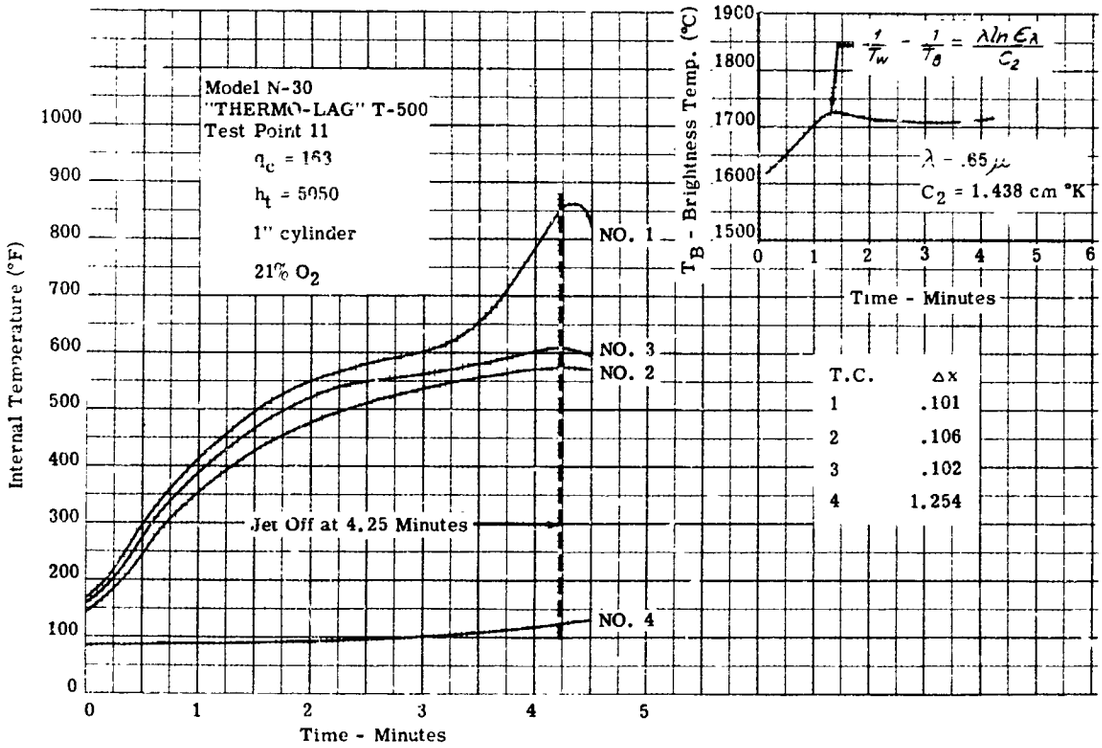

Figure A-38. Temperature - Time History of Model N-30

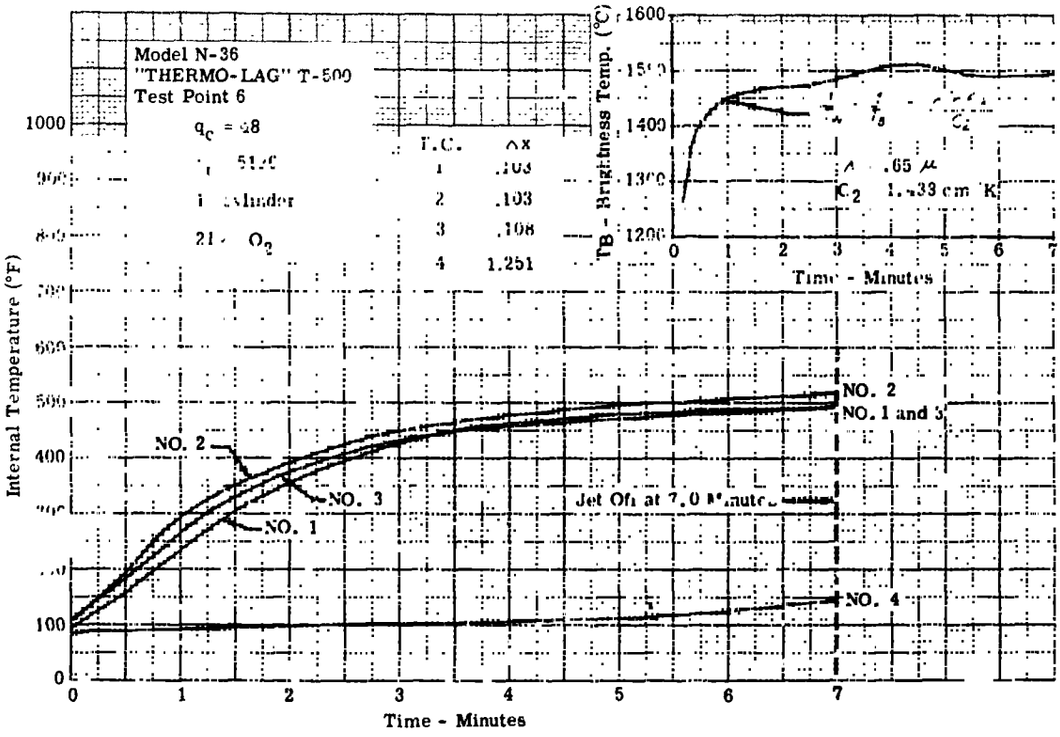

Figure A-40. Temperature - Time History of Model N-36

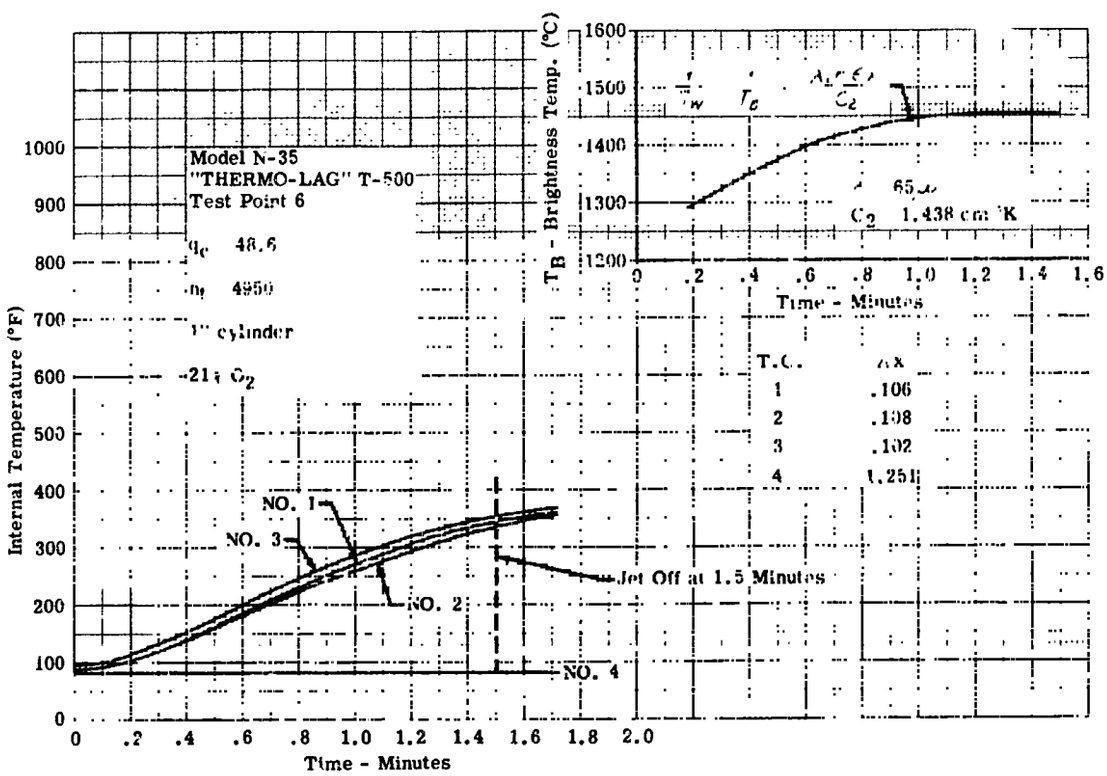

Figure A-39. Temperature - Time History of Model N-35

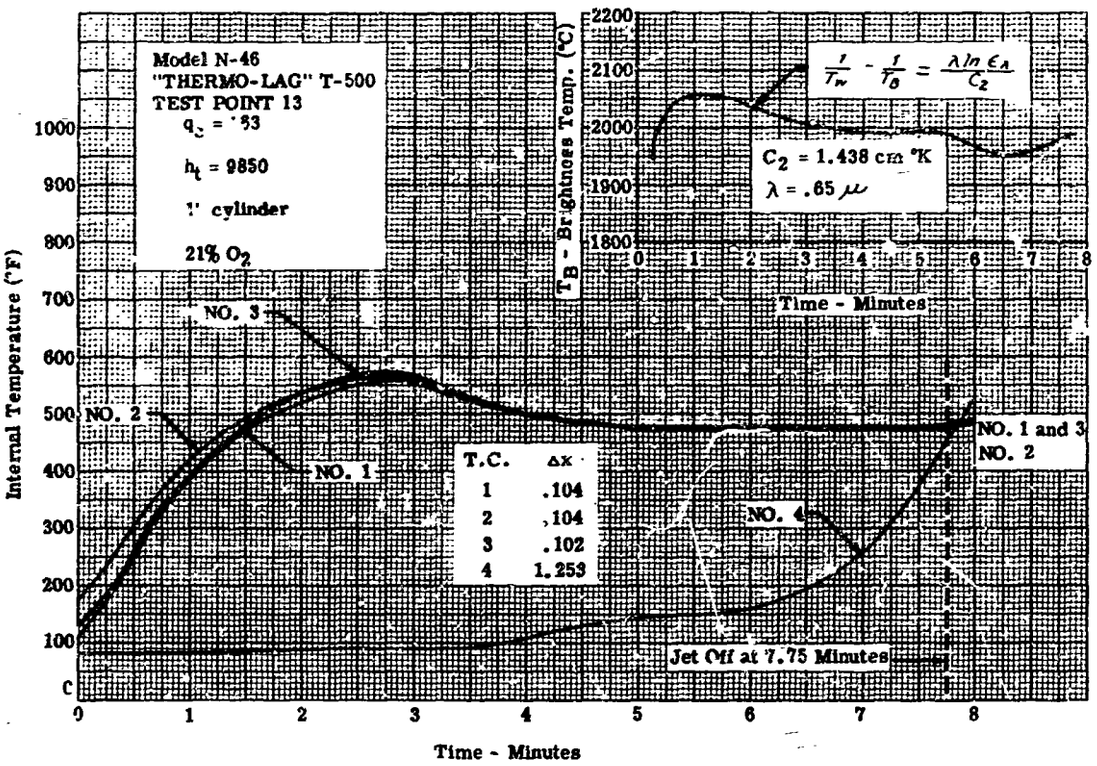

Figure A-41. Temperature - Time History of Model N-46

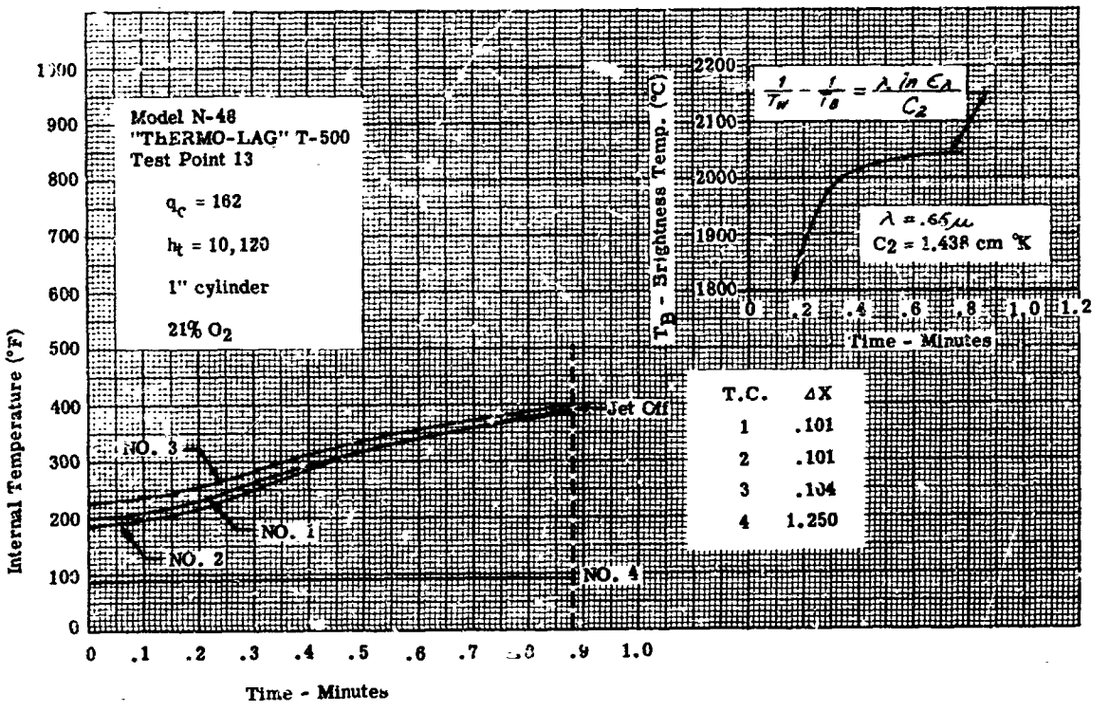

Figure A-42. Temperature - Time History of Model N-48

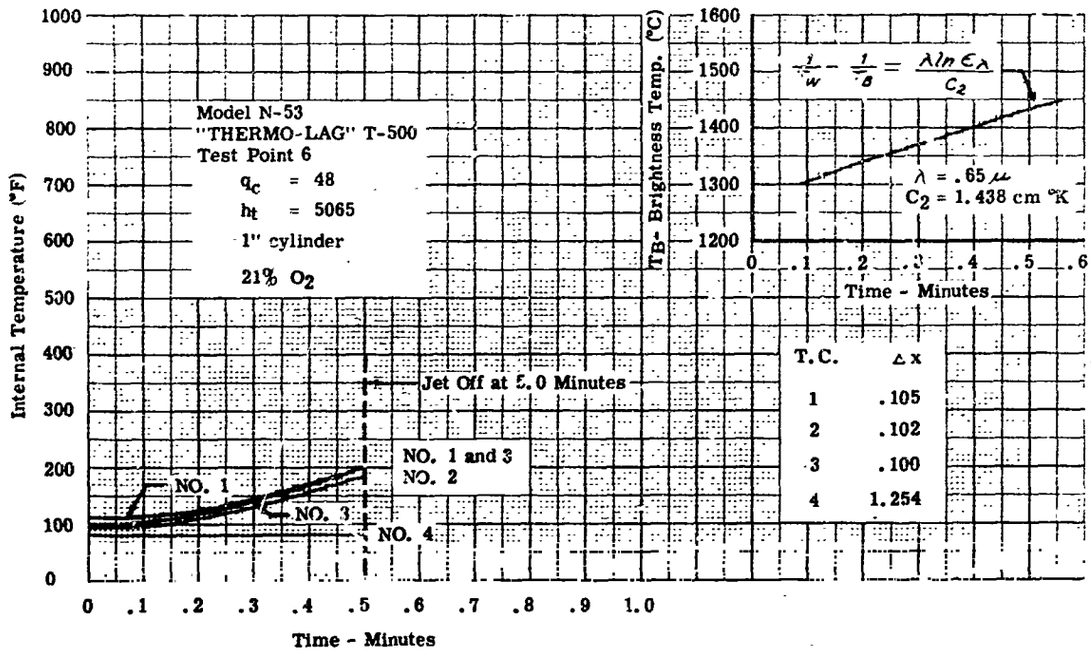

Figure A-43. Temperature - Time History of Model N-53

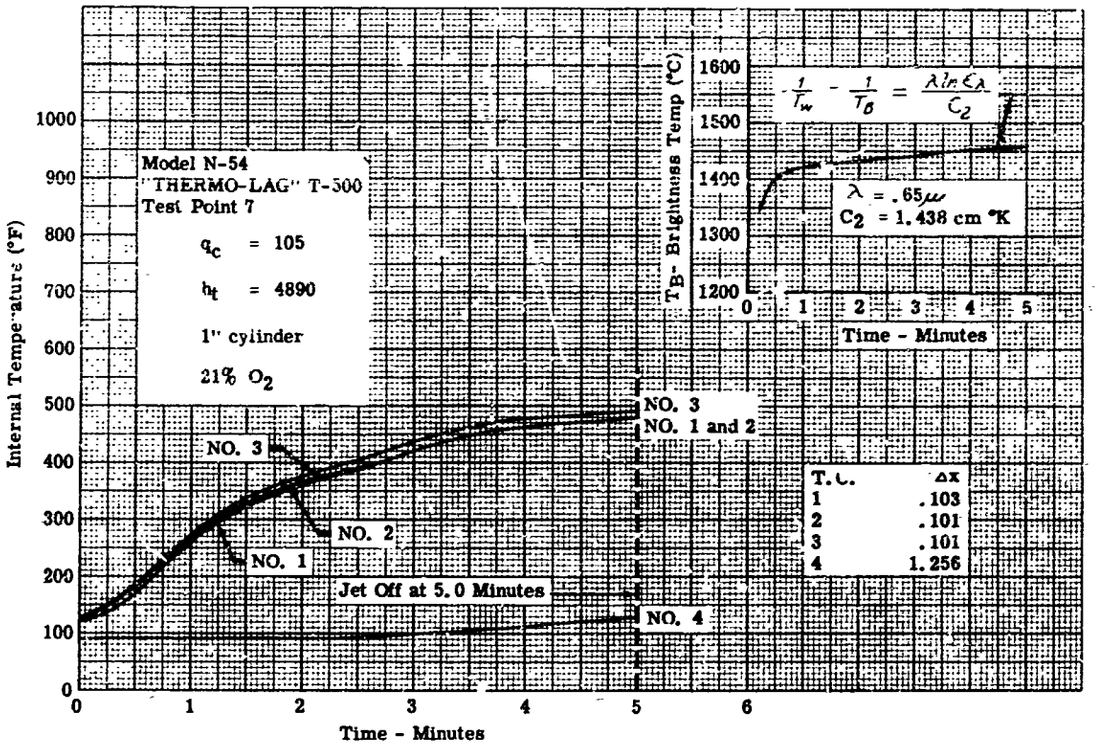

Figure A-44. Temperature - Time History of Model N-54

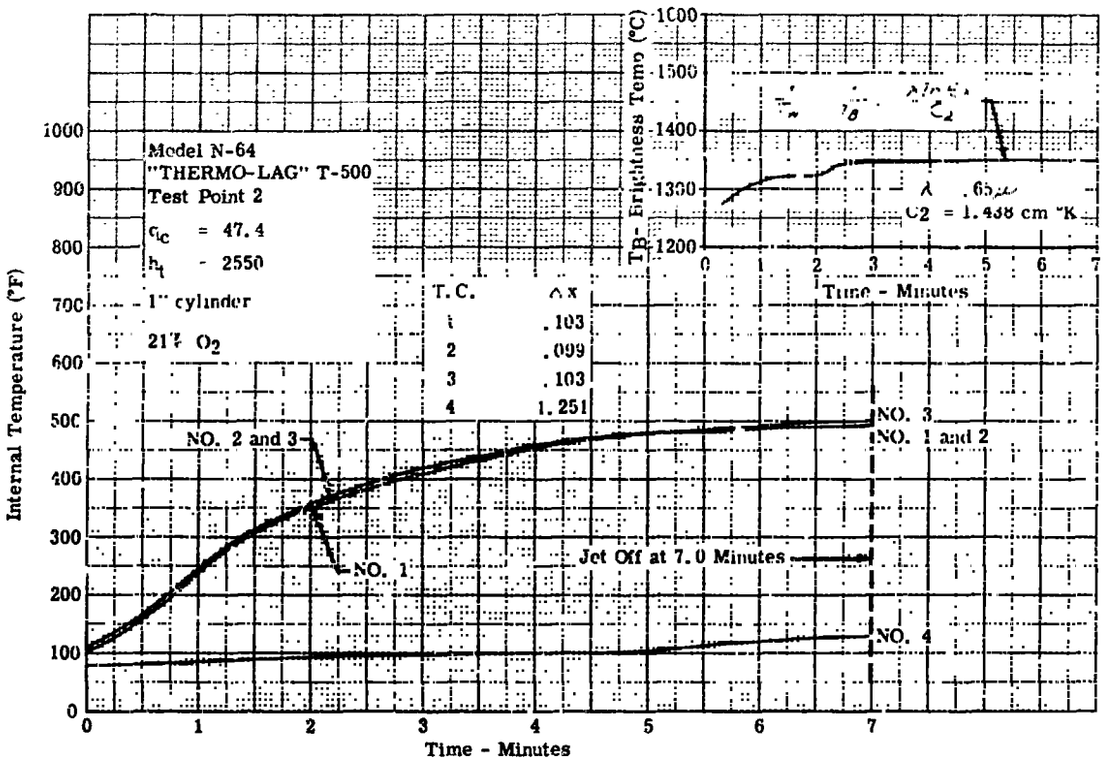

Figure A-45. Temperature - Time History of Model N-64

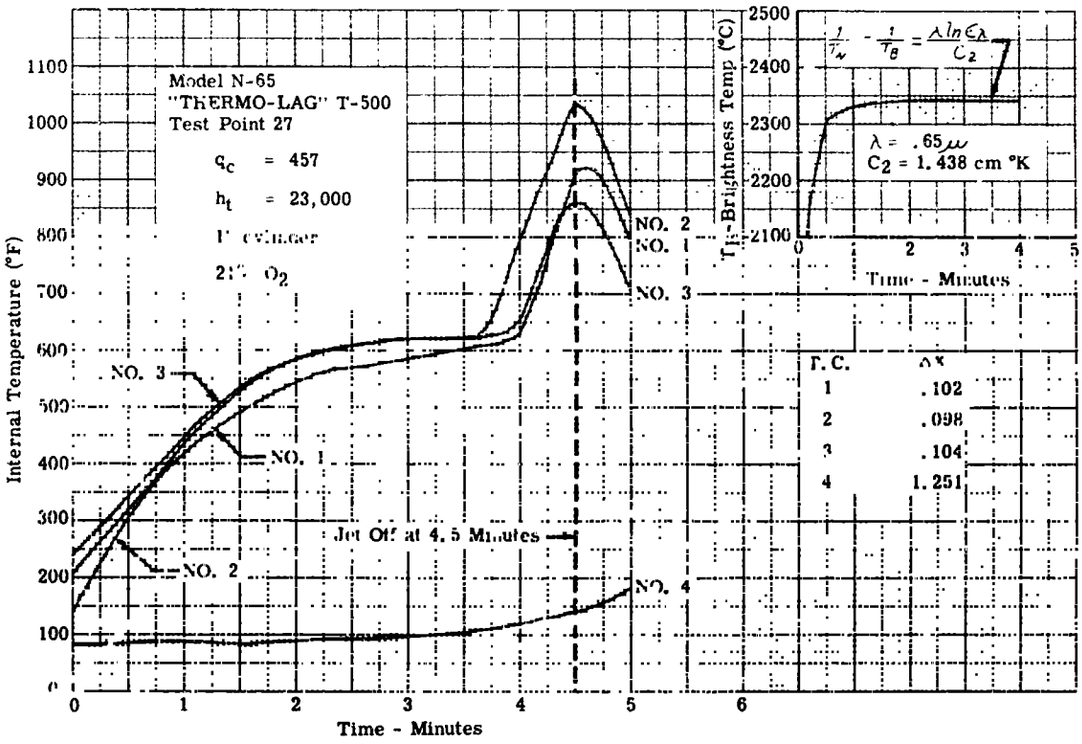

Figure A-46. Temperature - Time History of Model N-65

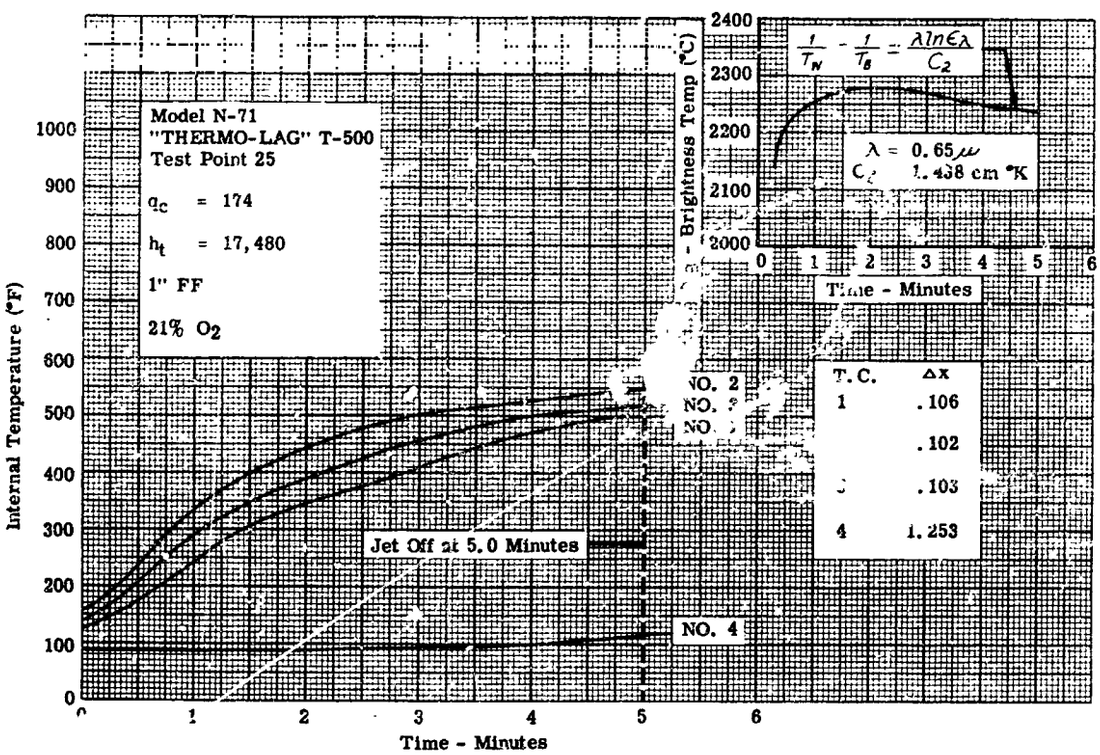

Figure A-47. Temperature - Time History of Model N-71

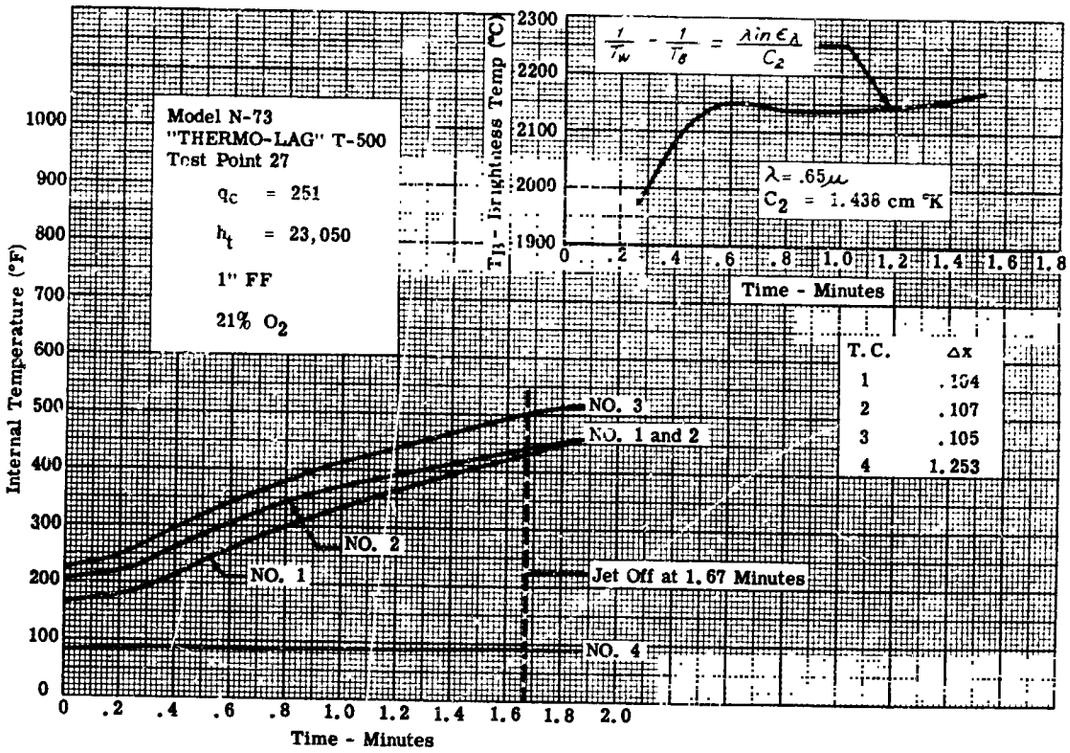

Figure A-48. Temperature - Time History of Model N-73

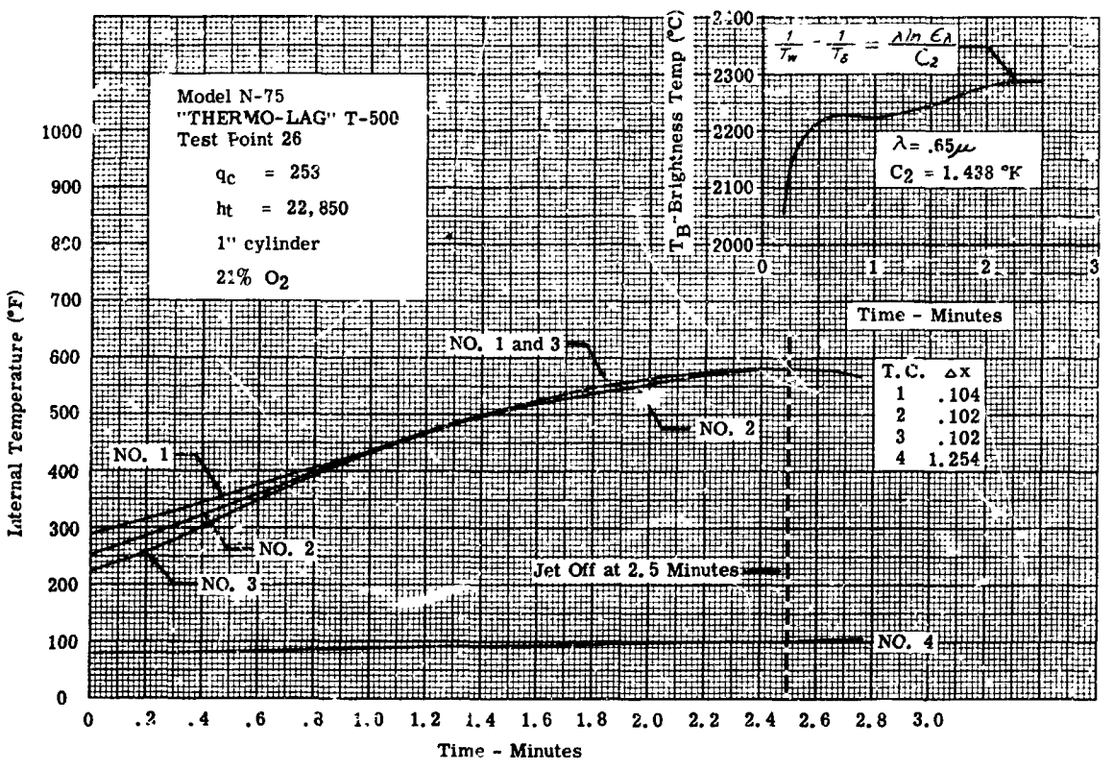

Figure A-49. Temperature - Time History of Model N-75

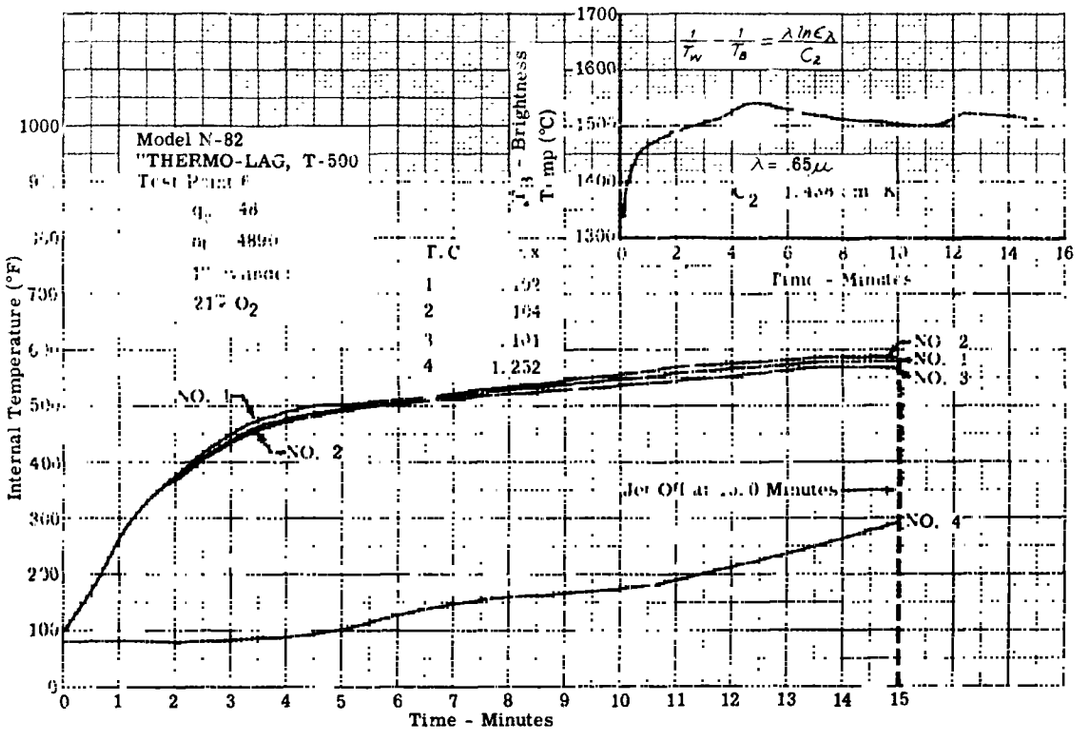

Figure A-50. Temperature - Time History of Model N-82

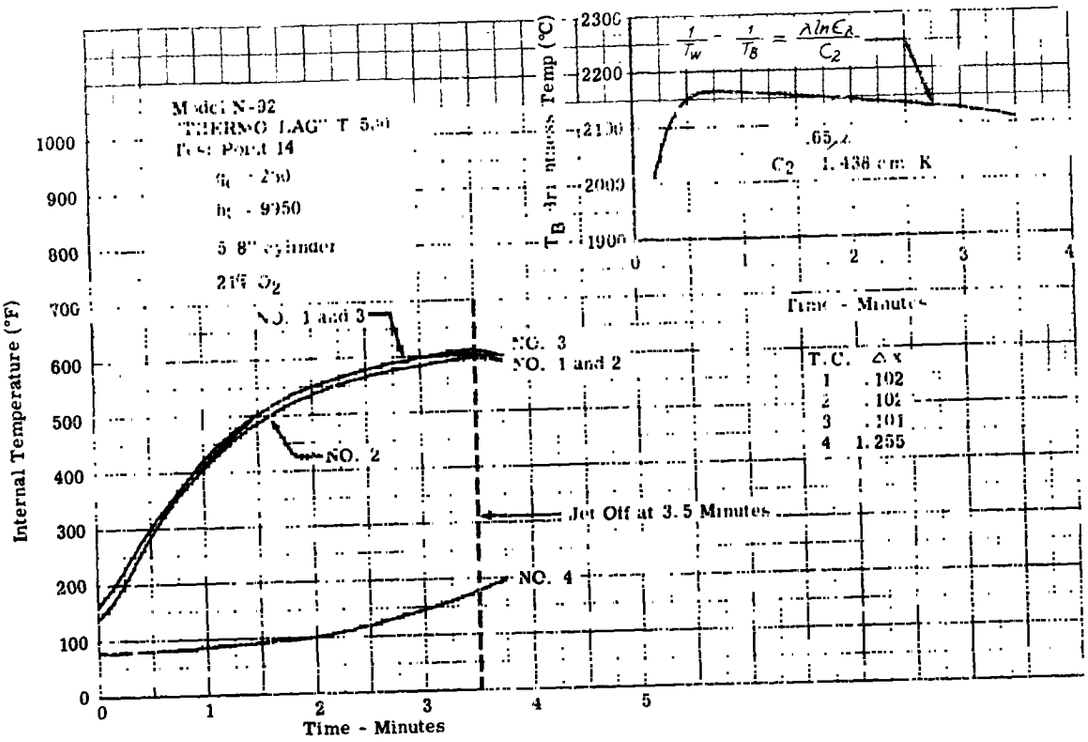

Figure A-51. Temperature - Time History of Model N-92

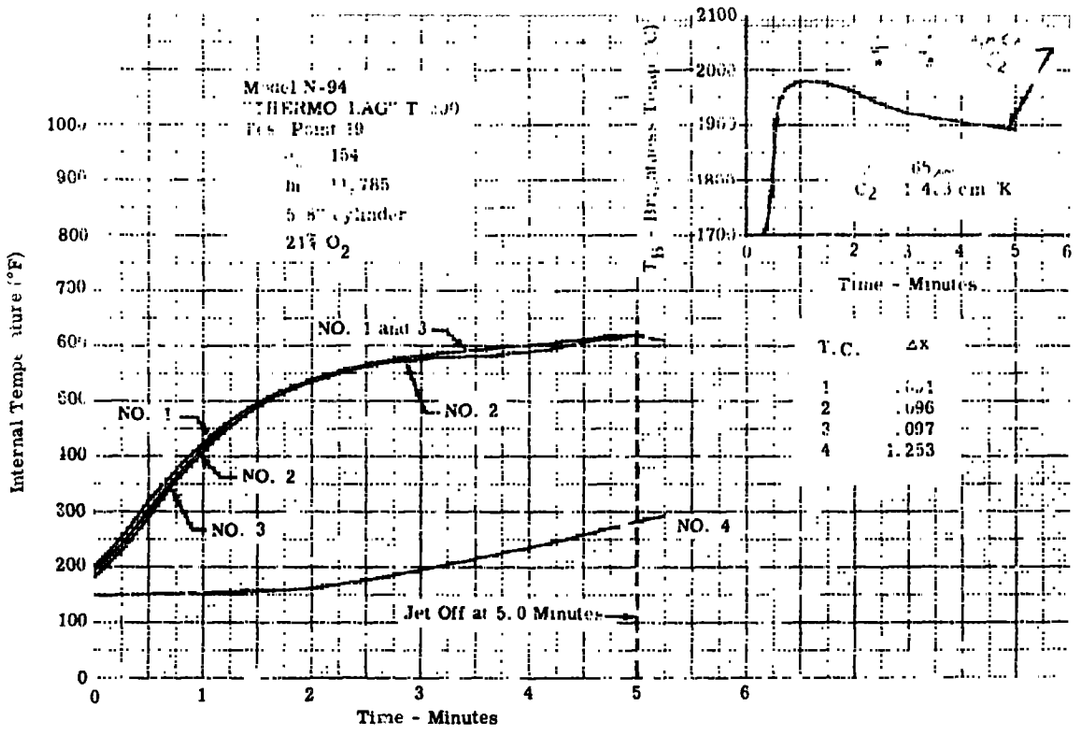

Figure A-52. Temperature - Time History of Model N-94

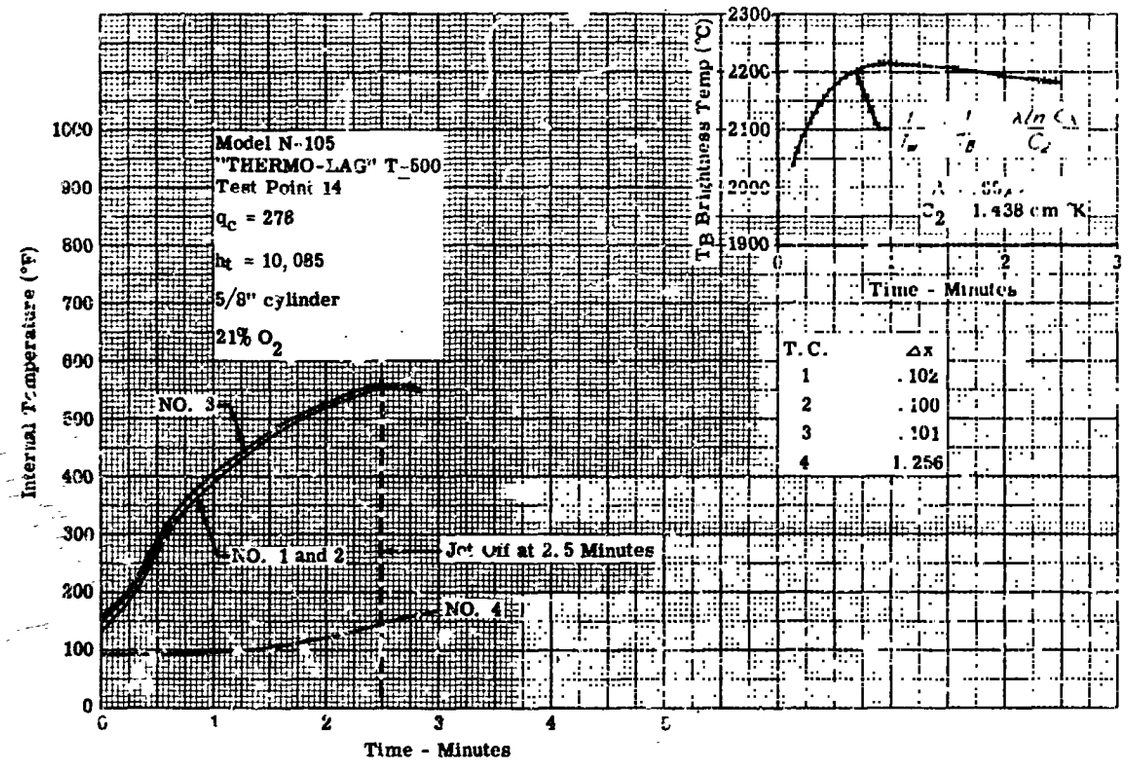

Figure A-53. Temperature - Time History of Model N-105

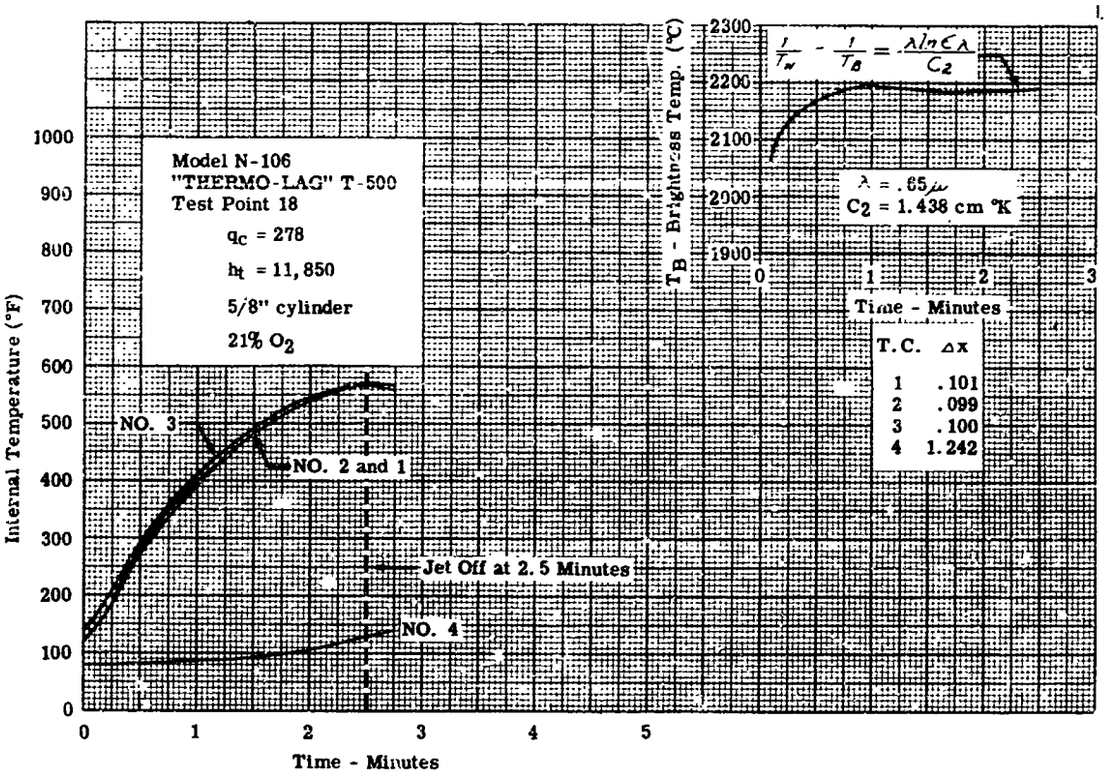

Figure A-54. Temperature - Time History of Model N-106

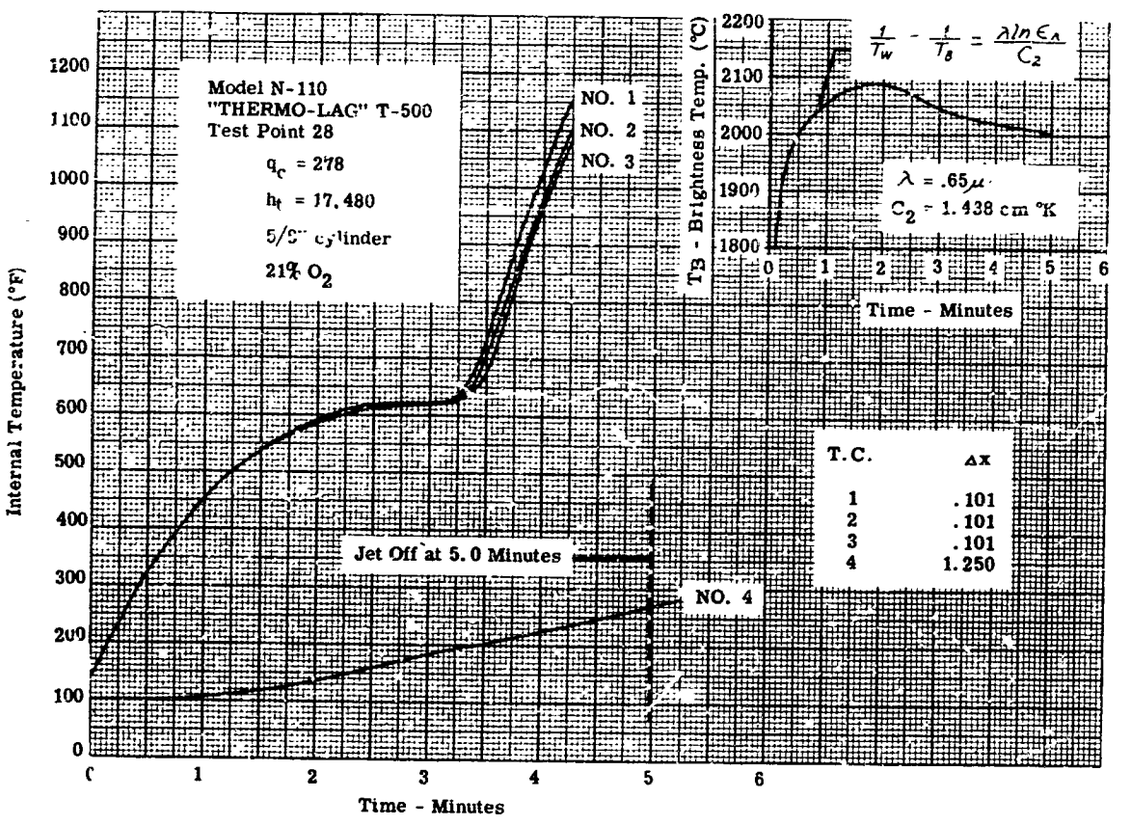

Figure A-55. Temperature - Time History of Model N-110

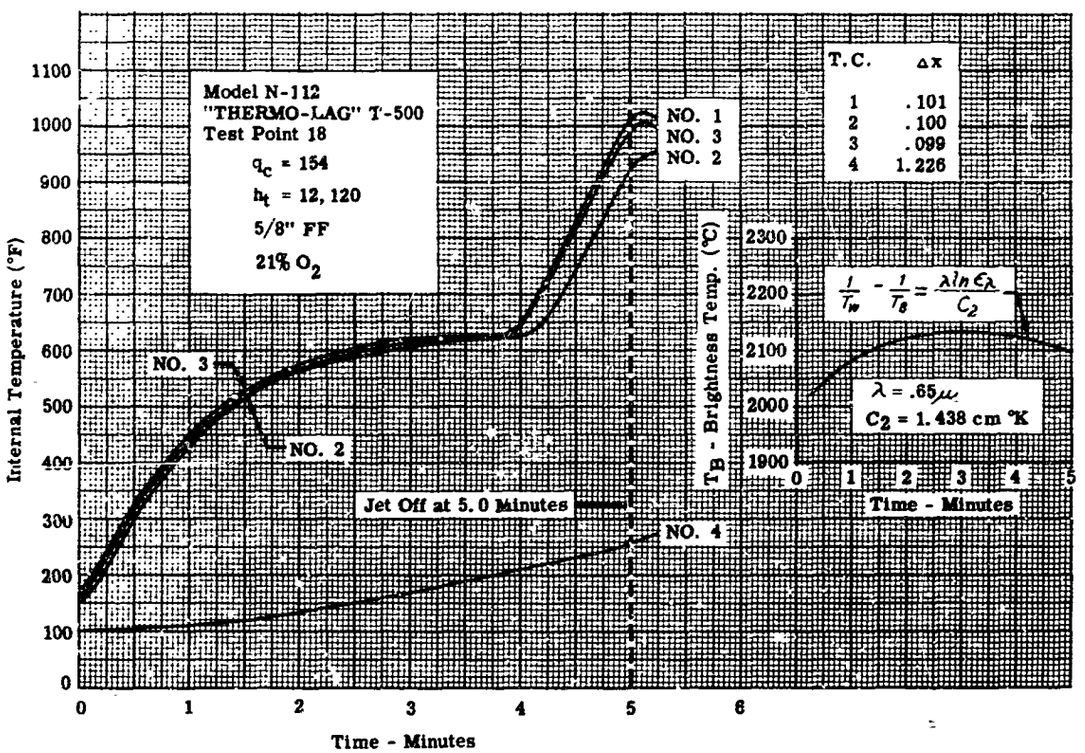

Figure A-56. Temperature - Time History of Model N-112

BLANK PAGE

APPENDIX B

SYMBOLS

The symbols used in this report are defined as follows unless otherwise specified:

GENERAL.

A	Area - FT^2
C	Specific heat - BTU/LBM-°F
D	Diameter - ft
F	View factor - dimensionless
g	Acceleration of gravity - 32.2 FT/SEC^2
g_c	Conversion factor - LBM-FT/SEC^2-LBF
h	Convective heat transfer coefficient - BTU/FT^2-SEC-°R
H	Enthalpy - BTU/LBM
J	Conversion factor - 778 LBM-FT/BTU
k	Thermal conductivity - BTU/FT-SEC-°R
K	Equilibrium constant - dimensionless
L	Length, thickness - FT
$\dot{m}$	Mass loss (or injection) rate - LBM/FT^2-SEC
M	Molecular weight - LBM/LB-MOLE
N	Permeability of porous matrix - LBM/FT
n	Mole fraction - dimensionless
p	Pressure - LBF/FT^2

Q	Heat effect - BTU
Q_D	Net heats of dissociation and decomposition - BTU/LBM
Q_L	Heat of sublimation - BTU/LBM
Q_{react}	Net heats of reaction - BTU/LBM
Q_s	Heat of pyrolysis of solid matrix - BTU/LBM
Q_t	Heat of phase transition of subliming salt - BTU/LBM
q	Heat flux - BTU/FT^2-SEC
q^*	Material efficiency - BTU/LBM
R	Universal gas constant - 10.71 LBF-FT/(LB-MOLE)-°R
r	Radius - FT
R_e	Reynolds number - dimensionless
ST	Stanton number - dimensionless
T	Temperature - °R
V	Velocity - FT
v	Specific volume - FT^3/LBM
W	Weight - LBM
w	Specific weight - LBM/FT^3
X	Distance, thickness, or linear recession - FT
$\dot{X}$	Linear recession rate - FT/SEC
x	coordinates
Y	Body dimension - FT
y	coordinates
z	coordinates

α	Transpiration cooling factor or coefficient of thermal expansion - IN./IN.-°C
β	Endothermic decomposition gradient with respect to temperature - BTU/LBM-°R
ϵ	Porosity - volume of gas/volume of system, or emissivity
ξ	Mass fraction - LBM of salt/LBM of system
θ	Time - SEC
θ, ψ	Planar angle - radian
ρ	Density - LBM/FT^3
μ	Viscosity - LBF-SEC/FT^2
τ	Wall shear stress - LBF/FT^2
Δ	Differential
σ	Stephan Boltzmann Constant - 0.1713×10^{-8} BTU/FT^2-HR-°R^4
ω	Solid angle - Steradian

SUBSCRIPTS

a	Apparent
$aero$	Aerodynamic
AW	Adiabatic wall
e	Outer edge of boundary layer
eff	Effective
G	Gas
i	Chemical species, = 1, 2 . . .
L	Local flow conditions
p	Constant pressure
rad	Radiation

S	Solid or sample
SM	Solid matrix
$stag$	Stagnation point
SW	Side wall
T,t	Total flow conditions
TR	Transition
W	Wall
x,y,z	Coordinates
0	No mass injection
$1,2,3\ldots$	Designation for specified area

SPECIAL SYMBOLS FOR STRESS ANALYSIS.

a	Inside radius of hole in a thick cylinder, IN.
A	Area of cross section, IN.^{2}
b	Outside radius of thick cylinder, IN.
E	Modulus of elasticity, PSI
G	Shear modulus, PSI
K	Bulk modulus, PSI
L	Length, IN.
P	Pressure, PSI
p	Load, LB
q	Shear flow, LB/IN.
r	Radius, IN.

t	Thickness, IN.
T	Temperature, °F
ΔT	Change in temperature, °F
u	Displacement in x-direction, IN.
U	Internal strain energy, IN.-LB
v	Displacement in y-direction, IN.
w	Displacement in z-direction, IN.
x	Distance along x-x axis, IN.
X	Indeterminate load, LB
y	Distance along y-y axis, IN.
z	Distance along z-z axis, IN.
α	Coefficient of linear thermal expansion, IN./IN./°F
γ	Shear strain
Δ	Change in length, IN.
ϵ	Unit strain, IN./IN.
ν	Poisson's Ratio
σ	Normal stress, PSI
τ	Shear stress, PSI
ω	Distributed load, LB/IN.

SUBSCRIPTS

B	Bond
C	Cylinder
i	Internal

o	Initial condition outer
r	Radial direction
θ	Angular direction